Analysis of Neutrophil Granulocytes in Experimental Head And Neck Cancer Development And Progression

Doctoral Thesis

In partial fulfillment of the requirements for the degree

"*Doctor rerum naturalium* (Dr. rer. nat.)"

to the
Faculty of Biology

at the
University Duisburg Essen

submitted by
Katrin Moses

born in Osterburg

August 2015

Die der vorliegenden Arbeit zugrunde liegenden Experimente wurden in der Forschungsabteilung der Hals-Nasen-Ohren Klinik des Universitätsklinikums Essen an der Universität Duisburg-Essen durchgeführt.

1. Gutachter: **Prof. Dr. Sven Brandau**

2. Gutachter: **Prof. Dr. Daniel Robert Engel**

Vorsitzende des Prüfungsausschusses: **Prof. Dr. Astrid Westendorf**

Tag der mündlichen Prüfung: **09.12.2015**

Contents

Abbreviations

Table 0.1: Abbreviations used in this thesis.

Abbreviation	Denotation
(v/v)	volume/volume
(w/v)	weight/volume
A	Ampere
AEC	3-amino-9-ethylcarbazole
BL6	immunocompetent mouse strain, C57BL/6JOlaHsd
BrdU	Bromodeoxyuridine (5-bromo-2'-deoxyuridine)
C_T	Cycle Threshold
C3H	immunocompetent mouse strain, C3H/HeNHsd
CatchUp	immunocompetent transgenic mouse strain, C57BL/6-Ly6g$^{tm2621(Cre\text{-}tdTomato)Arte}$
CatchUp$^{IVM\text{-}red}$	C57BL/6-Ly6g$^{tm2621(Cre\text{-}tdTomato)Arte}$ x B6.Cg-*Gt(ROSA)26Sor*$^{tm9(CAG\text{-}tdTomato)Hze}$/J
CD	Cluster of Differentiation
cDNA	complementary DNA
CFSE	Carboxyfluorescein succinimidyl ester
CXCR	CXC chemokine receptor
DAMP	Danger associated molecular patterns
DC	Dendritic cell
DMSO	Dimethylsulfoxid
DNA	Desoxyribonucleic Acid
DTT	Dithiothreitol
ECM	Extracellular matrix
EDTA	Ethylenediaminetetraacetic Acid
eGFP	enhanced Green Fluorescent Protein
ELISA	Enzyme linked immunosorbent assay
et al.	lat.: ET ALTERI
FACS	Fluorecense-Activated Cell Sorting
FC	Flow cytometry
FCS	Fetal Calf Serum
FSC	Forward Scatter
G	Gauge
G-CSF	Granulocyte colony stimulating factor
HMEC	Human Microvascular Endothelial Cells
HPV	Human papillomavirus
HRP	Horse radish peroxidase
HRPO	horseradish peroxidase
HSPC	Hematopoietic stem and progenitor cells

Table 0.1: (continued)

Abbreviation	Denotation
HyD-RLD	Hybrid reflected light detectors
IF	Immunofluorescence
Ig	Immunoglobulin
IHC	Immunohistochemistry
IMCES	Imaging Center Essen
IP	Intraperitoneal
ISO-1	4,5-Dihydro-3-(4-hydroxyphenyl)-5-isoxazoleacetic acid methyl ester
IVC	Individually ventilated cages
kDA	kilo-Dalton
LAD	Leukocyte adhesion deficiencies
LTR	Long terminal repeat
MACS	Magnetic activated cell sorting
MDSC	Myeloid derived suppressor cells
MFI	Mean fluorescence intensity
MIF	Macrophage Migration Inhibitory Factor
MMP	Matrix metalloprotease
MOPC	Murine OroPharynx Carcinoma cell line
mRNA	messenger RNA
NaCl	Sodium Chloride
nu/nu	athymic nude mice NMRI-*Foxn1*^{nu}/*Foxn1*^{nu}
PAGE	Polyacrylamide gelelectrophoresis
PAMP	Pathogen associated molecular patterns
PBS	Phosphate Buffered Saline
PE	Phycoerythrin
PI	Propidium Iodide
PMT	Photomultiplier tube
PMT	Photomultiplier tube
PVDF	Polyvinylidene Difluoride
qRT-PCR	Quantitative Real Time - Polymerase Chain Reaction
RNA	Ribonucleic Acid
ROI	Region of interest
RT	Room Temperature
RT	Reverse transcriptase
SCN	Severe congenital neutropenia
SDS	Sodium-Dodecyl-Sulfate
SN	Supernatant
SPF	Specific pathogen free animal housing
SSC	Side Scatter
SV40	Simian Virus 40

Table 0.1: (continued)

Abbreviation	Denotation
TAM	Tumor associated macrophages
TAN	Tumor associated neutrophils
TBS	Tris Buffered Saline
TEM	Transendothelial migration
TEMED	N,N,N',N'-Tetramethylethylendiamin
TMB	3,3',5,5'-Tetramethylbenzidine
Treg	regulatory T cell
Tris	Tris-hydroxymethyl-aminomethan
Tween	Polyoxyethylensorbitanmonolaurat
V	Voltage
VEGF	Vascular endothelial growth factor
WB	Western blot
WHO	World Health Organisation
x g	multiple of acceleration of gravity (g = 9.80665 $\frac{m}{s^2}$)
ZMB	Centre for Medical Biotechnology of the University Duisburg Essen

List of Figures

List of Tables

1 Introduction

1.1 The life cycle of neutrophil granulocytes

Polymorphonuclear neutrophil granulocytes were named after their staining characteristics in hematoxylin and eosin staining and their nuclear morphology. In contrast to the dark blue basophilic and bright red eosinophilic granulocytes, neutrophils stain neutral pink. As the most abundant white blood cell, they account for up to 70 % of human peripheral blood leukocytes. Neutrophils belong to the most rapidly responding cells of the innate immune system making them the essential first line defense against invading pathogens. This critical role for combating bacterial and fungal infections becomes apparent when an organism is affected by genetic neutrophil defects as for example in severe congenital neutropenia (SCN) or leukocyte adhesion deficiencies (LADs) in which neutrophils are unable to enter infected tissues[209, 74]. Accordingly, these patients suffer from augmented susceptibility to infections.

1.1.1 Granulopoiesis in the bone marrow and release to the periphery

When released to the peripheral circulation, neutrophils account for the most short-lived immune cells. Depending on the way of estimation in the respective studies, live time measurements range between a few hours and several days[152]. Therefore, essential constant production of neutrophils is carried out in the bone marrow resulting in the release of about 10^{11} cells per day. At this site, differentiation is talking place from multipotent hematopoietic stem cells via pluripotent progenitors, proliferating and lineage-committed myeloblasts, promyelocytes and myelocytes, further proceeding past metamyelocytes and band cells to mature segmented neutrophils. Development and lineage commitment is thereby strongly regulated by the transcription factors PU.1 and CCAAT/enhancer-binding protein α (C/EBPα) among others[166]. Most importantly, all phases of a neutrophils' life cycle are dominantly regulated by granulocyte colony stimulating factor (G-CSF). This role becomes apparent in G-CSF knockout mice, which develop chronic neutropenia[114]. Mechanistic evidence for an implication of G-CSF in lineage commitment was further provided by a study using G-CSF receptor knockout mice in a competitive repopulation assay[164]. While a low production of neutrophils was still found in those mice, the resulting mature neutrophils showed increased susceptibility to apoptosis indicating an additional role of G-CSF in neutrophil survival[118]. This underscores the central role of G-CSF for homeostasis of neutrophil while additional factors seem to be able to support granulopoiesis upon loss of G-CSF. Partial compensation, especially in situations called "emergency" granulopoiesis, can be mediated by granulocyte macrophage colony stimulating factor (GM-CSF), IL-6 and IL-3[129, 130, 154]. Neutrophil production is further regulated by a feedback mechanism from the phagocytes which remove apoptotic neutrophils from the circulation. This feedback involves IL-23 and subsequent IL-17 production[188]. Finally, freshly produced neutrophils have to be released to the periphery. This process is tightly regulated by the antagonistic receptors CXCR2 and CXCR4 and their respective ligands as well as G-CSF[42, 127, 210]. Thereby, stromal cell derived factor 1 alpha (SDF1α) attenuates neutrophil mobilization via CXCR4 activation[127]. CXCR2-binding ELR$^+$ (glutamic acid – leucine – arginine) chemokines further mediate mobilization via CXCR2[42] which is remarkably enhanced in the presence of G-CSF disrupting SDF1α mediated retention[210].

1.1.2 Peripheral challenges: Migration towards infection sites

As mentioned above, a high number of neutrophils is present in the peripheral circulation. However, migration to the site of infection is mandatory to exert their functions as first line defense against invading pathogens. Extravasation is initiated upon sensing of chemoattractants including formyl peptides (such as fMLP), leukotriene B(4) (LTB4), chemokines (such as IL-8) and cytokines like IL-6 and TNFα[115]. These are further derived from tissue resident cells like macrophages, dendritic cells (DCs) or fibroblasts sensing pathogen invasion[196]. Cytokine activated endothelial cells (EC) further present adhesion molecules as well as immobilized chemokines to mediate neutrophil attraction. First interaction is characterized by neutrophil tethering and rolling on the endothelial cell layer and is mediated by interaction of selectins[128]. Binding via selectins further activates cell surface integrins (LFA-1)[224] mediating slower rolling which is associated with sensing of presented chemokines[167]. These signals induce cytoskeletal rearrangements and activation of integrins (LFA-1, MAC-1, VLA4) resulting in firm adhesion to the endothelium[77]. Additionally, MAC-1 (macrophage-1 antigen, consisting of the integrins CD11b and CD18) dependent crawling is initiated which is necessary for localization to optimal extravasation sites[151]. Transendothelial migration (TEM), which can occur para- or trans-cellularly[214], and subsequent passing through pericytes and the basal membrane[9] finally results in neutrophil localization in the infected tissue. Further exposure to activating factors such as foreign pathogen associated molecular patterns (PAMPs) and endogenous damage associated molecular patterns (DAMPs) results in complete activation of neutrophil functions. Consequences of activation and associated functions will be described in the next section.

1.1.3 Effector functions: *Shimpū Tokkōtai* of the immune system

The *Shimpū Tokkōtai* were Japanese Special Forces which committed suicide attacks mainly against the US in the last years of World War II. Their activity is until now better known as kamikaze tactics. This terminology is further perfectly fitting for the actions of neutrophils as they are packed with deadly weapons and are always ready to die for the defense of the body. Neutrophil granules contain densely packed antimicrobial proteins and can be divided by content into three subtypes (primary, secondary and tertiary granules) according to the chronological order of their formation during differentiation[49].

Neutrophils sense pathogens and tissue damage associated with PAMP and DAMP release via a broad repertoire of innate immune receptors, primarily toll like receptors (TLR), resulting in activation and prolonged survival of the responding cell[62]. Thereby, exocytosis is one of the obvious responses to activation. Notably, exocytosis is more likely for granules that are formed later during development. This especially holds true for gelatinase (tertiary) granules and defensin-rich over defensin-poor azurophil (primary) granules[50]. Degranulation and release of secretory vesicles containing inflammatory modulators such as cytokines therefore induces first antimicrobial effects and attracts further immune cells. Main cytokines released by neutrophils are TNF-α, IL-1β, IL-8, macrophage inflammatory protein 1α (MIP-1α), and MIP-1β[110], which act primarily on neutrophils themselves as well as on monocytes, macrophages and endothelial cells. Further cytokine dependent interactions between neutrophils and DCs, B cells, NK and Th17 cells occur under specific circumstances[135]. A detailed overview of neutrophil derived cytokines and chemokines is provided by reference [124] implicating further interactions with additional T cell subsets. Neutrophil degranulation further in-

creases availability of cell surface receptors and integrins, which are also stored in the granula, resulting in a higher probability of additional activation and transmigration[49]. In the process of migration outside of the blood stream, neutrophils make use of specific proteins to modulate extracellular matrix (ECM) structure. Such proteins are matrix metalloproteinases (MMPs) which are also contained in tertiary granules[136]. By degradation of ECM structures, MMPs allow for tissue remodeling and simultaneously release further ECM bound molecules such as cytokines further promoting immune activation[148].
Importantly, Fcγ receptors which bind Fc fragments of antibodies, C-type lectins and complement receptors are transported to the cell surface during the process of degranulation and their activation induces phagocytosis of pathogens. Killing in the phagocytic vacuole is a multistep process. Initially, electrons enter the vacuole via NADPH oxidase producing superoxide radicals (O_2^-) resulting in an alkaline pH and a discharged membrane. O_2^- dismutates by the help of specific enzymes to hydrogen peroxide (H_2O_2) further increasing pH by H^+ consumption and leading to the accumulation of antimicrobial concentrations of these reactive oxygen species (ROS). Additionally, granular contents get incorporated by fusion of primary and secondary granules with the vacuole within 20 seconds after pathogen engulfment and high vacuolar pH buffers the acidic pH in these granules. The resulting pH is perfect for neutral proteases. K^+ further enters the vacuole to compensate charge separation by NADPH oxidase mediated electron transport and further activates neutral proteases which then potently kill engulfed pathogens[174]. As proteases are inactive in granules and do not meet according environments when released from the cell, these adjustment mechanisms are critical for killing activity in the vacuole as well as a matter of protection of the surrounding tissue when neutrophils undergo necrosis. Additionally, extracellular active proteases are inhibited by endogenous serine protease inhibitors (serpins)[100] which can in turn be inhibited by neutrophil derived MMP9[148]. In the phagocytic vacuole, influx of chloride further results in the formation of antimicrobial hypochlorous acid from H_2O_2 by granular myeloperoxidase (MPO)[98]. In total, killing is mediated by the vast body of microbicidal contents of the fused granules which become active by the adjusted environment in the vacuole and are supported by the production of ROS and oxidized halides. As these processes are highly toxic, phagocytosing neutrophils soon die in accordance with the *Shimpū Tokkōtai* analogy.
As an additional way of neutrophil mediated antimicrobial function, NETosis was described in the year 2004[17]. Formation of neutrophil extracellular traps (NETs) is associated with translocation of elastase from primary granules to the nucleus, where it cleaves specific histones and leads to chromatin decondensation[147]. Furthermore, ROS are indispensable for NET formation[57]. The resulting effector molecule-covered DNA net is then spit into the environment resembling a sticky and deadly trap for extracellular pathogens.
Further modulator functions of neutrophils are just arising to be recognized in the field and comprise interactions with the adaptive immune system. Therefore, neutrophil functions can not only be found during infections and autoimmunity, when the described mechanisms result in accelerated tissue damage, but also in the context of malignant diseases.

1.2 Cancer Immunology

Malignant disease is based on an accumulation of multiple independent alterations in the genome of one single cell which is in fact a very rare event. These changes can be attributed to external or genetic

factors and result in aberrant cell growth, proliferation and apoptosis by deregulation of signaling pathways. Thereby, the cells gain cancerous characteristics like self-sufficiency in growth signals, insensitivity to anti-growth signals, the ability to evade apoptosis, capability for tissue invasion and metastasis, a limitless replicative potential and sustained angiogenesis as summarized by Hanahan and Weinberg in 2000[70]. More recently, additional characteristics have been added to these core hallmarks which are not less of importance for malignant progression: deregulation of metabolic energy pathways and evasion of immune attack as well as genomic instability and tumor promoting inflammation were emerging in the last 15 years[71].

1.2.1 Immunosurveillance and Immunoediting

The immune system patrols the body continuously and is well trained by self tolerance mechanisms to not accidentally recognize and damage host tissue. According to this, a malignant tumor cell which arises in a host would not be detected. That this assumption does not hold true has been postulated by Burnet in 1957 suggesting the existence of tumor associated antigens resulting in continuous control of arising transformed cells by the immune system[21]. This process was named immunosurveillance of cancer. Therefore, a malignant cell has to evade the immune system as the result of a process that is called immunoediting which is a three-step process from elimination via an equilibrium phase resulting in tumor immune escape. The elimination phase contributes to immunosurveillance and is characterized by innate immune cell mediated recognition and killing of tumor cells, dendritic cell mediated cross priming of T cells and finally generation of tumor antigen specific T cells which home to the tumor origin resulting in an effective antitumor response[97]. By this process, most of the arising transformed cells get killed without further notice. Nevertheless, eradication of transformed cells puts a selection pressure on the malignant cells resulting in less immunogenic cell clones. This represents the second step, the equilibrium phase, which can take years before resulting in manifested tumor progression[97]. To finally escape immune control, additional adjustments take place in the tumor cells themselves as well as in the microenvironment. To this end, reduced tumor recognition is mediated by reduced antigen presentation via major histocompatibility complex class I molecules (MHC-I)[95]. According to the missing self hypothesis, cells with low MHC-I expression are eliminated by NK cells but tumors evade this regulation for example by additionally decreased expression of NK activating NKG2D (natural-killer group 2, member D) ligands[26]. Further immune ignorance has been postulated to take place by restriction of availability of tumor antigens[144]. Finally and probably most importantly, microenvironmental changes result in the formation of an immune privileged site. Local immunosuppression is thereby mediated by the presence of mainly tumor derived factors including vascular endothelial growth factor (VEGF), IL-10, Transforming growth factor beta (TGF-β), prostaglandin E2, soluble phosphatidylserine, Fas, FasL and MHC class I polypeptide-related sequence A (MICA)[97].

In the battle of immune evasion by the tumor, tumor cells do not act alone but also recruit and re-educate immune cells to promote tumor progression and immunosuppression. A central role in this context is subscribed to macrophages. Those can be alternatively activated resulting in a so called M2 phenotype which is characterized by secretion of anti-inflammatory molecules like IL-10, TGF-β and arginase1. Furthermore, general promotion of tumor angiogenesis, growth, metastasis, and immunosuppression has been described for M2 tumor associated macrophages (TAM)[73]. In addition,

tumoral factors are potent modulators of dendritic cell differentiation and it was demonstrated that immature DCs in tumor hosts mediate TGF-β dependent regulatory T cell (Treg) expansion thereby promoting tumor progression via immunosuppression[63]. Tregs are classically characterized by expression of cell surface CD25 and FoxP3 transcription factor activity and were associated with malignant disease very early on[58]. Their central role for tumor progression was demonstrated by antibody dependent depletion of the cell population expressing CD25 which resulted in complete block of tumor growth in leukemia, myeloma and sarcoma models[146] as well as melanoma[179]. The response to this treatment was mediated by induction of an antitumor cytotoxic T and NK cell activity[179]. Thus, a vast array of immune cells was indicated to be associated with tumor progression. In contrast, an involvement of neutrophils only started to be addressed by research and this advance further shapes the complexity of tumor associated inflammation.

1.2.2 Role of neutrophilic cells in human cancer

An association between high peripheral neutrophil counts and tumor progression as well as poor survival has been found for a variety of malignant diseases[201] and was generally identified as a sign of systemic inflammation. Additionally, more specific functional alterations in neutrophils became apparent in the last years. In head and neck cancer (HNC) patients, recent studies in our group demonstrated increased peripheral blood neutrophils and enhanced inflammatory activity[203]. Furthermore, neutrophils in HNC patients were characterized by lower inducible ROS production, reduced spontaneous apoptosis and by an increased number of immature cells[204]. Immature neutrophils were also found in the blood of terminal lung, breast and gastrointestinal cancer patients where they associated with poor prognosis[28]. In this line, reduced ROS by neutrophils was also demonstrated in acute lymphoblastic leukemia[198] and hepatocellular carcinoma[205]. A whole set of studies concentrated on the identification of the secretory patterns of neutrophils in oral cavity cancer patients. Thereby, they showed increased IL-1β and IL-1Ra release[88], higher VEGF and lower IL-18 secretion[89], a reduction in soluble tumor necrosis factor related apoptosis inducing ligand (TRAIL)[87] as well as an increase in the abundance of IL-17A and IL-17E in neutrophils in the tumor bearing hosts[61]. These findings implicate a functional involvement of tumor-modulated neutrophils in human tumor development and progression.

Among the neutrophil induced processes, promotion of angiogenesis is apparent by VEGF production which was also shown in a set of additional metastatic malignancies[108]. VEGF can directly act on endothelial cells promoting blood supply of the tumor. Further induction of angiogenesis was also described for MMP9 derived from peritumoral neutrophils in hepatocellular carcinoma[102]. Again, neutrophils exerted profound MMP9 expression in HNC patients as well[38]. The main mechanism by which MMP9 can directly influence angiogenesis is degradation of ECM and thereby release of ECM bound VEGF. ECM degradation furthermore enables mobility of cells and MMP9 can therefore also influence invasiveness of tumor cells. A direct link between neutrophils and tumor cell invasion was further suggested by our group showing that tumor infiltrating neutrophils induce invasion and migration promoting cortactin expression in tumor cells in orohypopharynx carcinoma[37]. Further association of neutrophils with metastasis was presented in hepatocellular and gastric cancers which was shown to depend on cell-cell contacts between tumor cells and neutrophils[217]. Finally, tumor associated neutrophils were also implicated in suppressing antitumor responses primarily by the re-

lease of arginase1 in non-small cell lung cancer[168] as well as glioblastoma multiforme patients[184]. Neutrophil derived arginase1 can profoundly suppress T cell responses by depletion of L-arginine. These findings draw a wide scaled picture of the multilayered functional consequences of neutrophil accumulation and infiltration in cancer patients. Murine models and advanced *in vitro* studies provide further insight into the mechanisms underlying these functions and will be described in the next chapter.
Additional complexity arises from the identification of distinct immunosuppressive neutrophil-related subsets which can be found in cancer patients. The so called granulocytic myeloid derived suppressor cells (MDSC) were first identified in mice and subsequently also emerged to be present in cancer patients. Even though identification is challenged in humans by the lack of Gr-1 antigen, which is present in mice, we recently suggested a phenotyping strategy specifically identifying human MDSC subsets[41]. In HNC patients, these cells comprised immunosuppressive immature neutrophilic cells with low density in gradient centrifugation and impaired chemotactic responses[15]. As immunosuppressive functions were also described for neutrophils, their implications in cancer progression are most probably overlapping. Furthermore, exact relations of both cell types are not yet well defined and are frequently discussed in the field[14].

1.2.3 Immune status in HNC

Head and neck tumors, which are most frequently resembling squamous cell carcinomas histologically, are mainly induced by two independent causative agents: human papillomavirus (HPV) infections and toxic nicotine abuse in combination with alcohol resulting in accumulation of genetic alterations[64, 6]. Both immunogenic viral antigens and nicotine and alcohol induce inflammatory processes which can likely result in malignant transformation[16, 56]. In case of HPV infections, expression of viral oncogenes further promotes carcinogenesis[226]. The resulting chronic inflammation often results in T cell exhaustion and inefficient tumor clearance.
Absolute numbers of $CD3^+$, $CD4^+$, and $CD8^+$ T lymphocytes were decreased in patients with HNC[107]. Furthermore, expansion of $CD8^+CD45RO^-CD27^-$ T cells was described, which are T cell receptor zeta chain negative and sensitive to apoptosis[106]. Thus, this cell type is rather unresponsive. Increased spontaneous apoptosis was also described for peripheral blood mononuclear cells (PBMC) as well as tumor infiltrating lymphocytes (TIL) of HNC patients[160] most likely contributing to decreased total T cell numbers. Furthermore, spontaneous apoptosis correlated with FasL expression in the tumor[160] potently removing tumor infiltrating T cells. Additional suppression of T cells in HNC patients is mediated by expansion of Tregs[190, 211] which show increased responsiveness to TLR stimulation and gain additional suppressive activities by the tumor derived DAMP high-mobility group protein B1 (HMGB1)[211, 212]. Next to the T cell compartment, tumor associated macrophages were also described to correlate with tumor progression as measured by metastasis and tumor stage[125]. On top of that, our group revealed expansion of immunosuppressive MDSC in HNC patients and further characterized central alterations in neutrophil granulocytes in this tumor entity as described above.

1.3 Models of tumor-neutrophil and neutrophil-tumor interaction

While patient material is only able to give insight into the current status of an individual state of disease, mechanistic knowledge can be obtained by further experimental models. Complex context can therefore be simplified and mimicked in *in vitro* setups. To this end, many cancer cell lines have been established and can be utilized to study responses of immune cells to tumoral factors. Furthermore, direct effects of isolated immune cells on tumor cells are investigated. Thereby, single cell interactions can be dissected. Transplantable as well as chemically or genetically induced tumors in mice resemble a unique opportunity for the investigation of tumor immune interactions in the living organism. As the murine and human immune systems are closely related, such mouse models are often used to mechanistically study disease progression. Neutrophils have been investigated in both models as described in this chapter.

1.3.1 Neutrophil-tumor crosstalk *in vitro*

For the analysis of functional properties, human neutrophils can be isolated from the peripheral blood. Only their short life span limits the *in vitro* applicability of these cells. Nonetheless, important findings have been made which help to understand the complex interaction between tumor cells and neutrophils. Using supernatants from tumor cell lines, survival promoting effects of tumoral factors as well as chemotactic properties on neutrophils were demonstrated[39, 203, 217, 215]. Furthermore, functional links to tumor promoting properties have been made. For example, angiogenesis promoting functions of neutrophil derived tissue inhibitor of metalloproteinase (TIMP)-free MMP9 have been identified in chorio-allantoic membrane (CAM) assays and by analysis of HUVEC (human umbilical vein endothelial cell) spheroid sprouting[8, 10]. Additional studies demonstrated that MMP9 release by neutrophils can be induced by tumor derived factors, which lead to an activation of the p38 mitogen-activated protein kinase (MAPK)[38]. Furthermore, immunosuppressive activity was identified to be mediated not only by arginase1 in response to IL-8[168] but also by oxidative stress. H_2O_2 was herein identified to induce T cell dysfunction *in vitro* which was mediated by impaired T cell actin dynamics[173, 99].

Next to that, additional studies concentrated on the direct feedback effects of neutrophils on cancer cells. A study from our group indicated neutrophil release of factors like MMP9 in response to HNC tumor supernatants which in turn resulted in increased tumor cell invasion and ECM adhesion[39]. Another study convincingly demonstrated a similar feedback effect especially on hepatocellular carcinoma cells by induction and release of HGF from neutrophils[86]. Further invasion promoting capacities on fibrosarcoma cells have been suggested for neutrophil derived serine proteases, namely elastase, cathepsin G and proteinase-3, which were shown to activate proMMP-2[178]. In a breast cancer model, direct interaction of neutrophils and cancer cells was assessed. Thereby it was found that these cell-cell interactions induced oncostatin M release from neutrophils which promoted an invasive phenotype of the breast cancer cells[157]. It was further demonstrated in a similar setting that interaction via ICAM-1 on tumor cells and β2 integrins on neutrophils (e.g. CD11b) was mandatory to enhance migratory capacities of breast tumor cells[191]. As invasiveness is also closely linked to metastasis, several studies also addressed neutrophil aided tumor cell extravasation in sophisticated *in vitro* settings. Neutrophil induced tumor cell transendothelial migration was herein first shown in a HUVEC migration assay and was also dependent on ICAM-1–MAC-1 (CD11b/CD18) interaction[215].

Further evidence for this mechanism was provided in an extravasation assay which included blood flow conditions where melanoma cell derived IL-8 induced MAC-1 increase on neutrophils and resulted in enhanced melanoma cell extravasation[83].
The described findings indicate that a complex functional interplay between neutrophils and tumor cells was identified by *in vitro* studies. These studies were ultimately required for our current understanding of *in vivo* processes. Nevertheless, culture systems always harbor one major disadvantage which is the lack of cell components that cannot be mimicked due to tissue complexity. *In vitro* studies therefore need to be verified by additional approaches to ensure the *in vivo* validity of the identified mechanisms.

1.3.2 Neutrophils in murine tumor models

In the murine system, mechanistic analysis can be realized by diverse interventions ranging from chemical inhibitors to genetic modifications. These possibilities result in a vast array of studies on tumor-immune interaction in mice. Murine neutrophils are identified by the expression of the myeloid integrin CD11b and the neutrophil specific marker Ly-6G. As Ly-6G can be detected by Gr-1 specific antibodies, which also bind to the monocytic Ly-6C antigen, one has to closely examine results from studies using Gr-1 for identification of neutrophils (and also monocytes). Additionally, differentiation between neutrophils and MDSC is impossible in murine hosts as MDSC have been described as $CD11b^+Gr\text{-}1^+$ cells in tumor bearing mice[175] which accounts for all neutrophils. To prevent misunderstandings, this study prefers to stick to the phenotypic identification by CD11b and Ly-6G. Nevertheless, accumulation of these cells in the tumor bearing host is a central characteristic in most studies. Tumor induced changes in $CD11b^+Ly\text{-}6G^+$ cell differentiation and function thereby include modulation of granulopoiesis in the bone marrow[111, 126] and extramedullary sites like the spleen have also been suggested as a reservoir of $CD11b^+Ly\text{-}6G^+$ cells in some tumor models[30]. The tumor microenvironment is furthermore capable of attracting and functionally activating $CD11b^+Ly\text{-}6G^+$ cells for example by the presence of the inflammatory chemokines CXCL1[138] and CXCL5[225]. Based on their important roles in inflammatory and homeostatic neutrophil trafficking the respective receptors CXCR2 and CXCR4[42] were suggested early on to be involved in recruitment of $CD11b^+Ly\text{-}6G^+$ cells to the tumor[171]. Consequently, CXCR2 blockade and knockout experiments resulted in diminished $CD11b^+Ly\text{-}6G^+$ cell infiltration into the tumor and decreased $CD11b^+Ly\text{-}6G^+$ cell associated tumor promoting angiogenesis[91], metastasis[219] and immunosuppression[79]. Mechanistically, murine studies provided and verified many functional connections between neutrophils and tumors which could also be applied to the human system as described below.
According to the human studies, MMP9 and VEGF mediated tumor angiogenesis was also supported in several murine tumor models[218, 103]. The role of MMP9 was further strengthened in knockout mice for either the MMP inhibitor TIMP2 or MMP9 itself in which neutrophil induced angiogenesis was either enhanced or reduced, respectively[68, 11]. Mechanistically, increased signal transducer and activator of transcription 3 (STAT3) activity was demonstrated to be associated with promotion of angiogenesis[90, 103]. On top of these findings, also a MAC-1 / ICAM1 dependent metastasis promotion could be verified *in vivo*. This has been demonstrated by β2 integrin knockout experiments[200] as well as by novel intravital imaging techniques[185].
As indicated by the term myeloid derived suppressor cells, immunosuppression by $CD11b^+Ly\text{-}6G^+$-

cells has been extensively studied in murine cancer models. The identified mechanisms include T cell suppression by Treg expansion[176, 29], arginase 1 and inducible nitric oxide synthase (iNOS) activity[194, 85, 19], block of T cell homing mechanisms[137, 72], Th17 polarization[27], TCRζ chain downregulation[131] and cysteine sequestration[186]. Knockout studies further demonstrated the central role of the MyD88 innate immune receptor adapter molecule for suppressive functions of CD11b$^+$-Ly-6G$^+$ cells on T cells[81]. Additionally, suppression of NK cells was indicated by cell-cell contact dependent inhibition of STAT5 activation[117] and direct NKG2D downregulation[45] by membrane bound TGFβ in spleen and liver of tumor bearing mice[113]. These variant mechanisms for CD11b$^+$-Ly-6G$^+$ cell mediated immunosuppression demonstrate the key role of these cells once induced by a tumor and further imply that specific tumor derived factors decide about the mode of action of CD11b$^+$Ly-6G$^+$ cells.

On top of various protumoral functions of CD11b$^+$Ly-6G$^+$ cells, recent studies provided evidence for a critical role of CD11b$^+$Ly-6G$^+$ cell localization in different organs within the tumor host on their functional properties. For example, Fridlender and coworkers[55] demonstrated that CD11b$^+$Ly-6G$^+$ cells from the spleen and tumor obtained protumoral gene expression changes compared to resting neutrophils. This was supported by a second study comparing resting and mobilized neutrophils from naive mice to MDSC from tumor bearing mice[221]. Furthermore, tumor infiltrating cells showed a pronounced upregulation of immunomodulatory cytokines and protumoral factors compared to spleen derived CD11b$^+$Ly-6G$^+$ cells from tumor bearing hosts[55]. Similarly, in a murine prostate cancer model, Gr-1$^+$ cells isolated directly from the tumor site, but not those from the spleen, showed high suppressive activity without need for additional *ex vivo* activation[76]. These studies conclusively demonstrate the necessity of neutrophil activation by tumoral factors in the tissue for the exertion of their complete protumoral repertoire.

Noteworthy, protumoral functions do not resemble the complete portrait of CD11b$^+$Ly-6G$^+$ cell tumor interactions. Mostly associated with therapeutic interventions, CD11b$^+$Ly-6G$^+$ cell activation was shown to be associated with potent antitumoral effector functions[13]. Probably the most cited example for this dichotomy is a study from Fridlender *et al.* in 2009[54]. They could show differential phenotypes associated with distinct gene expression patterns of tumor infiltrating CD11b$^+$Ly-6G$^+$ cells upon TGFβ blockade compared to untreated tumor bearing mice resulting in what they call a N1 rather than the "usually" occurring N2 tumor associated neutrophil (TAN). This terminology was chosen in analogy with proinflammatory and antitumoral M1 and protumoral M2 TAM. Another example is Bacillus Calmette-Guérin (BCG) induced immunotherapy of bladder cancer which is only effective upon the presence of neutrophils mediating the key antitumoral response[193]. Additionally, also intrinsic antitumoral properties of G-CSF stimulated neutrophils have been described with the inhibition of lung metastasis formation in murine breast cancer models[66]. This process involved the production of H_2O_2 which was further supported by a recent study to promote tumor cell killing after c-Met activation in CD11b$^+$Ly-6G$^+$ cells[52]. Taken together, these studies demonstrate the complex interaction between CD11b$^+$Ly-6G$^+$ cells and the tumor which is highly dependent on respective tumoral factors and therefore depends on detailed characterization of the model and the cancer entity in patients. Notably, a detailed analysis of CD11b$^+$Ly-6G$^+$ cells in murine HNC models is missing and would be beneficial for further investigation of neutrophil-HNC interactions.

1.3.3 Antibody mediated depletion as major technique for investigation of neutrophil functions

To address the in vivo relevance of CD11b$^+$Ly-6G$^+$ cells, many studies make use of antibody mediated depletion. For this purpose, researchers use antibodies directed against either Gr-1 (clone RB6-8C5), which is binding to Ly-6G as well as Ly-6C even though with lower affinity, or Ly-6G specific monoclonal antibodies (mAb)[32]. Efficient depletion of CD11b$^+$Ly-6G$^+$ cells is rapidly induced upon injections of αGr-1 mAb and provided important insight into short term models of infection[33, 24]. In contrast to depletion in infectious disease models, multiple and continuous injection of antibodies has to be applied for most tumor models to obtain longer depletion of neutrophils. Questions about the technique arose with a recent study by Ribechini *et al.* demonstrating that bone marrow derived CD11b$^+$Ly-6G$^+$ cells seemed to be resistant to antibody mediated depletion due to anti-apoptotic MCL-1 expression[163] which might additionally interfere with longer depletion periods. Limitations of the technology were also highlighted in a report suggesting that hepatic CD11b$^+$Ly-6G$^+$ cells are not depleted by Gr-1 mAb in tumor bearing mice[123]. In spite of that, many studies showed important mechanistic relationships between neutrophils and tumor progression using this technique.
Significant contribution to the understanding of neutrophil mediated tumor progression was made by studies with intermediate depletion periods of about one to two weeks. In such a setting, angiogenesis promoting functions of CD11b$^+$Ly-6G$^+$ cells was verified in a melanoma model[90]. A number of studies could further show the essential contribution of CD11b$^+$Ly-6G$^+$ cells to tumor cell metastasis. In this regard, CD11b$^+$Ly-6G$^+$cells were shown to be critical for lung colonization by fibrosarcoma cells[200] and by a lung cancer cell line[187]. In the 4T1 breast cancer model, a functional link has been described for CD11b$^+$Ly-6G$^+$ cell abundance and metastasis to lung[182] as well as liver[195]. Additionally, depletion of CD11b$^+$Ly-6G$^+$ cells was implied to induce immune response activation in a genetic glioma model[59] as well as by the lung cancer study of Srivastava *et al.*[187] who were the only ones so far reporting more than one mechanism of CD11b$^+$Ly-6G$^+$ cell protumor function in one study. These studies indicated that effects of neutrophils on tumor progression can occur rapidly and are therefore measurable within one to two weeks. Nevertheless, many studies also went for longer depletion periods of three weeks and longer which is essentially also required for genetic and toxin induced tumor models due to the slow onset of disease. These studies include the first description of tumor growth delay by granulocyte depletion in a nude mouse model in 1995[150]. Essentially, these studies verified CD11b$^+$Ly-6G$^+$ cell effects on tumor growth in different tumor models[84, 4, 197, 113, 139, 67, 92, 117] which was mainly contributed to an activation of antitumor immune responses during Gr-1 or Ly-6G depletion[84, 113, 54]. Thus, functional implications of CD11b$^+$Ly-6G$^+$ cells in tumor progression were observed in murine models using both intermediate and long-term depletion.
It has to be noted that depletion schemata highly vary between studies. The applied treatment regimens range from low abundance (100 µg twice per week)[54] to high availability of antibody (500 µg three times per week)[92]. Furthermore, the point of time of initiation of depletion may also differ and direct comparison of effects on tumor establishment and advanced progression are rarely mentioned. A recent study of Mishalian *et al.* indicated a late over early activity of CD11b$^+$Ly-6G$^+$ cells in lung carcinoma and mesentheloima models in which a CD11b$^+$Ly-6G$^+$ cell priming switch only occurred with tumor progression[133]. Additionally, also the choice of antibody has to be considered, as αGr-1 mAb potentially also depleted other cell subsets which might interfere with interpretation of

results[24, 32].
Regardless of varying treatments and limitations of the technique, all of these studies highlight the power of antibody mediated depletion to unravel important aspects of neutrophil biology. Nevertheless, limitations and variables also arise from the differences between tumor models. Surprisingly, a detailed and longitudinal analysis of the efficacy and functional consequences of antibody mediated depletion of CD11b$^+$Ly-6G$^+$ cells in the various compartments of tumor bearing mice is missing. Furthermore, it is largely unknown how the appearance of a tumor and thereby induced CD11b$^+$Ly-6G$^+$ cell modulation in the host may affect the process of neutrophil depletion.

Aim of the study

As described in the previous chapter, significant progress has been made in the understanding of neutrophil induced tumor progression in mouse models, which also reflect functional relationships to human malignant diseases. In head and neck cancer (HNC) patients, recent studies from our group indicated the importance of neutrophil granulocytes and identified further modulatory activity of HNC cells on human neutrophils *in vitro*[15, 203, 39]. Accordingly, analysis of these interactions in a murine model would provide a desirable tool for investigation of neutrophil functions in the tumor-immune crosstalk, which was not yet described in a HNC model. Studies in other tumor models reported a number of protumoral functions of neutrophils and it was suggested that infiltration into the tumor is a critical process for the activation of protumoral functions of neutrophils[55]. Contrary, accumulation of immunosuppressive neutrophils[1] in spleen and blood was also described as a key characteristic of many tumor models suggesting that these cells are also affected by the tumor in the periphery. Furthermore, it is not clear yet, whether protumoral neutrophils are specifically promoted to exert one single function or whether they are able to affect tumor progression by several means being for example angiogenesis and immunosuppression at the same time. A major tool to address these questions is provided by antibody mediated Ly-6G$^+$ cell depletion, which is often used in experimental tumor models. As neutrophils are highly modulated in the same tumor models and this modulation affects activation as well as differentiation of these cells[30, 223, 111], an interference between proceeding tumors and CD11b$^+$Ly-6G$^+$ cell depletion might occur. Nevertheless, the actual efficacy of neutrophil depletion is often not monitored and detailed analysis in long-term depletion experiments are lacking. Additional interest should be put into the function of the Ly-6G protein as such, which is targeted by these depletion regimens. Albeit no specific role was yet found for this molecule, antibody mediated ligation could either activate unknown pathways or interfere with its potential functions. A role for Ly-6G in CD11b$^+$Ly-6G$^+$ cell trafficking has been proposed[208] but was not confirmed in different experimental settings[75] and therefore remains elusive. The presented study will address several questions arising from the above stated proceedings in the field of neutrophil oncology as outlined below.

1. In the first part of this thesis, CD11b$^+$Ly-6G$^+$ cell frequencies as well as functional activation will be investigated in a HNC model. A main point of interest in this part of the study is the tissue specific localization of CD11b$^+$Ly-6G$^+$ cells and their organ dependent functions in the tumor bearing host during advanced disease progression.

[1] also called granulocytic myeloid-derived suppressor cells (MDSC)

2. Next, this study will focus on the impact of neutrophils on HNC progression and tumor growth. Using antibody mediated depletion of Ly-6G$^+$ cells, the role of neutrophils during the stages of tumor establishment and advanced disease progression will be assessed. Further analyses will address potential simultaneous functions by which CD11b$^+$Ly-6G$^+$ cells mediate tumor progression in the specific stage.

3. A major part of this study concentrates on the evaluation of neutrophil depletion efficacy in the tumor bearing host. To this end, this study will longitudinally analyze the effects of neutrophil depletion on frequency and function of these cells in different tissue compartments of the tumor bearing host.

4. In the final part of this thesis, a pilot study is presented aiming at the identification of Ly-6G mediated and tumor related functions in knockout mice. In a small experimental setup using the CatchUp mice[75] in the HNC tumor model, tumor associated trafficking and immune effector interactions will be analyzed.

Taken together, this study will serve new and until know unrepresented insights into HNC-neutrophil and neutrophil-HNC interactions by establishment and functional analysis of a HNC mouse model. Furthermore, detailed and longitudinal analysis of external neutrophil modulation in experimental tumors will be provided for the first time.

2 Material

2.1 Biological material

The table lists cell lines used for this work and their origin. For description of culture media see table 2.11.

Table 2.1: Cell lines and respective culture conditions.

Cell line	Origin	Reference
B16F10	murine melanoma selected for formation of lung metastasis, BL6	Filder 1975[51]
EL4	murine T cell lymphoma known to induce high MDSC accumulation, BL6	Youn *et al.*2012[221]
FaDu	human pharynx squamous cell carcinoma	Rangan 1972[159]
HEK293T	human embryonic kidney, constitutively expressing simian virus40 (SV-40) large T antigen	DuBridge *et al.*[35]
HMEC	human microvascular endothel, immortalized	Ades *et al.*[3]
MOPC^{-}	murine oropharyngeal carcinoma, tonsil-derived, BL6	kindly provided by John Lee[213]
MOPC^{-eGFP}	derived from MOPC- cells by lentiviral transduction	established in this work
MOPC^{+}	murine oropharyngeal carcinoma, tonsil-derived, HPV E6/E7^{+}, BL6	see MOPC^{-}
UM22b	human HNSCC	provided by Thomas Hoffmann[80]
SCCVII	spontaneously arising squamous cell carcinoma of C3H mice	kindly provided by Reinhard Zeidler [145]

2.2 Animals

Common names of animals used in this work are listed in the following table including the official names according to the standardized international nomenclature.

Table 2.2: Animals and respective breeders.

Mouse strain (general name)	Official name	Breeder
athymic nude mice (nu/nu)	NMRI-*Foxn1^{nu}*/*Foxn1^{nu}*	animal facility, University Hospital Essen
BL6	C57BL/6JOlaHsd	animal facility of the University Hospital Essen or Harlan Winkelmann GmbH (Borchen, Germany)
C3H	C3H/HeNHsd	see BL6

Table 2.2: continued

Mouse strain (general name)	Official name	Breeder
CatchUp	C57BL/6-*Ly6g*$^{tm2621(Cre\text{-}tdTomato)Arte}$	animal facility of the Centre for Medical Biotechnology of the University Duisburg Essen
CatchUp$^{IVM\text{-}red}$	C57BL/6-*Ly6g*$^{tm2621(Cre\text{-}tdTomato)Arte}$ x B6.Cg-*Gt(ROSA)-26Sor*$^{tm9(CAG\text{-}tdTomato)Hze}$/J	animal facility of the Centre for Medical Biotechnology of the University Duisburg Essen

2.3 Consumable supplies

Table 2.3: Consumables used in this work.

Consumable	Manufacturer
0.45 µm filters	Corning, New York USA
12 well cell culture multiwell plate	Greiner bio-one, Frickenhausen Germany
23 G needle	BD Biosciences, Heidelberg Germany
24 well Millicell Cell Culture Insert	Merck Millipore, Darmstadt Germany
96 well cell culture plate flat bottom	Greiner bio-one, Frickenhausen Germany
96 well cell culture plate round bottom	Greiner bio-one, Frickenhausen Germany
BD Falcon transwell 3 µm	BD Falcon, Heidelberg Germany
BD Microlance 3 25G (orange)	BD Biosciences, Heidelberg Germany
BD Microlance 3 27G (grey)	BD Biosciences, Heidelberg Germany
BD Microlance 3 23G (blue)	BD Biosciences, Heidelberg Germany
BD Microlance 3 20G (yellow)	BD Biosciences, Heidelberg Germany
BD Microtainer tubes SST with separation gel	BD Biosciences, Heidelberg, Germany
Biosphere® pipette tips 10 µL	Sarstedt, Nümbrecht Germany
Biosphere® pipette tips 100 µL	Sarstedt, Nümbrecht Germany
Biosphere® pipette tips 1000 µL	Sarstedt, Nümbrecht Germany
Biosphere® pipette tips 20 µL	Sarstedt, Nümbrecht Germany
Biosphere® pipette tips, 200 µL	Sarstedt, Nümbrecht Germany
Bottle top filter 500mL GW45	TPP, Trasadingen Switzerland
Casy Cups	Roche Innovatis, BIelefeld Germany
CellTrics 100 µmfilters	Partec, Münster Germany
CellTrics 50 µmfilters	Partec, Münster Germany
Centrifuge tubes, 40 mL	Nalgene, Rochester USA
Centrifuge tubes, 50 mL	Greiner bio-one, Frickenhausen Germany
Coding plates for CryoPure tubes green	Sarstedt, Nümbrecht Germany
Coding plates for CryoPure tubes yellow	Sarstedt, Nümbrecht Germany
Combitips® plus 10 mL	Eppendorf, Wesseling-Berzdorf Germany
Combitips® plus 5 mL	Eppendorf, Wesseling-Berzdorf Germany
Cover slips round 12 mm	Carl Roth, Karlsruhe Germany
Cover slip round 18 mm	Carl Roth, Karlsruhe Germany
Cryomold® Biopsy 10x10x5 mm	Sakura Finetek, Staufen Germany

Table 2.3: continued

Consumable	Manufacturer
Cryomold® Intermediate 15x15x5 mm	Sakura Finetek, Staufen Germany
CryoPure 2.0 mL tubes with external thread	Sarstedt, Nümbrecht Germany
FEATHER® microtome blades C35	pfm medical, Collone Germany
ImmEdge wax pen	Vector, Peterborough UK
Immuno Plates Maxisorp F96	Nunc / VWR, Darmstadt Germany
Immuno Plates Maxisorp F96	Nunc / VWR, Darmstadt Germany
LD Columns	Miltenyi, Bergisch Gladbach Germany
LightCycler Capillaries (20 µL)	Roche Applied Science, Wiesbaden Germany
LS Columns	Miltenyi, Bergisch Gladbach Germany
Health care Respirator FFP3 1873V	3M Medica, Neuss Germany
Microtiter plate, 96 Well, half area UV transparent	Corning / VWR International, Darmstadt Germany
Millex-GP Filter Unit	Merck Millipore, Darmstadt Germany
Multiply-µStrip pro 4 tubes chain with lid	Sarstedt, Nümbrecht Germany
Omnican® 100, 30 G needle	B.Braun, Melsungen Germany
Pipette tips, clear (300 µL)	Sarstedt, Nümbrecht Germany
PP sealing foil	Kisker-Biotech, Steinfurt Germany
PPS blood-collecting device, V-cannula blue, 1,5×43mm	MediPac, Rheinbreitbach Germany
PVDF Western Blotting Membranes	Roche Applied Science, Wiesbaden Germany
Reaction tubes 0.5 mL, PP	Sarstedt, Nümbrecht Germany
Reaction tubes 1.5 mL without cap	Sarstedt, Nümbrecht Germany
Reagent and centrifuge tubes 15 mL	Sarstedt, Nümbrecht Germany
Rotilabo®-blotting paper 1.5 mm	Carl Rot, Karlsruhe Germany
S-Monovette® 10 mL 9NC (Citrat)	Sarstedt, Nümbrecht Germany
SafeSeal tube 2 mL	Sarstedt, Nümbrecht Germany
Superfrost Plus glass slides	Carl Rot, Karlsruhe Germany
SuperFrost® microscope slides	Langenbrinck, Emmendingen Germany
Syringes (1 mL, 2 mL, 20 mL)	Becton Dickision, Heidelberg Germany
Tissue culture dishes	Sarstedt, Nümbrecht Germany
Tissue culture flask T175	Sarstedt, Nümbrecht Germany
Tissue culture flask T25	Sarstedt, Nümbrecht Germany
Tissue culture flask T75	Sarstedt, Nümbrecht Germany
Tissue culture plate 24 well	Sarstedt, Nümbrecht Germany
Tissue culture plate 6 well	Sarstedt, Nümbrecht Germany
Transfer pipette 3.5 mL, sterile	Sarstedt, Nümbrecht Germany

2.4 Equipment

This section refers to general laboratory equipment and specialized analytical machines.

Table 2.4: Equipment used in the laboratory.

Instrument	Manufacturer
6-place swinging rotor	Hettich Zentrifugen, Tuttlingen Germany
Analytical balance AE260	Mettler-Toledo, Giessen Germany
Avanti J-26XP	Beckman Coulter, Krefeld Germany
Autolave VX75	Systec, Linden Germany
BD FACSAria I	BD Biosciences, San Jose USA
BD FACSAria III	BD Biosciences, Heidelberg Germany
BD FACSCANTO II	BD Biosciences, Heidelberg Germany
Bechtop UV Transilluminator	UVP, Upland USA
BioDoc-It®M26X	UVP, Upland USA
Caliper 100 mm	Roeser Medical, Bochum Germany
Carrier for slide carrier	Hettich Zentrifugen, Tuttlingen Germany
Casy Cell Counter + Analyser System version TT	Roche Innovatis, Bielefeld Germany
ChemiDoc-It®Imager	UVP, Upland USA
Centrifuge Mikro 200R	Hettich Zentrifugen,Tuttlingen Germany
Centrifuge Universal 320	Hettich Zentrifugen, Tuttlingen Germany
Centrifuge Universal 420R	Hettich Zentrifugen, Tuttlingen Germany
CO_2Incubator HERAcell 240 und 240i	Thermo Scientific, Langenseldbold Germany
Cordless Animal Clipper VET Isis GT420	Aesculap Suhl GmbH, Suhl Germany
Cryomicrotome HM500	Techno-Med, Bielefeld Germany
Dewar - transport container	Carl Roth, Karlsruhe Germany
Ear punch device GE30 (mouse earmarks)	CHIRMED, Schöneck Germany
ELISA-Washer ELx50	Biotek, Bad Friedrichshall Germany
Eppendorf Research pipette 0.5-10 µL	Eppendorf, Wesseling-Berzdorf Germany
Eppendorf Research pipette 20-200 µL	Eppendorf, Wesseling-Berzdorf Germany
Glass anti-roll plate 39.5mm	Techno-Med, Bielefeld Germany
Heating block Neoblock 1	Neolab, Heidelberg Germany
Ice box 2.5 L	Carl Roth, Karlsruhe Germany
InLab Routine Pro pH electorde	Mettler-Toledo, Giessen Germany
Incubator & shaker TH30	Edmund Bühler, Hechingen Germany
Inverse microscope CK2-TR	Olympus, Hamburg Germany
LC Carousel Centrifuge	Roche Applied Science, Wiesbaden Germany
Leica TCS SP8 MP microscope	Leica, Mannheim Germany
Laminar flow hood MSC-Advance 1.8	Thermo scientific, Langenseldbold Germany
liquid nitrogen tank LD25	Taylor-Wharton, Husum Germany
LightCycler	Roche Applied Science, Wiesbaden Germany
Lock ring for cyto chamber	Hettich Zentrifugen, Tuttlingen Germany
MACSQuant®VYB	Miltenyi, Bergisch-Gladbach Germany
Variomag Powertherm (magnetic stirrer & heat plate)	HP Medizintechnik GmbH, Oberschleissheim Germany
Manual HPLC Syringes 20+30 µL	Hamilton, Reno USA

Table 2.4: continued

Instrument	Manufacturer
Microcentrifuge Sprout	Kisker-Biotech, Steinfurt Germany
Microloop ear curettes, Langenbeck	
Microscopy Scissors	Carl Roth, Karlsruhe Germany
Microsurgical forceps MK 17	CHIRMED, Schöneck Germany
Minishaker 3D	Kisker-Biotech, Steinfurt Germany
MiniVent Type 845	Hugo Sachs Elektronik, March Germany
Multipette stream	Eppendorf, Wesseling-Berzdorf Germany
MyCycler PCR maschine	BioRad, Munich Germany
MyCycler Thermogr. Upgrade	BioRad, Munich Germany
Neubauer counting chamber improved	Carl Roth, Karlsruhe Germany
One-funnel chambers	Hettich Zentrifugen, Tuttlingen Germany
Panasocis -86°CUltra deep freezer	EWALD Innovationstechnik, Bad Nenndorf Germany
Pipetman-Pipette P10	Gilson, Limburg-Offheim Germany
Pipetman-Pipette P100	Gilson, Limburg-Offheim Germany
Pipetman-Pipette P1000	Gilson, Limburg-Offheim Germany
Pipetman-Pipette P20	Gilson, Limburg-Offheim Germany
Pipetman-Pipette P200	Gilson, Limburg-Offheim Germany
Pipettus rechargeable battery	Hirschmann, Eberstadt Germany
PowerPac Basic	BioRad, Munich Germany
Precision analytical balance AZ612	sartorius, Göttingen Germany
QuadroMACS^{TM} Separator	Miltenyi, Bergisch Gladbach Germany
Scotsman AF80 ice flaker	Scotsman, Vernon Hills USA
Screw Top Bottles, clear 2000 mL	Carl Roth, Karlsruhe Germany
Screw Top Bottles, clear 250 mL	Carl Roth, Karlsruhe Germany
Screw Top Bottles, clear 500 mL	Carl Roth, Karlsruhe Germany
Section extensor for HM500	Techno-Med, Bielefeld Germany
Seven Easy ph-Meter	Mettler-Toledo, Giessen Germany
Slide carriers for one chamber	Hettich Zentrifugen, Tuttlingen Germany
Spacer Plates 1.0 mm	BioRad, Munich Germany
Staining boxes acc. to Schiefferdecker	Carl Roth, Karlsruhe Germany
Synergy 2 Multi-Mode Reader	BioTek, Bad Friedrichshall Germany
Trans-Blot SD Semi-dry	BioRad, Munich Germany
Univentor 400 Anaesthesia Unit	Uno, Zvenaar Netherlands
Vortex Mixer VTX-300L	Kisker-Biotech,Steinfurt Germany
Watherbath	GFL, Burgwedel Germany

2.5 Chemicals

Table 2.5: Chemicals and other substances.

Chemicals and reagents	Manufacturer
7AAD Staining Solution	BD Bioscience, Heidelberg Germany
Acetic acid	Merck Chemicals, Darmstadt Germany
Aceton pure	AppliChem, Darmstadt Germany

Table 2.5: continued

Chemical and reagents	Manufacturer
40 % Arylamide/Bis solution, 37.5:1	Bio-Rad, Munich Germany
AEC Solution	Invitrogen™ Life technologies, Karlsruhe Germany
Ammonium persulfate	Serva Electrophoresis, Heidelberg Germany
Aqua B. Braun	B.Braun, Melsungen Germany
BD Calibrite Beads	BD Bioscience, Heidelberg Germany
BD CST Beads	BD Bioscience, Heidelberg Germany
BD FACS Flow Sheat Fluid	BD Bioscience, Heidelberg Germany
BD FACSRinse Solution	BD Bioscience, Heidelberg Germany
BD Shutdown Solution	BD Bioscience, Heidelberg Germany
BD Matrigel™ (HC)	BD Bioscience, Heidelberg Germany
Cell Proliferation Dye eFluor450	eBioscience, Frankfurt Germany
CellTrace™ CFSE	Invitrogen™ Life technologies, Karlsruhe Germany
Citrate Buffer (pH 6.0), Concentrate,	Invitrogen™ Life technologies, Karlsruhe Germany
CryoSure DMSO	Wak Chemie Medical, Bettingen Germany
Dako REAL Peroxidase-Blocking Solution	Dako, Hamburg Germany
DAPI	BioLegend, Fell Germany
Dihydrorhodamine 123	Invitrogen™ Life technologies, Karlsruhe Germany
DynaBeads®CD3/CD28, mouse	Invitrogen™ Life technologies, Karlsruhe Germany
Eosin B	Carl Roth, Karlsruhe Germany
Ethanol 99,5 %, Ph.Eur., reinst	Carl Roth, Karlsruhe Germany
Fibronectin from bovine plasma	Sigma-Aldrich, Taufkirchen Germany
Fluoprep	BioMerieux, Nürtingen Germany
Forene 100% (Isoflurane)	AbbVie, Ludwigshafen Germany
Hydrochloric acid	Carl Roth, Kalsruhe Germany
Immersol 518F	Carl Zeiss Microscopy, Jena Germany
Kaisers glycerol gelatine	Merck Chemicals, Darmstadt Germany
Ketamine 10 %	Ceva Tiergesundheit., Düsseldorf Germany
May-Grünwalds Eosin-Methylenblue solution	Merck Chemicals, Darmstadt Germany
Methanol pure Ph. Eur.	Applichem, Darmstadt Germany
Paraformaldehyde	Merck Chemicals, Darmstadt Germany
PEI	Sigma-Aldrich, Taufkirchen Germany
PolyFin®, Paraffin Embedding Wax	olysciences, Eppelheim Germany
Poly(vinyl alcohol)	Sigma-Aldrich, Taufkirchen Germany
2-Propanol reinst Ph. Eur., USP	AppliChem, Darmstadt Germany
QTracker 655	Life Technologies, Darmstadt Germany
Roti®-Histokitt II	Carl Roth, Kalsruhe Germany
Roti®-Histol	Carl Roth, Kalsruhe Germany
Shandon Instant Hematoxylin	ThermoScientific, Bonn Germany
Sodium butyrate	Merck Chemicals, Darmstadt Germany
sodium citrate tribasic dihydrate	Sigma-Aldrich, Taufkirchen Germany
Sodium chloride	Carl Roth, Karlsruhe Germany
0.9 % Sodium chloride solution	Fresenius Kabi, Bad Homburg Germany
Spectra™ Multicolor Protein Ladder	ThermoScientific, Bonn Germany

Table 2.5: continued

Chemical and reagents	Manufacturer
TEMED	Bio-Rad, Munich Germany
Tissue Tek®Mounting Media	Sakura Finetek, Staufen Germany
Viability Dye eFluor450	eBioscience, Frankfurt Germany
Viability Dye eFluor780	eBioscience, Frankfurt Germany
Xylazine 2 %	Ceva Tiergesundheit, Düsseldorf Germany

2.6 Ready to use reaction systems

Table 2.6: Reaction systems and kits.

Description	Manufacturer
Annexin V:PE Apoptosis Detection Kit	BD Biosciences, Heidelberg Germany
Anti-Ly-6G MicroBead Kit, mouse	Miltenyi, Bergisch Gladbach Germany
APO-DIRECT™ Kit	BD Biosciences, Heidelberg Germany
BD Cytofix/Cytoperm	BD Bioscience, Heidelberg Germany
BD OptEIA™ Mouse IFN-γ ELISA Set	BD Biosciences, Heidelberg Germany
CD3ϵ MicroBead Kit, mouse	Miltenyi, Bergisch Gladbach Germany
CD45R (B220) MicroBeads, mouse	Miltenyi, Bergisch Gladbach Germany
CPD Star®	Roche Applied Science, Wiesbaden Germany
FITC BrdU Flow Kit	BD Biosciences, Heidelberg Germany
human MIF DuoSet®ELISA Kit	R&D Systems, Wiesbaden Germany
Maxima™ SYBR™ Green qPCR Master Mix	ThermoScientific, Bonn Germany
mouse G-CSF DuoSet®ELISA Kit	R&D Systems, Wiesbaden Germany
mouse IL-6 DuoSet®ELISA Kit	R&D Systems, Wiesbaden Germany
mouse KC DuoSet®ELISA Kit	R&D Systems, Wiesbaden Germany
RNeasy®Micro Kit	Quiagen, Hilden Germany
RNeasy®Mini Kit	Quiagen, Hilden Germany
SuperScript II RT	ThermoScientific, Bonn Germany
VenorGeM Mycoplasma Kit	Minerva BioLabs, Berlin Germany

2.7 Plasmids

The following plasmids were used to establish a green fluorescent HNC cell line for intravital microscopy. This work was performed in kind cooperation with the Institute for Transfusion Medicine at the University Hospital Essen. The system was established originally in the group of Prof. Dr. Helmut Hanenberg in Düsseldorf[112].

Table 2.7: Three plasmid system for viral particle production.

Plasmid name	Description
pCD/NL-BH	helping plasmid encoding for structural and regulatory genes
pE01	capsule plasmid encoding modified foamyviral capsule protein

Table 2.7: continued

Plasmid name	Description
pCL6IEGwo	lentiviral genome-integrating plasmid, replication incompetent, encoding eGFP under SSFV promoter

2.8 Recombinant proteins and chemical inhibitors

This section includes recombinant proteins and inhibitors and their respective final concentrations used in this manuscript.

Table 2.8: Proteins and inhibitors.

Reagent	Concentration	Manufacturer
G-CSF	100 ng / mL	Chugai Pharm, Frankfurt Germany
ISO-1	50 µM	Calbiochem, Darmstadt Germany
mIL-2	50 U / mL	Roche Applied Science, Wiesbaden Germany

2.9 Antibodies

The following antibodies have been used. The table further indicates final concentrations of antibodies or applied dilutions if stock concentrations were unknown. Antibodies were purchased from the following manufacturers: R&D Systems, Wiesbaden, Germany; BioLegend, Fell Germany; Acris Antibodies, Herford Germany; Abcam, Cambridge UK; Miltenyi, Bergisch Gladbach Germany; BD Biosciences, Heidelberg Germany; eBioscience, Frankfurt Germany; BioXCell, West Lebanon USA; NEB / Cell Signaling, Frankfurt Germany; Santa cruz Biotechnoligies, Heidelberg Germany; Biozol / Cederlane, Munich Germany; AbD Serotec, Düsseldorf Germany; Dianova, Hamburg Germany.

Table 2.9: Antibodies used in different applications.

Antigen	Isotype	Clone	Modification	Manufacturer	usage [µg/mL]
Flow Cytometry					
h/m-Arg1	sheep poly		APC	R&D Systems	0.50
h/m-CXCR7	mouse IgG2a	8F11-M16	APC	BioLegend	5
h/m-NOS2	rabbit IgG1	4E5	none	Acris Antibodies	23.75
m-CD11b	rat IgG2a	3A33	PE/Cy7	Abcam	2
m-CD3ϵ	hamster IgG1	145-2C11	FITC	Miltenyi	0.3
m-CD4	rat IgG2a	RM4-5	V450	BD Biosciences	4
m-CD45R(B220)	rat IgG2a	RA3-6B2	APC	Miltenyi	0.66
m-CD49b	rat IgM	DX5	FITC	Miltenyi	dil: 1:10

Table 2.9: continued

Antigen	Isotype	Clone	Modification	Manufacturer	usage [µg/mL]
m-CD49b	rat IgM	DX5	PE	Miltenyi	dil: 1:10
m-CD62L	rat IgG2a	Mel-14	FITC	eBioscience	5
m-CD8α	rat IgG2a	53-6.7	V500	BD Biosciences	4
m-CXCR2	rat IgG2a	242216	APC	R&D Systems	1
m-CXCR4	rat IgG2b	2B11	APC	BD Biosciences	20
m-Ly-6C	rat IgG2a	ER-MP20	PE	Acris Antibodies	2
m-Ly-6C	rat IgG2a	HK1.4	Alexa488	BioLegend	2.5
m-Ly-6G	rat IgG2a	1A8	PerCP/-Cy5.5	BioLegend	2
Depletion					
isotype	rat IgG2a	2A3	none	BioXCell	200 µg
isotype	rat IgG2b	LTF-2	none	BioXCell	100/200 µg
m-CD8	rat IgG2b	2.43	none	BioXCell	100 µg
m-Gr-1	rat IgG2b	RB6-8C5	none	BioXCell	200 µg
m-Ly-6G	rat IgG2a	1A8	none	BioXCell	200 µg
Immunoblot					
h/m-GAPDH	rabbit IgG	14C10	none	Cell Signaling	dil: 1:5000
h/m-MIF	rabbit	FL-115	none	Santa Cruz	0.4
Histology					
h/m-MIF	rabbit	FL-115	none	Santa Cruz	2
m-Asialo GM1	rabbit poly		none	Cedarlane	dil: 1:5000
m-CD11b	rat IgG2b	M1/70.15.1	none	BioSource	0.5
m-CD31	rat IgG2a	MEC13.3	none	Santa Cruz	0.013
m-CD4	rat IgG2a	RM4-5	none	BD Bioscience	1
m-CD8α	rat IgG2a	KT15	none	AbD Serotec	2
m-FoxP3	rat IgG2a	FJK-16s	none	eBioschience	2.5
m-Ly-6G	rat IgG2a	1A8	PerCP/-Cy5.5	BioLegend	0.5
m-MCL-1	rabbit	Y37	none	Abcam	14.27
Secondary Antibodies					
rabbit	donkey IgG (H+L)		Alexa488	Dianova	IF dil: 1:200
rabbit	goat IgG (H+L)		AP	Dianova	WB dil: 1:15000
rabbit	goat IgG (H+L)		Cy3	Dianova	IF dil: 1:400
rabbit	goat IgG (H+L)		HRPO	Dianova	IHC dil: 1:50
rabbit	goat IgG (H+L)		PE	Dianova	FC dil: 1:200
rat	donkey IgG (H+L)		Cy3	Dianova	IF dil: 1:400

Table 2.9: continued

Antigen	Isotype	Clone	Modification	Manufacturer	usage [µg/mL]
rat	goat IgG (H+L)		Alexa488	Invitrogen	IF dil: 1:200
rat	rabbit $F(ab)_2$		HRPO	Dianova	IHC dil: 1:50
Isotype Antibodies					
isotype	mouse IgG2a	G155-178	APC	BD Bioscience	stock 50
isotype	rabbit IgG		none	Santa Cruz	stock 400
isotype	rat IgG2a		FITC	BioLegend	stock 500
isotype	rat IgG2a	54447	APC	R&D Systems	stock 25
isotype	rat IgG2b	A95-1	APC	BD Bioscience	stock 200
isotype	sheep IgG		APC	R&D Systems	stock 10

2.10 Oligonucleotides

The following table lists the primers used for qRT-PCR. The temperature temp x refers to the annealing temperature in the PCR program which is depicted in table 3.6. All primers were specific to murine gene sequences. Oligonucleotidec, including Random Primer Hexamer for cDNA Synthesis, were purchased from Invitrogen^{TM} Life technologies (Karlsruhe, Germany).

Table 2.10: Oligonucleotides for application in qRT-PCR.

Target	Direction	Sequence	Temp x [°C]	Amplicon [bp]
b-actin	forward reverse	ACCAACTGGGACGACATGGAGAA GTGGTGGTGAAGCTGTAGCC	60	380
TNFa	forward reverse	TCGGGGTGATCGGTCCCCAA GGTGGTTTGCTACGACGTGGGC	65	141
CCL17	forward reverse	GGCCGAGAGTGCTGCCTGGA GCCCTGGACAGTCAGAAACACGA	59	120
VEGF-A	forward reverse	CTTGTTCAGAGCGGAGAAAGC ACATCTGCAAGTACGTTCGTT	55	125
CCL2	forward reverse	CGGCTGGAGCATCCACGTGTT TAGCAGCAGGTGAGTGGGGC	65	63
CCL5	forward reverse	CCTCACCATATGGCTCGGACACC GCGCGAGGGAGAGGTAGGCA	66	57
CCL3	forward reverse	TGTACCATGACACTCTGCAAC CAACGATGAATTGGCGTGGAA	59	109
ICAM1	forward reverse	ACCCACCCCGCAGGTCCAAT CAGCCGAGGACCATACAGCACG	55	148

Table 2.10: continued

Target	Direction	Sequence	Temp x [°C]	Amplicon [bp]
ARG-1	forward reverse	GACCACGGGGACCTGGCCTT ACTGCCAGACTGTGGTCTCCACC	55	170
iNOS	forward reverse	TGGCAACATCAGGTCGGCCAT CGGGCATCTGGTAGCCAGCG	65	110
IL-10	forward reverse	GCTGGACAACATACTGCTAACC CCCAAGTAACCCTTAAAGTCCTG	59	57
MMP9	forward reverse	GCTGACTACGATAAGGACGGCA TAGTGGTGCAGGCAGAGTAGGA	62	136
MHCIIH2I/Ab	forward reverse	GTGTGCAGACACAACTACGAGG CTGTCACTGAGCAGACCAGAGT	61	133
CCR2	forward reverse	GGGAGACAGCAGATCGAGTG CAACCCAACCGAGACCTCTT	60	71

2.11 Buffers, solutions and media

Table 2.11: Composition of Solutions and Media.

Liquid	Recipe and Manufacturer
Accutase®Cell Dissociation Reagent	Invitrogen™ Life technologies, Karlsruhe Germany
5× AP buffer	100 mM Tris (Carl Roth) 100 mM sodium chloride (Carl Roth) 5 mM magnesium chloride hexahydtrate (Carl Roth) pH 9.5
10× azidePBS	1.5 M sodium chloride (Carl Roth) 27 mM potassium chloride (AppliChem, Darmstadt Germany) 81 mM twice hydrated disodium phosphate (Carl Roth) 15 mM monopotassium phosphate (Carl Roth) 150 mM sodium azide (AppliChem) pH 7.4
Biocoll separating solution	(density 1.077 g / mL, isotone) Biochrom, Berlin Germany
Blocking Buffer R&D ELISA	1 % BSA (AppliChem) 0.2 M sucrose (AppliChem) 7.7 mM sodium azide (AppliChem) 1× PBS
CASYton	Roche Innovatis, Bielefeld Germany

Table 2.11: continued

Liquid	Recipe and Manufacturer
Cell culture medium I (tumor cell lines & primary immune cells)	RPMI 1640 (Invitrogen™ Life technologies) 10 % [v/v] heat-inactivated FCS (Biochrom) 100 IU / mL penicillin (Invitrogen™ Life technologies) 100 µg / mL streptomycin (Invitrogen™ Life technologies)
Cell culture medium II (MOPC cells)	DMEM with L-glutamine, glucose, Na-pyruvate (Invitrogen™ Life technologies) F-12 Nutrient Mixture (Ham, Invitrogen™ Life technologies) 10 % heat inactivated FCS (Biochrom) 100 IU / mL penicillin (Invitrogen™ Life technologies) 100 µg / mL streptomycin (Invitrogen™ Life technologies) 10 µg / mL EGF (Invitrogen™ Life technologies) 10 mg / mL insulin (Sigma-Aldrich) 25 µg/ mL transferrin (Sigma-Aldrich) 0.25 µg/ mL chorera toxin (Sigma-Aldrich) 25 µg/ mL hydrocortisone (Sigma-Aldrich) 0.2 µg/ mL tri-iodo-thyronine (Sigma-Aldrich)
Cell culture medium III (HMEC cells)	Microvasular endothelial growth medium (provito, Berlin Germany) 10 % heat inactivated FCS (Biochrom)
Cell culture medium IV (HEK293T cells)	DMEM (4.5 g / l Glucose, PAA) 10 % heat inactivated FCS (Biochrom) 100 IU / mL penicillin (Invitrogen™ Life technologies) 100 µg / mL streptomycin (Invitrogen™ Life technologies) 100 U / mL L-glutamine (Life Technologies)
Cryo medium I (cell lines)	30 % basal medium 60 % heat inactivated FCS (Biochrom) 10 % DMSO (Wak Chemie Medical)
Cryo Medium II (immune cells)	90 % heat inactivated FCS (Biochrom) 10 % DMSO (Wak Chemie Medical)
diluted Giemsa solution (always fresh)	30 % 100 mM disodium phosphate (Carl Roth) 60 % 100 mM monosodium phosphate (Merck Chemicals) 10 % Giemsa solution (Merck Chemicals)
EILSA Diluent Solution	eBioscience, Frankfurt Germany
IMEM	Lonza, Basel Switzerland
Immunoblot transfer buffer	25 mM Tris (Carl Roth) 192 mM glycine (AppliChem) 20 % [v/v] methanol (AppliChem)
Laemmli running buffer	247.1 mM Tris (Carl Roth) 1918.2 mM glycine (AppliChem) 34.7 mM SDS (Carl Roth)
MACS buffer	0.5 % BSA (AppliChem) 2 mM EDTA (Serva Electrophoresis) 1× PBS

Table 2.11: continued

Liquid	Recipe and Manufacturer
Mouse Serum	Dianova, Hamburg Germany
PBS cell culture grade 10× PBS	Life technologies, Darmstadt Germany 1.37 M sodium chloride (Carl Roth) 26.8 mM potassium chloride (AppliChem) 81 mM disodium phosphate (Carl Roth) 14.7 mM monopotassium phosphate (Carl Roth) pH 7.4
Percoll	GE Healthcare, Freiburg Germany
Reagent Diluent R&D ELISA	1× PBS 1 % BSA (AppliChem)
Red blood cell lysis solution	Miltenyi, Bergisch Gladbach Germany
SDS lysis buffer freshly add	25 mM Hepes (pH 7.3, PAN Biotech) 0.1 % [w/v] SDS (Carl Roth) 1 % [v/v] Triton X-100 (Sigma-Aldrich) 10 mM EDTA (Serva Electrophoresis) 10 mM sodium pyrophsphate (Carl Roth) 10 mM sodium fluoride (Carl Roth) 125 mM sodium chloride (Carl Roth) 10 % PhosphoSTOP (Roche Applied Science) 1 % Protease inhibitor cocktail I (Calbiochem / Merck Millipore) 1 % Protease inhibitor cocktail III (Calbiochem / Merck Millipore)
5× SDS sample buffer	180 mM Tris/HCl pH 6.8 (Carl Roth) 2.88 % [w/v] SDS (Carl Roth) 20 % [v/v] glycerol (AppliChem) 8 % [v/v] 2-mercaptoethanol (Merck Chemicals) 0.2 % [w/v] bromophenol sodium salt (Serva Electrophoresis)
Sodium Carbonate Buffer (mIFNγ ELISA)	0.1 M sodium carbonate pH 9.5
Staining Buffer (intracellular)	azide PBS 1 % heat inactivated FCS (Biochrom)
10× TBS	20 mM Tris (Carl Roth) 1.5 M sodium chloride (Carl Roth) pH 7.2 - 7.4
TBS-T	1× TBS 0.1 % Tween-20 (AppliChem)
TMB solution	0.48 % [w/v] TMB (Sigma-Aldrich) 10 % [v/v] acetone (AppliChem) 90 % [v/v] ethanol (Carl Roth) 0.6 % [v/v] hydrogen peroxide (Merck Chemicals)
TMB Substrate Buffer	32.8 mM citric acid (Merck Chemicals) 0.02 % [v/v] Kathon (Christ Chemie AG, Reinach Germany) pH 4.1

Table 2.11: continued

Liquid	Recipe and Manufacturer
Trypsin, 0.25% with EDTA 4Na	Invitrogen^{TM} Life technologies, Karlsruhe Germany
Wash Buffer (ELISA) (ELISA)	1× PBS 0.05 % [v/v] Tween-20 (AppliChem) 0.05 % [v/v] Tween-20 (AppliChem)

2.12 Software

Table 2.12: Software.

Sofware	Producer
AxioVision	Carl Zeiss, Jena Germany
BD FACSDiva	BD Biosciences, Heidelberg Germany
Gen 5	BioTek, Bad Friedrichshall Germany
GIMP 2.6.7	The GIMP Development Team, http://gimp.org
GraphPad Prism V 4.00	GraphPad Software, Inc., La Jolla USA
ImageJ V1.48v	Wayne Rasband, National Institutes of Health, Bethesda USA
IMARIS	Bitplane, Zurich Switzerland
LAS X	Leica Microsystems, Mannheim Germany
LightCycler 3	Roche Applied Science, Wiesbaden Germany
MACS Quantify	Miltenyi, Bergisch Gladbach Germany
MikTex 2.9	Christian Schenk, Berlin Germany
ModFit LT	Verity Software House, Topsham USA
MS Office 2007 / 2010	Microsoft, Remond USA
Photoshop CS5	Adobe Systems, Munich Germany
R	The R foundation, Vienna Austria
VisionWorksLS	UVP, Upland USA

3 Methods

3.1 Cell biology

3.1.1 General cell culture techniques

Adherent tumor and endothelial cell lines were cultivated in 25 – 175 cm^2 cell culture flasks at 37°C with 5 % CO2 supply in their respective media which are listed in table 2.11. For passaging, cells were washed with 1×PBS and dislodged with trypsine/EDTA at 80 % confluence twice-weekly. After stopping the reaction with FCS, cells were collected, centrifuged (300 g, 7 minutes, 4°C) and resuspended in equal amounts of culture medium. Cell counting was performed in a Casy cell counter in cell line specific programs via electric conductivity. Cells were seeded according to their growth rate in their respective cell culture media. Presence of mycoplasma was constantly excluded by a PCR Kit used with supernatant from confluent cultures (VenorGeM, Minerva BioLabs). For experiments, cells were dislodged using the more gentle enzyme Accutase® after washing with PBS, counted as described above and seeded according to the respective protocol.

Cryoconservation

For cryoconservation approximately $5 \cdot 10^6$ cells were pelleted by centrifugation (300 g, 7 minutes, 4°C) and resuspended in 1 mL cryo medium (medium I was used for cell lines while medium II was more convenient for primary immune cells, see table 2.11). Cells were immediately put into an isopropyl alcohol-containing cryo box for enabling a constant cooling rate of 1°C per minute to -80°C. Long-term storage was performed in liquid nitrogen tanks. After cryoconservation, the cells were re-transferred to active culture by thawing and washing with the respective medium to immediately remove DMSO. The cells were then cultivated as described above.

Generation of cell line supernatants

To generate standardized supernatants (SN) from tumor cell lines, cells were dislodged with Accutase and seeded at a density of $2 \cdot 10^6$ cells / mL of the respective culture medium. After 24 hours, SN were collected and centrifuged to remove cell debris and dead cells. Cell free SN were frozen at -20°C until analysis.

3.1.2 Establishment of a green fluorescent cell line via lentiviral transduction

S2 work was carried out in kind cooperation in the Institute for Transfusion Medicine at the University Medical Center in Essen. The system was established originally in the group of Prof. Dr. Helmut Hanenberg in Düsseldorf[112] and contains a plasmid encoding for the target protein (plasmid vector) as well as a helping plasmid and a capsule plasmid (see also table 2.7). The helping plasmid encodes the structural proteins gag and pol as well as the regulatory proteins vif, vpr, vpu, rev and tat under the control of the CMV promoter. The third plasmid encodes for CMV promoter driven expression of a modified foamyviral capsule protein, which is ensuring a broad host and tissue tropism. During particle formation, the plasmid vector is transported into the viral particles and later transferred into the transduced cells. It is further capable of integrating into the target cell genome by long terminal repeats (LTR) and therefore resulting in stably transduced cells. Viral particles are replication incompetent by a deletion in the U3 region of the 3'-LTR of the viral expression cassette. HEK293T cells

enable for the replication of episomal plasmids, which carry a Simian Virus 40 (SV40) origin of replication, by expression of the SV40 large-tumor antigen [35] and were therefore used for viral particle production.

Generation and purification of viral particles

Viral particles were produced in HEK293T cells using the plasmids listed in table 2.7 in a 175 cm^2 flask. For transfection of the cells, plasmids (0.5 µg / mL pE01, and 3.75 µg / mL NL-BH and pCL6) were packed in positively charged particles by mixing rigorously with 22.5 µg / mL Polyethylenimine (PEI) in DMEM and incubation for 30 minutes at room temperature in the dark. 70 - 90 % confluent cells were supplied with 6 mL PEI-DNA particles and 12 mL DMEM 15 % FCS, 1.5 % penicillin, streptomycin and L-glutamine (PSG) and incubated over night. Particles were taken up by endocytosis during this time [12]. To induce CMV promoter activity, new medium was supplemented with 10 mM sodium butyrate and incubated for 6 - 8 hours. This way, viral titers could be boosted to up to 1200 % [158, 112]. For collecting viral particles, cells were supplied with new medium (culture medium IV) and virus was produced for 18 - 22 hours before purification. To harvest viral particles, culture medium was filtered through 0.45 µm pores into a centrifuge tube that is leak proof for aerosols (40 mL, Nalgene). Viral particles were sedimented at 25000g for 90 minutes at 4°C and resuspended in HEPES buffered IMDM medium with 20 % FCS. Purified viral particles were stored at -80°C until used.

Stable transduction of target cells

For transduction, target cells ($MOPC^-$) were seeded in 6 well plates in varying densities and were left to adhere. Viral particles were added in different dilutions for 24 hours. Cells were washed carefully and observed for stress symptoms by light microscopy. Transduction efficiency was checked by fluorescence microscopy and cells with least stress symptoms and highest transduction efficiency were chosen for further expansion. Expanded mixed cell populations were sorted for eGFP expression using a BD FACSAria I flow cytometer. The resulting cell line contained >98 % $eGFP^+$ cells among living cells and is referred to by the name $MOPC^{-eGFP}$. No differences in growth behavior by MTT assay *in vitro* as well as *in vivo* and morphology have been observed between the modified cells and the parental cell line $MOPC^-$.

3.1.3 Primary cell isolation

Isolation of human neutrophils

Human neutrophils were isolated via density gradient centrifugation. Due to their specific density they colocalize with erythrocytes in a gradient with a 1.077 g / mL polysucrose solution and can be separated from mononuclear cells by this approach. Working fast and at constant room temperature allows isolation of viable, resting neutrophils.

Venous blood was taken in collection tubes containing 3.2 % trisodium citrate solution (S-Monovette®). After 1:1 dilution with PBS, blood was carefully loaded on the cell separation solution and subjected to the gradient centrifugation at 300 g for 30 minutes with minimal acceleration and without break. Mononuclear cells were removed and the pellet containing neutrophils and erythrocytes was collected. Next, erythrocytes were sedimented by applying the same volume 1 % PVA for 20 minutes. The neutrophil containing upper phase was collected and pelleted by centrifugation for 5 min-

utes at 300 g. Remaining erythrocytes were removed by hypotonic lysis in 0.2 % NaCl for 50 seconds with subsequent readjustment of osmolarity. Cells were maintained in cell culture medium I and applied to experiments after a 30 minutes resting phase.

Murine immune cell isolation from different tissues

All cell types were cultivated in cell culture medium I.

For the isolation of peripheral blood leukocytes, the mouse was sacrificed by an overdose of inhalation anesthesia (isoflurane). The peritoneum was opened directly and blood was taken from the aorta using a 25 gauge (G) needle and a 1 mL syringe. Blood was transferred into a tube containing 20 % [v/v] 3.8 % sodium citrate and mixed gently to prevent clotting. Blood cells were either stained directly (see whole blood staining in section 3.1.8) or after removal of erythrocytes by hypotonic lysis using distilled water for 10 seconds followed be readjustment of osmolarity with 2× PBS. After lysis, cells were washed and applied to further analysis.

Splenocytes were isolated by a mechanical procedure. To this end, the spleen was perforated and rinsed with PBS using a 23 G needle. Remaining leukocytes were dissociated from the soft tissue by mechanical pressure using the plugger of a 20 mL syringe. A single cell solution was obtained by separation of cell clumps using a 23 G needle. Erythrocytes were lysed as described above after centrifugation of the cell suspension. Resulting clumps, which were derived from soft tissue components, were removed by filtration through 50 µm cell strainers. Cells were counted as described above and applied to further analysis.

Bone marrow cells were isolated from the femur. Skin and surrounding muscles were removed and the bone was sterilized in 70 % ethanol prior to opening. Opened bones were rinsed with PBS using a 23 G needle until the bone turned white. A single cell solution was obtained by separation of cell clumps using a 23 G needle. Erythrocytes were lysed as described above after centrifugation of the cell suspension. Resulting clumps were removed using 50 µm cell strainers. Cells were counted as described above and applied to further analysis.

Lymph nodes were isolated from close proximity to the tumor localization (draining lymph node). Lymph nodes were cut into pieces and further minced with the plugger of a 20 mL syringe. The suspension was directly filtered using a 50 µm cell strainer and counted as described above.

Leukocytes from the liver were isolated after gentle dissection of the organ. Liver pieces were meshed using the plugger of a 20 mL syringe and filtered through a 50 µm cell strainer. The cell suspension was centrifuged at 460 g for 10 minutes and the cell pellet was applied to a Percoll gradient to purify leukocytes from dead hepatocytes. To this end, cells were resuspended in PBS 5 % FCS and mixed with isotonic 90 % Percoll solution to a final concentration of 32.5 % Percoll. Gradient centrifugation was carried out at 850 g for 25 minutes without break. By this procedure, the hepatocytes remain in the Percoll solution while the leukocytes sediment to the pellet which was gently washed with PBS 5 % FCS afterwards. Erythrocytes were lysed as described above followed by another filtration using a 50 µm cell strainer. Tumor infiltrating cells were isolated by mechanical dissociation of the tissue using the plugger of a 20 mL syringe. Erythrocytes were lysed as described above after centrifugation of the cell suspension. Resulting clumps were removed using 50 µm cell strainers.

3.1.4 Cell enrichment and purification by magnetic cell separation

Magnetic cell separation or magnetic activated cell sorting (MACS) is based on the characteristic expression of cell surface proteins on different types of immune cells. Specific antibodies were used to detect these proteins and coupled to magnetic beads either directly or indirectly by biotin. Sorting was performed using appropriate MACS columns placed in a MACS Separator, which is a strong permanent magnet. Thereby, the MACS Column provides a magnetic field which retains labeled cells. Columns were equilibrated by addition of 2 - 3 mL MACS buffer and after binding of the cells they were washed three times with the same amount of MACS buffer if not indicated differentially. Elution was achieved by removing the column from the magnet and rinsing the column with MACS buffer.

Depletion of $B220^+$ cells from splenocytes

To enhance enrichment of other cell types, B cells were first removed from isolated splenocytes. To this end, CD45R (B220) Micro Beads (Miltenyi) were used according to manufacturer's instructions. Isolated splenocytes were directly labeled using B220 specific micro bead coupled antibody (clone RA3-6B2, 10 µL / 10^7 cells) for 15 minutes at 4°C. After washing, cells were resuspended in MACS buffer and applied to a LD column as describes above. The cells which passed the column were collected and further processed as the $B220^-$ splenocytes.

T cell enrichment

$B220^-$ splenocytes were used for T cell isolation by using the CD3ϵ MicroBead Kit according to the manufacturer's protocol. In brief, up to 10^7 cells were labeled using 10 µL biotin coupled hamster-anti-mouse CD3ϵ for 10 minutes. After washing with MACS buffer, 20 µL anti-biotin micro beads were added for the same amount of cells and incubated for 15 minutes. Separation in a LS column was performed as described above after washing the cells again. The retained T cell-enriched population was eluted and subjected to proliferation experiments as described below.

Isolation of Ly-$6G^+$ neutrophils

For the isolation of murine neutrophils from isolated BL6 splenocytes, B220 depletion was performed as described above. Additionally, the Ly-6G MicroBead Kit was applied according to manufacturer's instructions. Cells were labeled using biotin coupled rat-anti-mouse Ly-6G antibody (50 µL / 10^8 cells) for 10 minutes. Anti-biotin micro beads were directly added (100 µL for the same amount of cells) and incubated for another 15 minutes. Washed cells were applied to a LS column and washed 5 times before purified cells were eluted from the column. Ly-$6G^+$ cells were used for direct analysis or cultured over night in cell culture medium I to assess survival.

3.1.5 Fluorescence-activated cell sorting

Fluorescence-activated cell sorting (FACS) is a method for isolating cell subsets based on cell surface expression of antigens by flow cytometry. For this isolation, the cells are detected as described in section 3.1.8 and after detection the stream is broken into individual droplets containing one cell each. At this step, an electrical charge is put on the droplet based on the measured properties and the adjustments by the experimentator. When passing the electrostatic deflection system, charged droplets are adjusted to get collected in different tubes. For the isolation of different immune cells, a

BD FACS Aria III was used, which was provided by the Imaging Center Essen (IMCES) in the Institute for Experimental Immunology and Imaging at the University Hospital Essen.

Isolation of tdTomato$^+$ neutrophils

For the isolation of neutrophils from CatchUp mice, tdTomato expression was used. Expression of the fluorescent protein is regulated as described in section 3.2.1 in these mice and is restricted to neutrophils. Therefore, additional labeling was not necessary leaving the cells as untouched and inactive as possible. Cells from different organs were prepared as described in section 3.1.3. Cell suspensions isolated from tumor tissue were further stained for dead cells using viability dye eFluor780 in PBS for 20 minutes. Cell sorting was carried out in cell culture medium I using the gating shown in figure A.1. The resulting neutrophil population was >98 % pure and was directly applied to cytospins, RNA isolation or T cell suppression assays.

T cell isolation

Splenocytes were labeled using anti-CD3ϵ-FITC antibody to isolate T cells from CatchUp mice. Labeling was carried out as described in section 3.1.8 using freshly filtered solutions. Cell sorting was carried out in cell culture medium I using the gating shown in figure A.2. T cells were of >99 % purity and subsequently used for T cell proliferation assays.

3.1.6 T cell proliferation

Polyclonal activation was used to assess proliferative capacities of T cells as well as suppressive properties of neutrophils. Cells were purified as described above and labeled using either Carboxyfluorescein succinimidyl ester (CFSE) or Cell Proliferation Dye eFluor450. For CFSE labeling, cells were pre-warmed at a maximum concentration of $1 \cdot 10^7$ / mL in RPMI, supplied with 5 µM CFSE for 15 minutes and the uptake was stopped by the addition of the same volume FCS. To label cells with eFluor450, $1 \cdot 10^7$ cells / mL were stained with 10 µM of the dye for 20 minutes at room temperature and stopped with 4-5× culture medium I for 5 minutes on ice. After washing both T cells could be supplied to the proliferation assay. The assay was carried out in 96 well round bottom plates in cell culture medium I supplemented with additional 50 U / mL mIL2 to maintain T cell survival. Proliferation was induced using CD3 and CD28 antibodies coupled to beads (DynaBeads) in a 1:1 T cell to bead ratio for 3 days. For the suppression of T cell proliferation, purified Ly-6G$^+$ cells were added in different Ly-6G : T cell ratios.

3.1.7 Transendothelial migration assay

The migration of neutrophils through an endothelium was to be mimicked by this assay. To this end, a 3 µm cell culture insert transwell system was equipped with an endothel cell monolayer prior to performing the migration assay.

Three µm cell culture inserts for 24 well plates were coated with 50 µg / mL fibronectin in PBS for 30 minutes and washed twice with PBS afterwards. Endothelial cells (human microvascular endothelial cells, HMEC) were added at $1 \cdot 10^5$ cells per insert and grown surrounded by cell culture medium III at 37°C and 5 % CO_2 to form a monolayer. Confluence of endothelial cells was assessed by hematoxylin and eosin staining and microscopic observation as follows. The staining procedure was performed

using the intact transwell, which was additionally coated and not to be used in the assay. Cells were fixed in methanol, stained with Shandon Instant Hematoxylin and directly transferred into acidified 0.1 % Eosin solution for 30 seconds each. After rinsing with desalted water, the transwell membrane was excised using sharp forceps, placed on a glass slide and mounted with Kaiser's glycerol gelatine. Confluence was usually achieved after a period of two days.
For performing the transendothelial migration assay, the cell culture insert was placed into a new well of a 24 well culture plate containing either cell culture medium as a control or tumor supernatants delivering chemotactic signals. Pretreatment of SN with 50 µM of the MIF inhibitor ISO-1 (4,5-Dihydro-3-(4-hydroxyphenyl)-5-isoxazoleacetic acid methyl ester inhibiting MIF tautomerase activity) was performed for 30 minutes prior to the experiment at 37°C. $5 \cdot 10^5$ isolated neutrophils were seeded on to the endothelial monolayer and were allowed to migrate for 4 hours at 37°C and 5 % CO_2. Additionally, the same amount of neutrophils was seeded and incubated in a well without insert and served as maximum migration control.
After the migration period, cell culture inserts were removed, migrated cell suspensions were mixed in the well and migrated cell numbers were determined using the Casy cell counter. Percentages of migrated cells refer to the cell numbers counted in the maximum migration control.

3.1.8 Flow cytometry

Flow cytometry can be utilized to detect, measure and analyze physical and chemical characteristics of cells or other particles. An advanced application of flow cytometry is fluorescence activated cell sorting (FACS) as described in section 3.1.5. In general, the cells enter a fluid stream in which they are led through a laser beam. Detectors are located in line with the laser beam (forward scatter, FSC) and vertical (side scatter, SSC). FSC represents information on cell size and volume whereas SSC measures refraction of light by the cells representing granularity and inner complexity. Fluorescence mediated by transgenic expression of fluorescent proteins or fluorescently coupled antibodies can be measured by special filters and detectors depending on the instrument settings. Measurements were carried out on a BD FACSCanto II machine with 3 fixed-wavelength lasers (488, 633 and 405 nm) providing detection on 8 photomultiplier tubes (PMT).

Cell surface staining

Staining of cell surface epitopes was generally carried out using fluorochrome coupled antibodies in a 96 well round bottom plate. Cells were washed with PBS prior to staining. Primary antibodies were diluted in PBS 3 % mouse serum and 10 % FCS, which was supposed to block unspecific binding, and incubated with the cells for 20 minutes at 4°C. Next, cells were washed with PBS and dead cells were stained using viability dyes diluted in PBS. After another wash, cells were resuspended in azide PBS and directly analyzed in the flow cytometer. Gating always included doublet exclusion and 100 % cells was set to living cells with a characteristic FSC SSC appearance of leukocytes. Antibodies used for flow cytometry and applied concentrations are listed in table 2.9.

Whole blood staining

Citrate mixed blood was transferred to a new 1.5 mL reaction tube. Antibodies were added in the titrated dilutions that were also used for normal surface staining (see table 2.9) and incubated at

4°C for 20 minutes. Erythrocytes were lysed directly after staining. For small amounts of blood (up to 10 µL from tail vein blood), lysis was performed using distilled water as described in section 3.1.3. In all other cases, 1× Red blood cell lysis solution (Miltenyi) was applied for 5 minutes (blood:buffer ratio 1:10). After lysis, cells were sedimented at 460 g for 5 minutes, resuspended in azide PBS and analyzed in the flow cytometer. Unstained cells were recorded for the correct adjustment of population gates.

Intracellular staining

Many molecules are located inside of cells and cannot be detected on the surface. To stain intracellular molecules, cells had to be permeabilized to gain access to those epitopes. Cell surface molecules were stained prior to permeabilization if a combination of both was stained. Cells were washed with PBS and permeabilization was performed using BD Cytofix / Cytoperm, which is based on PFA, for 20 minutes at 4°C. Cells were washed, resuspended in antibody containing Perm Wash Buffer and incubated for 30 minutes at 4°C. If secondary antibody staining was necessary, it was carried out the same way. For measurement, which was performed immediately, cells were resuspended in Staining Buffer.

BrdU staining

For the detection of integrated BrdU, an extended intracellular staining protocol was used according to the instructions of the BrdU FITC Flow Kit (BD). Surface staining was performed in advance and permeabilization was carried out as described above. Permeabilization was stabilized using Cytoperm Plus Buffer for 10 minutes. After washing, cells were refixated with Cytofix / Cytoperm for 5 minutes and washed again. A DNase digestion was performed at a concentration of 300 µg / mL for 1 hour at 37°C to release the incorporated BrdU. After washing with Perm Wash Buffer, BrdU was stained using a FITC coupled specific antibody in Perm Wash Buffer for 20 minutes at room temperature. After staining, cells were directly measured in the flow cytometer in Staining Buffer.

Proliferation of T cells

Proliferation experiments were set up as described in section 3.1.6 using CFSE or Cell Proliferation Dye eFluor450-labeled cells. Upon cell division, the fluorochrome content of the parental cell is equally distributed to the daughter cells resulting in a reduction of emitted fluorescence intensity by 50 %. Therefore, proliferation was easily assessable by flow cytometry. Additionally, CFSE-labeled T cell-enriched cultures were stained with α-CD4-V450 and α-CD8-V500 to identify T cells while eFluor450-labeled pure T cell suppression assays were stained with α-Ly-6G-PerCP/Cy5.5 to exclude surviving neutrophils prior to measurement as described above. Analysis was carried out using ModFit software as demonstrated in figure 3.1. The analysis considers the proportion of the mother population as well as the number of generations produced and results in the proliferation index ($\text{proliferation}_{\text{index}}$). For calculation of suppressive capacity, the following equation was used with the relative modification being either suppression or additional induction of proliferation.

$$\text{no proliferation: } proliferation_{index} = 1 \tag{1}$$

$$induced_{index} = proliferation_{index} - 1 \tag{2}$$

$$modification[\%] = 100 \cdot \frac{induced_{index}(modified)}{induced_{index}(normal)} \tag{3}$$

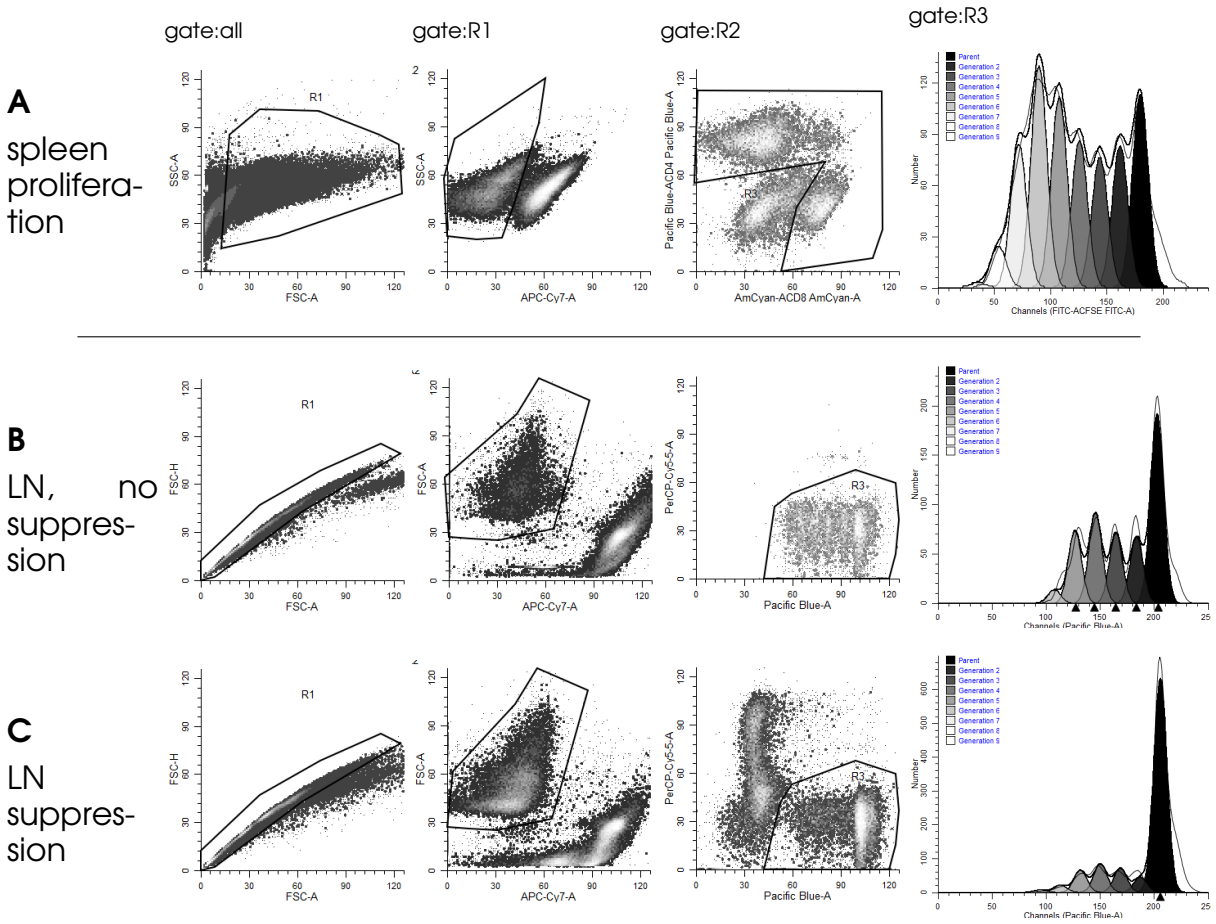

Figure 3.1: Analysis of proliferation assays. Representative plots from ModFit mediated proliferation analysis are shown. (A) Assay was performed with T cell enriched splenocytes. Proliferation of CD4 and CD8 positive living cells was analyzed (gate R3). (B+C) Suppression assay was carried out with labeled lymph node (LN) cells. Gate R3 was set to Proliferation dye positive cells which are negative for Ly-6G. One example for maximum proliferation (B) and suppression by a 1:1 bone marrow Ly-6G+ cell : LN T cell ratio (C) is given.

Detection of apoptosis

For the determination of apoptosis, cells were stained for the presence of phosphatidylserine on the cell surface by AnnexinV membrane binding, which resembles an early apoptotic phase, and for 7AAD incorporation which is taking place upon membrane dysfunction by dead, necrotic and late apoptotic cells. Treated cells were washed with PBS and resuspended in 1× Annexin binding buffer (provided by the AnnexinV:PE Kit, BD) containing AnnexinV-PE and 7AAD in a 1:100 dilution each. Staining was carried out for 15 minutes at 4°C and was followed by addition of Annexin binding buffer and direct analysis in the flow cytometer. Surviving cells were identified by being AnnexinV and 7AAD double negative. To ensure the correct adjustment of gates, unstained cells were measured as a control.

Reactive oxygen species

Reactive oxygen species (ROS) can be detected using Dihydrorhodamine 123. The chemical penetrates into the cells and is oxidized by ROS to rhodamine which is not able to leave the cell again but can be detected by its fluorescence ($\lambda_{ex}/\lambda_{em}$ 508/529 nm). Cells were isolated and rested for 60 min-

utes in culture medium at 37°C 5 % CO_2. Dihydrorhodamine 123 was added to a final concentration of 2.5 µg / mL and incorporated for 15 minutes under culture conditions. The reaction was stopped by incubation of ice for 15 minutes and samples were directly measured in the flow cytometer without washing.

Data analysis

FACSDiva 8 Software was used for the analysis of flow cytometry data except for the analysis of td-Tomato expression, which was assessed using MACSQuantify software because data was acquired at a MACSQuant machine. The term 'all cells' or 'all leukocytes' always refers to singlet, living cells with characteristic leukocyte forward and side scatter properties as depicted in figure 3.2[2]. Further gating for distinct cell populations was carried out with the help of unstained control cells. Expression of cell surface receptors and intracellular mediators was assessed via median fluorescence intensities (MFI) with the help of fluorescence minor one (FMO) controls using isotype antibodies in the same concentrations as specific antibodies for the respective molecule and were calculated as described below.

$$\Delta Median = MFI_{specific} - MFI_{FMO} \tag{4}$$

3.1.9 Enzyme linked immunosorbent assay

Serum preparation

For the analysis of serum cytokine content, mice were euthanized and blood was taken as described in section 3.1.3. Instead of using sodium citrate, blood was collected in tubes with separation gel. Tubes were placed to an upright position for 30 minutes to leave blood to coagulate. Cellular components and serum were separated by centrifugation at 6000 g for 10 minutes. The separation gel localizes between serum and cellular components in this procedure providing a physical barrier. Serum was frozen in these tubes at -80°C until analyzed.

Cytokine determination by ELISA

This assay for the antibody mediated detection of proteins in solutions such as culture supernatants and sera is performed by enzyme linked immunosorbent assay (ELISA). A sandwich-like approach was applied here using either Duo Set Kits from R&D or BD OptEIA Set Kits according to manufacturer's instructions. Antibody concentrations as well as highest standard concentrations are listed in table 3.1. Nunc Maxisorb plates were coated with the provided capture antibody in PBS[3] over night at 4°C. Next, antibody solution was removed and unspecific binding was blocked using Blocking Buffer (R&D) or Assay Diluent (BD) for 1 hour at room temperature. Plates were also stored at this step for later usage at 4°C. After washing, 50 µL of each sample was applied to the plate in triplicates. Dilution was performed in advance in Reagent Diluent (R&D) / Assay Diluent (BD) if necessary. A standard dilution in 7 steps and a blank sample without protein were run on each plate in triplicates to enable

[2] Noteably, all cells were acquired using the same voltages for SSC and FSC photomultiplier tubes
[3] For mIFNγ, coating was performed in sodium carbonate buffer. Please refer to table 2.11 for buffer composition.

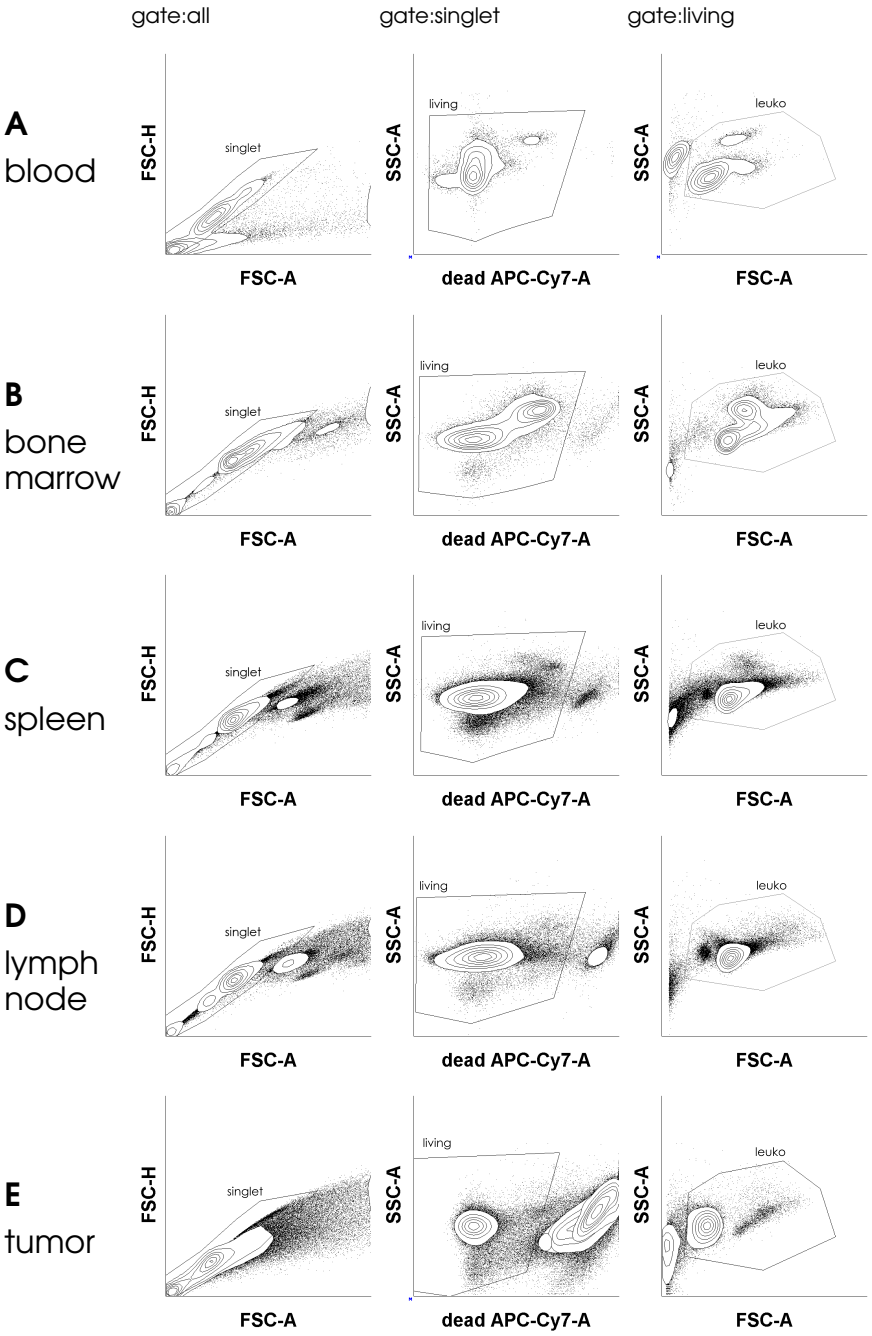

Figure 3.2: General gating strategy for analysis of flow cytometry. Cells were isolated from different mouse tissues and applied to flow cytometry. Voltages on photomultiplier tubes were the same for all cell types. Shown are representative contour plots of the respective analysis. Further analysis will refer to the leukocyte gate (leuko) as 'all leukocytes' or 'all cells'. This gate refers to the usual leukocyte SSC and FSC properties but does not necessarily contain leukocytes only.

quantification. Serum samples were run in duplicates. Binding by capture antibody occurred during a time interval of 2 hours at room temperature or over night at 4°C. The plate was washed using Washing Buffer to remove unbound protein and detection antibodies were used to verify binding of the protein of interest. For BD ELISA, biotinylated detection antibodies were combined with horse radish peroxidase (HRP) coupled streptavidin and incubated in Assay Diluent for 1 hour before proceeding with the detection step. For R&D Kits, biotinylated detection antibody was incubated for 2 hours prior to washing and separate incubation with HRP coupled streptavidin was carried out for 45 minutes. Detection was performed using the HRP catalyzed oxidation of 3,3',5,5'Tetramethylbenzidine (TMB) to TMB diimine, which is of blue color. After washing the plates, TMB substrate buffer and TMB solution were freshly mixed in a ratio of 20 : 1 and color reaction was taking place. The reaction was immediately stopped after 20 minutes by addition of half as much 2N sulfuric acid turning TMB yellow, which was directly measured in a Synergy II plate reader at 450 nm using Gen5 software. Concentrations were calculated according to the standard curve that derived from the standard dilutions.

Table 3.1: Concentrations of antibodies and standards used in the ELISA technique.

Analyte	Capture AB	Detection AB	Sensitivity	Manufacturer
hMIF	5.6 µL / mL	5.6 µL / mL	15.6 – 1000 pg / mL	R&D
mKC	5.6 µL / mL	5.6 µL / mL	31.25 – 2000 pg / mL	R&D
mG-CSF	5.6 µL / mL	5.6 µL / mL	15.6 – 1000 pg / mL	R&D
mIL6	5.6 µL / mL	5.6 µL / mL	15.6 – 1000 pg / mL	R&D
mIFNγ	5.6 µL / mL	5.6 µL / mL	15.6 – 1000 pg / mL	BD

3.2 Animal experiments

3.2.1 Animals

All animal experiments have been performed in accordance with the animal ethics committee of the state of North Rhine-Westphalia and the University of Duisburg-Essen and were carried out according to the German guidelines for experimental animal welfare. Mice were housed under standard specific pathogen free (SPF) conditions in individually ventilated cage (IVC) racks with a 12-hours circadian rhythm. Six- to eight-week old BL6, C3H and athymic nude nu/nu mice were used in the experiments. CatchUp$^{\text{IVM-red}}$ were generated by crossing CatchUp with B6.Cg-*Gt(ROSA)26Sor*$^{tm9(CAG\text{-}tdTomato)Hze}$/J mice as previously described[75] in kind cooperation with the group of Prof. Matthias Gunzer at the ZMB in Essen. CatchUp mice carry a transgene which induces the expression of the fluorescence protein tdTomato under the control of the Ly-6G promoter. tdTomato expression is enhanced in the CatchUp$^{\text{IVM-red}}$ litters because of Ly-6G specific Cre expression, which is activating additional tdTomato expression at the *ROSA26* locus. CatchUp mice were used at any age up to six month. Male and female mice were used in all experiments.

3.2.2 Tumor models

To induce tumors, murine tumor cell lines were injected into the respective hosts at different sites. All tumor injections were carried out under anesthesia by intraperitoneal (IP) application of ketamine and xylazine dosed at 100 mg / kg and 10 mg / kg body weight respectively and diluted in 0.9 % NaCl for injection of 10 µL / g body weight. Reasons for anesthesia are given in the following paragraphs.

Subcutaneous tumors

Subcutaneous tumor growth is a frequently used localization of transplantable tumors. The tumor cells are injected to the subcutaneous space over the dorsal flank of the mouse. This location bears several advantages and was chosen for those reasons: it causes minimal pain or discomfort throughout the experiment and it is very well accessible, facilitating a precise tumor volume measurement (see below).

Mice were anesthetized to enable shaving of the area of injection and thereby decreasing variability in tumor size estimation. $1 \cdot 10^6$ cells were thoroughly washed in PBS, resuspended in 100 µL PBS and injected to the dorsal flank using a 27 G needle. Cells were kept on ice to maintain viability. Mice were carefully observed until they woke up from anesthesia. Tumor size was determined by caliper measurement in two dimensions (a and b). Experimental end points were defined by a tumor size of 2 cm in one dimension if not stated differently. The following equation was used for calculation of ellipsoidal tumor volume:

$$V_{Tumor} = a \cdot b \cdot c \cdot \frac{\pi}{6} \tag{5}$$

$$\text{with } a < b \tag{6}$$

$$c \approx a \tag{7}$$

$$\Rightarrow V_{Tumor} = a^2 \cdot b \cdot \frac{\pi}{6} \tag{8}$$

Orthotopic tumors

The term orthotopic describes the implantation of the tumor cells to the organ of origin in this context. This localization is considered more clinically relevant due to the establishment of a more representative microenvironment. The orthotopic model was used for HNC cell lines by transplantation of the cells to the Musculus myohyoideus reflecting a localization that is in close proximity to the original tumor site.

Mice were anesthetized to enable the injection procedure which is done through the mouth of the mouse. $5 \cdot 10^5$ or $1 \cdot 10^6$ cells, MOPC$^{-/+}$ or SCCVII respectively, were thoroughly washed in PBS, resuspended in 30 µL PBS and injected to the floor of the mouth using a 27 G needle. Cells were kept on ice to maintain viability. Mice were carefully observed until they woke up from anesthesia. Mice were scaled daily because proceeding tumors of this location were known to cause weight loss due to reduced food uptake. Experiments were ended upon a weight loss of > 20 %.

Cutaneous ear tumors

The ear was chosen as tumor location for intravital microscopy because it is easily accessible and can be imaged in a multiphoton microscope without surgical interventions. Tumor cell injection cannot be performed as standardized as for the other two locations in this case because the final injection

volume may differ. $0.2 \cdot 10^6$ cells were prepared as described above and resuspended in 10 µL PBS per mouse. Mice were anesthetized and fixed to the working surface with one ear facing upwards. The ear was additionally fixed to the left index finger and the cell suspension (approximately 10 µL) was carefully injected using a 30 G needle in a out-to-inwards directionality.

Matrigel-tumor mixtures

Basement membrane matrix (Matrigel^{TM}) was used to give additional stromal support to tumor cells upon injection. The mixture contains extracellular matrix (ECM) components like growth factors and matrix proteins. Matrigel-tumors were transplanted to the subcutaneous location. In contrast to the subcutaneous protocol, cells were first resuspended in 50 µL PBS and mixed with the same volume Matrigel^{TM} to a final concentration of 5 mg protein / mL solution. Equipment had to be pre-cooled and placed on ice for the whole procedure because Matrigel^{TM} solidifies at room temperature. Upon injection to the flank of the mouse, a Matrigel^{TM} ball formed and supported tumor cell seeding. For this reason, one fifth of the usual cell amount was injected in matrix-supported tumors.

3.2.3 Depletion of Ly-6G$^+$ cells and T cells

For the depletion of different immune cell subsets, an antibody-mediated elimination technique was applied. Specific monoclonal antibodies were injected via the intraperitoneal route (for treatment regimens see table 3.2). Injections were performed using a 27 G needle with a total injection volume of 200 µL antibody dilution in 0.9 % NaCl per mouse. In control groups, the respective isotype antibody was applied the same way. Elimination of cells could be checked by flow cytometry of peripheral blood. For this reason, blood was taken from the lateral tail veins by tapping with a 27 G needle and subsequent transfer into tubes prepared with 5 µL 3.8 % sodium chloride solution to prevent coagulation. Flow cytometric analysis was performed as described in section 3.1.8. Alternatively, blood could also be transferred to a glass slide and spread thinly and evenly using a rectangular cover slip. These blood smears were applied to a Pappenheim's staining for morphological determination of granulocyte numbers (see section 3.4.3).

Table 3.2: Treatment regimens for depletion of different immune cells.

Target	clone	isotype	AB /mouse [µg]	treatment interval
CD8 T cells	2.43	rIgG2b, LTF-2	100	weekly
Gr-1 mainly neutrophils	RB6-8C5	rIgG2b, LTF-2	200	3 days
Ly-6G neutrophils	1A8	rIgG2a, 2A3	200	3 days

3.2.4 *in vivo* BrdU assay

Bromodeoxyuridine (5-bromo-2'-deoxyuridine, BrdU) is a analogue of thymidine that can be taken up by all cells and is incorporated in replicating DNA. For this reason, systemic availability of BrdU leads to the presence of this nucleoside in all cells that underwent cell division during the presence of the compound. BrdU$^+$ cells can be detected by specific antibodies after DNA denaturation.

Mice were injected with 1 mg BrdU in 200 µL PBS IP. After two hours, mice were killed and organs were either frozen for histology or isolated cells were analyzed via flow cytometry.

3.2.5 Noninvasive intravital microscopy

Intravital imaging is a state of the art technique to investigate cell motility and the effect of different kinds of interventions in the living animal. By combining transgenic expression of fluorescent proteins and transferable targeted or non-targeted fluorescent molecules, a wide array of cells and processes can be visualized. Multiphoton microscopy is based on an excitation of the electrons of a fluorophore using long-wavelength photons of which two have to excite one electron simultaneously to get it to the higher energy level. The red-shifted excitation wavelength enables deeper tissue penetration due to less scattering effects. Furthermore, an additional decrease of background signal is achieved by two-photon excitation. Due to this technique it is possible to realize noninvasive imaging if the region of interest in close proximity to the skin. An ear tumor model was chosen to enable intravital noninvasive imaging in the tumor. Ear skin is very thin and tumors were located directly underneath the keratinocytes. For these experiments, CatchUp$^{IVM\text{-}red}$ animals have been used to visualize Ly-6G^{+} cells without additional labeling steps. MOPC$^{\text{-}eGFP}$ cells were transplanted to identify tumoral regions by eGFP fluorescence as described in section 3.2.2. 100 µL Qdot non-targeting nanocrystals (QTracker 655, 1 µM) were injected intravenously (IV) to assess vasculature. Mice were initially anesthetized by IP injection of ketamine and xylazine dosed at 100 mg / kg and 10 mg / kg body weight respectively and diluted in 0.9 % NaCl for injection of 10 µL / g body weight. Maintenance of anesthesia for the imaging period was performed by inhalation of a 1.2 % isoflurane oxygen mixture which was applied via a ventilation unit to the intubated mouse with 250 strokes per minute at 250 µL volume per stroke. Body temperature was retained using a heating pad adjusted to 37°C. The mouse was adjusted on the pad and the ear was shaved and further immobilized on a plastic syringe to ensure best accessibility with the objective. To this end, a mixture of Vaseline and paraffin in a ratio of 4:1 [w/w] was used to minimize potential irritations of the ear skin and heated to 50°C prior to application. Imaging was performed with a Leica TCS SP8 MP microscope with simultaneous detection via Hybrid reflected light detectors (HyD-RLD) and photomultiplier tubes (PMT) using a HCX IRAPO L25x/0.95 water objective. Excitation was mediated at 960 nm using a Coherent Chameleon Vision II Ti:Saph-Laser. Filter settings are depicted in table 3.3.

Table 3.3: Filter settings used for intravital microscopy.

Target structure	**Target fluorophore**	**Filter path**	**Detector**
Neutrophils	tdTomato transgene	BS RSP560 + BS RSP620 + BP585/40	HyD
Tumor cells	eGFP transgene	BS RSP560 + BS RSP495 + BP525/50	PMT
Blood vessels	Qdots 655	BS RSP560 + BS RSP620 + BP660/30	HyD

Table 3.3: continued

Target structure	Target fluorophore	Filter path	Detector
Collagen	SHG signal	BS RSP560 + BS RSP495 + BP485/30	PMT

3.3 Protein biochemistry

3.3.1 SDS-PAGE and Immunoblotting

Preparation of cell lysates

A defined number of cells was taken from the cell culture (see 3.1.1) and washed three times with PBS while handled on ice. For storage, cells were centrifuged at 300 g for 5 minutes at 4°C, supernatant was removed and the resulting dry pellet was maintained at -20°C. To lyse the cell pellets, cells were thawed on ice and resuspended in 1 mL SDS lysis buffer containing proteases and phosphatases inhibitors / $1 \cdot 10^6$ cells and incubated for 5 minutes on ice (for components see table 2.11). Incubation was followed by 10 minutes centrifugation at 12000 g and 4°C in a microcool centrifuge to remove cell debris. Clean protein lysates were transferred to a new tube, mixed with 5× SDS sample buffer (table 2.11) and denatured for 10 minutes at 95°C. Sample buffer contains β-mercaptoethanol to reduce disulfide bounds and SDS binding to lipophil protein regions and releasing not covalent boundaries. Due to the highly negative charge of bound SDS the proteins can be separated by size in the electric field.

Gel electrophoresis

Proteins were separated according to their molecular weight using a discontinuous sodium dodecyl sulfate (SDS) polyacrylamide gel electrophoresis as described by Laemmli[109]. The polyacrylamide gel is made up by a sacking gel and a separation gel differing in polyacrylamide concentration and pH-value. In the stacking gel, polyacrylamide concentration is low not allowing a separation of the proteins. Glycine is nearly uncharged at the low pH of 6.8 making it move slowly whereas chloride ions are highly charged creating a second electric field which is increasing the local field intensity. Negatively charged proteins move behind the chloride ions and were concentrated on small space this way. Reaching the separation gel the pH-value changes to 8.8 leading to a negative charge of glycine which rapidly pushes the proteins into the separation gel.

Table 3.4: Ingredients for SDS PAGE gels. Amounts for two gels are given

Volume		Reagent	Volume		Reagent
separation gel			**stacking gel**		
4.5	mL	40 % Acrylamide/Bisacrylamide	630	µL	40 % Acrylamide/Bisacrylamide
5	mL	3 M Tris pH 8.8	210	µL	3 M Tris pH 6.8
5.36	mL	distilled water	4.1	mL	distilled water
75	µL	20 % SDS	25	µL	20 % SDS

Table 3.4: continued

Volume	Reagent	Volume	Reagent
30 µL	TEMED	20 µL	TEMED
30 µL	10 % APS	20 µL	10 % APS

Preparation of the gels was performed by mixing the respective ingredients for the separation or stacking gel according to table 3.4. Ammonium persulfate (APS) and N, N, N', N'-tetramethylethylenediamine (TEMED) are added last to start the polymerization process. The separation gel is polymerized first while covered with isopropyl alcohol followed by the stacking gel containing the pockets for protein loading. A Bio-Rad system was set up to run the gel electrophoresis with 2 gels containing running buffer. Equal sample volumes referring to the same number of lysed cells were loaded using a 1 mL Hamilton syringe. For identification of protein size, one sample pocket was loaded with Spectra protein ladder. Separation was carried out at 80 V for about 2h.

Immunoblotting

Gel electrophoresis was followed by blotting the separated proteins onto a polyvinylidene difluoride (PVDF) membrane using a semi dry blotting technique. Gel and membrane were surrounded by 2 piles of Rotilabo®blotting paper without any air bubbles and adjusted at the anode of the blotting chamber with the membrane being located between gel and anode. Blotting was performed for 60 minutes at 25 V and a maximum current of 300 mA in transfer buffer.
Protein containing membranes were washed in TBS and eventually stored at 4°C until analysis. Unspecific binding sites were blocked with TBS-T 5 % BSA for 1 hour at room temperature followed by incubation with the primary antibody directed against the protein of interest (1 hour, RT) in blocking solution. Antibodies and dilutions are listed in table 2.9. Membranes were washed in TBS-T and stained with alkaline phosphatase-coupled secondary antibody in blocking solution for 1 hour. After washing, pH was equilibrated using AP buffer and detection was carried out by CPD Star®substrate-induced, AP-catalyzed chemiluminescent reaction, which was recorded in the ChemiDoc-It®using VisionWorksLS software.

Densitometric Analysis

Densitometric measurement of signal intensity was carried out using ImageJ software. To this end, the different lanes were selected and the lane intensities were converted to a profile plot. This plot shows a curve on which the background signal was eliminated by setting a threshold. The area defined by the profile and the threshold was then measured resulting in a value which was reflecting the amount of protein. Signal intensities of MIF were normalized to GAPDH.

3.4 Histology

3.4.1 Sample preparation

Cryotissue was used for the analysis of different organs of tumor bearing and naive mice. Tissues were excised from the mouse as fast as possible and adjacent tissue was removed. Tissues were washed

in PBS and embedded in Tissue-Tek®O.C.T.™ compound, which is a formulation of water soluble glycols and resins, as fast and as dry as possible in Cryomold®containers. Afterwards, embedded tissues were frozen on liquid nitrogen as fast as possible. Thereby, the embedding compound provides structural support for freezing as well as sectioning later on. The resulting tissue blocks were stored at -80°C.
Frozen sections were prepared at a cryomicrotome at -25°C after equilibrating block temperature. Consecutive sections of 5 µm thickness were collected on SuperFrost®microscope slides in representative regions of the tissue. Sections were dried for one day and either stained directly or stored at -80°C until staining. Hematoxylin and eosin staining was always performed prior to further analysis to verify tissue quality.
For the analysis of cultured or primary cells, adherent cell lines were grown on sterile cover slips in 24 well culture plates for 2 days until the desired confluence was reached. Cells on cover slips were directly applied to the respective staining. Suspension cells were applied to the cytospin technology for further processing. Therefore, a cytospin chamber was assembled and 50000 - 100000 cells were given into the chamber in 100 µL FCS. The cells were then spun onto the microscope slide for 4 minutes at 40 g using the respective rotor. FCS was removed and the chamber was disassembled releasing the microscope slide, which was dried prior to staining or storage at -80°C.

3.4.2 Hematoxylin and eosin staining

The hematoxylin and eosin staining (HE stain) is probably the most common staining method in classical histology and often used for differentiation of tissue structures. The two staining components result in blue colored basophilic structures (especially nuclei) by hematoxylin and red to pink appearing acidophilic substances, which are most proteins and therefore results in pink cytoplasm, by eosin. Cryosections were completely thawed prior to staining. The staining is carried out after rehydrating the sections using decreasing alcohol concentrations. Staining in Shandon's Instant Hematoxylin was performed for up to 1 minute followed by blueing under running tap water. Next, eosinophilic staining was performed for 3 minutes in 0.5 % acidified aqueous eosin solution. Staining was followed by a wash in desalted water and subsequent dehydration in increasing alcohol concentrations. Sections were cleared in xylene, mounted using Roti®Histokitt and analyzed by light microscopy.

3.4.3 Pappenheim's staining

The Pappenheim panoptic staining technique was used on blood smears or cytospins on microscopic slides for the visualization of granulocytes and precursors. Slides were first stained with neutral May-Grünwald solution, containing methylene blue and eosin in methyl ethanol, for 2 minutes and left in water for the same time to develop staining. The second staining step was performed for 10 minutes in diluted Giemsa solution followed by washing the same way. Specimens were dried and subsequently mounted using Roti®Histokitt.

3.4.4 Immunhistochemical staining

This technique was used to specifically stain selected antigens with a color reaction for subsequent quantification. Antigens were detected by specific antibodies and peroxidase coupled secondary an-

tibodies facilitated a peroxidase mediated conversion of soluble 3-amino-9-ethylcarbazole (AEC) to a red precipitate.
Cryosections were thawed, dried and surrounded with wax (ImmEdge pen) to keep staining solutions in place. All following steps were carried out in a humid chamber. Fixation was performed using BD Cytofix / Cytoperm for 30 minutes. After washing with PBS, peroxidase block was applied for 15 minutes to minimize background signal from endogenous peroxidases. Washing with PBS was followed by incubation with primary antibody, diluted according to table 2.9 in PermWash buffer, at 4°C over night. Antibody was removed by washing three times in PBS before the buffer was exchanged for TBS. Tissues were incubated with two peroxidase conjugated secondary antibody consecutively to enhance signals. Both secondary antibodies were diluted 1:50 in TBS 10 % FCS and 20 % mouse serum, incubated for 30 minutes and followed by three washes with TBS. Visualization of bound antibodies was performed by peroxidase mediated color reaction of the AEC substrate solution within 10 minutes. Residual substrate was removed by washing three times in TBS. Tissues were rinsed with desalted water before counterstaining nuclei with Shandon Instant Hematoxylin for 10 seconds and blueing-up with running tap water. After another rinse with distilled water, tissues were mounted using Kaiser's glycerol gelatine and analyzed by light microscopy.

3.4.5 Immunofluorescence staining

Cytospins, cover slips or thawed cryosections were stained for antigen expression using specific antibodies. Cells were permeabilized using Cytofix / Cytoperm for 30 minutes and washed with PBS. Primary antibodies were diluted in Perm Wash buffer and cells were stained for 60 minutes. After washing 3 times with PBS, cells were incubated with fluorescently-coupled secondary antibodies in PBS 5 % BSA for 30 minutes with addition of the nuclear staining reagents DAPI (1:36000) or 7AAD (1:200). Cells were washed again and mounted using the aqueous mountant Fluoprep. Analysis was carried out as fast as possible after solidification of mounting medium at 4°C.

3.4.6 Apoptosis detection by TUNEL staining

Staining of apoptotic cells in cryotissues was performed by a TUNEL assay. TUNEL thereby refers to Terminal deoxynucleotidyl transferase dUTP nick end labeling and detects DNA fragmentation which is a process induced during apoptosis. To this end, a modification of the APO-DIRECT^{TM} Kit was applied. Buffers were provided by the kit.
Cryosections were thawed, dried and surrounded with wax (ImmEdge pen) to keep staining solutions in place. All following steps were carried out in a humid chamber. Fixation was performed for 30 minutes in 3 % PFA and after washing with PBS further fixation was added using 70 % ethanol for accessibility of the nuclear structures. After washing with WashBuffer, enzymatic labeling of DNA double strand breaks was performed in the presence of 15 U TdT enzyme and 0.04 nM FITC-labeled dUTPs in the provided reaction buffer for 1 hour at 37°C. The reaction was stopped using Rinse Buffer and nuclei were stained by DAPI diluted in RinseBuffer for 20 minutes. After washing in PBS, tissues were mounted using Fluoprep.

3.4.7 Image acquisition and quantification techniques

Microscopy was carried out using Axioskop 2 and AxioVision software. Fluorescence was excited using a 50W halogen lamp and detected using appropriate filters. Images were taken at 200× or 400× magnification with an AxioCam MRc 5 camera for further quantification.
Immunohistochemical staining of cell subsets were counted by hand on 4 representative photomicrographs and represented as positive cells per region of interest (ROI). On some occasions, quantification by ImageJ was performed. Therefore, colors were split by the *Colour Deconvolution* function and after threshold adjustment, positively stained area was measured (as percentage of total area).
Fluorescence intensity was quantified on photomicrographs taken under exactly the same conditions using ImageJ. If negative staining resulted in fluorescence signal, it was subtracted from the fluorescence intensity of the specific staining.

3.5 Molecular biology

3.5.1 Isolation of RNA and reverse transcription

Total RNA was isolated directly from PBS-washed and pelleted cells. RNeasy Mini or Micro Kits were used depending on the number of cells, for more or less that $2 \cdot 10^5$ cells respectively. Isolation was performed according to manufacturer's instructions. In short the cells were lysed using RLT buffer containing 1 % β-mercaptoethanol, homogenized using a QIAshredder spin column and equilibrated for binding by 70 % ethanol. Purification of RNA was further conducted on a RNeasy spin column, which is a silica membrane affinity column system, including several washing steps to remove DNA, protein and salt contents. For removal of DNA, an additional DNase digestion was performed when using the Micro Kit. RNA was eluted from the column using 30 or 14 µL RNase free water, respectively for Mini or Micro isolation. This procedure provides an enrichment of mRNA because of the membrane selectivity for RNA molecules >200 nucleotides. Determination of RNA concentration and purity was carried out by photometric analysis using the Synergy II plate reader at 260 and 280 nm for high sample volumes only.
200 ng RNA or the total eluate were directly set up in a reverse transcriptase (RT) reaction using the SuperScript™ II RT kit. Primer annealing on RNA templates was performed using 20.833 ng / µL random primer and 0.833 mM dNTP mix for 5 minutes at 65°C. After incubation with 1× first strand buffer and 0.011 M DTT for 2 minutes at 25°C, 10 units / µL reverse transcriptase were added and run according to table 3.5. The resulting complementary DNA (cDNA) was stored at -20°C.

Table 3.5: Reverse transcriptase reaction.

Temperature	Time
25°C	10 minutes
42°C	50 minutes
70°C	15 minutes

3.5.2 Transcript Quantification by qRT-PCR

SYBR Green is an asymmetrical cyanine dye that binds to double stranded DNA. The DNA-dye complex absorbs blue light at λ_{max} = 494 nm and emits green light at λ_{max} = 521 nm. By measuring the fluorescence after every elongation phase, the dye can be used to visualize the amplification of DNA

during the polymerase chain reaction (PCR), which is therefore called quantitative real time PCR. The PCR cycle, at which a significant exponential increase in fluorescence is detected, is directly correlated with the amount of DNA template that was present in the beginning of the reaction. This cycle is called the Cycle Threshold (C_T) and was used for further quantification.
qRT-PCR was performed on 10 ng target cDNA in Maxima^{TM} SYBR^{TM} Green mix using 0.5 µM of forward and reverse primers for the gene of interest. The reaction was run and read in a LightCycler®-capillary based system according to the program shown in table 3.6. Primer sequences and respective annealing temperatures are listed in table 2.10. β-actin was analyzed as internal standard. Data acquisition and analysis was performed using LightCycler 3 software.

Table 3.6: qRT-PCR program.

Purpose	Temperature	Time	slope [°C/sec]	Data?
Initial denaturation				
Denaturation	95°C	10 min	20	None
Amplification 40 cycles				
Denaturation	95°C	15 sec	20	None
Annealing	x°C	30 sec	20	None
Extension	72°C	30 sec	20	Single
Melting curve				
Denaturation	95°C	0 sec	20	None
Reannealing	57°C	15 sec	20	None
Denaturation	98°C	0 sec	0.1	Continuous
Cooling of the carousel				
Cooling	40°C	10 sec	20	None

3.5.3 Data analysis and hierarchical clustering

Differential expression was analyzed by the $2^{-\Delta\Delta C_T}$ method [120]. Expression was normalized to the internal standard and the difference between different treatments or cellular localization was assessed depending on the aim of the experiment as shown in equation 10. Due to the exponential relation of the DNA amount to the respective cycle, the normalized difference of mRNA which was present in the original samples is described logarithmically. The resulting value represents the fold difference in expression in the analyzed samples.

$$\Delta C_T = C_T(target) - C_T(internalStandard) \tag{9}$$

$$\Delta\Delta C_T = \Delta C_T(sample) - \Delta C_T(referenceSample) \tag{10}$$

$$relativeExpression = 2^{-\Delta\Delta C_T} \tag{11}$$

Hierarchical clustering and heatmaps were generated using R software with the Euclidean distance as distance metric and by applying complete linkage clustering.

3.6 Statistics

Statistical analysis was carried out using GraphPad Prism software. Statistical significance was assessed with either student's *t*-test for comparison of two groups with equal variances or one way ANOVA with Bonferroni post hoc testing for more than two groups. Results were considered significant at $p \leq .05$.

4 Results

4.1 Role of HNC tumors in modulating neutrophil physiology

As the field of tumor immunology grew rapidly in the last decades, many studies concentrated on the role of T regulatory cells (Treg) and macrophages[73, 2]. Currently, neutrophils ($CD11b^+Ly\text{-}6G^+$ cells) have just started to emerge as important cell type in this context. Since then, different studies used mouse models to further characterize $CD11b^+Ly\text{-}6G^+$ cell functions in spontaneous, induced or transplantable tumor settings[14]. However, no head and neck cancer (HNC) model had been established in this context so far. Recent studies from our group indicated tumor promoting functions of neutrophils in HNC patients which were inducible by tumor derived factors, such as the cytokines macrophage migration inhibitory factor (MIF) and CXCL8[39, 203]. Therefore, the first part of this work aimed at the characterization of possible HNC mouse models to investigate functional implications of neutrophils in tumor bearing mice. One criterion for these models was to specifically resemble characteristics of phenotypes that have been found with patient-derived or tumor factor-treated neutrophils in the human system.

4.1.1 HNC cells interact with murine and human neutrophils via the MIF-chemokine receptor axis

Neutrophil functions in immune cell-cancer interactions were highly debated in the literature because different studies could show both, pro- or antitumoral functions of these cells. When research proceeded with looking for the respective mechanisms, it became clear that the microenvironment is a key player for determining neutrophil functions. Data from our group suggested tumor derived chemokines and cytokines as important inducers of a protumoral neutrophil phenotype in HNC patients and human neutrophil tumor interactions[39, 203]. For this reason, tumor derived MIF was chosen to be analyzed in more detail in this section as well as the potential of murine $CD11b^+Ly\text{-}6G^+$ to respond to this cytokine.

Human neutrophils migrate through endothelial cells in response to tumor derived MIF

We previously showed chemotactic properties of tumor derived MIF in a transwell assay[39]. This assay is in principle testing the general migratory potential that can be induced without the need of integrin activation which is important for neutrophil extravasation. To assess whether MIF is capable of inducing infiltration of neutrophils into the tumor tissue, an assay was established to mimic migration of immune cells through an endothelium. Additional activation of integrins is indispensable for the neutrophils to pass through this endothelial monolayer. First, tumor supernatants (SN) were tested for their capacity to induce transendothelial migration (TEM). FaDu and UM22b cell lines were used for the production of SN because their SN were shown to possess chemotactic properties on neutrophils and contain notable amounts of MIF (1000 and 2000 pg / mL respectively). The TEM assay was set up as described in section 3.1.7. Healthy donor neutrophils were seeded on a HMEC monolayer (figure 4.1A) and were left to migrate towards different tumor SN for 4h. Both, FaDu and UM22b SN, induced neutrophil migration through an endothelial monolayer (figure 4.1B), which was dependent on the neutrophil donor and on the cell line used for SN production. To investigate the impact of MIF in this process, SN were incubated with the chemical antagonist ISO-1[122] to inhibit

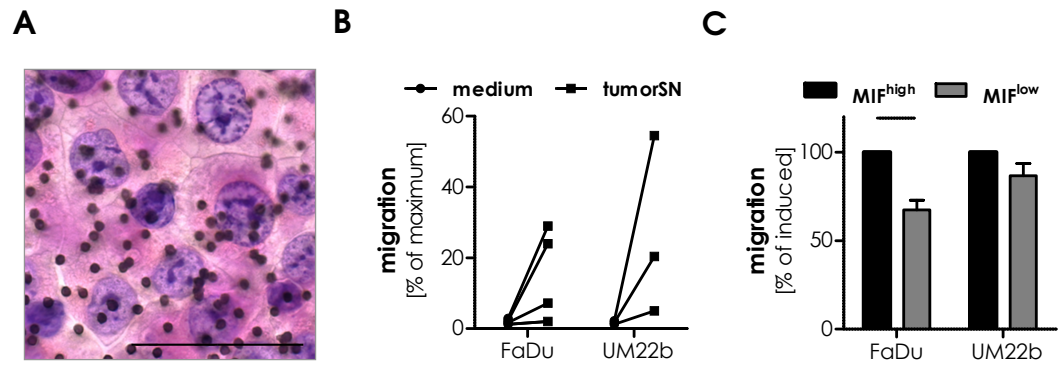

Figure 4.1: Tumor-derived MIF induces neutrophil transendothelial migration. Human neutrophils were isolated by density gradient and applied to an *in vitro* transendothelial migration assay (TEM) using a HMEC monolayer grown on a 3 µm pore transwell insert. Tumor supernatant (SN) from different cell lines was used as attractant. **A** HMEC monolayer was stained with hematoxylin and eosin directly on the transwell membrane. A representative photomicrograph was taken at 630 × magnification (scale represents 50 µm). **B** $5 \cdot 10^5$ neutrophils were added to the upper well of a TEM setup and migrated towards either basic culture medium or tumor SN for 4 h. Migrated cells were counted. Maximum migration was reflected by the cell count of neutrophils in a well without transwell insert. **C** Tumor SN was pretreated with either DMSO or 50 μM of the MIF inhibitor ISO-1 for 30 minutes. $5 \cdot 10^5$ neutrophils were added to the upper well of a TEM setup and migrated towards either DMSO or ISO-1 SN reflected as MIF^{high} and MIF^{low}, respectively. After 4 h, migrated cells were counted. Bars represent mean±SEM of 5 (FaDu) and 3 (UM22b) independent experiments. Line indicates $p \leq .05$ by paired t-test.

MIF activity prior to the TEM assay. The induced migration was reduced to less than 70 % by inhibition of MIF in FaDu SN while the effect was much lower in UM22b SN. It was concluded that tumor derived MIF is indeed capable of inducing transendothelial migration of human neutrophils which might result in tumor infiltration by these cells.

Murine HNC cell lines express MIF *in vitro* and *in vivo*

As a next step, MIF expression was verified in murine cell lines as it is a potential modulator of $CD11b^+Ly\text{-}6G^+$ cell numbers and activation in tumor bearing mice. Available murine HNC cell lines were SCCVII, which derived from C3H mice, and BL6 derived MOPC cells, of which both subtypes, HPV16 E6/E7 positive ($MOPC^+$) and negative ($MOPC^-$), were used. Additional cell lines from different cancer entities, being B16F10 melanoma and EL4 T cell lymphoma, were used as a reference as they were described to induce $CD11b^+Ly\text{-}6G^+$ cell modulation[222]. Expression of MIF was first determined in cultured cells. Western Blot (WB) analysis of equal cell numbers showed varying expression of the 12 kDa protein in relation to GAPDH (figure 4.2A). SCCVII and $MOPC^-$ HNC cells expressed the highest detectable MIF amounts in conjunction with B16F10 cells. To confirm these results, SCCVII and $MOPC^-$ cells were grown on cover slips, stained for MIF and analyzed by fluorescence microscopy (immunofluorescence, IF). The IF analysis indicated a higher expression of MIF by $MOPC^-$ cells compared to SCCVII, which was not observed by WB, suggesting that production and release of the cytokine might also be dependent on cell confluence and stress during the experiment. Representative photomicrographs are shown in figure 4.2B. Because of the variability of MIF expression, presence of the cytokine was further verified in tumors derived from the respective cell lines. To this end, $5 \cdot 10^5$ HNC tumor cells were injected orthotopically into their respective hosts and grown for about 2 weeks. Resulting tumors were prepared as described in section 3.4.1 and analyzed for MIF expression

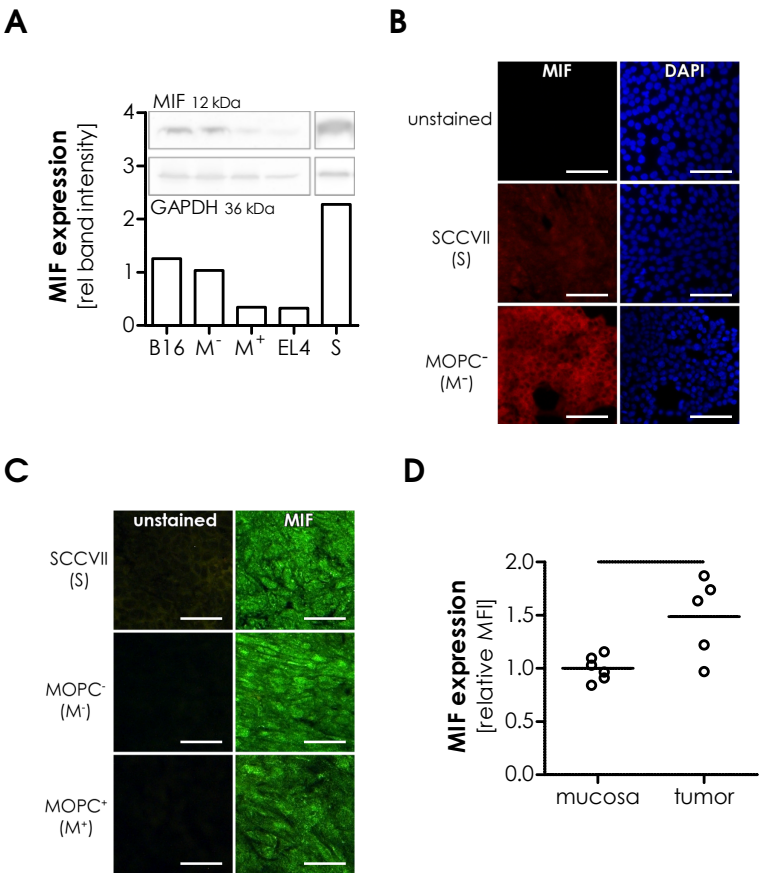

Figure 4.2: MIF is expressed by murine HNC cell lines. **A** $2 \cdot 10^5$ cells were lysed and analyzed by Western Blot. Membranes were stained against MIF and GAPDH and ImageJ densitometry was performed. One representative of 3 experiments is shown. Bars indicate band intensity of MIF/GAPDH. Abbreviations: B16=B16F10, M^-=MOPC$^-$, M^+=MOPC$^+$, S=SCCVII. **B** Cells were grown on cover slips for 2 days and stained for MIF in Cy3. Nuclei were stained by DAPI. One representative of 2 experiments is shown. Pictures were taken at 200× magnification and processed identically. The scale represents 50 µm. **C** Orthotopic tumors from C3H (SCCVII) and BL6 mice (MOPC$^-$) were prepared for histology. Cryosections were stained for MIF in Alexa488. Pictures were taken as described in B and are representative for 3 - 4 mice. **D** Mean fluorescence intensity (MFI) of MIF was quantified on stained tissue as shown in C. Tumor tissue from MOPC$^-$ tumors was compared to healthy mucosa from the same animal. Line indicates significance at $p \leq .05$ as tested by paired t-test.

by fluorescence microscopy. All murine HNC tumors expressed MIF without major differences (figure 4.2C). Expression was confirmed for B16F10 subcutaneous (SC) tumors as well (data not shown). To evaluate the amounts of MIF, which were effectively produced by the tumor tissue, healthy mucosa from MOPC$^-$ tumor bearing mice was collected and stained as well. Fluorescence intensities were determined in healthy epithelial regions and in the tumor tissue of the respective mice (figure 4.2D). MIF expression by tumor tissue was found to be higher than epithelial expression in 4 out of 5 tumors. These results indicate that murine cancer cell lines, especially derived from the head and neck region, share upregulated MIF expression with human tumors which might lead to a modulation and attraction of CD11b$^+$Ly-6G$^+$ cells in tumor bearing mice which is consistent with our previous results in HNC patients.

CXCR2 and CXCR4 are expressed on CD11b$^+$Ly-6G$^+$ cells in different compartments of naive BL6 and C3H mice

Tumor derived chemokines such as CXCL1 and CXCL5 regulate both the migration and functional activation of CD11b$^+$Ly-6G$^+$ cells[225, 138]. Furthermore, recruitment of CD11b$^+$Ly-6G$^+$ cells to the tumor was described to be mainly CXCR2 and CXCR4 dependent, as these receptors share important roles in inflammatory and homeostatic neutrophil trafficking[42, 171]. As MIF is another ligand for CXCR2, CXCR4 and also CXCR7[199], the expression of these receptors was analyzed on CD11b$^+$Ly-6G$^+$ cells in naive mice of the strains C3H and BL6. The cells were identified by flow cytometry as described in

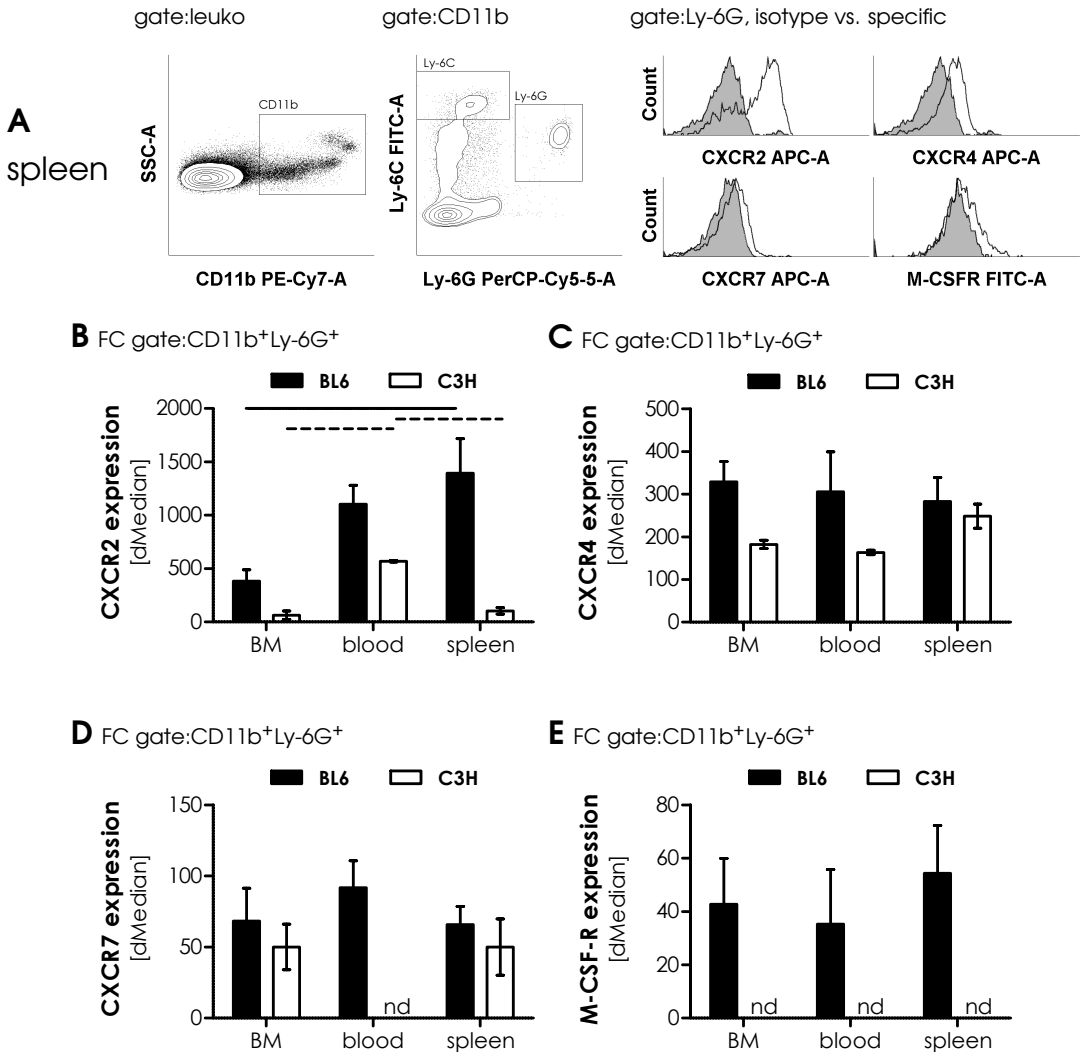

Figure 4.3: Chemokine receptor expression by CD11b$^+$Ly-6G$^+$ cells in naive mice. Cells were isolated from bone marrow (BM), blood and spleen of naive BL6 (n=4) and C3H (n=3) mice and were analyzed by flow cytometry. Representative results are shown in **A** for BL6 splenocytes indicating the gating strategy and CXCR expression in histograms (filled curve=isotype stained cells, FMO; open curve=specific antibody signal). Cells were analyzed for the expression of CXCR2 **B**, CXCR4 **C**, CXCR7 **D** and M-CSF-receptor **E**. 'nd' indicates that these cells have not been analyzed for the respective receptor (nd=not determined). Data are shown as mean±SEM. Lines indicate significance as tested by one way ANOVA with $p \leq .05$.

figure 3.2 and 4.3A. CXCR2 expression was most abundant on the surface of CD11b$^+$Ly-6G$^+$ cells compared to the other receptors especially when cells were derived from peripheral compartments (see histogram for spleen derived cells in figure 4.3A). CXCR2 expression is regulated upon mobilization of the cells from the bone marrow with increasing expression in spleen and blood in BL6 and in the blood in C3H mice (figure 4.3B). In contrast, CXCR4 (figure 4.3C) and CXCR7 expression (figure 4.3D) were not differentially regulated in the analyzed CD11b$^+$Ly-6G$^+$ cells of different tissue compartments of naive mice. M-CSF-receptor, which is present on macrophages, monocytes and precursor cells as well as myeloid derived suppressor cells (MDSC)[222], was analyzed in addition to the chemokine receptors and was hardly detectable on CD11b$^+$Ly-6G$^+$ cells from naive mice, as expected (figure 4.3E). These results confirm the general capability of CD11b$^+$Ly-6G$^+$ cells to respond to HNC derived factors.

Chemokine receptors CXCR2 and CXCR4 are differentially expressed on CD11b$^+$Ly-6G$^+$ cells in HNC tumor bearing mice

After having shown that CD11b$^+$Ly-6G$^+$ cells express receptors for HNC derived factors in naive mice, receptor expression was determined in tumor bearing mice in different compartments including the tumor itself. To this end, mice were inoculated with $5 \cdot 10^5$ HNC cells orthotopically (MOPC and SCCVII in BL6 and C3H mice, respectively) and isolated cells were analyzed by flow cytometry after two to three weeks of tumor growth. Comparable to naive mice, CXCR2 (figure 4.4A) was expressed mainly in the periphery (blood and spleen) in tumor bearing BL6 mice. In tumor bearing C3H mice, expression of CXCR2 was increased in the bone marrow compared to naive and did not differ between bone marrow and spleen derived CD11b$^+$Ly-6G$^+$ cells. Low CXCR2 expression was found in tumor infiltrating CD11b$^+$Ly-6G$^+$ cells in BL6 mice, which is consistent with high intratumoral CXCR2 ligand availability and ligand-induced receptor downregulation[48, 220]. In contrast to CXCR2 expression, CXCR4 and CXCR7 expression did not vary as much between the compartments (figure 4.4B+C). A slight decrease of CXCR4 expression was observed in splenic CD11b$^+$Ly-6G$^+$ cells of tumor bearing BL6 mice (figure 4.4B). CXCR4 and 7 expression was further unchanged in tumor infiltrating CD11b$^+$-Ly-6G$^+$ cells. Despite overall low expression of M-CSF-R, slightly elevated levels were observed in bone marrow and tumor derived CD11b$^+$Ly-6G$^+$ cells (figure 4.4), suggesting a MDSC like phenotype of CD11b$^+$Ly-6G$^+$ cells in these tissues in the HNC model.
Collectively, these data characterize a chemokine-chemokine receptor axis which potentially results in trafficking and accumulation of CD11b$^+$Ly-6G$^+$ cells in HNC bearing mice. These tumor models therefore also resemble the relation of HNC tumors and neutrophils in HNC patients which is partially mediated by homologous CXCR ligands.

4.1.2 Expansion of CD11b$^+$Ly-6G$^+$ cells correlates with tumor progression

Peripheral neutrophil counts are easily accessible in humans and in cancer patients, and increased neutrophil numbers often associates with a poor overall survival[201]. In HNC patients, we previously described alterations in neutrophil function and the appearance of immunosuppressive subsets[15, 204]. Comparable observations were also shown for several murine tumor models[222] but not for HNC. After having demonstrated that potential ligands for CD11b$^+$Ly-6G$^+$ cells are expressed by murine HNC tumors, accumulation of these cells was analyzed in the described tumor models. To

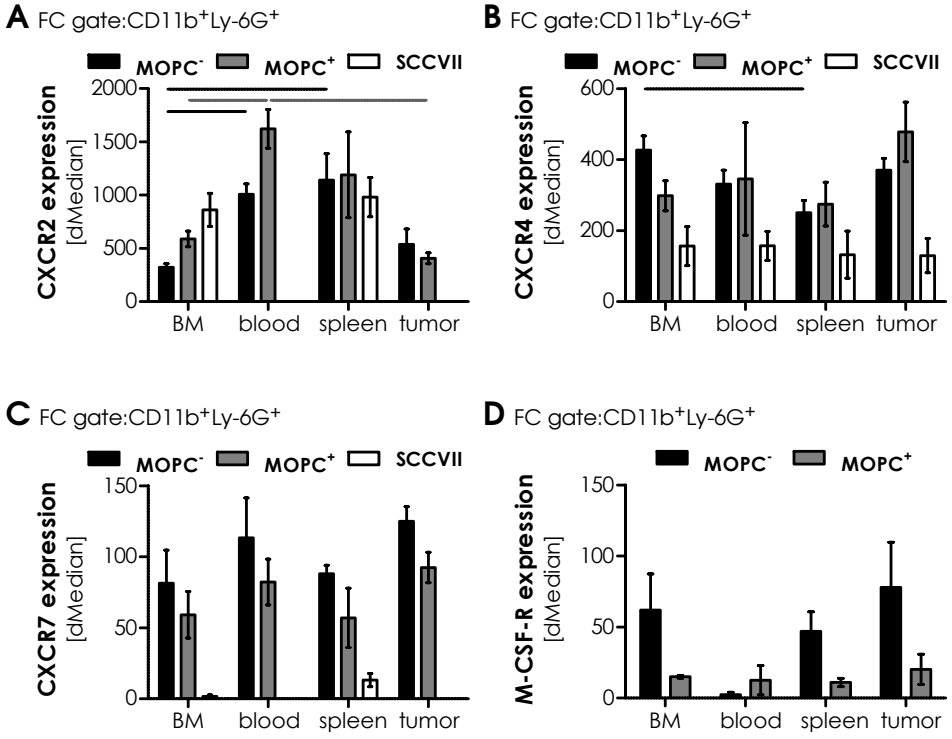

Figure 4.4: CD11b$^+$Ly-6G$^+$ cell expression of CXC receptors in tumor bearing mice. BL6 (n=5 per tumor cell line) and C3H mice (n=4) have been injected with the indicated HNC cell lines orthotopically. Mice were sacrificed after two to three weeks upon weight loss. Bone marrow, blood, spleen and tumor infiltrating cells were isolated and analyzed by flow cytometry. CXCR2 **A**, CXCR4 **B**, CXCR7 **C** and M-CSF-R **D** expression was evaluated on CD11b$^+$Ly-6G$^+$ cells. Data are shown as mean±SEM. Lines indicate significance as tested by one way ANOVA among mice with the same tumor with $p \leq .05$.

this end, orthotopic (ortho) as well as subcutaneous (SC) tumor locations were compared in their capability of inducing changes in CD11b$^+$Ly-6G$^+$ cell abundance in different tissue compartments.

HNC tumors increase the frequency of CD11b$^+$Ly-6G$^+$ cells in the blood of tumor bearing mice

In cancer patients, including our studies as described above, blood is frequently analyzed and many changes were found in this compartment. To evaluate whether similar changes take place in the murine models, blood was analyzed in this first characterization. For this purpose, BL6 and C3H mice were injected with the respective HNC cell lines at orthotopic and subcutaneous locations as described in section 3.2.2. EL4 tumors served as a reference cell line and were injected subcutaneously. Accumulation of CD11b$^+$Ly-6G$^+$ cells in EL4 tumor bearing animals was previously described[222]. Blood was analyzed by flow cytometry after two to three weeks of tumor growth. Representative analyses are shown in figure 4.5A for BL6 and figure 4.5B for C3H naive and tumor bearing mice indicating an increase in numbers of analyzed cells. Detailed analysis in SC tumors revealed accumulation of CD11b$^+$Ly-6G$^+$ cells in BL6 but not C3H mice (figure 4.5C). Furthermore, SC MOPC$^-$ tumors induced slightly higher amounts of CD11b$^+$Ly-6G$^+$ cells than EL4 tumors. In contrast, frequencies of peripheral blood CD11b$^+$Ly-6G$^+$ cells consistently increased in both mouse strains independent of the injected tumor cell line in orthotopic tumor bearing mice (figure 4.5D). To compare all experiments,

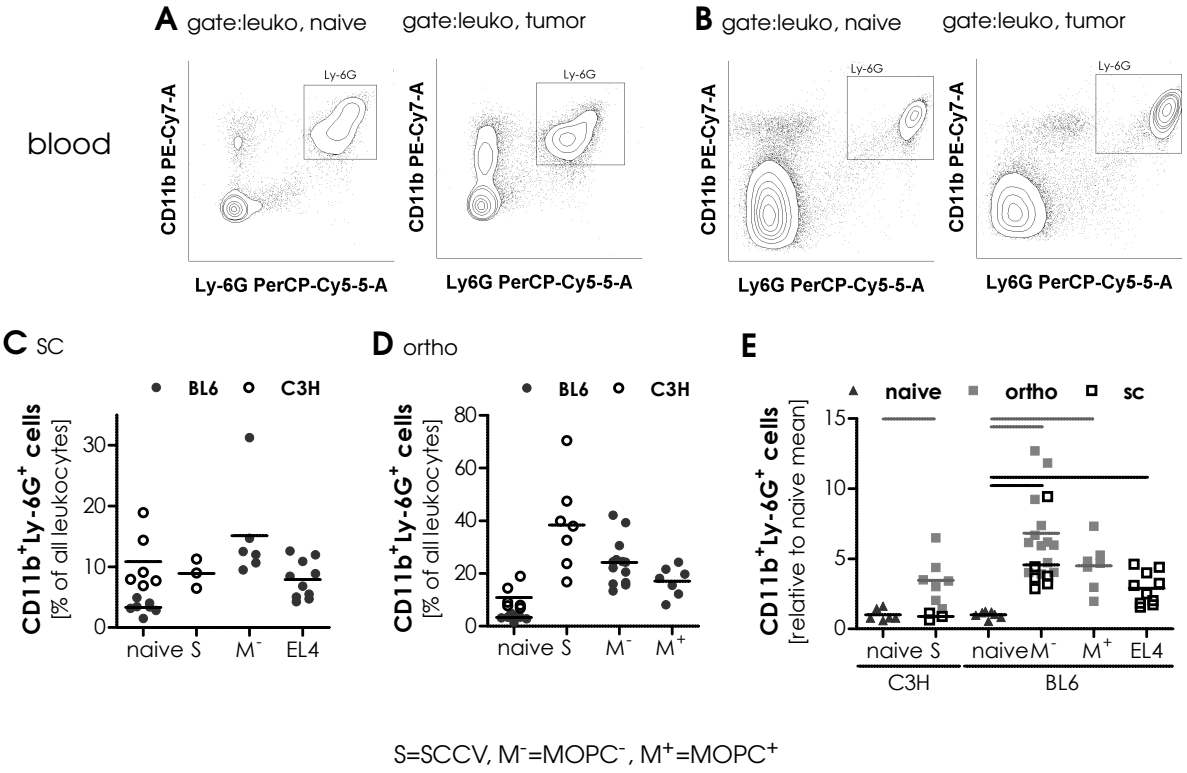

S=SCCV, M⁻=MOPC⁻, M⁺=MOPC⁺

Figure 4.5: CD11b⁺Ly-6G⁺ cells accumulate in blood of tumor bearing mice. BL6 and C3H mice were injected with the indicated tumor cell lines at different locations. Tumor bearing and naive mice were sacrificed after two to three weeks. Blood was taken from the abdominal aorta and was analyzed by flow cytometry. **A** and **B** show representative contour plots for CD11b⁺Ly-6G⁺ cells from naive and tumor-bearing BL6 (**A**, tumor=MOPC⁻ ortho) and C3H mice (**B**, tumor=SCCVII ortho). Frequency of CD11b⁺Ly-6G⁺ cells was analyzed in SC **C** and ortho **D** tumor-bearing mice. The relative accumulation to the mean of the respective naive group (naive mean=1) is depicted in **E**. Data are shown as single measurements. Lines indicate significance as tested by one way ANOVA within mouse strains with $p \leq .05$ (only shown in **E**).

the relative induction of CD11b⁺Ly-6G⁺ cells was assessed by adjusting the mean of the naive mouse groups to 1. While accumulation of CD11b⁺Ly-6G⁺ cells is most prominent in orthotopic tumor bearing mice especially for MOPC⁻ tumors, this difference between tumor locations is not statistically significant. These results confirm modulatory effects of HNC tumors on peripheral blood CD11b⁺-Ly-6G⁺ cells. Furthermore, on comparison to the well established EL4 cell line, it would imply that modulation by HNC tumors represents a strong effect.

CD11b⁺Ly-6G⁺ cells expand in spleens of HNC tumor bearing mice

As a next step, accumulation of CD11b⁺Ly-6G⁺ cells in the spleen was assessed. The spleen has been described as a major site of myelopoiesis in tumor bearing mice[223] and is therefore an important reservoir of CD11b⁺Ly-6G⁺ cells. To analyze splenic composition in HNC bearing animals, BL6 and C3H mice were injected with the respective cell lines as indicated in the figure at orthotopic and subcutaneous administration sites. EL4 mice were used as a reference in BL6 mice with SC tumor administration. After two to three weeks of tumor growth, splenocytes were isolated and frequency of CD11b⁺Ly-6G⁺ cells was determined by flow cytometry. Representative FC plots already indicated increased numbers of CD11b⁺Ly-6G⁺ cells in tumor bearing BL6 (figure 4.6A) and C3H mice (figure 4.6B). When analyzing SC tumors, an increased frequency was only apparent in EL4 tumor bearing

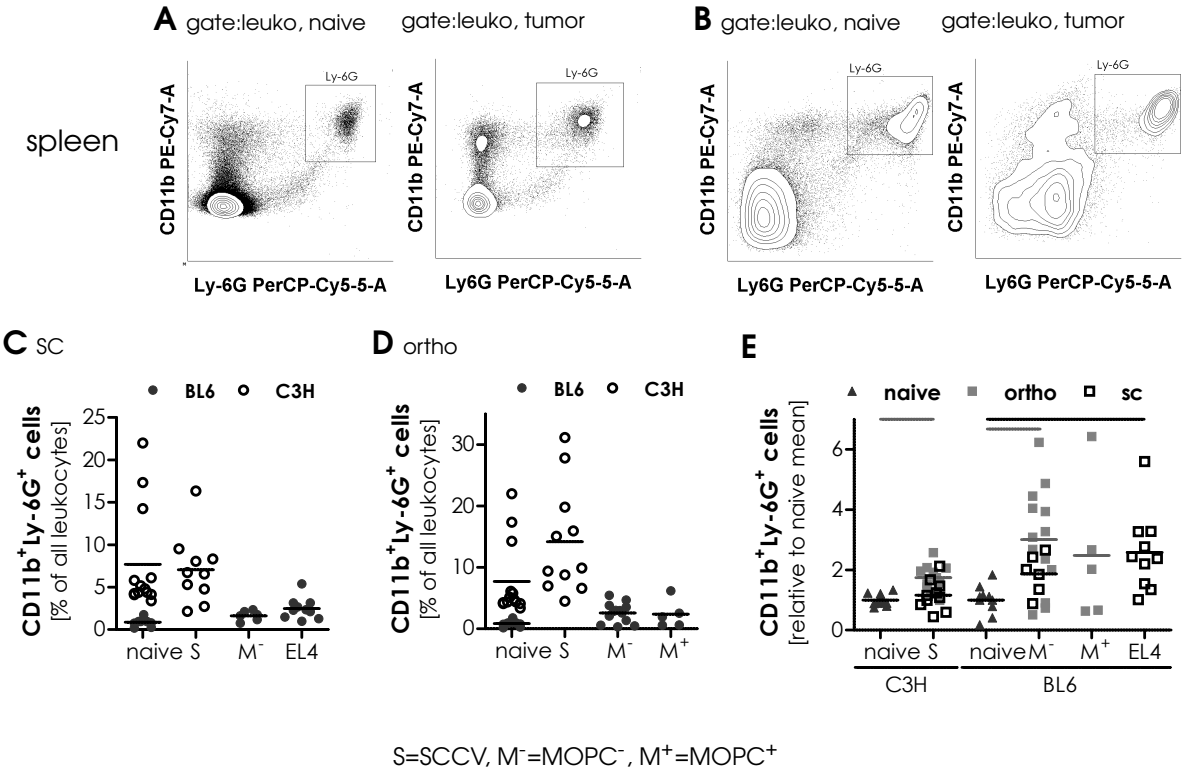

Figure 4.6: CD11b$^+$Ly-6G$^+$ cells accumulate in the spleen of tumor bearing mice. BL6 and C3H mice have been injected with the indicated tumor cell lines at different locations. Tumor bearing and naive mice were sacrificed after two to three weeks and cells were isolated from the spleen. Analysis for CD11b$^+$Ly-6G$^+$ cells was performed by flow cytometry as also indicated in **A** and **B** for naive and tumor-bearing BL6 (**A**, tumor=MOPC$^-$ ortho) and C3H mice (**B**, tumor=SCCVII ortho). Frequency of CD11b$^+$Ly-6G$^+$ cells was analyzed in SC **C** and ortho **D** tumor-bearing mice. The relative accumulation to the mean of the respective naive group (naive mean=1) is depicted in **E**. Data are shown as single measurements. Lines indicate significance as tested by one way ANOVA within mouse strains with $p \leq .05$ (only shown in **E**).

animals compared to naive (figure 4.6C). In line with the data obtained from analysis of blood cells, orthotopic tumors induced a more distinct increase in the frequency of CD11b$^+$Ly-6G$^+$ cells. To minimize inter experimental variances, data was adjusted to the mean frequency in the respective naive group (figure 4.6E). Relative accumulation of CD11b$^+$Ly-6G$^+$ cells in the spleen was clearly induced in tumor bearing mice with ortho tumors showing slightly higher induction than SC tumors. These data demonstrate modulation of the splenic CD11b$^+$Ly-6G$^+$ reservoir in HNC tumor bearing mice especially for orthotopic tumor locations.

HNC tumor progression correlates with the accumulation of CD11b$^+$Ly-6G$^+$ cells

The previous findings showed that CD11b$^+$Ly-6G$^+$ cell frequencies differ between naive and HNC tumor bearing animals. Next, it was of major interest whether these changes depended on the general intervention induced by tumor injection or on tumor size and time of tumor progression. To test this, MOPC$^-$ and SCCVII cells were injected into BL6 and C3H mice, respectively. After two to three weeks of tumor growth, CD11b$^+$Ly-6G$^+$ cell frequencies were assessed as described above and tumors were explanted to determine tumor weight. In BL6 animals with MOPC$^-$ tumors, splenic CD11b$^+$Ly-6G$^+$ frequencies correlated positively with tumor weight while peripheral blood cell numbers showed a marginal positive correlation (figure 4.7A). Furthermore, splenic and peripheral blood CD11b$^+$Ly-

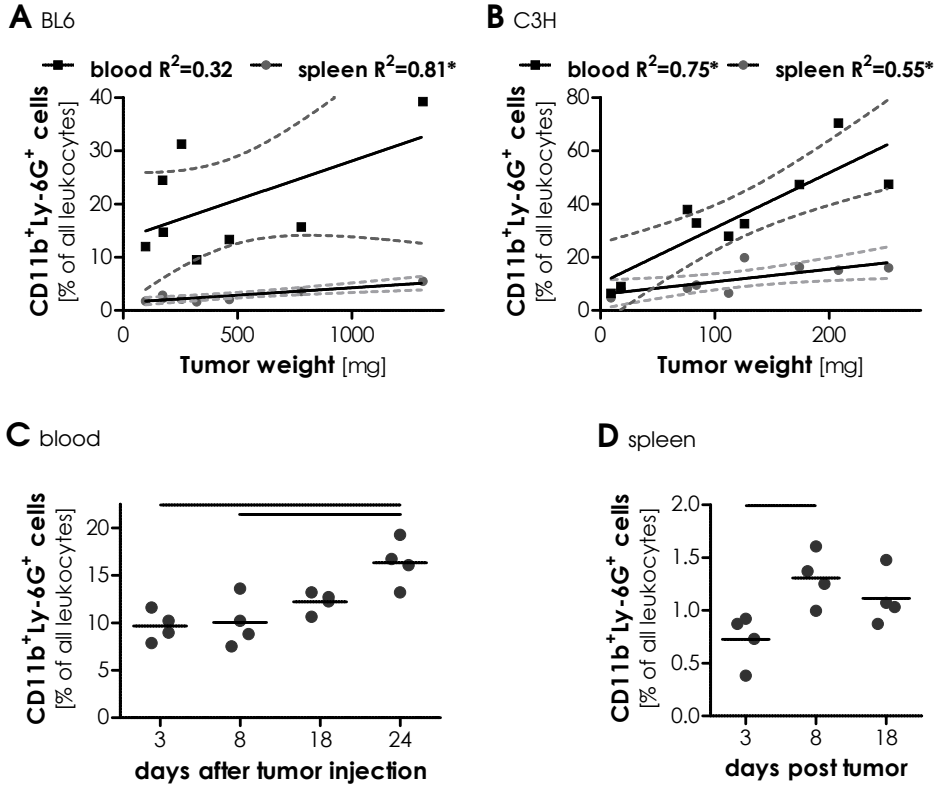

Figure 4.7: CD11b$^+$Ly-6G$^+$ cell accumulation is time and tumor size dependent. BL6 and C3H mice have been injected with MOPC$^-$ or SCCVII cells, respectively, at different locations. **A+B** Tumor bearing were sacrificed after two to three weeks and cells were isolated from the spleen and blood. Flow cytometry data for CD11b$^+$Ly-6G$^+$ cells was correlated with the weight of the excised tumor for BL6 **A** and C3H mice **B**. Lines indicate linear regression and dotted lines represent the respective 95 % confidence band of the best fit. Significant correlation was observed for all data sets except BL6 blood with $p \leq .05$ (indicated by *). **C+D** MOPC$^-$ SC tumor-bearing mice were killed after the indicated periods. Frequency of CD11b$^+$Ly-6G$^+$ cells was analyzed in blood **C** and spleen **D** of these mice. Data are shown as single measurements. Lines indicate significance as tested by one way ANOVA with $p \leq .05$.

6G$^+$ cell frequencies were dependent on tumor weight in C3H mice with SCCVII tumors (figure 4.7B). For identification of time dependent accumulation, BL6 mice were inoculated with SC MOPC$^-$ tumors and frequencies of CD11b$^+$Ly-6G$^+$ cells were assessed after different periods of tumor growth. While no changes were observed in the first week in blood (figure 4.7C), increased frequencies in the spleen were already detectable after 8 days of tumor growth (figure 4.7D). With further tumor progression, blood CD11b$^+$Ly-6G$^+$ cell counts also started to increase slightly after 18 days and accumulated significantly 24 days after tumor cell injection (figure 4.7C).

Collectively, these data demonstrate tumor dependent accumulation of CD11b$^+$Ly-6G$^+$ cells in the described mouse model. Time dependent increase in CD11b$^+$Ly-6G$^+$ cell frequencies has already been described in other tumor models[223]. However, this is the first study to demonstrate that in a murine HNC model this is also the case. It was demonstrated that tumor progression induced accumulation of CD11b$^+$Ly-6G$^+$ cells in the blood of tumor bearing animals, while the tumor affected splenic neutrophils in a very early stage of tumor development. The low slope of the correlation between splenic CD11b$^+$Ly-6G$^+$ numbers and tumor weight in advanced tumors further confirmed that the splenic CD11b$^+$Ly-6G$^+$ cell reservoir is affected in earlier stages of tumor development and

does not increase so much in the analyzed advanced stages. However, the peripheral blood CD11b$^+$-Ly-6G$^+$ cell frequency was demonstrated to be highly dependent on tumor weight during advanced tumor progression.

4.1.3 HNC tumors are infiltrated by Ly-6G$^+$ cells

CD11b$^+$Ly-6G$^+$ cells can affect peripheral immune responses thereby influencing tumor progression[45, 137, 176]. Nevertheless, infiltration into the tumor is a critical step for inducing local effects such as angiogenesis and tissue remodeling[91]. Furthermore, modulation by tumor derived factors is most likely taking place at tumoral sites. It was therefore mandatory to assess the infiltration of tumor tissue by CD11b$^+$Ly-6G$^+$ cells in the HNC models. To this end, mice were inoculated with the HNC cell lines SCCVII, MOPC$^-$ and MOPC$^+$ at SC and ortho administration sites. After two to three weeks of tumor growth, tumors were isolated and applied to histological analysis or flow cytometry. EL4 tumor bearing mice were analyzed by flow cytometry as well. Histological characterization demonstrated infiltration of polymorphnuclear Ly-6G$^+$ cells in murine HNC tumor tissue (figure 4.8A+B). All analyzed tumors were infiltrated with Ly-6G$^+$ cells. While SCCVII cells attracted more Ly-6G$^+$ cells than MOPC$^-$ tumors at the SC tumor location (figure 4.8C), ortho tumors did not differ clearly in the density of infiltrating cells (figure 4.8D). Flow cytometric analysis further confirmed increased infiltration in SCCVII SC tumors (figure 4.8E). Varied infiltration of all ortho tumors was also observed by this technique (figure 4.8F). Compared to EL4 tumors, infiltration of HNC was remarkably high. Furthermore, orthotopic tumors were consistently higher infiltrated than SC tumors within BL6 tumor bearing mice. Surprisingly, when correlating tumor weight and Ly-6G$^+$ cell infiltration as determined by histology, SC infiltration was dependent on tumor weight (figure 4.8G) while ortho tumors were constantly infiltrated independent of tumor progression (figure 4.8H).
Consistently, this data demonstrated HNC infiltration by Ly-6G$^+$ cells. Infiltration was most pronounced in orthotopically localized tumors which also induced higher peripheral accumulation of CD11b$^+$Ly-6G$^+$ cells. Furthermore, density of infiltration was only found to correlate with tumor weight in established SC tumors.

4.1.4 Assessing the infiltration of adaptive and innate immune cells in experimental HNC tumors

As already indicated in the beginning of this chapter, tumors are not only primarily infiltrated by CD11b$^+$Ly-6G$^+$ cells. The tumor immune crosstalk is rather characterized by strikingly heterogeneous immune cell populations. These include T cells which can be roughly differentiated into CD4$^+$ and CD8$^+$ cells but also comprise of T regulatory cells and Th17 cells[96]. The tumor immunoscore is further complicated by additional infiltration by cells of the innate immune system such as NK cells and monocytes giving rise to tumor associated macrophages[30]. To gain insight into the general immunogenicity of the described HNC mouse model, the tumoral infiltration of additional immune cells was assessed in the following section.

Infiltration of T cells: CD4 in SC and CD8 cells in ortho HNC tumors

T cells are potential antitumor effector cells. Especially CD8 T cells can be directly cytotoxic on tumor cells. Nevertheless, T cell infiltration is not necessarily associated with good clinical outcome

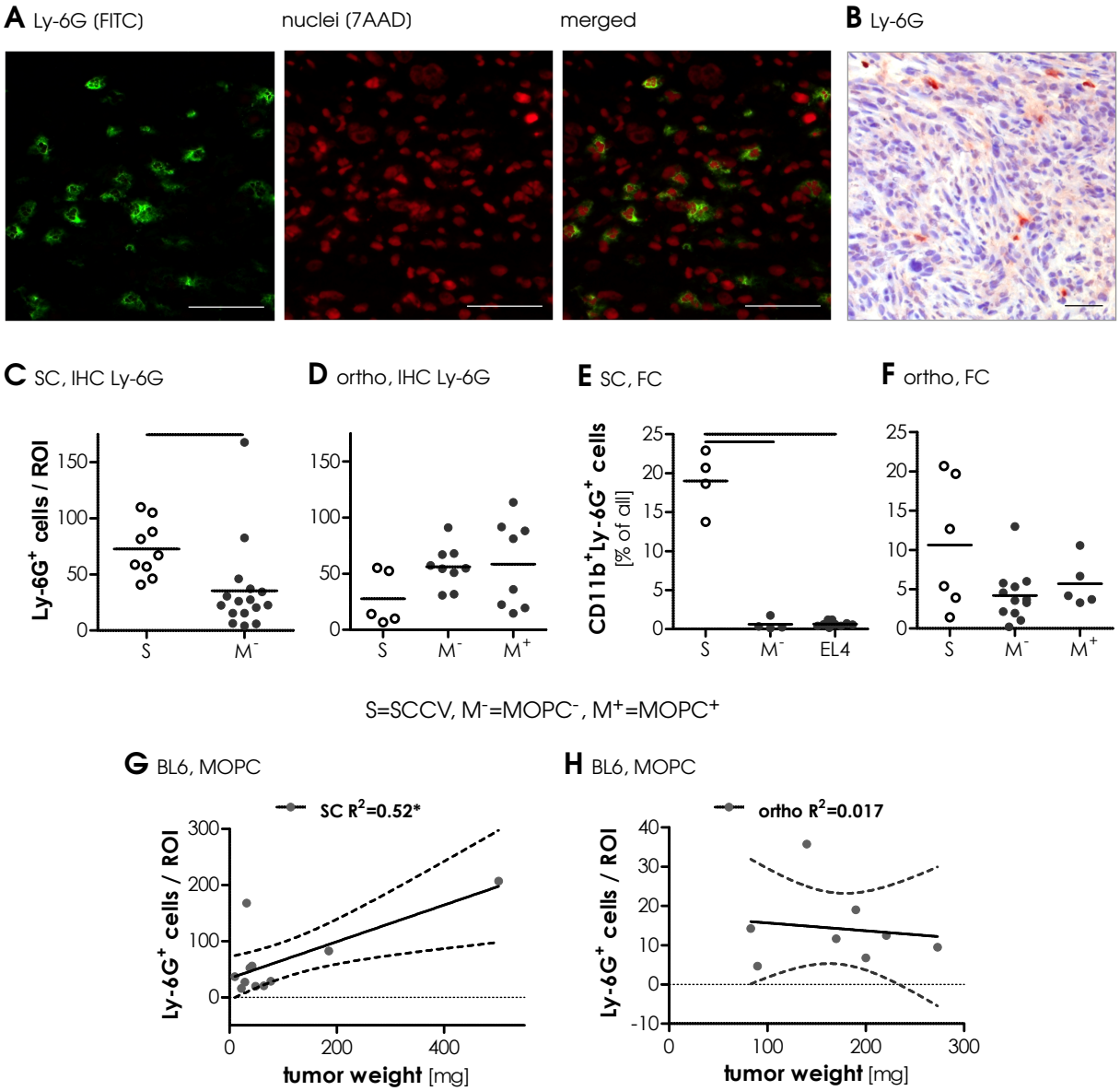

Figure 4.8: Infiltration of Ly-6G cells in the tumor tissue. BL6 and C3H mice have been injected with the respective tumor cells at different locations. Tumor-bearing were sacrificed after two to three weeks and tumor tissue was analyzed. **A** Cryosections were stained for Ly-6G(FITC) and 7AAD. A representative example is shown at 400× magnification. **B** Immunohistochemical staining for Ly-6G is presented at 200× magnification (=$\frac{1}{4}$ROI). The scale represents 50 µm for all photomicrographs. Four of these regions of interest (ROIs) per tumor were manually counted for the number of infiltrating cells as shown in **C** for SC and in **D** for ortho tumors. **E+F** Flow cytometry for $CD11b^+Ly\text{-}6G^+$ cells was performed for different tumors of the SC **E** and ortho **F** administration sites. Immunohistochemical results of BL6 animals as shown in **C+D** were applied to linear regression analysis versus the weight of the respective explanted tumor (**G** for SC and **H** for ortho). Lines indicate linear regression and dotted lines represent the respective 95 % confidence band of the best fit. Significant correlation is indicated by * with $p \leq .05$.

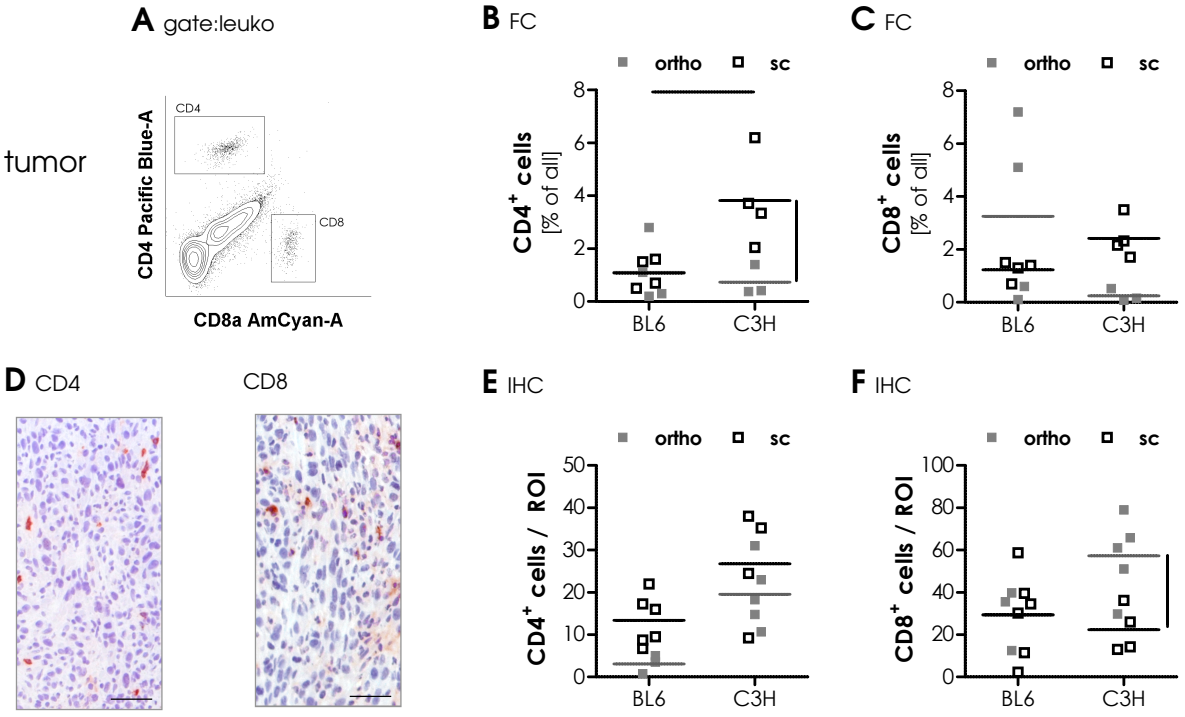

Figure 4.9: Differential T cell infiltration in HNC tumors. BL6 and C3H mice were injected with MOPC$^-$ or SCCVII cells at different locations. Tumor-bearing mice were sacrificed after two to three weeks and tumor tissue was analyzed. **A-C** Flow cytometry was performed for CD4 and CD8 T cells as indicated in **A**. Frequencies of CD4 **B** and CD8 cells **C** were analyzed. **D-F** Cryosections were stained for CD4 or CD8 by immunohistochemistry. Photomicrographs were taken at 200× magnification at four ROIs per tumor. Representative examples are shown in **D** (scale represents 50 µm). Staining was analyzed by manual counting of tumor infiltrating CD4 **E** and CD8 cells **F**. Single tumors are shown as data points and lines indicate means (horizontal) and significance (vertical) as tested by one way ANOVA with $p \leq .05$.

as also regulatory T cells are often found in tumor tissues. To characterize whether T cells infiltrate experimental HNC tumors, BL6 and C3H mice were injected with the MOPC$^-$ or SCCVII tumor cells at the SC or orthotopic site. After two to three weeks of tumor growth, tumors were excised and either subjected to flow cytometry or immunohistochemistry for the analysis of infiltrating CD4 and CD8$^+$ cells (FC gating and representative photomicrographs are shown in figure 4.9A and D). By flow cytometry, frequencies of CD4$^+$ cells were highest in SCCVII SC bearing C3H mice (figure 4.9B). In accordance with CD4 aided CD8 T cell infiltration[69], frequencies of CD8$^+$ cells were also elevated in SCCVII SC versus ortho tumors but did not differ significantly (figure 4.9C). Immunohistochemistry confirmed highest infiltration of CD4$^+$ cells in SCCVII SC tumor but differences were not as clear as in flow cytometry (figure 4.9E). Contrary, CD8$^+$ T cells were most abundant in SCCVII ortho tumors in the histological analysis. In sum, T cells were found to infiltrate HNC tumors in the described mouse model which was dependent on mouse strain and tumor location.

Infiltration of monocytes and NK cells is independent of HNC tumor location

Innate immune cells can differentially affect tumor progression. While NK cells are potential tumor killers, macrophages can be alternatively activated to promote tumor progression and immature dendritic cells further induce immune tolerance[73, 63]. Tumor associated, M2 macrophages are derived from peripheral blood monocytes or monocytic myeloid derived suppressor cells which can be iden-

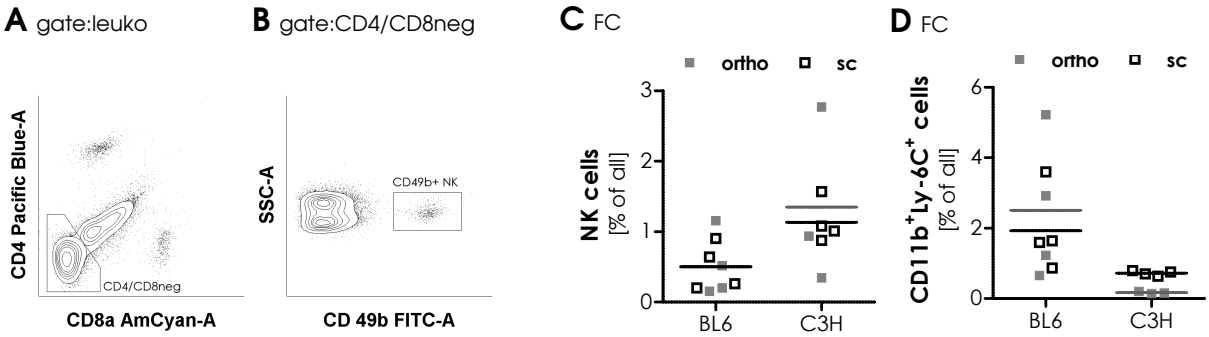

Figure 4.10: Innate immune cell infiltration in HNC tumors. BL6 and C3H mice were injected using MOPC$^-$ or SCCVII cells at different locations. Tumor-bearing mice were sacrificed after two to three weeks and tumor tissue was analyzed. Flow cytometry was performed for CD4 and CD8 negative (as shown in **A**) and CD49b$^+$ NK cells **B**. Frequencies of thereby identified NK cells were analyzed **C**. Monocyte frequencies were assessed by CD11b and Ly-6C positivity **D**. Infiltration did not differ significantly.

tified by the markers CD11b and Ly-6C[222]. For the identification of additional innate immune cell infiltration in HNC tissues, NK cells and monocytes were analyzed by flow cytometry in two to three-week grown SCCVII and MOPC$^-$ tumors. NK cells were therefore identified by CD4 and CD8 negativity and expression of CD49b[7] as shown in figure 4.10A and B. NK cell infiltration did not differ between SC and ortho localization of either SCCVII nor MOPC$^-$ tumors with SCCVII tumors being generally slightly higher infiltrated than MOPC$^-$ (figure 4.10C). For monocytic cells, this trend was reversed and higher frequencies of CD11b$^+$Ly-6C$^+$ cells were present in BL6 tumor bearing mice without difference in localization.

Taken together, the analysis of the composition of tumoral infiltration showed the highest immune infiltrate in SCCVII SC tumors with high CD11b$^+$Ly-6G$^+$ as well as T and NK cell infiltration. T cell infiltration further tended to depend on tumor localization while innate immune cells had consistent tumor type specific infiltration patterns. Additional functional analysis would be necessary to identify direct implications of these differential infiltration patterns.

4.1.5 Importance of CD11b$^+$Ly-6G$^+$ cell localization for regulatory functions

As CD11b$^+$Ly-6G$^+$ cells are modulated at different sites in the tumor bearing host, their functions may differ depending on the tissue specific localization. One functional implication of CD11b$^+$Ly-6G$^+$ cells is immunosuppression which can occur on several sites being the tumor tissue itself as well as in the periphery including the secondary lymphoid organs[153]. Further functions seem to be restricted to the tumor site like promotion of angiogenesis and tissue remodeling resulting in invasion and metastasis[53]. Whether all cells of the population are capable of exerting these functions or functional responses have to be induced by a local phenotypic shift was investigated by a seminal study from Fridlender and colleagues. They presented differential gene expression patterns of naive CD11b$^+$Ly-6G$^+$ cells compared to CD11b$^+$Ly-6G$^+$ cells from tumor bearing mice and between both of them compared to tumor infiltrating Ly-6G$^+$ cells demonstrating the significance of intratumoral localization[55]. These data prompted us to investigate gene expression and functional properties of CD11b$^+$Ly-6G$^+$ cells from different compartments of HNC bearing hosts.

Bone marrow and spleen derived CD11b$^+$Ly-6G$^+$ cells have equal immunosuppressive capabilities

It was suggested in the literature that immunosuppressive properties of CD11b$^+$Ly-6G$^+$ cells are dependent on maturation and localization of these cells[60, 76] in tumor models. This study therefore asked whether bone marrow derived and splenic CD11b$^+$Ly-6G$^+$ cells from HNC tumor bearing mice differ in their capability of suppressing T cells. For this purpose, it was first tested whether splenic immunosuppression might be a mechanism in this tumor model. To this end, spleen tissue from naive and MOPC$^-$ tumor bearing BL6 mice was analyzed for the number of Ly-6G$^+$ cells and proliferating Ki67$^+$ cells by immunohistochemistry. As already demonstrated by flow cytometry in section 4.1.2, this analysis confirmed accumulation of Ly-6G$^+$ cells in tumor bearing mice (figure 4.11A and C, black symbols). Coincidentally, a reduction of proliferating cells was observed suggesting a reduced immune activation in HNC tumor bearing mice (figure 4.11B and C, grey symbols). As a next step, direct suppressive activity of Ly-6G$^+$ cells was assessed. Bone marrow derived Ly-6G cells were isolated from MOPC$^-$ tumor bearing BL6 mice and were added to polyclonally activated and labeled T cells. Proliferation of T cells and respective suppression by the added cells was assessed after three days by flow cytometry. In a ratio of 1 to 10 Ly-6G$^+$ cells to T cells, only minor suppressive activity was observed, whereas up to 80 % of proliferation was suppressed when adding equal numbers of Ly-6G$^+$ to T cells (figure 4.11D). To compare different origins of Ly-6G$^+$ cells, isolation was performed from spleen as well. To this end, MOPC$^-$ tumor bearing CatchUp animals were used to facilitate pure isolation of Ly-6G$^+$ cells by sorting for tdTomato signal. T cell suppression assay was performed according to the bone marrow suppression but different cell ratios were used. Splenic Ly-6G$^+$ cells had minor suppressive activity in a 1 to 20 (Ly-6G$^+$ to T cell) mixture and showed ratio dependent increase of T cell suppression (figure 4.11E). Even though both assays are not directly comparable because different donor mouse strains were used, splenic Ly-6G$^+$ cells seemed to be equally suppressive in lower effector to target ratios than bone marrow derived Ly-6G$^+$ cells. In an exemplary experiment, this trend was not reproduced in a 1:5 ratio with cells derived from the same CatchUp animal (figure 4.11F). Collectively, suppressive activities were demonstrated to be equal for both spleen and bone marrow derived Ly-6G$^+$ cells from HNC tumor bearing animals.

Tumor infiltrating CD11b$^+$Ly-6G$^+$ cells upregulate protumoral modulators

As mentioned in the beginning of this chapter, intratumoral localization adds another level of activation to CD11b$^+$Ly-6G$^+$ cells. HNC tumor derived factors furthermore proved to induce a protumoral phenotype in human neutrophils in *in vitro* studies[39, 203]. A protumoral activation was therefore also hypothesized for intratumoral CD11b$^+$Ly-6G$^+$ cells in our HNC model. For an initial study, splenic and intratumoral CD11b$^+$Ly-6G$^+$ cells were analyzed from MOPC$^-$ SC tumor bearing BL6 mice by flow cytometry. In tumor infiltrating CD11b$^+$Ly-6G$^+$ cells, cell surface expression of CD11b was increased, which may indicate local activation of these cells (figure 4.12A). Intracellular effector molecules showed no consistent regulation in this analysis. While iNOS was slightly increased (figure 4.12B), Arginase1 protein expression was rather decreased in tumor infiltrating CD11b$^+$Ly-6G$^+$ cells (figure 4.12C). As effector proteins could be released to the microenvironment prior to analysis, gene expression was to be assessed for further analysis of the activation status of tumor infiltrating CD11b$^+$Ly-6G$^+$ cells. To isolate Ly-6G$^+$ cells as gentle as possible, CatchUp mice were used and tdTomato$^+$ cells were sorted without additional antibodies that might further activate the cells. For

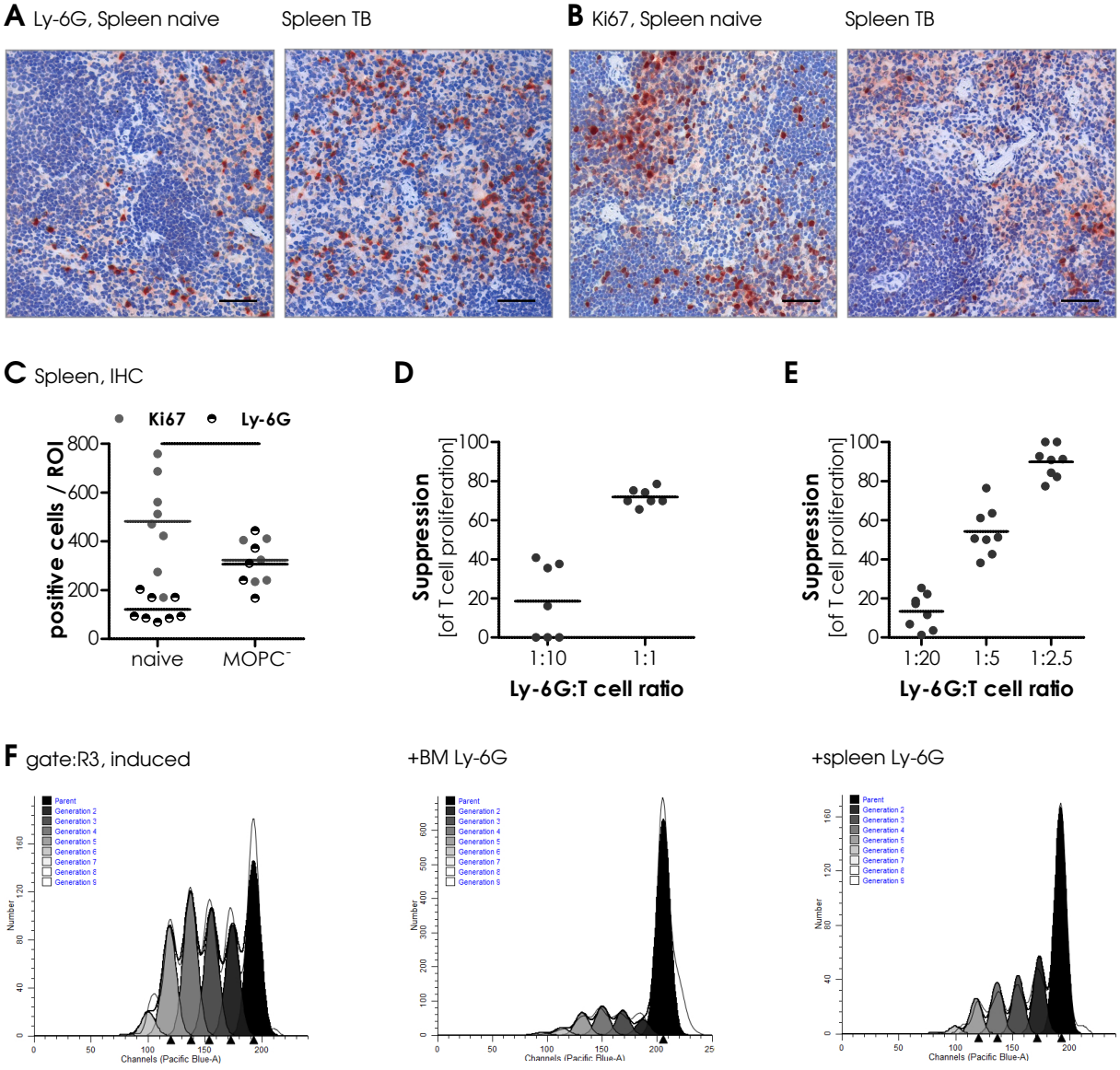

Figure 4.11: T cell suppression by splenic and bone marrow derived Ly-6G cells. **A-C** Spleen cryosections from tumor-bearing and naive BL6 mice were stained for Ly-6G and Ki67. Representative photomicrographs for Ly-6G **A** and Ki67 **B** are shown at 200 × magnification with a scale representing 50 µm. **C** Positive cells were counted in 4 ROIs and each symbol indicates the mean of a mouse. The line indicates significance at $p \leq .05$ as determined by student's *t*-test. **D-F** Bone marrow derived Ly-6G$^+$ cells were isolated from tumor bearing BL6 mice by MACS technique. Ly-6G$^+$ cells from spleen were isolated from CatchUp mice by sorting of tdTomato$^+$ cells. T cells were isolated from the respective animals by sorting for CD3ϵ stained cells. Proliferation dye 450-labeled T cells were stimulated by 50 U / mL IL2 and CD3/CD28 Beads and Ly-6G cells were added in different ratios. Proliferation was assessed by flow cytometry after three days and suppression by Ly-6G cells from bone marrow **D** and spleen **E** was calculated. Representative histograms for induction of proliferation, suppression by bone marrow-derived Ly-6G cells and suppression by spleen-derived Ly-6G cells are shown in **F**.

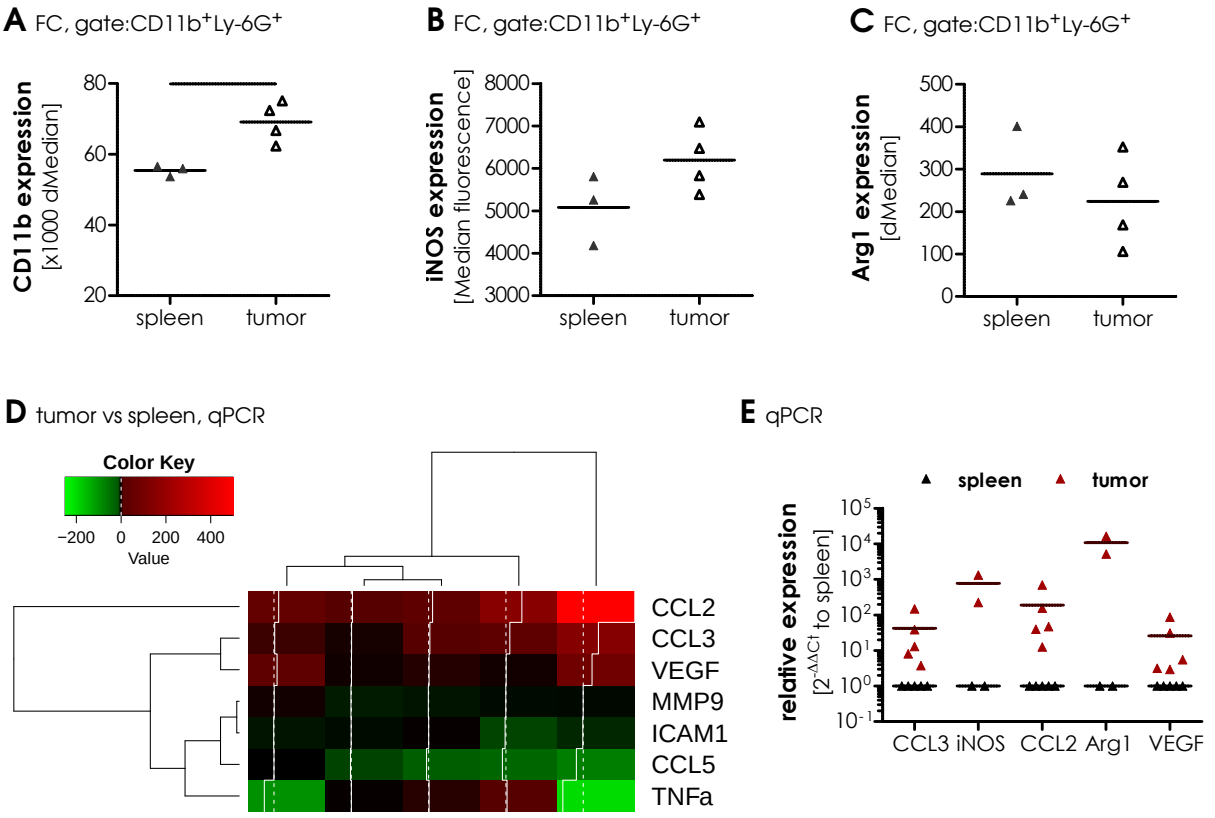

Figure 4.12: Tumor infiltration results in activation of protumoral mediators. BL6 and CatchUp mice were injected with MOPC$^-$ cells SC. **A** Spleen and tumor were isolated from BL6 animals after two weeks and analyzed by flow cytometry. Cells were stained for CD11b and Ly-6G and median cell surface expression of CD11b **A** as well as intracellular iNOS **B** and Arg1 **C** were analyzed on these cells. **D+E** Ly-6G$^+$ cells were isolated from tumors and spleens of five CatchUp animals by sorting for tdTomato signal. mRNA expression was assessed by qPCR. Relative gene expression was calculated after normalization to β-actin comparing tumor and spleen-derived cells in a hierarchical clustering analysis **D**. Selected increased genes are shown in **E** also including iNOS and Arg1 which were only detectable in two animals.

five CatchUp animals, cells were isolated from spleen and tumor after three weeks of tumor growth. Gene expression analysis was performed on a set of target genes which are differentially regulated in pro versus antitumoral CD11b$^+$Ly-6G$^+$ cells as described by Fridlender *et al.*[54]. Differential gene expression of tumor infiltrating and spleen derived CD11b$^+$Ly-6G$^+$ cells could be demonstrated in an hierarchical cluster analysis (figure 4.12D). Antitumoral markers, such as ICAM-1 and TNFα, thereby clustered in a group that is downregulated in tumor versus splenic Ly-6G$^+$ cells. Furthermore, upregulation of the chemokines CCL2 and CCL3 was very pronounced in the tumor, which may result in attraction of additional immune cells and thereby promoting tumor associated inflammation. Consistently upregulated genes were summarized in figure 4.12E by the $2^{-\Delta\Delta C_T}$ analysis versus spleen. Thereby it became apparent that also angiogenesis promoting VEGF is highly induced upon infiltration in the tumor. Only in two out of five animals, Arg1 and iNOS mRNA was detectable in both groups. Nevertheless, upregulation was induced in tumor infiltrating CD11b$^+$Ly-6G$^+$ cells in the mice with positive PCR results for Arg1 and iNOS. Thus, intratumoral activation of CD11b$^+$Ly-6G$^+$ cells is crucial for inducing a protumoral phenotype shift.

Taken together, a HNC mouse model was established resembling tumor cell immune interactions

which can also be found in HNC patients. CD11b$^+$Ly-6G$^+$ cells further accumulated in the periphery of advanced HNC tumor bearing mice. Functionally, it was possible to show immunosuppressive functions of CD11b$^+$Ly-6G$^+$ cells independent of localization in bone marrow or spleen of HNC tumor bearing mice. Additionally, infiltration into the tumor tissue further activated Ly-6G$^+$ cells as seen by cell surface CD11b expression and induction of a protumoral gene expression pattern. Immunosuppressive activity of intratumoral CD11b$^+$Ly-6G$^+$ cells was implied by induction (gene expression) and release (low protein content) of Arginase1 and induction of iNOS expression (mRNA and protein). These data suggest several levels of suppression of antitumor responses by CD11b$^+$Ly-6G$^+$ cells in HNC hosts and additional protumoral functions that become activated upon infiltration into the tumor tissue. These HNC models with either SC or orthotopic localization are therefore well suited for the analysis and further characterization of CD11b$^+$Ly-6G$^+$ cell protumoral activities.

4.2 Implication of Ly-6G$^+$ cells in HNC tumor progression

It has been demonstrated that HNC tumors in murine models interact with CD11b$^+$Ly-6G$^+$ cells and induce their accumulation in the periphery. A general status of T cell suppression may be mediated by these cells in the HNC hosts. Furthermore, infiltration and activation in the tumor microenvironment was described in the previous chapter. Nevertheless, additional immune cells were shown to infiltrate these experimental tumors and these carry the potential of influencing tumor progression as well. At least some of these cells might be attracted by CD11b$^+$Ly-6G$^+$ cell derived chemokines further complicating the tumor-immune cell crosstalk. The next part of this study therefore aimed to analyze the importance of CD11b$^+$Ly-6G$^+$ cells for tumor progression in this HNC model by either direct or indirect effects. To this end, CD11b$^+$Ly-6G$^+$ cell depletion was utilized as a technique that is often used to analyze granulocyte functions in different disease states such as infection, autoimmunity and cancer[24, 32, 119]. αGr-1 (clone RB6-8C5) and αLy-6G (1A8) monoclonal antibodies (mAb) were used to deplete CD11b$^+$Ly-6G$^+$ cells. For the analysis of longitudinal tumor growth, application of antibodies was continued throughout the experiment in a three-days interval.

4.2.1 Effect of neutrophil depletion on establishment of tumors and progression of advanced tumors

As tumor progression is characterized by different stages, it is therefore possible that neutrophils could promote all or a number of these stages. While immune evasion and vascularization are critical during the establishment of a tumor, invasiveness and metastasis become more important in advanced disease[206]. In experimental tumors, similar phases can be found. Upon tumor injection, seeding to the organ takes place, which can be supported by structural remodeling and adjustment of the microenvironment. Initial tumor growth can furthermore only occur upon induction of vascularization. If immunosuppression is not mediated, experimental tumors can get rejected after one week[101]. Supporting invasiveness further results in enhanced tumor growth. Therefore, implication of CD11b$^+$Ly-6G$^+$ cells was assessed during tumor cell seeding as well as during late progression in this HNC model.

Advanced tumors grow independent of CD11b$^+$Ly-6G$^+$ cells

A study by Mishalian and colleagues suggested that murine CD11b$^+$Ly-6G$^+$ cells are only implicated in

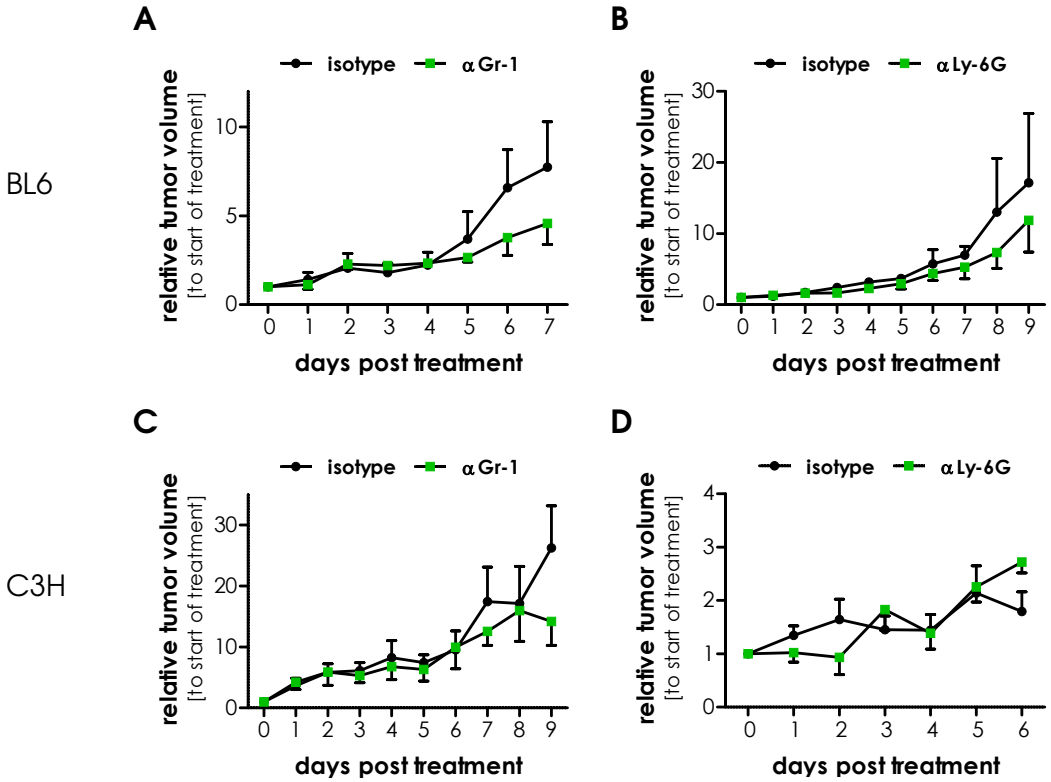

Figure 4.13: Advanced tumor growth proceeds relatively independent of Ly-6G cells. Tumor-bearing mice (n=4-5) were continuously treated with CD11b$^+$Ly-6G$^+$ cell-depleting antibodies as soon as a tumor size of 3-5 mm was reached in one dimension. Tumor growth was assessed in BL6 (**A+B**, MOPC$^-$) and C3H mice (**C+D**, SCCVII) treated with either αGr-1 **A+C** or αLy-6G **B+D**. Data are presented as mean±SEM of the relative volume to the tumor volume when starting treatment (tumor size at start of treatment was set to 1).

advanced tumor progression in a model using lung tumor or mesothelioma cells[133]. To investigate whether a similar mechanism is present in the described HNC models, established tumor bearing mice were depleted of CD11b$^+$Ly-6G$^+$ cells. To this end, the SC tumor model was chosen to enable the determination of exact tumor volumes. MOPC$^-$ and SCCVII tumors were monitored daily under continuous depletion of Ly-6G$^+$ cells. In BL6 mice, tumor growth was slightly reduced after 5 days of depletion using αGr-1 antibody (figure 4.13A). This tendency was confirmed when using αLy-6G to more specifically address CD11b$^+$Ly-6G$^+$ cells (figure 4.13B). Nevertheless, these differences only account for very small effects as no statistical significance was obtained. Contrary, this trend was even smaller in SCCVII tumor bearing C3H mice when depleting with αGr-1 (figure 4.13C). Surprisingly, a slight early reduction of tumor growth was observed when SCCVII tumors were depleted using the αLy-6G antibody but this is reverted into unchanged progression after day 2 (figure 4.14D). In sum, only a minor influence on advanced tumor progression could be demonstrated for CD11b$^+$Ly-6G$^+$ cells in the HNC tumor model.

CD11b$^+$Ly-6G$^+$ cells mediate tumor establishment

An effect of CD11b$^+$Ly-6G$^+$ cells on advanced tumor progression was not confirmed in this study. Therefore, the mechanism indicated in the study by Mishalian did not seem to be shared by the herein used HNC cell lines. They also indicated that early tumor growth can not be affected by depletion because CD11b$^+$Ly-6G$^+$ cells did not enter their tumors in early stages but were located in the tumor

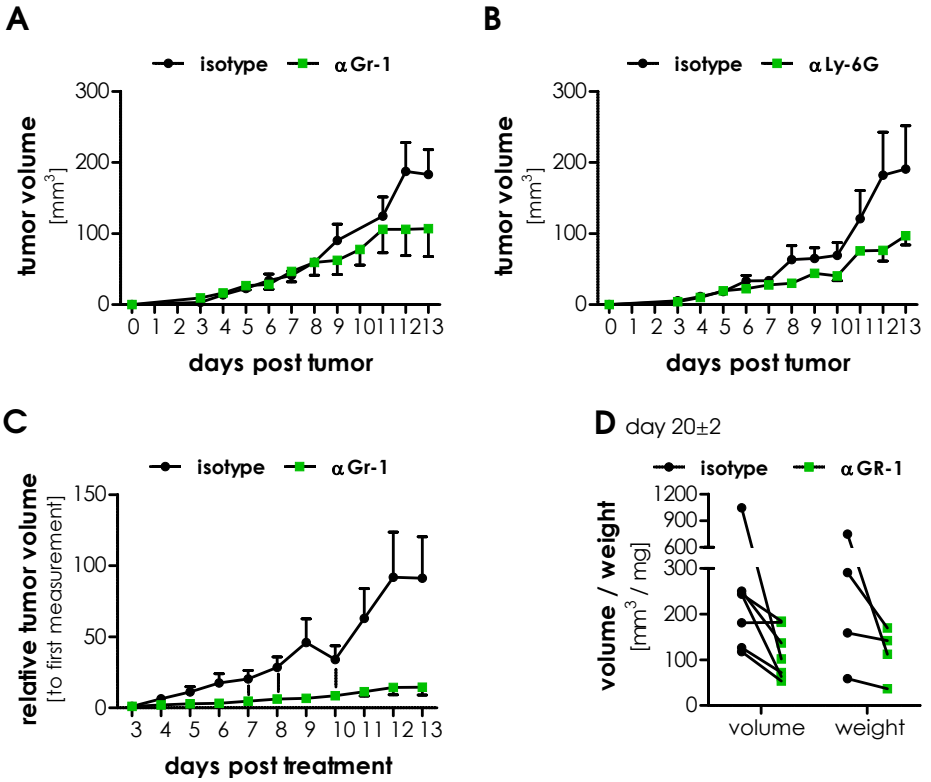

Figure 4.14: Ly-6G cells mediate tumor establishment. BL6 mice (n=4) were depleted of CD11b$^+$Ly-6G$^+$ cells by injection of specific antibodies. After 2 days, MOPC$^-$ tumor cells were injected SC and tumor size was determined under continuous antibody applications. Depletion was carried out using either Gr-1 **A** or Ly-6G **B** specific antibodies. Relative tumor volume was calculated to day 3, which was the first day of tumor measurement for Gr-1 depleted animals **C**. Data are presented as mean±SEM and lines indicate significant differences calculated by student's *t*-test with $p \leq .05$. Final tumor volume and weight of tumor explants from Gr-1 treated animals was assessed at days 18-22 **D**.

periphery[133]. Contrary, immunohistochemistry indicated considerable infiltration of CD11b$^+$Ly-6G$^+$ cells within the first days in the HNC model (data not shown). As a consequence, the impact of this early presence of CD11b$^+$Ly-6G$^+$ cells in HNC tumor bearing mice was analyzed. For this analysis, BL6 mice were depleted of CD11b$^+$Ly-6G$^+$ cells and MOPC$^-$ tumor cells were injected SC into the CD11b$^+$Ly-6G$^+$ cell free mice 2 days after start of treatment. Tumor growth was monitored to evaluate an influence of CD11b$^+$Ly-6G$^+$ cells on this stage of tumor progression and treatment was continued during the whole experiment. First, both isotype and αGr-1 treated animals developed small tumors within three days. After one week, a reduced tumor size became apparent in the depleted group (figure 4.14A). To confirm that this effect was mediated by the absence of Ly-6G and not Ly-6C cells, the experiment was repeated using αLy-6G antibody. Again, tumors appeared simultaneously but depleted animals consistently develop slow growing tumors (figure 4.14B). The reduced tumor growth was even more pronounced when analyzing the relative tumor volume to day 3, which indicates the speed of tumor progression (figure 4.14C). Accordingly, final tumor volumes and weights, as measured between day 18 and 22 when the experiment was finished, were reduced in αGr-1 treated animals compared to respective isotype treated controls (figure 4.14D).

Collectively, this data provides strong evidence for an implication of CD11b$^+$Ly-6G$^+$cells in early tumor formation and seeding in the HNC model. Furthermore, late tumor progression is less affected

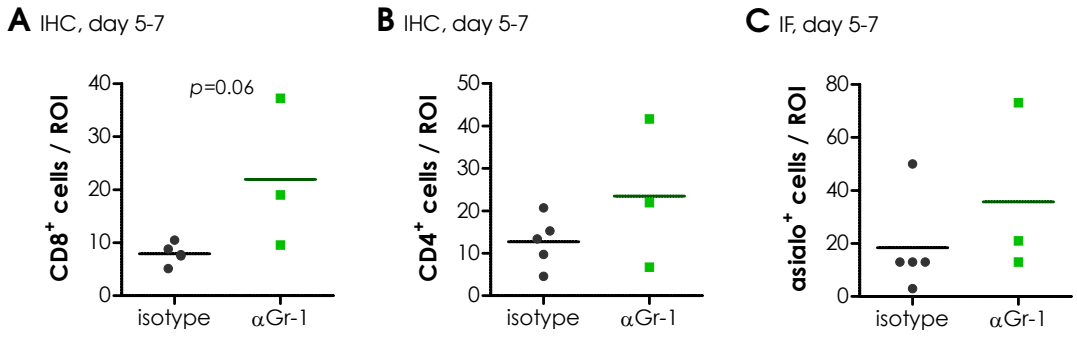

Figure 4.15: Enhanced T cell infiltration in depleted tumors. BL6 mice were depleted of CD11b$^+$Ly-6G$^+$ cells using αGr-1 mAB. After 2 days, MOPC$^-$ tumor cells were injected SC and antibody application was continued. Tumors were isolated 5-7 days after tumor cell injection and analyzed by immunohistochemistry (T cells) and fluorescence microscopy (NK cells). Tumor infiltrating CD8 **A** and CD4 **B** T cells as well as asialo$^+$ NK cells **C** were assessed by manual counting of 4 ROIs per tumor at 200× magnification.

by the presence or absence of CD11b$^+$Ly-6G$^+$ cells.

4.2.2 T cell dependent delay of early tumor growth

The presence of CD11b$^+$Ly-6G$^+$ cells enhanced HNC tumor growth especially in the early phase of tumor progression. Nevertheless, differences in tumor volumes were rather manifested with some delay while formation of the first visible small tumor nest was not affected. It is therefore likely that an antitumoral adaptive immune response is hosted in neutropenic tumor bearing mice. As a next step, it was obvious to analyze the role of anti tumor effector cells in growth delay by CD11b$^+$Ly-6G$^+$ cell depletion.

Early tumor infiltration and immune cell distribution is changed upon depletion

Potential antitumor effector cells are T as well as NK cells which can attack tumor cells directly via perforin and granzyme and by Fas ligation[180]. To investigate whether CD11b$^+$Ly-6G$^+$ cells in the HNC model suppress these antitumor effectors thereby facilitating especially early tumor progression, tumor tissues were analyzed in the early establishment phase. For this purpose, MOPC$^-$ cells were injected into CD11b$^+$Ly-6G$^+$ cell depleted and undepleted BL6 mice. Tumors were isolated between day 5 and 7 of tumor progression and analyzed by immunohistochemistry. Early tumors were found to be consistently higher infiltrated with T cells when mice were treated with αGr-1 antibody (figure 4.15). This trend was most clearly observed for CD8$^+$ cells (figure 4.15A) but also CD4$^+$ cell density increased slightly (figure 4.15B). NK cell infiltration was assessed by fluorescence microscopy on the same tumors but for these cells, no differential infiltration was found (figure 4.15C). Thus, enhanced T cell infiltration in Gr-1 depleted mice indicated a T cell suppressive function for CD11b$^+$Ly-6G$^+$ cells in the HNC model.

T cells partially mediate delayed tumor growth

After having shown that T cells can enter CD11b$^+$Ly-6G$^+$ cell depleted tumors more easily than in neutrophil competent mice, the impact of this infiltration had to be determined. Do T cells in neutropenic mice mediate delayed tumor progression? To answer this question, a combination of Gr-1 and CD8 depletion was performed. BL6 mice were continuously depleted using antibodies against

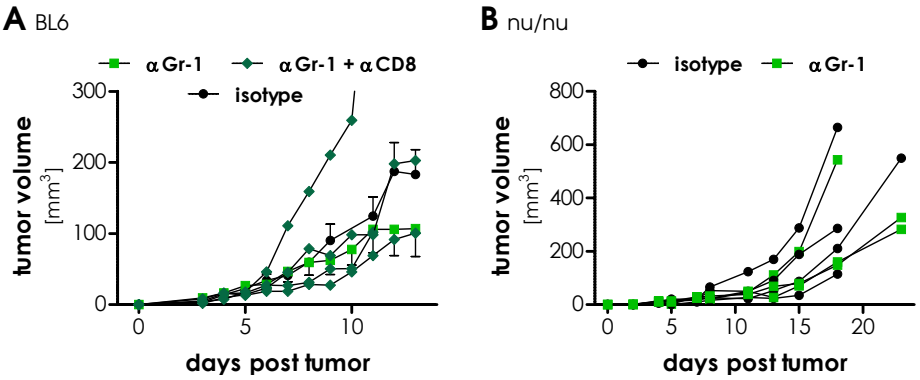

Figure 4.16: Depletion of CD8 T cells does not necessarily diminish Gr-1 depletion effects. **A** BL6 mice (n=4) were depleted of either CD11b$^+$Ly-6G$^+$ cells alone using αGr-1 mAB or CD11b$^+$Ly-6G$^+$ cells and CD8 T cells by additional application of the mAB 2.43. After 2 days, MOPC$^-$ tumor cells were injected SC and tumor size was determined under continuous antibody applications. Data are presented as mean±SEM for the Gr-1 group and single growth curves are shown for Gr-1 + CD8 depletion. **B** Athymic nude mice were injected with MOPC$^-$ tumor cells with or without depletion by Gr-1 mAB and tumor growth was monitored. Single growth curves are shown.

CD11b$^+$Ly-6G$^+$ cells or both cell types and MOPC$^-$ cells were injected SC to monitor tumor progression. Again, Gr-1 depletion reduced tumor growth, but additional CD8 depletion did not ultimately result in abolishment of this effect (figure 4.16A). Only in two out of four double depleted animals, tumor growth was enhanced compared to the Gr-1 depleted group. To exclude additional effects by CD4 T cells, a tumor growth analysis was carried out in athymic nu/nu mice. These mice lack mature T cells of both types and are therefore unable to mount an antitumor T cell response. nu/nu mice were depleted of CD11b$^+$Ly-6G$^+$ cells using αGr-1 antibody and MOPC$^-$ tumor cells were injected to monitor tumor growth. Two out of three depleted and one out of four undepleted tumors grew slowly in nu/nu mice but one of the depleted tumors also grew nearly as fast as the fastest undepleted tumor (figure 4.16B). Therefore, Gr-1 cells do not seem to influence tumor growth in nu/nu mice as they do in BL6 mice.

This data indicate that T cells are implicated in reduction of tumor growth by CD11b$^+$Ly-6G$^+$ cell depletion. T cells infiltrated depleted tumors to a higher extent than CD11b$^+$Ly-6G$^+$ cell competent tumors. Nevertheless, depletion of CD8$^+$ cells alone was not capable of restoring normal tumor growth in all mice. Equal tumor growth in nu/nu mice independent of the presence of Ly-6G$^+$ cells suggests that both CD8 and CD4 T cells might be involved in the observed growth delay.

4.2.3 CD11b$^+$Ly-6G$^+$ cells facilitate tumor establishment by structural remodeling of host tissue

Early tumor growth was slowed in Gr-1 and Ly-6G depleted animals. At least in BL6 animals, not only CD8 T cells were responsible for reduction of tumor growth. To investigate additional mechanisms by which CD11b$^+$Ly-6G$^+$ cells could mediate tumor progression, tumor vascularization was assessed. Induction of VEGF expression in tumor infiltrating neutrophils as shown in section 4.1.5 already indicated an influence of CD11b$^+$Ly-6G$^+$ cells on tumor angiogenesis. This was furthermore shown by studies in other tumor models where depletion was used as well[90]. Furthermore, vessel density was reduced in depleted orthotopic MOPC$^-$ tumors but not in SC tumors when analyzed after one to

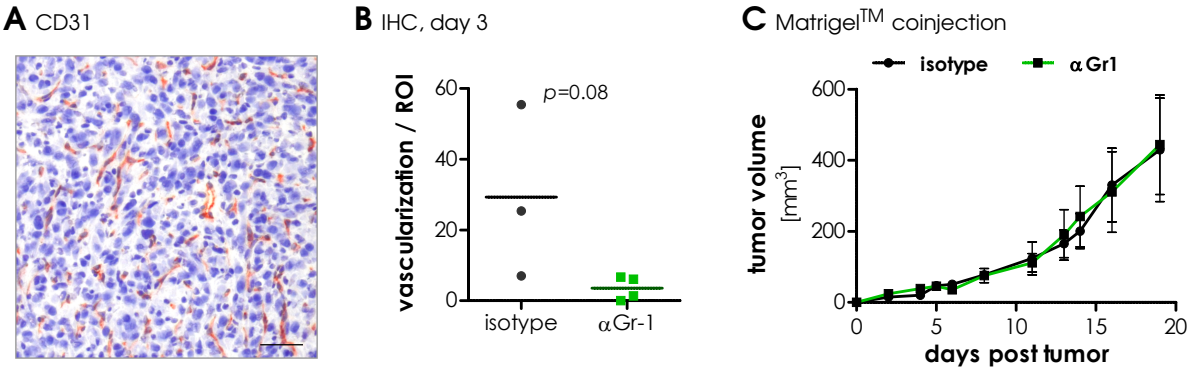

Figure 4.17: Ly-6G cells provide structural support for the tumor. Intratumoral vessel density was assessed by immunohistochemical staining **A** (scale represents 50 µm). Vessel density was analyzed in MOPC$^-$ tumors isolated at day 3 from mice which were depleted by αGr-1 or treated with isotype mAB. To this end, the number of CD31$^+$ vessels was counted manually in 4 ROIs per tumor at 200× magnification **B**. Significance was tested by student's *t*-test. BL6 mice were depleted using αGr-1 and injected with tumor cells in a PBS Matrigel^{TM} mixture. Tumor growth was followed for 20 days **C**.

two weeks (data not shown). To assess a very early effect on tumor vascularization, BL6 mice were depleted of neutrophils using αGr-1 antibody and MOPC$^-$ cells were injected into either depleted or isotype treated mice. Tumor vascularization was assessed as soon as a small tumor mass was visible at day 3 after tumor cell injection. Analysis was carried out by immunohistochemical staining of CD31 identifying endothelial cells (figure 4.17A). Microvessel density, as reflected by the number of CD31$^+$ cells per region of interest, was remarkably reduced in CD11b$^+$Ly-6G$^+$ cell depleted tumors (figure 4.17B). To demonstrate that support by induction of angiogenesis and tissue remodeling is inducing neutrophil enhanced tumor seeding, this support was mimicked by coinjection with Matrigel^{TM}. Matrigel^{TM} MOPC$^-$ mixtures were injected SC into Gr-1 depleted or isotype treated BL6 mice and tumor growth was monitored. Notably, Matrigel^{TM} tumors grew faster than in the normal SC model even though only one fifth of the normal cell number was injected. Tumor growth was unaffected by depletion of CD11b$^+$Ly-6G$^+$ cells in this growth factor rich tumor model (figure 4.17C). Accordingly, direct tumor support by growth factors, vascularization and tissue remodeling is involved in CD11b$^+$-Ly-6G$^+$ cell mediated tumor establishment.

Taken together, the presented data indicate a crucial role of CD11b$^+$Ly-6G$^+$ cells in establishment of HNC tumors rather than promoting advanced tumor progression. The underlying mechanism was identified by a lack of Ly-6G$^+$ cell mediated T cell suppression as well as missing structural and angiogenesis inducing support for tumor cell seeding by CD11b$^+$Ly-6G$^+$ cells. Furthermore, it is unique that both mechanisms could be described in one study thereby implicating that tumor associated CD11b$^+$Ly-6G$^+$ cells mediate diverse protumoral functions simultaneously.

4.3 Detailed characterization of neutrophil depletion in tumor bearing mice

Tissue specific functional activity of Ly-6G$^+$ cells is only starting to emerge[55] and beside *ex vivo* analysis of isolated cells, *in vivo* depletion is often used to assess functional implications of these cells. The data presented in this study also convincingly demonstrated how antibody mediated depletion can reveal mechanisms of CD11b$^+$Ly-6G$^+$ cells in tumor bearing hosts. Nevertheless, it was also indicated in chapter 4.1.2 that CD11b$^+$Ly-6G$^+$ cell dynamics are affected by tumor burden in this HNC model in accordance with studies in other tumor models[222]. As tumor derived factors inducing myeloid cell expansion might interfere with the applied technique of antibody mediated depletion, this part of the study aimed to investigate the efficacy of CD11b$^+$Ly-6G$^+$ cell depletion in HNC tumor bearing mice.

4.3.1 The phases of CD11b$^+$Ly-6G$^+$ cell depletion in the peripheral blood

As peripheral blood is easily available in small amounts, the efficacy and duration of antibody mediated *in vivo* depletion is usually only monitored in blood by most of the studies. This study therefore started to assess depletion efficacy in the peripheral blood in HNC bearing mice as well.

Complete peripheral blood depletion

The presence of a tumor was shown to induce peripheral blood expansion of CD11b$^+$Ly-6G$^+$ cells (chapter 4.1.2). To assess whether this expansion can be overcome by antibody mediated depletion and to investigate the efficacy of the treatment, MOPC$^-$ tumor bearing mice were depleted using αGr-1 or αLy-6G antibodies starting at a tumor size of 5 mm. Depletion was continued by antibody application on every third day and Ly-6G$^+$ cell frequencies were monitored in tail vein blood by flow cytometry daily. In accordance with many other studies which analyze treated animals after 24 hours, Ly-6G$^+$ cells were drastically reduced after one day and also remained completely depleted for several days for both αGr-1 (figure 4.18A) and αLy-6G (figure 4.18B) treatment. A comparable efficacy was demonstrated in SCCVII bearing C3H animals (not shown). To further verify flow cytometry results, blood smears from identically treated BL6 animals were analyzed microscopically using Pappenheim's staining. No segmented or banded neutrophil granulocytes were observed by this technique for the same period of observation while Ly-6G negative eosinophils remained present (not shown). Thus, HNC tumor burden does not interfere with the onset of antibody mediated depletion.

Rebound of CD11b$^+$Ly-6G$^+$ cells upon continued depletion pressure

Many cancer studies, including this one, monitor and treat tumor bearing mice for longer than one week with CD11b$^+$Ly-6G$^+$cell depleting antibodies. In a majority of studies, the treatment approached or exceeded three weeks[197, 4, 54, 67, 92, 113, 139, 150] with depletion efficacy being often only mentioned in the methods section but not directly demonstrated. This study therefore analyzed peripheral blood depletion for a longer period in mice carrying HNC MOPC$^-$ tumors. Depletion was achieved by αGr-1 injection in 5 mm tumor bearing mice and was repeated every third day. Starting with normal Ly-6G$^+$ cell numbers (figure 4.19A), complete depletion was induced rapidly and was stable for at least 5 days in the peripheral blood (figure 4.19B). Nevertheless, after some additional time on day 10, Ly-6G$^+$ cells started to be detectable (figure 4.19C) and two weeks after start of treatment, normal Ly-6G$^+$ cell frequencies were present in the blood of continuously treated tumor bearing animals (figure 4.19D). Thus, complete depletion was found to be very transient in the peripheral blood of

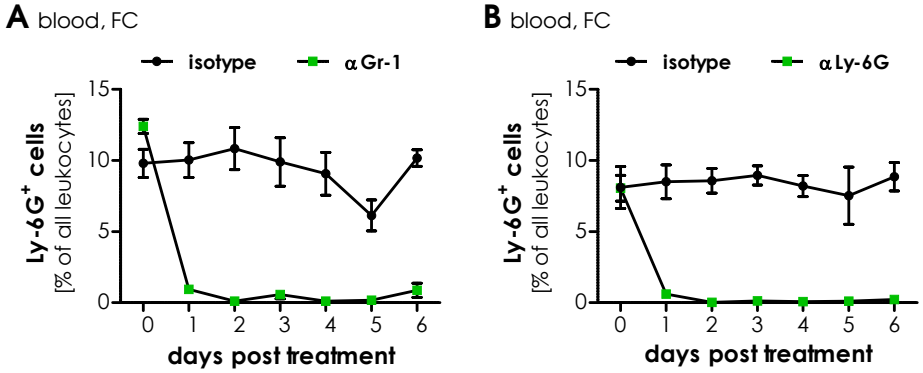

Figure 4.18: Ly-6G cells are depleted from the peripheral blood for several days. MOPC$^-$ tumor-bearing mice were continuously depleted using either αGr-1 **A** or αLy-6G mAB **B** starting at a tumor size of 3-5 mm. Frequencies of peripheral blood Ly-6G$^+$ cells were determined daily in tail vein blood by flow cytometry.

tumor bearing animals. Ly-6G$^+$ cells started to reappear to detectable numbers after approximately one week under continued antibody applications and reached normal levels after some additional days which was consistent over several experiments as summarized in figure 4.19E. Using αLy-6G antibody to deplete neutrophils resulted in similar kinetics of CD11b$^+$Ly-6G$^+$ cell rebound as well as when depleting in tumor bearing C3H mice (not shown).
These data demonstrate for the first time that CD11b$^+$Ly-6G$^+$ cells rebound upon antibody mediated depletion within two weeks under continued antibody application. Treatment with Ly-6G$^+$ cell depleting antibodies thereby is divided into two phases: the complete peripheral blood depletion phase and the phase of CD11b$^+$Ly-6G$^+$ cell rebound. Notably, it was not possible to prolong the complete peripheral depletion phase neither by increasing antibody application frequencies nor by switching epitope specificity of the applied antibody between Gr-1 and Ly-6G (not shown).

4.3.2 Total peripheral blood depletion phase - the resistant neutrophil reservoir

As already indicated above, depletion is most often monitored in the peripheral blood but tissue specific functions of CD11b$^+$Ly-6G$^+$ cells are critical for several effector functions. Furthermore, recent studies revealed depletion resistance of bone marrow cells in naive mice[163] as well as inefficient depletion in the liver in experimental tumor models[123]. Based on these observations, depletion efficacy was monitored in different tissue compartments of HNC tumor bearing mice in the present study.

Undepleted bone marrow cells are covered with depletion antibody

When analyzing the function of cells by depleting the respective cell type, it is critically important that the targeted cells are removed from the organs in which they exert these functions. Given the above stated studies, different organs were analyzed during the complete peripheral blood depletion phase. To this end, MOPC$^-$ tumor bearing mice were depleted of neutrophils using αGr-1 or αLy-6G antibodies. The organs of interest were isolated after several days of treatment and analyzed by flow cytometry for CD11b and Ly-6G positive cells. By αGr-1 antibody treatment, significant reduction of the frequency of CD11b$^+$Ly-6G$^+$ cells was observed in all organs except for liver (figure 4.20A). The same holds true for bone marrow and spleen from mice treated with αLy-6G antibody (figure 4.20B).

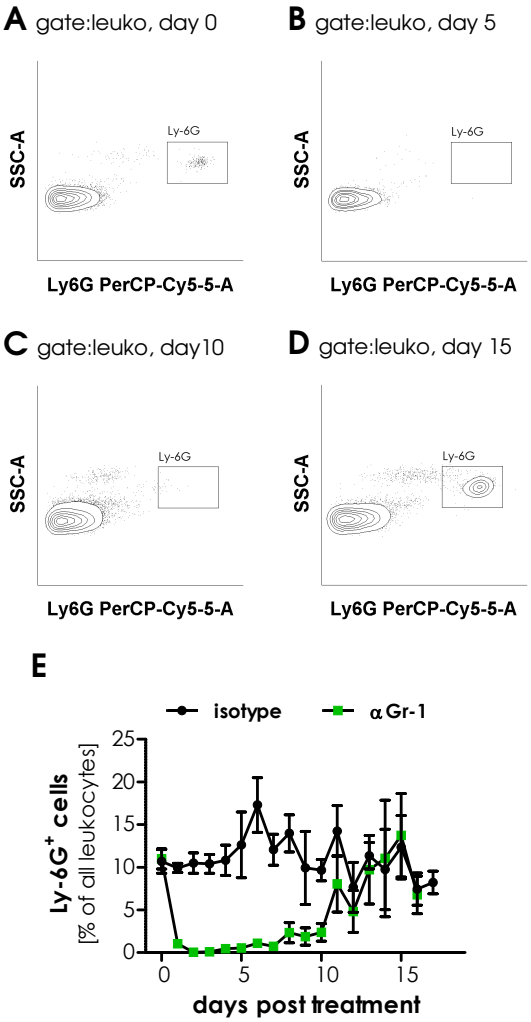

Figure 4.19: Ly-6G cell reappear under depletion pressure. MOPC$^-$ tumor-bearing mice were continuously depleted using αGr-1 mAB. Frequencies of peripheral blood Ly-6G$^+$ cells were determined in tail vein blood by flow cytometry. **A-D** show representative flow cytometry plots at different stages of depletion being day 0 (**A**, before antibody injection) as well as day 5 **B**, day 10 **C**, showing the first reappearing cells, and day 15 **D**, indicating increased numbers of Ly-6G$^+$ cells. **E** shows means±SEM of 6 experiments with 36 mice in total, which have been measured on different days.

Surprisingly, a prominent reduction of stained cells was also observed in the bone marrow. Detailed analysis of the progression of depletion in the bone marrow revealed normal CD11b$^+$Ly-6G$^+$ cell frequencies already at day 10 preceding peripheral blood reappearance and an increase by 50 % at day 16 (figure 4.20C). When analyzing day 4-5 flow cytometry results in more detail, unchanged numbers of CD11b positive cells become apparent in Gr-1 depleted animals during complete peripheral blood depletion (figure 4.20D). This indicated limitations in conventional flow cytometry for the detection of these cells in antibody treated animals. Overestimation of Ly-6G$^+$ cell depletion in the bone marrow was further validated by directly staining isolated cells with anti-rat secondary antibody which was able to bind to the *in vivo* antibody coated bone marrow derived Ly-6G$^+$ cells (figure 4.20E). As these results were alarming for the estimation of depletion efficiency in other organs as well, a similar analysis was carried out in spleen derived cells. CD11b$^+$Ly-6G$^+$ cell frequencies are much lower in this organ under normal conditions and the described analysis was not able to confirm any antibody coverage on CD11b$^+$Ly-6G$^+$ cells from splenocytes of depletion antibody treated animals (figure 4.20F and G). These results reveal that depletion is rather inefficient and classical flow cytometry for Ly-6G$^+$ cell counts is not reliable in bone marrow due to epitope masking by the depletion antibody while similar antibody coating was not observed in other organs during peripheral blood depletion.

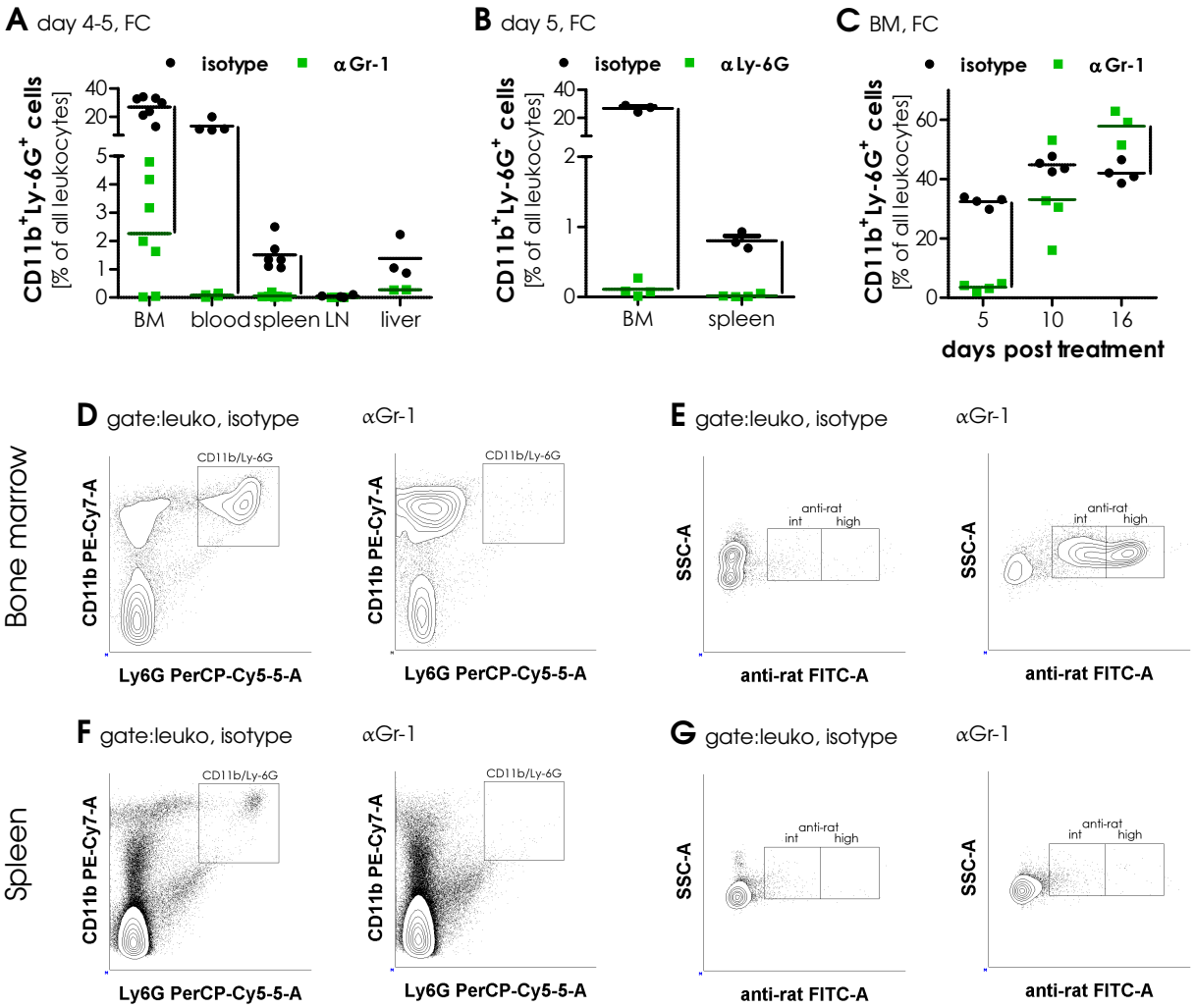

Figure 4.20: Bone marrow cells are not depleted but covered with antibody. MOPC$^-$ tumor-bearing mice were continuously depleted using αGR-1 or αLy-6G mAB as indicated. CD11b$^+$Ly-6G$^+$ cells were analyzed by flow cytometry in different organs. **A** Gr-1 treated animals were analyzed for frequencies of CD11b$^+$-Ly-6G$^+$ cells in bone marrow, spleen, blood, liver and lymph nodes (LN) on day 4-5 after depletion. **B** Bone marrow and spleen from Ly-6G treated animals was measured on day 5 after tumor injection. **C** Time dependent changes in bone marrow of Gr-1 treated animals were assessed on day 5, 10 and 16. Flow cytometry plots of bone marrow cells indicate an increase in Ly-6G negative cells in **D**, which stain positive for anti-rat FITC secondary antibody **E** on day 5 after start of treatment. Similar analysis in spleen derived cells did not show the same result (**F and G**.

Viable cells reside in tumor tissue and spleen

This study demonstrated that conventional flow cytometry for surface markers is not the ideal method for detection of Ly-6G$^+$ cells under depletion pressure at least in the bone marrow. As a consequence, validation of tissue specific depletion was to be achieved by immunohistochemistry of cryotissues. For this purpose, MOPC$^-$ tumor bearing mice were depleted using Gr-1 antibody and analysis was carried out during the complete peripheral blood depletion phase. Microscopic analysis revealed the presence of residual Ly-6G$^+$ cells in spleens and tumor tissue of treated animals (figure 4.21A). Quantification of splenic Ly-6G$^+$ cell density revealed significant reduction to 10-50 % of normal levels in αGr-1 treated mice (figure 4.21B) and to 25-55 % by αLy-6G treatment (figure 4.21C). Nevertheless, considerable numbers of Ly-6G$^+$ cells were present under treatment and were not detected before. Notably, depletion efficacy seemed to be much higher when analyzing flow cytometry data (see figure 4.20B and the previous paragraph). Still, antibody coverage was not observed in spleen derived cells. Therefore, another mechanism seems to lead to limited Ly-6G$^+$ cell detection in the spleen by flow cytometry. In addition, reduction of Ly-6G$^+$ cells in the tumor tissue was even less efficient and did not even reach statistical significance. In order to analyze viability of intratumoral Ly-6G$^+$ cells, we took advantage of the novel CatchUp$^{IVM\text{-}red}$ model[75]. In these mice, neutrophils are detectable by Ly-6G specific Cre-mediated activation of tdTomato reporter gene expression and can therefore be visualized for intravital microscopy. For this purpose, eGFP expressing MOPC$^-$ cells were generated as described in section 3.1.2 to identify tumor tissue. MOPC^{-eGFP} cells were injected into the cutis of the ear resulting in growth of a solid tumor within one week. In this setting, it was possible to noninvasively follow neutrophils in the tumor of living mice under treatment with αGr-1. Additional intraveneous (IV) injection of fluorescently labeled nanocrystals facilitated visualization of vascular structures. As shown in a series of images over a time of 17.5 minutes in figure 4.21D, this technology confirmed the presence of residual tumor infiltrating Ly-6G$^+$ cells and further demonstrated that these cells were viable and migratory.

Taken together, different tissues were shown to host viable depletion resistant Ly-6G$^+$ cells during the phase of complete peripheral blood depletion in the HNC model. As these organs, such as spleen and the tumor itself, are also sites of protumoral functions by neutrophils, these results suggest careful interpretation of studies in which efficacy and duration of depletion are not monitored and documented in detail. Furthermore, incomplete depletion in these organs might constitute to accelerated CD11b$^+$Ly-6G$^+$ cell rebound.

4.3.3 Counteracting depletion - enhanced granulopoiesis and CD11b$^+$Ly-6G$^+$cell survival

Even though many studies, including this one, report antitumoral effects of CD11b$^+$Ly-6G$^+$ cell depletion by long term application of antibodies, this study clearly demonstrated limited efficacy of this treatment with peripheral blood CD11b$^+$Ly-6G$^+$ cells reappearing after several days. This raises the question for the source and mechanism of depletion rebound in HNC tumor bearing mice.

Systemic effects of depletion are found in the serum

Systemic changes in the serum proteome can be induced by HNC tumors[203]. As these factors may affect CD11b$^+$Ly-6G$^+$ cells and granulopoiesis in untreated as well as in depleted mice, serum cy-

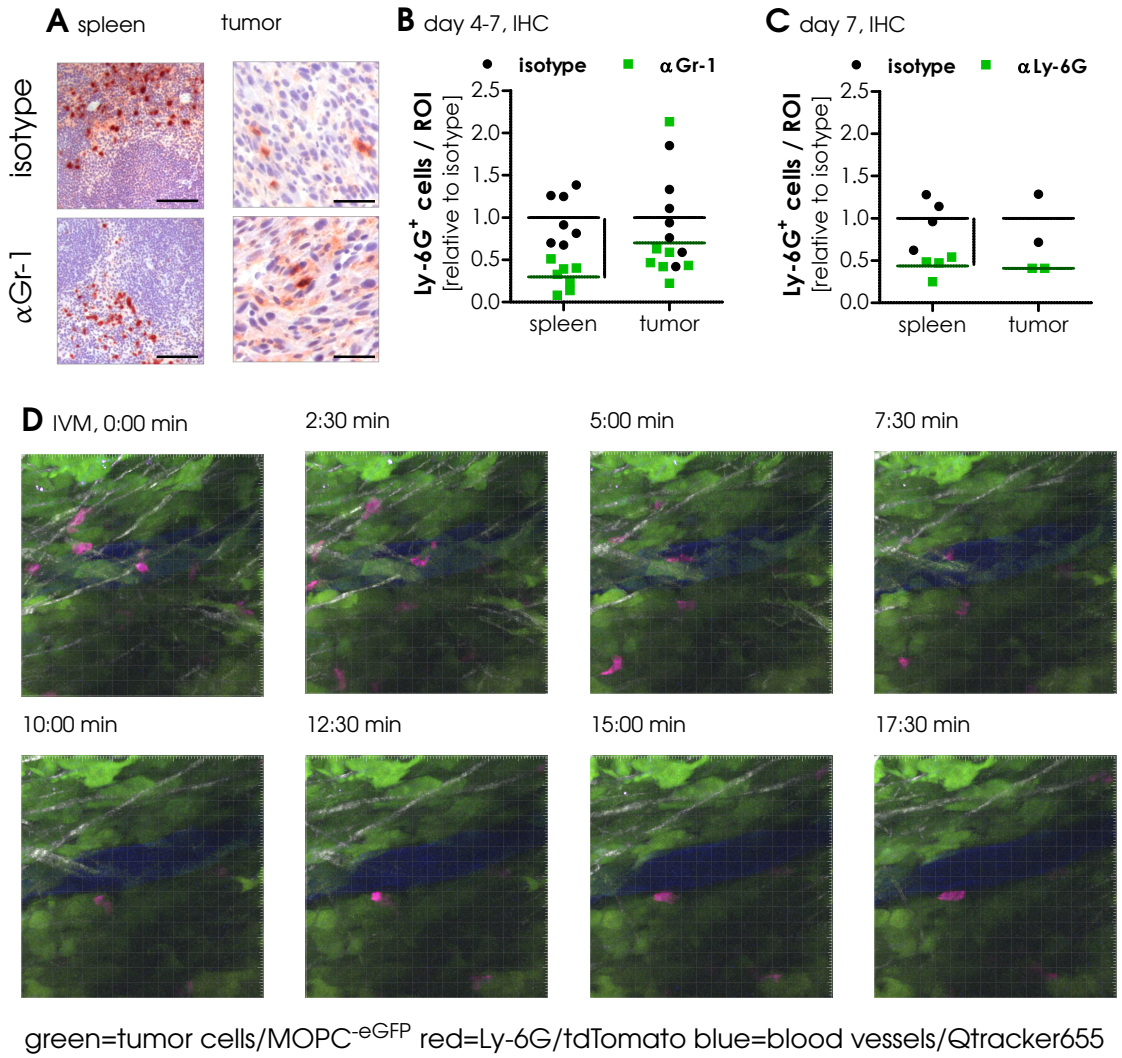

Figure 4.21: Viable Ly-6G$^+$ cells are present in tumor tissue and spleen. BL6 or CatchUp mice bearing MOPC$^-$ tumors were depleted of CD11b$^+$Ly-6G$^+$ cells. **A-C** Immunohistochemical staining of cryosections from spleens and tumors of BL6 mice were analyzed for Ly-6G$^+$ cells manually on 200× magnified photomicrographs (representative see **A**, scale represents 50 µm) at day 4-7 after depletion. Four ROIs were analyzed per tumor for αGr-1 **B** or αLy-6G **C** treated animals. The mean value of the respective isotype group was set to 1. Lines indicate significant decreases as calculated by student's *t*-test with $p \leq .05$. **D** CatchUp$^{IVM\text{-}red}$animals bearing ear tumors were depleted using αGr-1. Intravital imaging was carried out on day 2 after depletion. Blood vessels were visualized by IV injection of Qtracker 655. Maximum intensity projection of a 30 µm stack is shown for 8 different points in time spread over 17 minutes and 30 seconds as indicated.

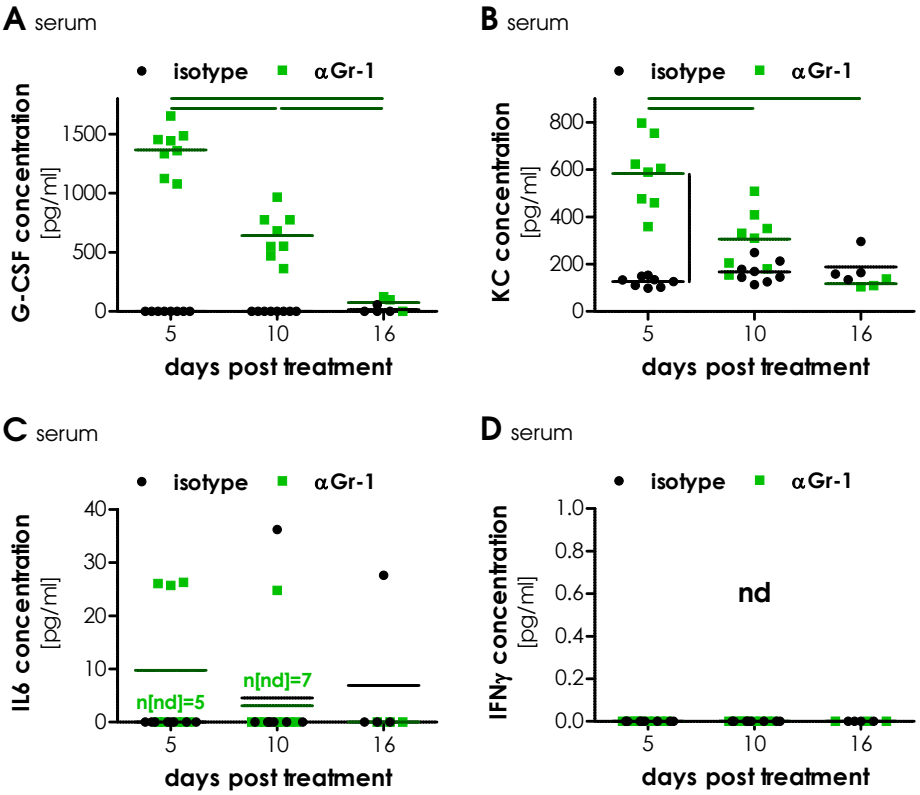

Figure 4.22: Granulopoiesis inducing cytokines increase upon depletion of Gr-1$^+$ cells. MOPC$^-$ tumor bearing BL6 mice were continuously depleted of Ly-6G$^+$ cells by αGr-1 treatment. Mice were sacrificed at different intervals of treatment and blood was taken for analysis of serum parameters. Serum concentrations of G-CSF **A**, KC **B**, IL6 **C** and IFNγ **D** were determined by ELISA. Lines indicate significance as calculated by one way ANOVA with $p \leq .05$.

tokine content was analyzed by ELISA at different stages of depletion in MOPC$^-$ tumor bearing BL6 mice. G-CSF was not detectable in naive or small tumor bearing mice but upon depletion with αGr-1 antibody, this granulopoiesis driving factor was dramatically increased (figure 4.22A). Highest G-CSF levels were present during complete peripheral blood depletion and decreased rapidly in accordance with CD11b$^+$Ly-6G$^+$ cell repopulation of the host. In addition, serum levels of KC, which only slightly increased upon tumor progression, were highly increased at the same time as G-CSF probably inducing CD11b$^+$Ly-6G$^+$ cell mobilization (figure 4.22B). KC serum concentration decreased upon depletion rebound as well. Given the natural function of CD11b$^+$Ly-6G$^+$ cells in antimicrobial defense, depleted mice could easily suffer from infections which could also result in the increase of the described cytokines. Notably, no generalized signs of infections were observed in the treated animals. Nevertheless, serum concentrations of additional infection associated cytokines were analyzed in depleted animals to exclude an underlying inflammation. IL-6 was not elevated in either control nor depleted mice in any phase of depletion (figure 4.22C). In accordance, IFNγ was not detectable in any sample (figure 4.22D) therefore excluding general infections in depleted mice. Thus, granulopoiesis modulating cytokines are highly induced upon depletion while infections are not present.

Depletion induces granulopoiesis in the spleen

CD11b$^+$Ly-6G$^+$ cells reappear after several days of complete depletion in the peripheral blood which

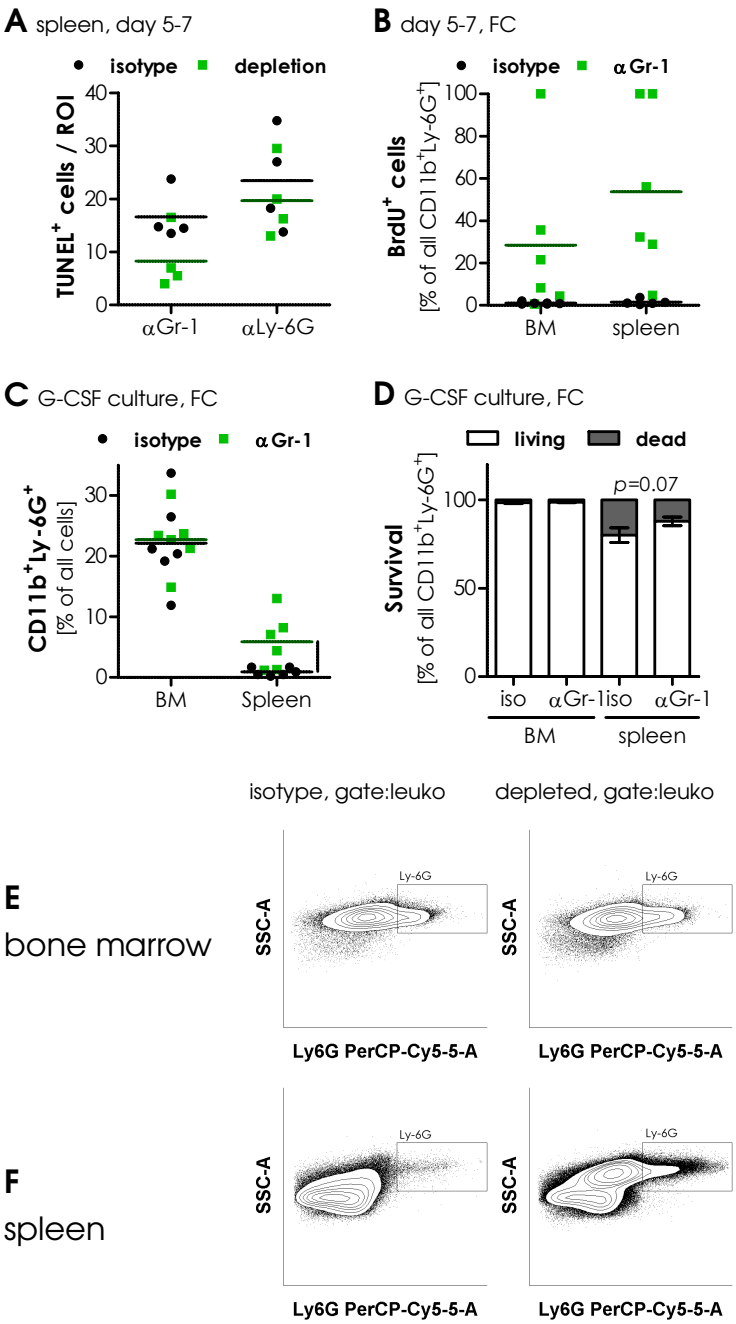

Figure 4.23: Depletion enhances extramedullary granulopoiesis. MOPC$^-$ tumor bearing BL6 mice were continuously depleted of Ly-6G$^+$ cells. **A** Spleens were analyzed for apoptotic cells by TUNEL staining on cryosections of day 5-7 after start of treatment. **B** Proliferation in bone marrow and spleen was assessed by BrdU injection 2 hours prior to analysis in mice at day 4-8 after start of treatment. Analysis was carried out by flow cytometry. **C-F** Bone marrow cells and B220 depleted splenocytes from mice at day 4-8 after start of treatment were isolated and cultured for 5 days in the presence of 100 ng / mL G-CSF. Frequency of CD11b$^+$Ly-6G$^+$ cells was assessed by flow cytometry **C**. Survival was assessed in the same cultures by analysis of viability dye staining within the population of CD11b$^+$Ly-6G$^+$ cells **D**. Representative FC plots are shown for bone marrow **E** and spleen **F**. Significance was assessed by student's *t*-test with $p \leq .05$.

is associated with increased granulopoiesis inducing cytokines in the periphery. Bone marrow and spleen are major sites of granulopoiesis[177, 30]. Given the relative inefficacy of depletion at these sites compared to blood, these organs were analyzed during complete peripheral blood depletion as potential sources of Ly-6G$^+$ cell development and maturation. As a first step, cellular turnover in the spleen of CD11b$^+$Ly-6G$^+$ cell depleted MOPC$^-$ tumor bearing mice was assessed. To this end, cryotissue was collected at day 5-7 after start of continuous treatment and apoptosis was analyzed by TUNEL assay. Apoptotic cells were not elevated in spleens of either αGr-1 nor αLy-6G treated mice but rather trended towards reduced numbers as shown in figure 4.23A. Therefore, increased cellular turnover in the spleen of depleted mice was excluded. To further identify the source of Ly-6G$^+$ cell production in tumor bearing depleted mice, BrdU was incorporated *in vivo* for two hours before analyzing different organs by flow cytometry. Despite a great variability among αGr-1 treated animals, a clear and very substantial increase in the percentage of BrdU$^+$ among Ly-6G$^+$ cells was noted in bone marrow and spleen (figure 4.23B). It is noteworthy that this increase was more pronounced in spleen than bone marrow. The potential of both organs to produce CD11b$^+$Ly-6G$^+$ cells during complete peripheral blood depletion was further assessed by *in vitro* culture in the presence of G-CSF for 5 days. Bone marrow produced constant amounts of CD11b$^+$Ly-6G$^+$ cells independent of treatment as determined by flow cytometry (figure 4.23C and E). Remarkably, splenocyte cultures of isotype treated tumor bearing mice produced only minor amounts of CD11b$^+$Ly-6G$^+$ cells while splenocytes demonstrated enhanced granulopoietic capacities upon αGr-1 treatment (figure 4.23C and F). When analyzing survival in these cultures, bone marrow CD11b$^+$Ly-6G$^+$ cells were constantly viable and survival of splenic CD11b$^+$Ly-6G$^+$ cells was prolonged in cultures from αGr-1 treated mice (figure 4.23D).
Collectively, this data provides strong evidence for preferential induction of extramedullary rather than bone marrow granulopoiesis in tumor bearing mice under αGr-1 depletion pressure. This process is potentially driven by high systemic levels of G-CSF and KC.

4.3.4 Immature regulatory Ly-6G$^+$ cells drive the CD11b$^+$Ly-6G$^+$ cell rebound phase

Long term antibody mediated depletion of CD11b$^+$Ly-6G$^+$ cells is often performed in murine cancer studies including this study in chapter 4.2. Simultaneously, tumor driven modulation of neutrophil differentiation and biology has been described[30, 223] and is also present in the HNC model (chapter 4.1). This study further aims to identify the role of the tumor during CD11b$^+$Ly-6G$^+$ cell rebound and the fate of the arising Ly-6G$^+$ cells as they appear during the rebound phase in long term experiments.

Accelerated CD11b$^+$Ly-6G$^+$ cell rebound in tumor bearing animals

As mentioned above, an influence of tumor derived factors on the outcome of depletion is not unlikely. In serum samples, induction of KC was also more pronounced in tumor bearing mice compared to naive mice when depleting with αGr-1 (not shown). To evaluate the influence of tumor burden on the dynamics of depletion and rebound, MOPC$^-$ tumor bearing and naive mice were subjected to αGr-1 depletion and peripheral blood was monitored by flow cytometry. Between day 9 and 11 after onset of depletion, Ly-6G$^+$ cell frequencies already started to increase rapidly in tumor bearing mice in contrast to naive mice (figure 4.24A). Only a small number of naive mice (2/10) started to enter CD11b$^+$Ly-6G$^+$ cell rebound as defined by Ly-6G$^+$ cell frequencies >2 %. In contrast, as many as 7 out of 11 tumor bearing mice displayed complete CD11b$^+$Ly-6G$^+$ cell rebound at the given time

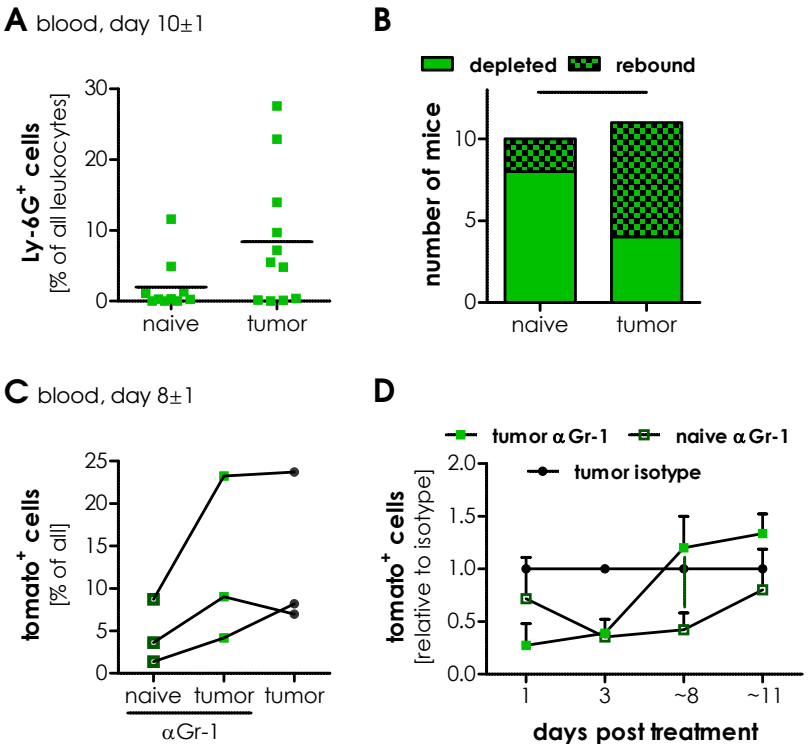

Figure 4.24: CD11b$^+$-Ly-6G$^+$ cell rebound is enhanced by the tumor. Naive and MOPC$^-$ tumor bearing BL6 or CatchUp mice were continuously depleted using αGr-1. Frequencies of Ly-6G$^+$ cells were assessed in tail vein blood by flow cytometry on day 9-11 in BL6 animals **A**. The number of depleted mice versus mice in the rebound phase was analyzed using 2 % as cut off value and was tested by Chi^2 test **B**. For CatchUp mice, a similar trend is shown on day 7-9 for tdTomato$^+$ cells in tail vein blood **C** and the progression of depletion and rebound is indicated by relative tdTomato numbers to isotype **D**. Significance was assessed by student's *t*-test with $p \leq .05$ between naive and tumor bearing animals and is indicated by a vertical line.

(figure 4.24B). To exclude detection limitations in flow cytometry in this critical phase, a similar experiment was performed using CatchUp mice. Thus, Ly-6G$^+$ cells could be monitored in the flow cytometer without external antibody dependent detection but by tdTomato signal. Differential CD11b$^+$Ly-6G$^+$ cell rebound was confirmed in these mice with an earlier onset of 2 days at day 7 to 9 after start of treatment (figure 4.24C). When analyzing tdTomato$^+$ cells relative to simultaneously treated isotype controls, fast CD11b$^+$Ly-6G$^+$ cell rebound became apparent in MOPC$^-$ tumor bearing animals while naive mice entered CD11b$^+$Ly-6G$^+$ cell rebound more slowly (figure 4.24D). These data indicate that reappearance of Ly-6G$^+$ cells is accelerated by the presence of an HNC tumor in two different mouse strains and using two different flow cytometric detection methods.

Prolonged survival of reappearing immature cells in the spleen

Reappearing cells are present during an experiment as soon as depletion is carried out for longer than one week in tumor bearing mice. As indicated in section 4.3.3, increased survival was present in CD11b$^+$Ly-6G$^+$ cells generated *ex vivo* from spleens of depleted animals during complete peripheral blood depletion. Increased survival is also associated with lower maturation stages and these were further linked to suppressive activities[153]. Survival and maturation was therefore analyzed in Ly-6G$^+$ cells from mice with CD11b$^+$Ly-6G$^+$ cell rebound under constant antibody applications. Splenic Ly-6G$^+$ cells were isolated from BL6 MOPC$^-$ tumor bearing mice in the rebound phase by MACS technique and cultured *ex vivo* for 24 hours. Survival, as determined by flow cytometry for AnnexinV and 7AAD double negative cells, was increased in cells from animals in the rebound phase compared to the respective isotype control mice (figure 4.25A). For additional morphological analysis, MOPC$^-$ tumor bearing CatchUp mice were depleted using αGr-1 until CD11b$^+$Ly-6G$^+$ cells rebound and Ly-6G$^+$ cells were isolated by FACS from spleen and bone marrow. Anti-apoptotic mechanisms were

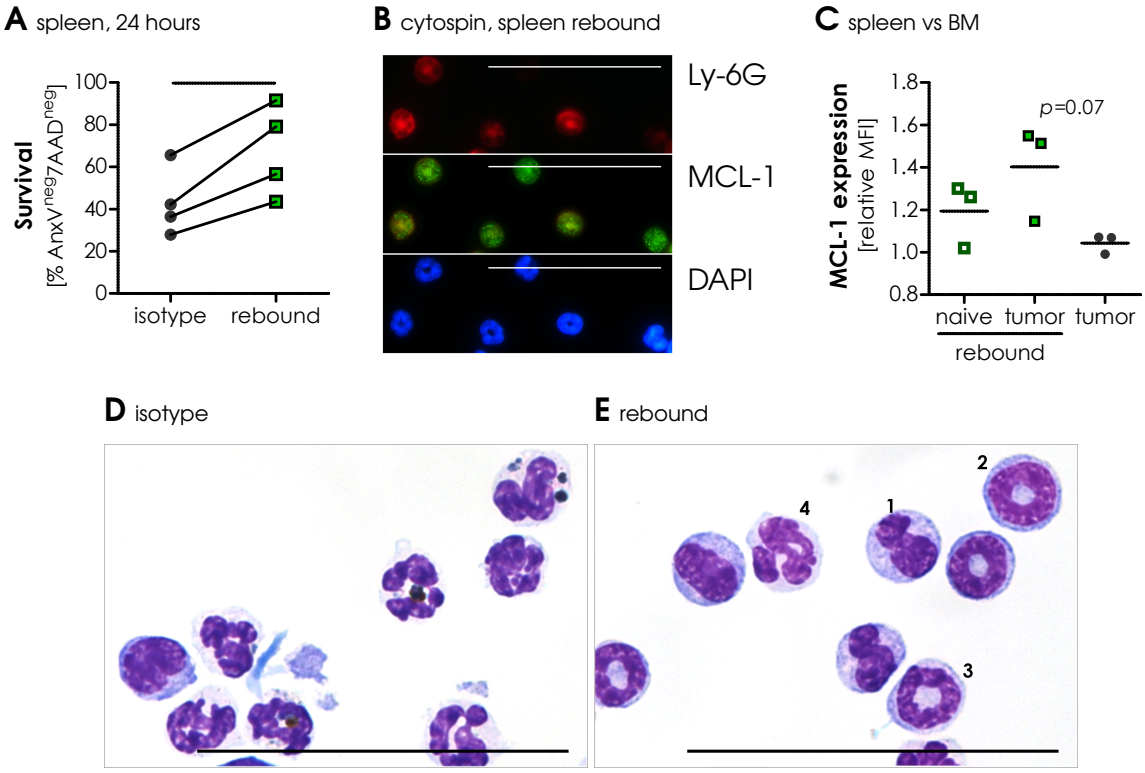

Figure 4.25: Depletion is followed by expansion of long-lived Ly-6G cells. MOPC$^-$ tumor bearing BL6 or CatchUp mice were continuously depleted using αGr-1. **A** Ly-6G cells were isolated by MACS from spleen of BL6 mice after CD11b$^+$Ly-6G$^+$ cell rebound and cultured for 24 hours before survival was assessed by AnnexinV 7AAD flow cytometry. **B-E** tdTomato$^+$ cells were isolated by FACS from bone marrow, blood and spleen of CatchUp animals in the rebound phase. Cells were analyzed by cytospin. MCL-1 was stained (representative photomicrograph at 1000× magnification **B**) and analyzed on 4 ROIs at 400× magnification for fluorescence intensity by ImageJ. Spleen Ly-6G cell MCL-1 expression is indicated relative to a bone marrow specimen of the same batch **C**. Pappenheim staining of cytospin indicate nuclear morphology at 1000× magnification for isotype treated animals **D** and those which rebound from depletion **E**. The scale represents 50 µm for all photomicrographs. 1 = myelocyte, 2 = metamyelocyte, 3 = banded, 4 = segmented

investigated as survival was enhanced despite continuous antibody treatment, because depletion antibodies were discussed to act via inducing apoptosis[1, 163]. To this end, cytospin preparations were stained for the Bcl-2 family member MCL-1 and expression was analyzed by quantification of fluorescence intensity. Notably, Ly-6G^{high} as well as Ly-6G^{int} tdTomato$^+$ cells expressed MCL-1 (figure 4.25B). Mean fluorescence intensity was normalized to a simultaneously processed bone marrow sample. MCL-1 expression analysis thereby indicated that splenic and bone marrow derived Ly-6G$^+$ cells express similar levels of the anti-apoptotic protein in tumor bearing untreated mice. More importantly, expression was enhanced in spleen derived Ly-6G$^+$ cells after CD11b$^+$Ly-6G$^+$ cell rebound in tumor bearing mice while bone marrow expression remained constant (figure 4.25C). Cytospin preparations of spleen derived cells were also analyzed for morphological differences by Pappenheim stain. Cells isolated from isotype treated animals mainly composed of mature neutrophils with characteristically segmented nuclei (>90 %, figure 4.25D). In contrast, a high proportion of immature cells was identified among preparations from rebound phase animals (figure 4.25E). According to the nuclear morphology, tdTomato$^+$ cells from spleens in the rebound phase contained some mature segmented cells and a mixture of myelocytes, metamyelocytes and banded neutrophils. In summary, these results

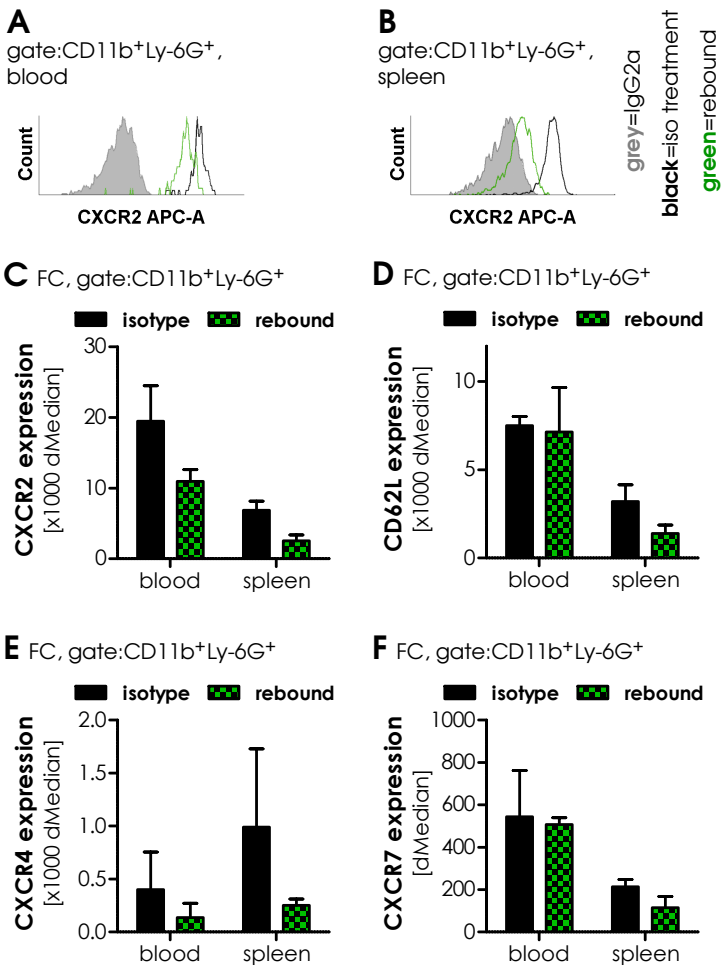

Figure 4.26: Reappearing cells show activated surface marker expression. MOPC$^-$ tumor bearing BL6 mice in the rebound phase of Gr-1 depletion were analyzed by flow cytometry. Representative histograms for CXCR2 expression on blood **A** and spleen derived CD11b$^+$Ly-6G$^+$ cells **B** are presented. CD11b$^+$Ly-6G$^+$ cells were analyzed for CXCR2 **C**, CD62L **D**, CXCR4 **E** and CXCR7 **F** expression. Means±SEM of three mice are shown.

demonstrate for the first time that tumor induced factors counteract Gr-1 depletion and strengthen anti-apoptotic signals in the rebound phase under constant depletion pressure possibly resulting in faster complete CD11b$^+$Ly-6G$^+$ cell rebound.

Activated phenotype by surface marker expression

This study indicated earlier that reappearing cells are characterized by prolonged survival and immature phenotype. In addition to the maturation status, activation can also induce survival and modulate functional properties. Both maturation and activation are associated with differential cell surface expression of CXC chemokine receptors[165, 42]. To identify the phenotype of reappearing cells in HNC bearing mice, cell surface expression of CXCRs as well as L-selectin, which is downregulated upon activation[93], was analyzed by flow cytometry in blood as well as in spleen. CXCR2 was prominently regulated on rebound CD11b$^+$Ly-6G$^+$ cells with decreased cell surface levels of the receptor in blood and spleen of αGr-1 treated animals (figure 4.26A-C). Contrary, L-selectin was unchanged in blood but low in spleen derived CD11b$^+$Ly-6G$^+$ cells in the depletion rebound phase (figure 4.26D) suggesting an activated phenotype in spleen but not blood. Additionally, CXCR4 was highly variable in isotype treated animals but constantly low on CD11b$^+$Ly-6G$^+$ cells that rebound from depletion indicating decreased shuttling to the bone marrow (figure 4.26E). Finally, CXCR7 was unchanged by the treatment (figure 4.26F). Collectively, cell surface expression of different markers indicate a mixture of

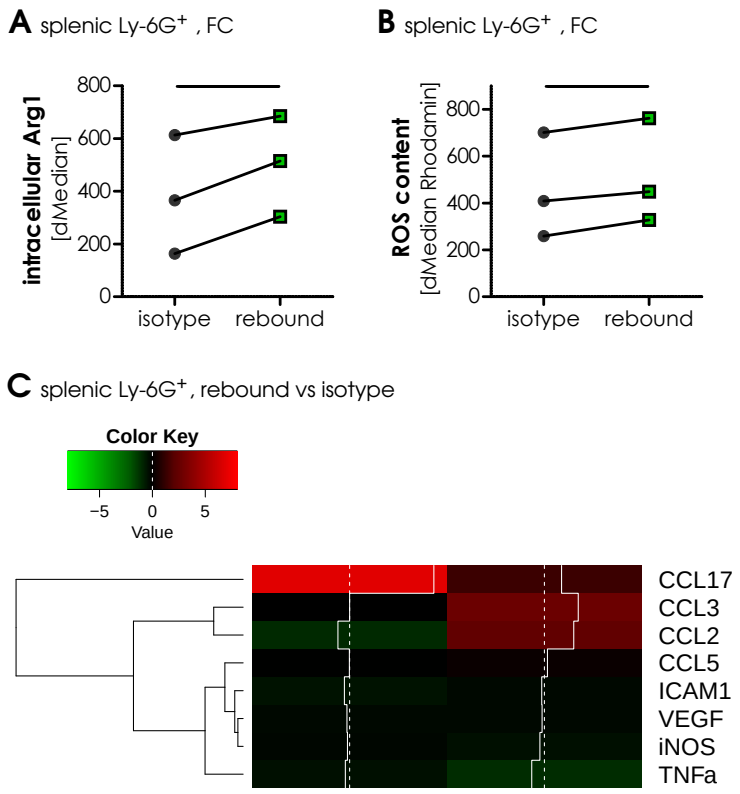

Figure 4.27: Reappearing Ly-6G cells express inflammatory modulators. MOPC$^-$ tumor bearing BL6 mice in the rebound phase of Gr-1 depletion were sacrificed and Ly-6G$^+$ cells were isolated from the spleen by MACS technique. Intracellular Arginase1 (Arg1) **A** and reactive oxygen species (ROS) **B** content was assessed by flow cytometry. Significance was calculated by paired student's *t*-text with $p \leq .05$. **C** mRNA expression of different genes was analyzed by qPCR from 2 exemplary pairs of mice. Data was normalized to β-actin and relative differences between rebound and isotype treated Ly-6G$^+$ cells were visualized in a heatmap after hierarchical clustering of genes using R software.

activated and immature CD11b$^+$Ly-6G$^+$ cell phenotypes as already shown partially by morphological analysis.

Regulatory molecules are differentially expressed in rebound CD11b$^+$Ly-6G$^+$ cells

Reappearing CD11b$^+$Ly-6G$^+$ cells were demonstrated to share immature and activated phenotypes. Both can be associated with immunomodulatory and protumoral functions. It was therefore crucial to analyze functional mediators in these cells which are coming up during long term depletion experiments. To this end, MOPC$^-$ tumor bearing BL6 mice were continuously depleted using αGr-1 and Ly-6G$^+$ cells were isolated from the spleen during CD11b$^+$Ly-6G$^+$ cell rebound. Flow cytometric analysis of the intracellular effector molecules arginase1 and reactive oxygen species (ROS) displayed expected interexperimental variability, but levels were consistently induced in αGr-1 treated animals in the rebound phase compared to controls (figure 4.27A and B). Finally, using a panel of candidate marker genes for tumor associated neutrophil polarization[54], gene expression was measured in two pairs of cells from rebound and isotype treated animals by qPCR. Data were visualized by hierarchical clustering suggesting changed regulatory properties of CD11b$^+$Ly-6G$^+$ cells in the rebound phase (figure 4.27C). The most prominent and consistent changes were observed in CCL17 upregulation and reduced TNFα expression. Both indicate a polarization towards a protumoral phenotype as TNFα was described in conjunction with an antitumoral phenotype and CCL17 mediated regulatory T cell recruitment by neutrophils in another study[54, 132].

In summary, the presented data provides evidence for a limited applicability of long term depletion in tumor bearing mice. Tissue specific depletion was shown to be incomplete and granulopoiesis was rapidly induced in the spleen resulting in CD11b$^+$Ly-6G$^+$ cell rebound. Furthermore, the results

of the final experiments suggest that Ly-6G$^+$ cells, which reappear under depletion pressure, have an immature and immunoregulatory phenotype. The presence of residual, depletion resistant, migratory intratumoral Ly-6G$^+$ cells, enhanced extramedullary granulopoiesis and the rapid reappearance of immature regulatory cells should therefore be considered when using αGr-1 treatment to analyze *in vivo* functions of neutrophils and MDSC in tumor bearing mice.

4.4 Role of Ly-6G in tumor-neutrophil interactions

Neutrophil specific expression of Ly-6G has been used for identification and depletion of these cells in mice for a long time. Although identified as a key neutrophil marker, surprisingly, the function of this molecule was unknown until recently. In 2012, Wang *et al.* published a study suggesting that ligation of Ly-6G with nondepleting antibody doses results in reduced migratory properties of CD11b$^+$Ly-6G$^+$ cells[208]. They identified an association of Ly-6G and β2-integrins which was crucial for β2-integrin dependent migration. This is in line with a study indicating that the structurally related molecule CD177 on human neutrophils can interact with PECAM and transendothelial migration can be diminished by blocking CD177[169]. However a recent study poignantly demonstrated that Ly-6G knockout neutrophils are functionally normal and do not lack migratory properties using the CatchUp model[75]. This suggests an antibody dependent effect in the earlier studies and leaves Ly-6G without function again. To assess potential functions of Ly-6G in neutrophil-tumor interactions, CatchUp animals have been used in this study for comparison of heterozygous Ly-6G competent and homozygous Ly-6G knockout mice.

4.4.1 Differential tumor growth in Ly-6G KO animals

As CD11b$^+$Ly-6G$^+$ cells have been demonstrated in the earlier chapter to be involved in progression of the HNC tumor model, tumor progression was analyzed in hetero and homozygous CatchUp animals. To this end, MOPC$^-$ cells were injected SC into the respective hosts and tumor volume was monitored over time. Differential tumor growth became apparent during the course of disease while initial tumor formation was not affected in both female (figure 4.28A) and male (figure 4.28B) mice. Surprisingly, Ly-6G knockout resulted in accelerated tumor growth suggesting an antitumoral function of the molecule. Furthermore, tumor growth between male and female mice also differed substantially.
Collectively, a tumor promoting environment was suggested by the presented results in homozygous CatchUp animals with Ly-6G knockout.

4.4.2 Ly-6G is dispensable for infiltration into tumor tissue but affects gene expression

This study indicated differential tumor growth in Ly-6G knockout and competent mice. Possible mechanisms could be mediated by migratory deficiencies upon lack of Ly-6G as indicated in an earlier study[208] as well as a modulation of neutrophil effector functions. This study therefore assessed tumor infiltration as well as several effector genes to elucidate the mechanism of differential tumor growth.

Ly-6G KO neutrophils infiltrate into MOPC tumors

As indicated above, Ly-6G could be involved in migratory properties of neutrophils. To address mi-

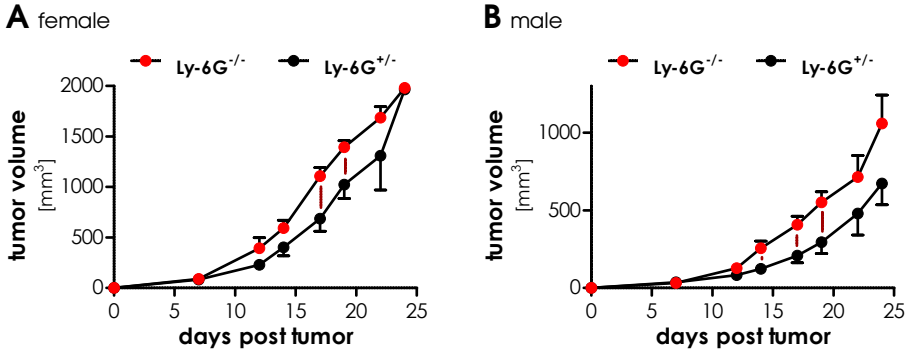

Figure 4.28: Ly-6G knockout affects growth of HNC tumors. Homozygous (Ly-6G$^{-/-}$) and heterozygous (Ly-6G$^{+/-}$) CatchUp mice were injected with MOPC$^-$ tumors SC and tumor growth was evaluated in female **A** and male mice **B**. Data are presented as mean±SEM of 4-5 mice. Statistical significance is indicated by vertical lines and was assessed by student's *t*-test with $p \leq .05$

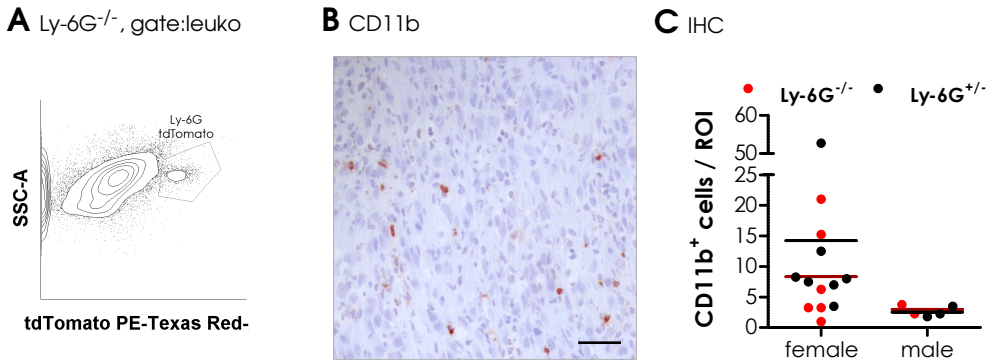

Figure 4.29: Ly-6G knockout cells infiltrate tumor tissue normally. Tumors were excised from MOPC$^-$ bearing CatchUp animals. Flow cytometry was performed for identification of tdTomato$^+$ cells in homozygous (Ly-6G$^{-/-}$) mice **A**. Number of CD11b$^+$ cells was assessed in the tumor by immunohistochemistry on cryosections. 4 ROIs of 200× magnification (as shown in **B**, scale represents 50 µm) were analyzed manually in heterozygous (Ly-6G$^{+/-}$) and Ly-6G knockout (Ly-6G$^{-/-}$) mice **C**.

gration into the tumor tissue in the HNC model, MOPC$^-$ cells were injected SC into Ly-6G competent as well as knockout CatchUp animals and tumor tissue was analyzed after three weeks of tumor growth. Using flow cytometry, tdTomato$^+$ cells were detectable in the tumor mass of Ly-6G$^{-/-}$ mice (figure 4.29A). As intratumoral localization is mandatory for CD11b$^+$Ly-6G$^+$ cell functions in this context, verification of the exact localization in this tumor mass was crucial. To this end, cryotissue from MOPC$^-$ tumors grown in the respective mice was analyzed. As Ly-6G was not available for identification of neutrophils in Ly-6G$^{-/-}$ mice, CD11b was stained in the available tissues. Examination of the immunohistochemical staining revealed that CD11b stained exclusively granulocytic cells in MOPC$^-$ tumors (figure 4.29B). CD11b and thereby granulocytic infiltration in MOPC$^-$ tumors did not differ between Ly-6G competent and knockout mice (figure 4.29C). Infiltrating cells were evenly distributed throughout the tumor tissue in all groups. Thus, Ly-6G deficient neutrophils are capable of migrating into HNC tissues normally.

CD11b$^+$Ly-6G$^+$ cells from Ly-6G KO mice exert differential gene expression

After demonstrating that intratumoral migration is not affected in Ly-6G deficient mice, a phenotypic

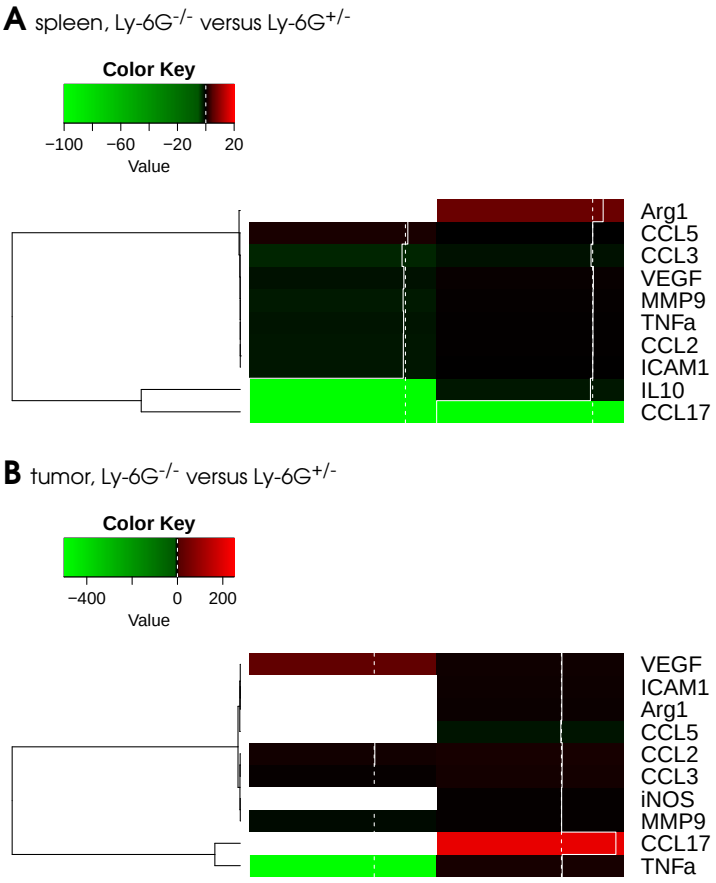

Figure 4.30: Differential gene expression in Ly-6G deficient versus competent CatchUp neutrophils. Ly-6G cells were isolated from spleen and tumor of 4 MOPC^{-} tumor bearing CatchUp animals (2 pairs of homo and heterozygous animals). Gene expression was analyzed by qPCR and processed via normalization to β-actin and relation of Ly-6G$^{-/-}$ to Ly-6G$^{+/-}$ gene expression. Heatmaps and hierarchical clustering for spleen derived **A** and tumor infiltrating **B** Ly-6G cells are shown indicating the differential gene expression in homo vs heterozygous cells.

difference between neutrophils from Ly-6G competent and deficient mice was likely. To address this hypothesis, gene expression of N1 and N2 polarization markers[54] was assessed in neutrophils isolated from MOPC^{-} tumor bearing mice with both genotypes. Isolated cells derived from tumor tissue and spleen of two pairs of mice. qPCR was performed to assess gene expression and visualization was operated by a heatmap and hierarchical clustering analysis. In the spleen, most markers were detectable and pronounced differential gene expression was found for the cytokine IL-10 and the chemokine CCL17 which are highly downregulated in neutrophils from Ly-6G deficient mice (figure 4.30A). The other markers were not consistently regulated in both mouse pairs and arginase1 was upregulated in one but not detectable in the other set of samples. Unfortunately, expression of many genes was also not detectable in one set of tumor infiltrating neutrophil samples, which was probably due to low cell numbers resulting in low RNA concentrations. The most remarkable changes in tumor infiltrating neutrophils were observed for CCL17 expression, again, but in the tumor it was upregulated in one out of two Ly-6G deficient neutrophil samples while it was not detectable in the other set (figure4.30B). This is of interest as CCL17 could mediate Treg recruitment[132]. Furthermore, antitumoral TNFα was downregulated in one pair of mice but unchanged in the second data set. Therefore a lower antitumoral N1 phenotype was not supported by this data. Upregulation, even though not to the same extent as for CCL17, was observed for the chemokines CCL2 and CCL3 and for VEGF.
Collectively, the mechanism of enhanced tumor growth in Ly-6G deficient animals was not mediated by affecting migratory properties of neutrophils in line with previous observations in the CatchUp model[75]. Gene expression analysis revealed reduced protumoral CCL17 and IL-10 expression in the spleen of Ly-6G deficient mice which is not in accordance with enhanced tumor growth. Furthermore,

enhanced CCL17 as well as CCL2, CCL3 and VEGF expression was demonstrated in tumor infiltrating neutrophils suggesting modulation of tumor associated inflammation and angiogenesis in Ly-6G deficient mice.

4.4.3 Differences in T cells from Ly-6G deficient mice

T cells can mediate antitumoral responses but are also regulated and suppressed by $CD11b^+Ly\text{-}6G^+$-cells in tumor bearing mice. Furthermore, differential influence of Ly-6G deficient neutrophils on T cells was indicated by gene expression analysis. Functional interaction between both cell types was therefore addressed in the next part of this study.

Ly-6G does not mediate T cell suppression

Decreased IL-10 and increased Arg1 expression by Ly-6G deficient neutrophils in the spleen of tumor bearing mice suggested an altered interaction between these cells and T cells. Furthermore, a differential capability for the regulation of T cells might be a mechanism by which Ly-6G competent and knockout neutrophils could influence tumor progression. To test this hypothesis, $tdTomato^+$ cells were isolated from spleens of $MOPC^-$ tumor bearing hetero and homozygous CatchUp mice. Proliferation dye labeled $CD3^+$ cells from heterozygous mice were stimulated using αCD3/αCD28 beads in the presence of 50 U / mL IL-2 and Ly-6G cells were added in different ratios. Proliferation of T cells was analyzed after 3 days of culture by flow cytometry (figure 4.31A). Ly-6G knockout neutrophils did not result in differential suppression of T cell proliferation in either a 1:20 (figure 4.31B), 1:5 (figure 4.31C) nor in a 1:2.5 neutrophil to T cell ratio (figure 4.31D). Thus, Ly-6G knockout neutrophils exerted normal T cell suppressive capabilities in an *ex vivo* polyclonal proliferation assay.

Tregs are not enhanced in the tumor tissue

T cell activation was not differentially affected by Ly-6G competent and knockout neutrophils. Nevertheless, enhanced CCL17 expression in one tumor of Ly-6G deficient animals suggested possible effects on T regulatory cells resulting in enhanced infiltration. To analyze the abundance of Tregs in the tumors, cryotissue of $MOPC^-$ SC tumors from the respective mice was analyzed by immunohistochemistry. $CD4^+$ T cells were found to equally infiltrate tumors from both genotypes (figure 4.32A and B). A high cell number was also found to express the Treg associated transcription factor FoxP3 in the nucleus (figure 4.32C). Treg infiltration into $MOPC^-$ tumors was slightly decreased in Ly-6G deficient females compared to Ly-6G competent mice from the same gender (figure 4.32D). Remarkably high numbers were observed when calculating the abundance of Tregs among tumor infiltrating $CD4^+$ cells in Ly-6G competent but not in knockout female mice (figure 4.32E). In heterozygous mice, between 66 and 100 % of infiltrating $CD4^+$ cells were made up of $FoxP3^+$ cells while in knockout mice this abundance ranged between 20 and 57 % and was therefore significantly reduced. Surprisingly, this was not apparent in the smaller group of male mice.

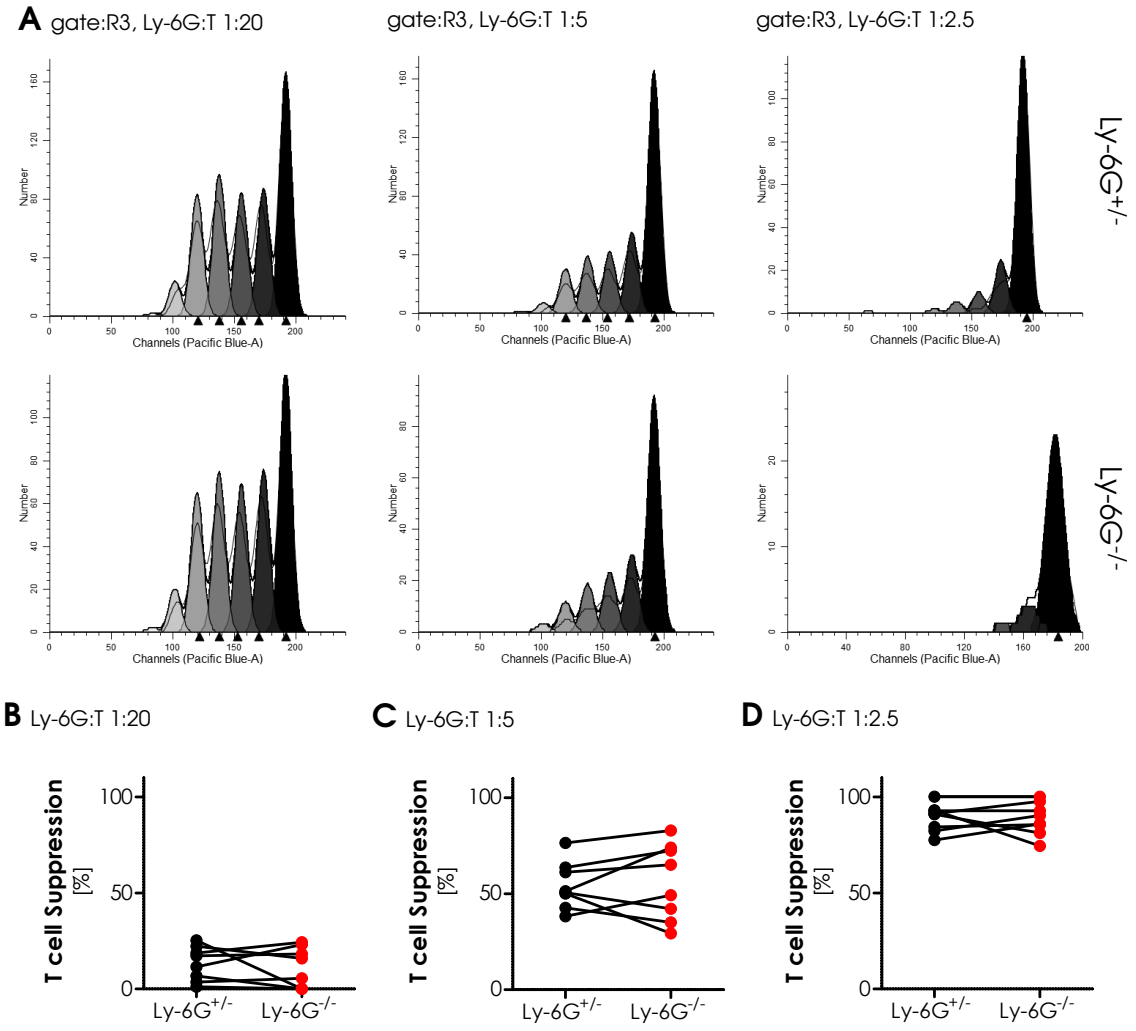

Figure 4.31: Equal T cell suppression by hetero and homozygous CatchUp Ly-6G cells. Ly-6G cells and CD3 T cells were isolated from the spleen of MOPC^{+} tumor bearing CatchUp animals and subjected to a T cell proliferation (stimulation of proliferation with 50 U / mL IL2 and CD3/CD28 Beads) and suppression assay using different Ly-6G to T cell ratios. Suppression of polyclonal proliferation is indicated in representative histograms for hetero **A-C** and homo **D-F** animals using 1:20 **A+D**, 1:5 **B+E** and 1:1 **C+F** Ly-6G:T cells. Analysis of homo and hetero animals processed on the same day are shown for the ratio of 1:20 **G**, 1:5 **H** and 1:1 **I** Ly-6G:T cells

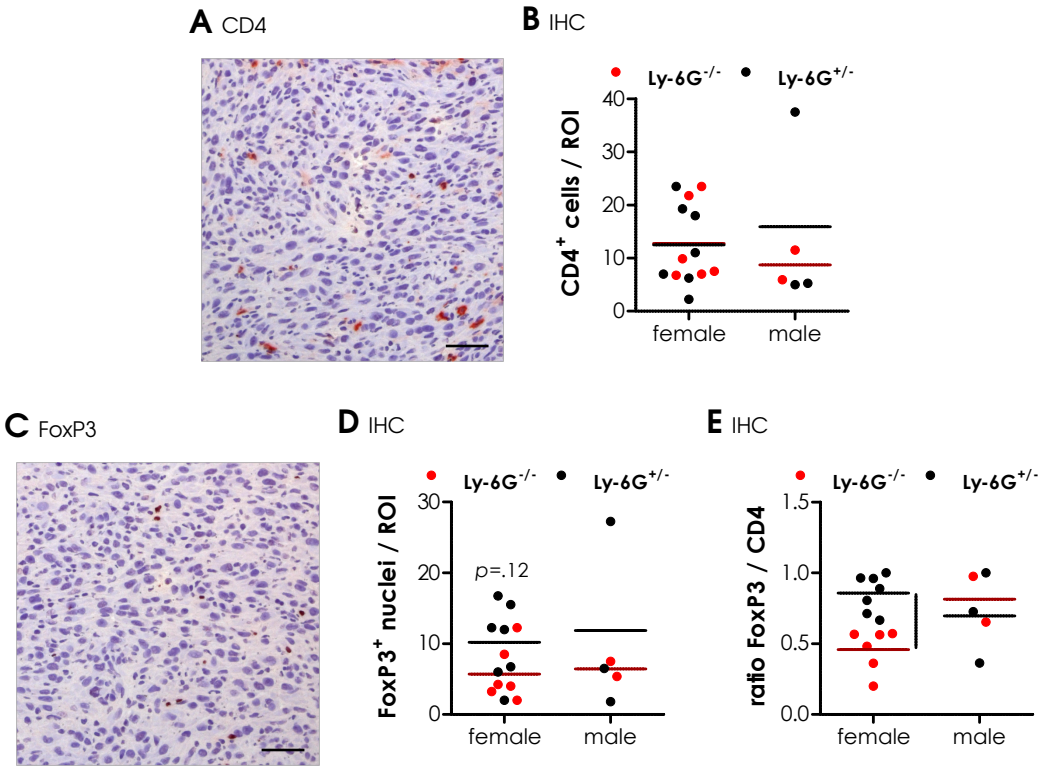

Figure 4.32: Treg tumor infiltration differs in homozygous CatchUp animals. Tumors were excised from MOPC$^-$ bearing CatchUp animals and analyzed by immunohistochemistry. Number of CD4$^+$ cells was assessed in the tumor on 4 ROIs of 200× magnification (as shown in **A**, scale represents 50 µm) and analyzed manually **B**. FoxP3$^+$ cells were analyzed the same way. A representative staining is shown in **C**. FoxP3$^+$ nuclei were counted manually **D** and the ratio of CD4 T cells and FoxP3$^+$ nuclei was calculated for each tumor **E**. Vertical line indicates statistical significance as determined by student's *t*-test with $p \leq .05$.

Consequently, this study promoted evidence for differential tumor promoting environments in Ly-6G competent and knockout mice. While neutrophils of both genotypes readily infiltrated HNC tumor tissue, gene expression suggested a modulation of tumor associated inflammation and angiogenesis in Ly-6G deficient mice. Interaction with T cells was further analyzed but suppressive capacities of neutrophils were not affected by presence or absence of Ly-6G. Surprisingly, reduced abundance of tumor infiltrating regulatory T cells was demonstrated in Ly-6G deficient mice which is not in line with enhanced tumor progression. Collectively, Ly-6G mediated modulation of tumor growth and defective T regulatory cell accumulation in Ly-6G knockout homozygous CatchUp animals would require further investigation. It is therefore rather likely that enhanced tumor progression is induced by affecting different tumor promoting cell types such as macrophages or by regulation of angiogenesis in these mice.

5 Discussion

This thesis investigated the role of neutrophils in the immunological tumor-host interaction in a mouse model of head and neck cancer. In the different parts of the study, the following questions and topics were addressed.

1. **Are CD11b$^+$Ly-6G$^+$ cells affected by HNC tumors in mice?** Yes, they are. A mouse model for HNC-CD11b$^+$Ly-6G$^+$ cell interaction was established. In this model, CD11b$^+$Ly-6G$^+$ cells were influenced by tumoral factors via the chemokine/CXCR2 axis. CD11b$^+$Ly-6G$^+$ cells rapidly accumulated in spleen and peripheral blood and cell frequencies increased with tumor progression. Furthermore, it was demonstrated that bone marrow and spleen derived CD11b$^+$Ly-6G$^+$ cells from HNC bearing mice have T cell suppressive capacities. Infiltration into the tumor tissue induced local activation of protumorigenic properties of CD11b$^+$Ly-6G$^+$ cells.

2. **Do CD11b$^+$Ly-6G$^+$ cells affect HNC tumor progression?** As indicated above, intratumoral CD11b$^+$Ly-6G$^+$ cells were characterized by a protumor phenotype. Further experiments suggested a distinct role of CD11b$^+$Ly-6G$^+$ cells especially in tumor establishment and adjustment of the tumor niche rather than in advanced tumor progression. Both inhibition of T cell function and potential effects on tumor angiogenesis as well as structural remodeling were suggested by the data presented in this study.

3. **Is experimental depletion of CD11b$^+$Ly-6G$^+$ cells affected by the presence of a tumor?** In addition to inducing changes in CD11b$^+$Ly-6G$^+$ cell development and biology, HNC also limited antibody mediated depletion of these cells. This study described a phase of complete depletion of CD11b$^+$Ly-6G$^+$ cells in the peripheral blood, which is followed by the reappearance of the cells despite continuous antibody application. During the complete peripheral blood depletion phase, detailed analysis revealed a reservoir of resistant CD11b$^+$Ly-6G$^+$ cells not only in the bone marrow but also in spleen and tumor. Furthermore, extramedullary granulopoiesis was highly induced in depleted animals, which showed remarkable high G-CSF and KC serum levels. These processes resulted in the CD11b$^+$Ly-6G$^+$ cell rebound during continuous depletion, which was found to be faster in HNC tumor bearing animals than in naive mice. It was also shown for the first time that reappearing CD11b$^+$Ly-6G$^+$ cells display a pronounced regulatory phenotype which might interfere with long term experiments.

4. **Does Ly-6G play a role in CD11b$^+$Ly-6G$^+$ cell-tumor interactions?** In a pilot study, this question was addressed in CatchUp mice. The Ly-6G knockout genotype resulted in accelerated tumor growth in a subcutaneous HNC model. While CD11b$^+$ cells equally infiltrated tumor tissue in both genotypes, gene expression revealed changes in T cell regulating cytokines. Surprisingly and not in accordance with accelerated tumor growth, regulatory T cell infiltration was decreased in tumors from Ly-6G$^{-/-}$ mice. Therefore, the function of Ly-6G was not fully elucidated in this initial study and requires more detailed analysis in the future.

Some of the main findings and controversies of this study will be discussed in the following sections.

5.1 Interaction of neutrophils and HNC

As described in section 1.3, many scenarios have been identified in which murine CD11b$^+$Ly-6G$^+$ cells and human neutrophils are affected by the tumor and may in turn affect tumor progression. The later include suppression of antitumor immunity as well as the direct or indirect promotion of angiogenesis, invasiveness and metastasis of tumor cells. Notably, these functions were usually described independent of each other in distinct models or tumor entities. In HNC patients, recent data suggested similar protumoral mechanisms of neutrophils[203] but a murine model for HNC-neutrophil interaction was not described so far. This thesis presented such a model and the central advances achieved in this model will be discussed in the next sections.

5.1.1 Effects of the tumor on CD11b$^+$Ly-6G$^+$ cell frequencies and functions

Recently, many tumor cell lines were described to induce CD11b$^+$Ly-6G$^+$ cell accumulation in tumor bearing mice. One study by Youn *et al.* compared several cell lines in their capacity of inducing CD11b$^+$Ly-6G$^+$ cell accumulation[222]. They presented that highest induction of CD11b$^+$Ly-6G$^+$ cells in BL6 mice is achieved by the EL4 lymphoma cell line. As human HNC was also associated with accumulation of neutrophils and immunosuppressive subsets[15, 203], a comparable HNC mouse models would represent a tool for detailed analysis of neutrophil-tumor interactions and possible interventions. Nevertheless, described HNC mouse models using tumor cell lines and chemical cancer induction were not shown to be associated with CD11b$^+$Ly-6G$^+$ cell modulation so far. The HNC model presented in this study was characterized to induce CD11b$^+$Ly-6G$^+$ cell accumulation in spleen and blood in relation to tumor progression (section 4.1.2). For comparability to other studies. this study used the EL4 cell line, which was characterized by Youn *et al.*[222], as a reference. Surprisingly, the reported CD11b$^+$Ly-6G$^+$ cell frequencies of 30 % of all splenocytes were not induced in this study by neither EL4 nor any of the tested HNC cell lines. Regardless of this difference, a significant induction of splenic CD11b$^+$Ly-6G$^+$ cell frequencies was demonstrated by the reference cell line in the presented study. This is also in line with a study from another group demonstrating a two-fold increase of splenic CD11b$^+$Ly-6G$^+$ cells upon EL4 tumor burden[123]. It was therefore concluded, that the difference to the Youn study was not due to differential activity of the reference tumor cell line. Potential explanations for the difference in detected cell numbers might include the mice themselves, which might have been obtained from different breeders, or diverging protocols for splenocyte isolation and flow cytometry procedures subsequently resulting in the detection of remarkably different cell numbers. Consequently, the herein presented changes in CD11b$^+$Ly-6G$^+$ cell distribution upon tumor burden were highly relevant and compared to well established tumor cell lines, the HNC tumors induced high amounts of these cells. This finding implicated a pronounced role of neutrophils in the course of HNC progression.

When demonstrating that CD11b$^+$Ly-6G$^+$ cells accumulate in a tumor model, the consequence of such a process gains interest. In the past, many studies concentrated on functional analysis of spleen and blood derived CD11b$^+$Ly-6G$^+$ cells. Especially when investigating myeloid derived suppressor cells (MDSC), these sources were chosen because of the robust accumulation in the respective organs in the course of tumor progression. As implicated by the terminology, immunosuppression is a central process of spleen derived MDSC function in these studies (summarized in reference [14]). Further data provided evidence for an impact of the tumor on bone marrow derived neutrophils,

which is in accordance with deregulated granulopoiesis[25]. This process could result in the release of immature cells from the bone marrow to the circulation where they were shown to be highly immunosuppressive[18, 60]. Thus, the induction of a higher number of immature CD11b$^+$Ly-6G$^+$ cells would further contribute to the general state of immunosuppression in tumor bearing mice. Nevertheless, it is unclear whether the immunosuppressive capacity is an intrinsic feature of CD11b$^+$Ly-6G$^+$ cells or whether it requires local activation. Regarding this question, a study in a prostate tumor model suggested that peripheral CD11b$^+$Ly-6G$^+$ cells from liver or spleen indeed require activation of iNOS by IFN-γ to gain T cell suppressive capacities[76]. To clarify intrinsic suppressive activity of CD11b$^+$Ly-6G$^+$ cells in the HNC model, spleen and bone marrow derived cells from tumor bearing mice were analyzed *ex vivo* in the presented study. Suppression of polyclonal T cell proliferation by splenic as well as bone marrow derived neutrophils was thereby confirmed (figure 4.11). In this experimental setup, production of IFN-γ by T cells is also induced (not shown) and could induce suppressive activities in both cell types. Nevertheless, in Ly-6G to T cell ratios of 1:2.5 or 1:1 only a few T cells were actually activated and the amount of IFN-γ production was therefore negligible. An intrinsic immunosuppressive capacity of CD11b$^+$Ly-6G$^+$ cells independent of organ specific localization was therefore indicated by the presented data in HNC bearing mice.

How are these neutrophil modulating processes induced? Tumor derived factors seem to be critical for the induction of neutrophil accumulation and functions[40]. As the microenvironment of each tumor entity differs, differential activation and subsequent functions of neutrophils arise. In line with this hypothesis, TGF-β was identified as a key factor driving a protumoral CD11b$^+$Ly-6G$^+$ cell phenotype. TGF-β blockade resulted in a phenotypic shift towards an antitumoral phenotype of CD11b$^+$-Ly-6G$^+$ cells in a mesothelioma and lung tumor model[54]. Additionally, TGF-β was recently indicated to promote a shift towards a neutrophil subset with immunosuppressive properties and low density among blood CD11b$^+$Ly-6G$^+$ cells[170] suggesting further peripheral effects of tumor derived factors. Additional cytokines are likely to promote comparable activations. For example, a recent study indicated that the role of neutrophils in HNC patients was induced by a tumor cell-neutrophil cross talk which was at least partly dependent on tumor derived macrophage migration inhibitory factor (MIF)[39]. In the present study, overexpression of MIF in murine HNC cell lines was demonstrated in comparison to healthy tissue (figure 4.2), which further strengthens the potential role of this molecule in HNC. Additionally, MIF might be one factor for induction of accumulation of CXCR2 and CXCR4 responsive cells like neutrophils (figures 4.4 and 4.7). KC, a more potent ligand for CXCR2, was also produced by the HNC cell lines (not shown). Both cytokines could result in the attraction of CD11b$^+$-Ly-6G$^+$ cells to the tumor tissue, which is likely to be induced by CXCR2 ligands. This assumption is based on receptor downregulation in the tumor tissue (figure 4.4), which was described to be induced by prolonged ligand exposure[48, 220]. It was therefore suggested, that in the HNC model the tumor induced a CXCR-ligand dependent modulation of neutrophils which could result in an activation of protumoral functions.

Despite the described peripheral functions of CD11b$^+$Ly-6G$^+$ cells, a local activation at the tumor site becomes more and more apparent as indicated in the previous paragraph. This is in line with studies demonstrating that not only peripheral neutrophil numbers but especially the amount of tumor infiltrating cells are clinically associated with poor outcome for example in HNC[207, 203]. Accordingly, a recent study suggested that immunosuppressive capacities of CD11b$^+$Ly-6G$^+$ cells are limited

to the site of ongoing inflammation in a prostate tumor model[76]. In detail, the authors showed T cell suppression by splenic CD11b$^+$Ly-6G$^+$ cells as well but tumor infiltrating cells were much more suppressive because they did not depend on T cell derived IFN-γ. Functionally, CD11b$^+$Ly-6G$^+$ cell infiltration into the tumor was shown to be required for the induction of a metastatic phenotype of fibrosarcoma cells in another study[200]. Furthermore, transcriptomic analysis offered the possibility of analyzing detailed phenotypic differences from small cell populations. A detailed comparison of naive neutrophils, peripheral neutrophils from tumor bearing mice and tumor infiltrating neutrophils was provided by Fridlender *et al.* in Balb/C mice[55]. The results demonstrated downregulation of structural genes and cytotoxicity in tumor infiltrating CD11b$^+$Ly-6G$^+$ cells and further characterized upregulation of immunoregulatory genes as a key mechanism induced in tumor bearing mice with peripheral CD11b$^+$Ly-6G$^+$ cells showing lower upregulation than tumor infiltrating CD11b$^+$Ly-6G$^+$ cells. Further upregulation of 13 chemokines was also presented by this group in tumor infiltrating cells compared to CD11b$^+$Ly-6G$^+$ cells from naive mice. This data demonstrated the broad character of intratumoral activation in the Balb/C mouse model. The present study also analyzed CD11b$^+$Ly-6G$^+$ cells from different localizations in HNC bearing BL6 and CatchUp mice on the BL6 background to evaluate similar intratumoral activations. Tumor infiltrating CD11b$^+$Ly-6G$^+$ cells were more activated than splenic CD11b$^+$Ly-6G$^+$ cells as determined by cell surface CD11b expression (figure 4.12A). Notably, CD11b upregulation is a general characteristic of tissue resident neutrophils as it is upregulated upon extravasation to enhance migration into the tissue[104]. Nevertheless, extravasation is generally also associated with activation but the fate of this activation in turn depends on the local factors[40]. In the HNC tumor, CD11b$^+$Ly-6G$^+$ cells furthermore exerted higher expression and release of Arg1 and higher protein content of iNOS compared to spleen derived cells (see figure 4.12), which suggested that increased immunosuppression is likely to be a feature of tumor infiltrating CD11b$^+$Ly-6G$^+$ cells in this model. Notably, iNOS was classified as part of a "N1" antitumor phenotype of CD11b$^+$Ly-6G$^+$ cells[54, 133] because of its proinflammatory function. Regardless of this classification, both iNOS and Arg1 were shown to be key mediators of CD11b$^+$Ly-6G$^+$ cell dependent T cell suppression and tumor promotion[36]. Therefore, iNOS was considered a tumor promoting factor in this model. Furthermore, intratumoral localization also affected mRNA expression of proangiogenic VEGF, suggesting that promotion of angiogenesis is not intrinsic to CD11b$^+$Ly-6G$^+$ cells but specifically induced at the tumor site. MMP9 would further support this function in the tumor but was not found to increase in comparison to spleen derived CD11b$^+$Ly-6G$^+$ cells. Adding even more complexity, the chemokines CCL2 and CCL3 were also highly expressed on mRNA levels in tumor infiltrating neutrophils in HNC tumors. By the production of these chemokines, recruitment of additional immune cells is mediated. CCL2 was implicated in a number of studies to recruit monocytic cells further promoting tumor progression[121, 134, 156]. Additional expression of CCL3 could recruit regulatory T cells and other CCR5 expressing leukocytes[172]. Furthermore, this chemokine was associated with enhanced angiogenesis in a lung tumor model by induction of MMP9 expression by macrophages, which in turn also promoted metastasis formation[216]. Collectively, these data suggest a profound activation of protumoral functions of CD11b$^+$Ly-6G$^+$ cells in the HNC tissue being suppression of antitumor responses, attraction of additional tumor promoting immune cells and direct as well as indirect promotion of angiogenesis. These complex activations demonstrated that CD11b$^+$-Ly-6G$^+$ cell effects on tumor progression might occur directly as well as indirectly via additional cell

lines further shaping the tumor microenvironment

The presented data indicated that HNC tumors affect neutrophils at different tissue compartments of the tumor bearing host. An intrinsic capacity of CD11b$^+$Ly-6G$^+$ cells in suppressing T cell activation was demonstrated. On top of that, accumulation in the periphery as well as migration towards the tumor tissue was induced by tumoral factors which locally activated versatile tumor promoting functions. Thereby, neutrophils are promoted to not only interfere with activation of immune responses but also mediate attraction of additional immune cells. The tumor tissue therefore becomes a major site of direct protumoral CD11b$^+$Ly-6G$^+$ cell activation while peripheral CD11b$^+$Ly-6G$^+$ cells from tumor bearing mice directly promote tumor growth via intrinsic immunosuppressive functions.

5.1.2 Impact of CD11b$^+$Ly-6G$^+$ cells on tumor progression

As mentioned before, neutrophils did not only accumulate during tumor progression but exerted specific tumor promoting functions as well. The detailed knowledge of neutrophil functions is central for understanding disease progression and for the development of potential therapeutic strategies. This does not only address the nature of the function itself as the timing of neutrophil activity is even more important. Next to their central role in acute inflammation, neutrophils were shown to substantially contribute to chronic inflammatory diseases by sensing danger associated molecular patterns (DAMPs) and releasing further immunogenic products[22]. Thereby, they could also be conductive to the establishment of malignant lesions as many cancer entities may result from inflammatory processes[44]. In transplantable experimental models, this process is of course lacking. Nonetheless, these experimental tumors proceed in different stages as well. In line, they need to establish first, evade recognition by the immune system and require stromal support and nutrient supply during the growth phase. Earlier studies already indicated that the tumor promoting activity of CD11b$^+$Ly-6G$^+$ cells might be limited to different stages of tumor progression in experimental models as well. Accordingly, Mishalian *et al.* presented that only late tumor progression is affected by Ly-6G$^+$ cell depletion because early tumors of the tested lung and mesothelioma cell lines neither attracted nor interacted with CD11b$^+$Ly-6G$^+$ cells[133]. To further analyze the contribution of CD11b$^+$-Ly-6G$^+$ cells to HNC progression in the models presented herein, antibody dependent depletion was applied in this study as well and was carried out during both phases, HNC establishment and seeding as well as advanced tumor progression (see section 4.2.1). Presence of CD11b$^+$Ly-6G$^+$ cells had only a slight effect on advanced HNC tumor progression in BL6 and hardly any effect in C3H mice (figure 4.13). In contrast, early tumor establishment and onset of progression was dependent on the presence of neutrophils especially in the BL6 HNC model (figure 4.14). These findings were contradictory to the results in the Mishalian study[133], which might be due to the different tumor models in both studies. A key difference between the HNC model and the lung and mesothelioma models of the Fridlender group is the onset of infiltration of Ly-6G$^+$ cells into the tumor tissue. Transplanted HNC tumors were infiltrated immediately after induction of tumor progression within a few days (data not shown) while in the other models, the authors stated that infiltration started at the stage of advanced tumor volumes. For this reason, CD11b$^+$Ly-6G$^+$ cells can take over important tumor promoting functions in the presented HNC models which was not possible in the Mishalian study. Furthermore, additional data from different tumor models indicated that early promotion of tumor formation by neutrophils in transplantable tumor models is not limited to tumors derived from HNC

cell lines[67, 90, 113, 139, 197, 200, 150]. For this reason, neutrophil induced tumor establishment was identified as a key process in experimental HNC tumors as these cells were attracted early on.
If an immune response is raised against transplanted tumor cells, this would result in the eradication of the tumor within a few weeks. Therefore, a central task during establishment of an experimental tumor is made up by the suppression of an immune activation or the blockade of the access of antitumor effector cells to the site of tumor formation. Immunosuppressive functions of $CD11b^+Ly\text{-}6G^+$ cells were demonstrated in a number of tumor models which also resulted in the name granulocytic myeloid derived suppressor cells (MDSC) for $CD11b^+Ly\text{-}6G^+$ cell in tumor bearing hosts[18, 183]. Detailed mechanisms of neutrophil induced suppression of antitumor immunity were summarized in section 1.3.2. In line with these mechanisms, Grizzle *et al.* showed that TS/A tumors get rejected in young mice which do not mount a neutrophil response while the tumor induces $CD11b^+Ly\text{-}6G^+$ cell accumulation in older mice resulting in the ability of tumor formation[67]. Another group also indicated that adoptive immunotherapy against the HER-2/neu antigen can only be effective in a transgenic breast tumor model if a combination with $CD11b^+Ly\text{-}6G^+$ cell depletion is performed[139]. Furthermore, anti-PD1 therapy, which should result in enhanced activation of antitumor T cells, was only effective in a model of rhabdomyosarcoma if $CD11b^+Ly\text{-}6G^+$ cell infiltration into the tumor was blocked as well[79]. These studies demonstrated the potential role of neutrophils in tumor associated immunosuppression not only for tumor formation but also for immune targeting therapies. The presented study indicated an early implication of $CD11b^+Ly\text{-}6G^+$ cells in the formation of experimental HNC (figure 4.14) and immunosuppression was therefore assessed as a potential mechanism of the observed growth delay. In histological analysis, antitumor effector cell infiltration was affected in the first days of tumor progression under $CD11b^+Ly\text{-}6G^+$ cell depletion (figure 4.15). T cell suppressive activity of $CD11b^+Ly\text{-}6G^+$ cells from HNC tumor bearing animals was further confirmed *in vitro* (figure 4.11) but simultaneous depletion of $CD11b^+Ly\text{-}6G^+$ and CD8 T cells did not resolve delay of tumor progression in all mice (tumor progression was benefited in 50 % of the double depleted mice as shown in figure 4.16). Furthermore, in nude mice, which are unable to mount a directed T cell response, Gr-1 depletion did only result in slightly but not significantly reduced tumor growth of BL6 derived $MOPC^-$ cells. Therefore, T cells seemed to be affected by $CD11b^+Ly\text{-}6G^+$ cells in the HNC model but they did probably not represent the only mechanism of $CD11b^+Ly\text{-}6G^+$ cell mediated HNC progression. Additional immune cells might also be affected by neutrophils in this model and should be analyzed in future studies in more detail. Based on an accumulation in the draining lymph node of HNC tumor bearing GR-1 depleted animals (data not shown), NK cells were a promising candidate for further analysis and have not been addressed in detail in this study. NK cells were shown to be manipulated by $CD11b^+Ly\text{-}6G^+$ cells via NKG2D downregulation[113, 45] resulting in reduced cytotoxicity by diminished perforin production[187, 117]. These antitumor effector cells were likely to be involved in reduced tumor progression upon $CD11b^+Ly\text{-}6G^+$ cell depletion in the HNC model. Even though their presence in the tumor upon depletion did not change very much, NK cells could be more cytotoxic in the absence of $CD11b^+Ly\text{-}6G^+$ cells. Conclusively, suppression of T cell responses presented as a potential mechanism of $CD11b^+Ly\text{-}6G^+$ cell mediated establishment of HNC tumors but additional mechanisms seem to be present in this model.
Another event of key importance to tumor formation is angiogenesis as a tumor mass is not able to exceed a volume of 2 mm^3 without vascular supply[141]. Angiogenesis is often taking place in accor-

dance with further changes in the local tissue structure including matrix remodeling, which enables the generation of a tumor niche. CD11b$^+$Ly-6G$^+$ cells were able to substantially take part in these processes by release of proteases and growth factors[218, 103] (for more details see section 1.3.2). In histological analysis, the presented study indicated that angiogenesis was affected in the first days of tumor progression under CD11b$^+$Ly-6G$^+$ cell depletion (figure 4.17B). Further Gr-1 depletion experiments using the matrix providing component Matrigel^{TM} indicated that the component substituted for a function of the neutrophils because depletion had no effect on these tumors (figure 4.17C). Matrigel^{TM} provides ECM structure as well as diverse growth factors to the tumor and promotes angiogenesis[149, 43], which ablated the effects observed by CD11b$^+$Ly-6G$^+$ cells depletion in the presented experiments. Therefore, an additional function of CD11b$^+$Ly-6G$^+$ cells was suggested by these experiments. CD11b$^+$Ly-6G$^+$ cell presence resulted in stromal support to HNC tumor cells, probably by matrix remodeling protease activities, during seeding and establishment of the tumor and further induced early angiogenesis.

While many studies concentrated on distinct functions of CD11b$^+$Ly-6G$^+$ cells in tumor progression (as described in section 1.3.2 and 1.3.3 in more detail), a simultaneous exertion of a combination of those functions was rarely addressed. Only one study by Srivastava *et al.* reported about two simultaneous functions of CD11b$^+$Ly-6G$^+$ cells in tumor bearing mice[187]. In a SC lung tumor model, they demonstrated neutrophil mediated T and NK cell suppression as well as promotion of angiogenesis, which was diminished after depletion of these cells. As the majority of studies presented data about one explicit function of CD11b$^+$Ly-6G$^+$ cells in the context of a tumor burden, it would be likely that several neutrophil phenotypes exist which are either proangiogenic, metastasis-promoting or immunosuppressive. The way of activation of these potential phenotypes is not clarified in detail. In contrast, gene expression of HNC infiltrating CD11b$^+$Ly-6G$^+$ cells suggested activation of diverse functions (figure 4.12), which made this study consider immunosuppression as well as angiogenesis and structural (stromal) support as possible causes of CD11b$^+$Ly-6G$^+$ cell mediated tumor progression in the HNC models. The experiments presented in sections 4.2.2 and 4.2.3 supported this hypothesis. It was presented that the absence of T cells as well as additional matrix reverse the delay of tumor formation and onset of progression by CD11b$^+$Ly-6G$^+$ cell depletion. This study therefore provided evidence for simultaneous proangiogenic and immunosuppressive functions of CD11b$^+$Ly-6G$^+$ cells in the establishment phase of HNC progression.

5.1.3 Potential role of the neutrophil molecule Ly-6G

In a pilot study, the importance of the neutrophil specific murine protein Ly-6G was furthermore addressed in the context of HNC progression. A role for Ly-6G in CD11b$^+$Ly-6G$^+$ cell integrin-mediated migration was suggested by a study of Wang *et al.* in 2012[208] but was not confirmed in a Ly-6G knockout model[75]. In line with these previous results in the CatchUp animals used herein, migration into HNC tumors was unaffected by the absence of Ly-6G (figure 4.29). It was therefore concluded that Ly-6G is dispensable for the migration of CD11b$^+$Ly-6G$^+$ cells. As Wang *et al.* used antibodies in their study to block Ly-6G function, antibody mediated activation or unspecific effects are most likely to be the underlying mechanism of their observation. Even though enhanced tumor growth was presented in Ly-6G knockout animals (see figure 4.28), this study lacks a comprehensive mechanism for this effect due to the small size of the studied groups. Further research would be necessary to identify the

exact implication of CD11b$^+$Ly-6G$^+$ cells in tumor growth differences between Ly-6G$^{-/+}$ and Ly-6G$^{-/-}$ mice. Unexpectedly, Tregs were reduced in tumors from Ly-6G$^{-/-}$ mice even though higher induction of CCL17 expression by a tumor infiltrating neutrophil could have been associated with higher Treg infiltration (as also described in reference [132], see figures 4.32 and 4.30). This result rather suggested a generalized defect of Treg cells in Ly-6G$^{-/-}$ CatchUp mice which could be further investigated but is not probable to be implicated in tumor progression. An antitumor role of Treg cells was so far only demonstrated in inflammation induced cancers such as colorectal cancer[47]. A comparable mechanism is rather unlikely in the presented transplantable SC tumor model. Increased expression of VEGF in tumor infiltrating CD11b$^+$Ly-6G$^+$ cells of two Ly-6G$^{-/-}$ versus Ly-6G$^{-/+}$ pairs suggested that further analysis should concentrate on tumor angiogenesis, which is likely to result in enhanced tumor growth. Nevertheless, the mechanism of a potential suppression or regulation of VEGF expression by Ly-6G remained elusive and further investigations would be required to draw comprehensive conclusions from the presented implication.

5.2 Limitations of experimental antibody mediated neutrophil depletion

Experimental elimination of neutrophils by depletion antibodies is a well established method, which is used to decipher the function of these cells in murine models of inflammation, infectious diseases and cancer. Nevertheless, a longitudinal analysis of treatment efficacy in different tissue compartments was not provided so far. The presented study revealed a number of limitations of the technique in a HNC tumor model by performing these analysis, which will be discussed in the following section.

5.2.1 Incomplete depletion in different tissues of tumor bearing mice

Application of Ly-6G depleting antibodies results in fast elimination of peripheral blood neutrophils within one day[23, 32] and blood is the most frequently tested organ when assessing depletion efficacy. If the thereby determined efficacy would be correct, the depletion would be the perfect tool for the analysis of CD11b$^+$Ly-6G$^+$ cell functions in murine models. However, first limitations of this techniques arose from the identification of undepleted CD11b$^+$Ly-6G$^+$ cell reservoirs in bone marrow of naive mice[163] and local CD11b$^+$Ly-6G$^+$ cells in the liver of tumor bearing animals[123]. These cells were detected as soon as 24 hours after antibody injection. Nevertheless, many studies carry out long term depletion especially in the field of oncology to assess tumor growth without assessing further tissue specific efficacy. In addition to CD11b$^+$Ly-6G$^+$ cells residing in bone marrow and liver, the presented study identified depletion resistant cells in spleen and tumor within 4 days of depletion using αGr-1 antibody[4] while peripheral blood cells were completely eradicated (see figure 4.18 and 4.21). Intratumoral cells were further characterized directly *in vivo* by noninvasive multiphoton microscopy and their viability and migratory capacity was demonstrated (figure 4.21). Of note, these cells from CatchUp animals with Ly-6G promoter dependent tdTomato expression had lower fluorescence intensity than intratumoral cells from undepleted mice (n=1, data not shown). This observation suggested a low Ly-6G promoter activity, which would be in line with a rather immature phenotype[78]. Therefore, insufficient intratumoral depletion might be due to a combination of limited antibody penetration in the tissue and low abundance of Ly-6G surface expression in a subset of immature tumor infiltrating CD11b$^+$Ly-6G$^+$ cells. Inefficient depletion was further confirmed

[4] Depletion was always carried out continuously with antibody injection every three days after start of treatment.

in HNC tumor bearing mice after αLy-6G mediated depletion, which was demonstrating a general functional disadvantage of the technique. Notably, CD8 depletion was found to be complete in the tumor tissue even after three weeks of antibody treatment (data not shown). Therefore, resistance to depletion might be an intrinsic feature of neutrophils probably due to their fast cellular turnover. Given the pronounced importance of intratumoral CD11b$^+$Ly-6G$^+$ cells as described in the previous section, inefficient depletion in the tumor should not be ignored. It is rather likely that these cells interfere with the desired study outcome as they might still be able to exert their protumoral function. Furthermore, immature cells were often described to be potentially more immunosuppressive than mature neutrophils[19, 60]. Nevertheless, many studies identified tumor promoting mechanisms of CD11b$^+$Ly-6G$^+$ cells using this technology. Several potential reasons for this controversy exist. Depletion could be more efficient in other tumor models for example because of a different tumor architecture and microenvironment which might not support the survival of CD11b$^+$Ly-6G$^+$ cells in the tumor during depletion. Another reason could be that the mechanisms described in these studies are the central reason for the progression of the described tumors. This would mean that having a high number of depleted neutrophils resulted in the break down of the tumor promoting mechanisms of these models, which can not be compensated by a small number of remaining CD11b$^+$Ly-6G$^+$ cells. Furthermore, residual CD11b$^+$Ly-6G$^+$ cells could also be functionally impaired. Such a scenario has been described by Ribechini *et al.* They reported the loss of suppressive activity of depletion resistant, antibody coated CD11b$^+$Ly-6G$^+$ cells in the bone marrow[163]. A similar response could be induced in CD11b$^+$Ly-6G$^+$ cells in other tissues if they were coated with the depletion antibody. Whether this is a possible mechanism and whether it also holds true for functions like promotion of angiogenesis remains to be determined by future studies. Incomplete depletion in a number of tissues as shown in this thesis anyway requests for more detailed analysis of depletion efficacy in upcoming cancer studies.

Detection of murine neutrophils can be easily performed by flow cytometry using the surface markers CD11b and Ly-6G. Therefore, flow cytometry is also frequently used in depletion studies to determine depletion efficacy. Although limited detection of depletion antibody-coated neutrophils was already demonstrated in bone marrow neutrophils[163], flow cytometry did not loose importance for this purpose. The use of secondary antibodies enabled for the detection of depletion antibody-coated cells as well. Surprisingly, the presence of resistant cells was not apparent in flow cytometry in the presented study. Spleen resident resistant cells were not detectable by neither CD11b and Ly-6G flow cytometry nor by using secondary antibodies (figure 4.20) but immunohistochemistry (IHC) revealed remarkable resistance to depletion by neutrophils in the very same organ (figure 4.21). These results indicated further limitations of flow cytometry for the sake of testing for depletion efficacy. Nevertheless, the reasons for these dramatic differences in both techniques remain elusive. A possible explanation could be the loss of these resistant Ly-6G$^+$ cells during the isolation procedure while they can not disappear from the intact organ that is analyzed by IHC. Furthermore, IHC could be more sensitive in detecting Ly-6G^{low} neutrophils which would be missed by a flow cytometry strategy that is looking for classical Ly-6G^{high} mature cells. A low expression of Ly-6G by residual neutrophils was also suggested by intravital microscopy as discussed above. Nevertheless, limitations of flow cytometry are alarming because virtually all studies either do not check or report depletion efficiency at all[202, 113, 155], check depletion efficacy only in the peripheral blood[54, 90, 139, 150, 189], analyze addi-

tional organs only by flow cytometry[84, 197, 161, 116, 181] or directly state that CD11b$^+$Ly-6G$^+$ cell numbers are only reduced[59, 92, 116, 139, 182, 187, 140]. These facts highlight the importance of the data presented in this study and suggest careful monitoring as well as choice of monitoring techniques when considering depletion of neutrophils.

5.2.2 Mechanisms of CD11b$^+$Ly-6G$^+$ cell rebound

As neutrophils are the key cell type of immediate immune responses against invading pathogens, their life cycle is closely regulated (see also section 1.1.1). Keeping in mind that these cells possess a remarkably short life span, fast mechanisms are likely to exist to regulate neutrophil numbers in case of acute infection or loss of cell numbers. This mechanism is called "emergency granulopoiesis" and is characterized by accelerated hematopoietic stem and progenitor cell (HSPC) proliferation[114]. Cain *et al.* indicated in their study on emergency granulopoiesis that this proliferative response is a consequence of the inflammation and G-CSF driven exhaustion of the bone marrow neutrophil pool[23]. They further demonstrated that the number of bone marrow neutrophils inversely correlated with HSPC proliferation 48 hours after a single dose injection of different amounts of αGr-1 antibody. This response resulted in a reconstitution of bone marrow neutrophil numbers within 4 days after single dose αGr-1 treatment[5] and was preceded by a G-CSF response, which peaked between day 1 and 2 after antibody injection. In the presented study, a remarkable increase in serum G-CSF was detected on day 5 after start of continuous αGr-1 treatment even though bone marrow repopulation was already induced (see figures 4.22 and 4.20). This result indicated that upon continuous antibody presence and tumor burden, additional regulatory mechanisms take place to adjust neutrophil numbers. In line, the cytokine KC was also increased in the treated animals. As a consequence of high levels of CD11b$^+$Ly-6G$^+$ cell stimulating factors, an increased level of granulopoiesis was observed in spleen derived cells from tumor bearing, depleted animals (see figure 4.23). This is in line with data showing tumor- as well as G-CSF-induced mobilization of progenitor cells to the spleen and the resulting enhancement of this organ as a site of extramedullary granulopoiesis[25, 30]. As CD11b$^+$Ly-6G$^+$ cell modulation is also a key characteristic of tumor progression in the HNC model and many other studies, potential interference of tumor burden with antibody mediated depletion was tested in the presented study. The emergency-like granulopoiesis in response to neutrophil depletion was observed in both naive and tumor bearing mice in this study. Of note, the presence of a tumor accelerated this process and resulted in earlier rebound of neutrophils in the peripheral blood (figure 4.24). These findings suggested that cancer related inflammation potentiates the depletion induced granulopoiesis albeit the mechanisms responsible for this effect still need to be elucidated.
Even though granulopoiesis is enhanced under depletion pressure, the resulting CD11b$^+$Ly-6G$^+$ cells would still be depleted by the applied antibodies. Based on this assumption, long term studies were designed and carried out. A depletion period of three weeks can be found in a number of studies in the field of tumor immunology[150, 84, 4, 197, 113, 54, 139, 67, 92, 117]. Nevertheless, data presented in this study reliably demonstrated a profound CD11b$^+$Ly-6G$^+$ cell rebound during long term depletion, which is taking place after about ten days (figures 4.19 and 4.24). This fact raises the question of the mechanism of rebound under depletion pressure. To assess this question, the mode of action of antibody induced depletion is of importance, which is a topic of vivid debate. Most likely, antibody binding and

[5] αGr-1 was dosed at 100 µg per mouse IP. Detection was carried out including a secondary antibody.

ligation of Ly-6G results in activation and apoptosis of the affected cell[163], which is probably at least partly involving complement factors[1] leading to the final elimination of sequestered, dying cells by phagocytes especially in spleen, liver and bone marrow[20]. For bone marrow compensation of depletion, an antiapoptotic mechanism has been suggested by Ribechini *et al.* involving enhanced expression of the Bcl-2 family member MCL-1 in bone marrow resident CD11b$^+$Ly-6G$^+$ cells[163]. In section 4.3.4, it was shown that upon rebound during continuous depletion, MCL-1 is especially increased in spleen derived CD11b$^+$Ly-6G$^+$ cells while its expression in bone marrow resident CD11b$^+$Ly-6G$^+$ cells was comparable to the control group. Furthermore, survival of spleen derived CD11b$^+$Ly-6G$^+$ cells was also increased (figure 4.25) suggesting a similar antiapoptotic mechanism taking place in the rebound phase. The described compensatory mechanisms ultimately resulted in the reappearance of neutrophils with an immature phenotype. It is rather likely that these cells could also get depleted by the antibody when they undergo maturation. But their immature status in combination with their high numbers enabled the process of CD11b$^+$Ly-6G$^+$ cell rebound during long term depletion.
The presence of high numbers of immature neutrophils during the rebound phase of long term depletion challenges the applicability of these experimental settings. The function and phenotype of these cells is central to the interpretation of all studies with depletion periods of more than one week. Immature myeloid cells including CD11b$^+$Ly-6G$^+$ cells exert immunosuppressive activity in infectious diseases[65] as well as in cancer[5, 60]. Furthermore, key effector mediators of immature myeloid suppressive cells are Arginase1[143] and reactive oxygen species (ROS)[105]. Both mediators were also found to be constitutively increased in the immature cells resulting from rebound during long term depletion in the present study (figure 4.27). Furthermore, reduced non-specific, αCD3 and αCD28-induced T cell proliferation was observed in mixed splenocyte cultures from mice in the rebound phase (data not shown) indicating an increased state of peripheral T cell suppression in these animals. Finally, the reappearing CD11b$^+$Ly-6G$^+$ cells were tested for expression of anti- and protumoral phenotypic markers. This set of markers originally derived from a study by Fridlender *et al.* who observed an antitumoral phenotypic shift of tumor infiltrating neutrophils[6] upon TGF-β inhibition[54]. In the present study, the most remarkable changes between isotype-treated and depletion-resolved spleen-derived CD11b$^+$Ly-6G$^+$ cells were an upregulation of CCL17 and a simultaneous downregulation of TNF-α expression, which are representatives from the protumor "N2" and the antitumor "N1" group, respectively. It was therefore concluded, that a phenotypically protumoral N2 shift is taking place in peripheral CD11b$^+$Ly-6G$^+$ cells from tumor bearing mice after long term depletion is resolved. These changes could further result in increased Treg expansion as CCL17 was recently shown to be a key mediator in CD11b$^+$Ly-6G$^+$ cell-Treg crosstalk[132]. These results are of central importance for long term depletion experiments, as they demonstrate the presence of immature immunomodulatory neutrophils which are capable of interfering with the study outcome.

5.2.3 Consequences for data interpretation

In conclusion, it is not advisable to carry out long term depletion using neutrophil specific antibodies especially under CD11b$^+$Ly-6G$^+$ cell modulating conditions such as HNC and other tumor models. Even though many studies found detailed mechanisms of CD11b$^+$Ly-6G$^+$ cell mediated tumor progression using this technique, they very likely worked in a tumor model with very strong neutrophil

[6] In the respective study termed tumor associated neutrophils (TAN)

mediated effects. Nevertheless, in many models as well as in human disease, a majority of functions could be shared between related cell types. In line with this, other cells like monocytes could take over for neutrophil mediated functions like immunosuppression and promotion of angiogenesis[82, 137], which would not be affected by single cell type depletion. Therefore, the complex crosstalk between the various cell types that are implicated in tumor progression is hard to be dissected experimentally. For this reason and with the knowledge of the limitations presented in this study, one conclusion is central: Especially studies which show no effect of neutrophil depletion on tumor progression (and probably also in the context of other disease models) might have been affected by the phenomena of incomplete depletion and CD11b$^+$Ly-6G$^+$ cell rebound. This key conclusion is not only applicable for published data but is of particular interest for the first part of the presented study. It was demonstrated that the presence of CD11b$^+$Ly-6G$^+$ cells is more important for tumor establishment and formation than for advanced and established tumor progression in a transplantable HNC model (figures 4.13 and 4.14). As incomplete depletion and CD11b$^+$Ly-6G$^+$ cell reappearance was demonstrated in the same model, the role of CD11b$^+$Ly-6G$^+$ cells in advanced tumor progression is very likely underestimated by the presented data. The growth curves in section 4.2.1 were recorded during a period between one to two weeks after induction of CD11b$^+$Ly-6G$^+$ cell depletion and compensatory cell expansion was therefore not present for the longest part of observation as rebound started around day ten. Nevertheless, resistant undepleted cells were present throughout the experiment. As the activity and fate of these cells is not clarified yet, their capacity of compensating for the loss of many CD11b$^+$-Ly-6G$^+$ cells is hard to be estimated. It is still very likely, that resistant cells are capable of exerting similar functions as immature reappearing cells, thereby interfering with the outcome of the study by immunosuppression and promotion of tumor growth. A higher impact of CD11b$^+$Ly-6G$^+$ cells in advanced tumor progression in the HNC model is therefore likely.
Taken together, the presented study provided evidence for limited applicability of long term antibody mediated neutrophil depletion especially in murine tumor models. Furthermore, depletion has to be monitored critically in more organs than peripheral blood and with more methods than flow cytometry to ensure the best possible quality of data interpretation.

5.3 Therapeutic implications

An association between high peripheral neutrophil counts and tumor progression as well as poor survival has been found for a variety of malignant diseases[201]. Further functional alterations of neutrophils in respective patients included neutrophil survival, ROS and cytokine production and further mediators like VEGF and MMP9 which directly affect tumor progression (see section 1.2.2). On the other hand, chemotherapeutic agents were shown to rapidly induce neutropenia, which might cause severe side effects and delays in therapy[31]. Given the important antimicrobial roles of neutrophils, infections could arise from severe neutropenia resulting in longer hospitalization and increased treatment costs. As a compensatory treatment for such side effects, G-CSF arose as a tool for limiting neutropenia especially in phases of high dose treatment as for example in adjuvant breast cancer therapies[46]. A similar study in HNC resulted in an unexpected improvement of survival[192]. Nevertheless, G-CSF is known to drive mobilization of HSPCs in humans as well and this treatment could also result in the accumulation of immunoregulatory cells in line with the data from the depletion experiments in the presented study. This effect might further interfere with treatment outcome and

could even result in accelerated tumor progression. Remarkably, Di Maio *et al.* showed in an analysis of three randomized trails in advanced non-small cell lung cancer that mild therapy-induced neutropenia was actually associated with longer survival in comparison to patients who did not develop neutropenia[34]. Thus, regulation and manipulation of neutrophil numbers in cancer patients under treatment resembles a balance act between risk of infections and interference with treatment outcome.

As manipulation of neutrophil cell numbers proved difficult for the reasons discussed above, other modes of neutrophil manipulation might be more promising. Earlier studies and the first part of this study implicated CXCR2 ligands as key mediators of neutrophil attraction to the tumor. Given the intratumoral activation of neutrophils, which was discussed earlier, this infiltration process might be a promising target for future therapies. Promising results were achieved in murine tumor studies using antagonists to CXCR2[79, 92] and safety of CXCR2 inhibition was already demonstrated in two studies dealing with respiratory diseases for treatment periods of 4 weeks[142] as well as 6 month[162]. Besides migratory blockade, which might also interfere with migration towards infection sites, neutrophil phenotypic shift could be a potential starting point for further treatment. In this way, the antitumoral potential of neutrophils would be efficiently used to strike back cancer progression. Such strategies could include interference with response modifiers such as TGF-β and IFN-β[54, 90] or activation of neutrophil cytotoxic and immune activating functions via microbial compounds[94, 193]. Further translational research will be needed to define potential treatment regimens aimed at modulating neutrophil numbers, migration, localization or function. Effectiveness of such treatments would have to be determined for the respective tumor entity as the distinct microenvironment in the tumor mass also affects treatment outcome. To this end, tumor models as presented in this study are key tools for preclinical evaluation of possible interventions.

5.4 Conclusions

In this study, a murine HNC model was developed to investigate interactions between CD11b$^+$Ly-6G$^+$ cells and the tumor. This model was characterized by expansion of CD11b$^+$Ly-6G$^+$ cells in blood and spleen of tumor bearing animals, which was not demonstrated before in HNC. Central experiments presented local activation of CD11b$^+$Ly-6G$^+$ cells in the tumor tissue. Thus, this model represents major characteristics of neutrophil-HNC interactions in human cancer patients as reported in former studies[38, 39, 203, 204]. In these HNC models, this study further strengthened the hypothesis, that neutrophil mediated effects in the tumor bearing host were not limited to one direction but that these cells rather exert a number of functions. Among these, immunosuppression as well as promotion of angiogenesis were suggested as mechanisms in HNC. Importantly, this study was able to provide evidence that protumorigenic CD11b$^+$Ly-6G$^+$ cells are not necessarily entrained by the tumor during tumor progression to become protumorigenic as it was put forward by earlier studies[133]. Instead, CD11b$^+$Ly-6G$^+$ cells have intrinsic capacities to quickly promote early processes such as establishment and formation of tumor cell accumulations at least in transplantable tumor models.
Finally, the presented thesis contains unprecedented longitudinal analyses of the efficacy of antibody mediated Ly-6G$^+$ cell depletion in different tissue compartments of tumor bearing mice. Incomplete depletion of neutrophils was thereby indicated in spleen and tumor in experimental tumor models and was further followed by rapid expansion of immunoregulatory immature granulocytic cells. Therefore, future long term studies on modulation and function of CD11b$^+$Ly-6G$^+$ cells require Ly-6G$^+$ depletion techniques which are more sophisticated and effective than antibodies. With the development of Ly-6G-Cre mice[75], genetically driven specific depletion of Ly-6G$^+$ cells may become available in future studies.

Summary

In contrast to other cells of the immune system, the role of neutrophils in cancer has only started to emerge in the last decades. Previous studies of our group showed that high infiltration of neutrophil granulocytes in head and neck cancer (HNC) tissues correlated with poor survival of patients with advanced disease. Further *in vitro* studies indicated that human neutrophils are manipulated by tumor cells to acquire a protumoral phenotype. Neutrophil manipulation by experimental tumors was also described for a variety of tumor types in murine models but HNC models were not yet tested in this respect. Therefore, at first, this study addressed the effect of murine experimental HNC on CD11b$^+$-Ly-6G$^+$ cells in the tumor bearing host and, secondly, the role of these cells in HNC progression. A central method for these analyses was the antibody mediated depletion of Ly-6G$^+$ cells. In this regard the efficacy of depletion in different organs of the host and the impact of tumor burden on depletion efficacy were analyzed. Finally, a pilot study in the last part concentrated on a potential role of the murine neutrophil specific molecule Ly-6G for CD11b$^+$Ly-6G$^+$ cell function during neutrophil-tumor interaction.

In the transplantable HNC models presented herein, tumors induced accumulation of CD11b$^+$Ly-6G$^+$ cells in the periphery (blood and spleen). Tumors transplanted to an orthotopic site were superior to subcutaneous tumors in this respect. This accumulation correlated with tumor progression in line with observations in HNC patients. Infiltration into the tumor tissue further activated Ly-6G$^+$ cells and induced a protumoral gene expression pattern including increased expression of immunosuppressive Arg1 and iNOS, proangiogenic VEGF and a cytokine pattern that was distinct from splenic Ly-6G$^+$ cells.

Using antibody mediated depletion, CD11b$^+$Ly-6G$^+$ cells were found to be mainly implicated in HNC cell seeding and establishment of a tumor while the presence of neutrophils did not further promote advanced tumor progression. The experiments suggested that neutrophils promoted tumor establishment by different mechanisms involving the regulation of T cell functions as well as by providing structural support and inducing angiogenesis.

A detailed characterization of antibody mediated neutrophil depletion (using αGr-1 as well as αLy-6G antibodies) revealed that the depletion in the peripheral blood could be divided into an initial one-week complete depletion phase, which was followed by the reappearance of Ly-6G$^+$ cells (rebound phase) despite continued antibody treatment. A depletion resistant pool of viable neutrophils resided in the tumor tissue, spleen and bone marrow during complete peripheral blood depletion. Reappearance of neutrophils during the rebound phase was accompanied by enhanced extramedullary granulopoiesis and occurred faster in tumor bearing mice than in naive mice. Reappearing CD11b$^+$-Ly-6G$^+$ cells displayed an immature phenotype and strongly expressed immunoregulatory molecules. In the last part, comparison of neutrophils from Ly-6G$^{+/-}$ and Ly-6G$^{-/-}$ mice suggested that the molecule Ly-6G is not involved in neutrophil-to-tumor migration. Nevertheless, enhanced HNC progression was observed in Ly-6G$^{-/-}$ mice. The underlying mechanism remains to be determined in future studies.

In summary, the presented HNC models were shown to possess characteristics of the human disease in terms of tumor-neutrophil interactions. Therefore, further functional analysis as well as therapeutic interventions involving neutrophil functions could be carried out in these models. Depletion experiments showed that CD11b$^+$Ly-6G$^+$ cells strongly promote early phases of tumor growth in this

model, most likely by influencing antitumor activity of T cells and by modulation of the recipient tissue niche. During tumor progression, Ly-6G$^+$ cells expand in the blood, spleen, bone marrow and tumor and display tissue specific alterations in function and gene expression. Analysis of Ly-6G$^+$ cells in later phases of tumor growth is limited by the rapid re-appearance of these cells despite continuous treatment with depleting antibodies which is mediated by enhanced extramedullary granulopoiesis and by the presence of viable, migratory, depletion resistant cells in bone-marrow, spleen and tumor. This transient, short-term nature of Ly-6G$^+$ cell depletion in the periphery and the continuous presence of tissue resident depletion resistant cells emphasize the need for careful monitoring and cautious interpretation of negative results in murine models of tumor-neutrophil or tumor-myeloid derived suppressor cell interaction.

Zusammenfassung

Die Rolle von Neutrophilen im Zusammenhang mit Krebserkrankungen fand in der Tumorimmunologie lange Zeit wenig Beachtung und wird erst seit einigen Jahren intensiv bearbeitet. In Kopf-Hals-Tumor (KHT)-Patienten mit fortgeschrittenem Tumorstadium konnten vorherige Studien in unserer Gruppe zeigen, dass eine starke Infiltration des Tumorgewebes mit einer schlechten Überlebensrate assoziiert ist. Daraufhin wurden *in vitro* Untersuchungen durchgeführt, welche zeigten, dass humane Neutrophile in Anwesenheit von tumoralen Faktoren einen tumorfördernden Phänotyp annehmen. Weiterhin sind in der Literatur einige experimentelle Tumorsysteme beschrieben, welche eine tumorfördernde Veränderung von Neutrophilen beschreiben. Untersuchungen zur Rolle von Neutrophilen in murinen KHT Modellen liegen bisher nicht vor. Aus diesem Grund war es ein Hauptziel des ersten Teils der vorliegenden Arbeit, Neutrophile ($CD11b^+Ly\text{-}6G^+$) in murinen KHT Modellen zu charakterisieren und deren Rolle in Bezug auf die Progression des experimentellen Tumors zu identifizieren. Als zentrale Methode diente hierfür die antiköpervermittelte Depletion von $Ly\text{-}6G^+$ Zellen, welche im weiteren Verlauf der Arbeit näher auf ihre Effektivität in unterschiedlichen Geweben untersucht wurde. Weiterhin wurde der Einfluss der Tumorpräsenz auf die Effektivität der antikörpervermittelten Depletion analysiert. In einer abschließenden Pilotstudie sollte außerdem eine potentielle Funktion des neutrophilenspezifischen Proteins Ly-6G, das nur in der Maus vorkommt, im Kontext der Funktion von Neutrophilen in der Interaktion mit Tumoren untersucht werden.
Initiale Untersuchungen der vorliegenden Arbeit deuten auf eine Interaktion von Tumorzellen und Neutrophilen hin, welche zu einer tumorprogressionsabhängigen Expansion von $CD11b^+Ly\text{-}6G^+$ Zellen in der Peripherie (Blut und Milz) führte. Orthotop transplantierte Tumoren lösten in diesem Zusammenhang eine stärkere Expansion als subkutane Tumoren aus. Diese Beobachtungen deckten sich mit Daten aus vorherigen Studien in KHT Patienten. Weiterhin konnte demonstriert werden, dass die Lokalisation im Tumor zu einer weiteren Aktivierung der $CD11b^+Ly\text{-}6G^+$ Zellen führte und dass dies die Expression eines tumorfördernden Genexpressionsprofils zur Folge hatte. Dieses war charakterisiert durch immunsuppressive Gene wie Arg1 und iNOS und Gefäßversorgung förderndes VEGF und beinhaltete außerdem verschiedene Cytokine, die weitere Immunzellen anlocken können. Im weiteren Verlauf konnte durch antikörpervermittelte Depletion der Neutrophilen eine zentrale Funktion in der Entstehungsphase der transplantierten Tumoren festgestellt werden, während bereits etablierte Tumoren weniger stark von der Unterstützung durch $CD11b^+Ly\text{-}6G^+$ Zellen abhingen. Auf funktioneller Ebene wurden durch die gezeigten Experimente verschiedene Mechanismen zur neutrophilenvermittelten Tumorentstehung nahegelegt, wobei sowohl die Regulation von T Zellen als auch eine eher strukturelle Unterstützung des Gewebeumbaus und der Gefäßversorgung eine Rolle spielten.
Im nächsten Schritt wurde die antikörpervermittelte Depletion von $Ly\text{-}6G^+$ Zellen in einem der KHT Modelle näher betrachtet. Hierbei konnte die Depletion im peripheren Blut in verschiedene Stadien eingeteilt werden. Eine vollständige Depletion wurde während der ersten Behandlungswoche beobachtet und obwohl die Antikörperdosierung fortlaufend aufrechterhalten wurde, kam es nach circa zehn Tagen zu einem Wiederauftreten von $Ly\text{-}6G^+$ Zellen. Während der vollständigen Depletion im Blut wurde außerdem eine depletionsresistente Population von lebendigen $Ly\text{-}6G^+$ Zellen im Tumorgewebe sowie in der Milz und im Knochenmark identifiziert. Weiterhin wurde die vollständige Depletionsphase durch die Gegenwart eines Tumors weiter verkürzt. In diesem Zusammenhang kon-

nte eine verstärkte extramedulläre Granulopoese festgestellt werden, die zu einer Ansammlung von Neutrophilen führte, welche einen unreifen Phänotyp aufwiesen und weiterhin durch eine hohe Expression von immunmodulierenden Molekülen charakterisiert waren.
Im letzten Teil wurde gezeigt, dass die Migration von $CD11b^{+}Ly\text{-}6G^{+}$ Zellen in das Tumorgewebe nicht von der Expression des Moleküls Ly-6G auf der Zelloberfläche abhängt. Trotzdem konnte ein gesteigertes Tumorwachstum in $Ly\text{-}6G^{-/-}$ Tieren beobachtet werden. Im Rahmen dieser Studie war es nicht möglich einen zugrundeliegenden Mechanismus zu identifizieren.
Zusammenfassend konnte in der vorliegenden Arbeit erstmalig gezeigt werden, dass eine Auswahl von murinen KHT Modellen Charakteristika der humanen Erkrankung im Hinblick auf eine Interaktion von Tumor und Neutrophilen widerspiegelt. Das beschriebene Modell kann für weiterführende funktionelle Analysen tumorassoziierter Neutrophiler sowie zur Testung möglicher therapeutischer Interventionen genutzt werden. Depletionsexperimente deuteten darauf hin, dass besonders die frühe Tumorprogression in diesen Modellen stark durch $CD11b^{+}Ly\text{-}6G^{+}$ Zellen beeinflusst wird indem diese die antitumorale Funktion von T Zellen einschränken und außerdem zur Etablierung einer lokalen Nische für die Tumoretablierung beitragen. Während der anschließenden Tumorprogression expandieren $Ly\text{-}6G^{+}$ Zellen in Blut, Milz und im Tumorgewebe und weisen dabei gewebespezifisch veränderte Funktionen auf, welche mit distinkten Genexpressionsmustern einhergehen. Eine Analyse der $CD11b^{+}Ly\text{-}6G^{+}$ Zell Funktionen in diesen späteren Phasen der Tumorprogression ist mittels Antikörperbehandlung durch deren Widererscheinen unter Depletionsdruck, welches durch depletionsresistente Zellen und verstärkte extramedulläre Granulopoese induziert wird, nur limitiert möglich. Diese Charakteristika des Depletionsverlaufes unterstreichen die zwingende Notwendigkeit einer peniblen Überwachung der Depletion und implizieren, dass negative Ergebnisse in murinen Krebsmodellen zur funktionellen Rolle von Neutrophilen oder MDSCs[7] besonders vorsichtig interpretiert werden müssen.

[7] suppressive Zellen der myeloiden Linie, aus dem Englischen: *Myeloid derived suppressor cells*

References

[1] K. B. Abbitt, M. J. Cotter, V. C. Ridger, D. C. Crossman, P. G. Hellewell, and K. E. Norman. Antibody ligation of murine Ly-6G induces neutropenia, blood flow cessation, and death via complement-dependent and independent mechanisms. *J Leukoc Biol*, 85(1):55–63, Jan 2009.

[2] D. O. Adeegbe and H. Nishikawa. Natural and induced T regulatory cells in cancer. *Front Immunol*, 4:190, 2013.

[3] E. W. Ades, F. J. Candal, R. A. Swerlick, V. G. George, S. Summers, D. C. Bosse, and T. J. Lawley. HMEC-1: establishment of an immortalized human microvascular endothelial cell line. *J Invest Dermatol*, 99(6):683–690, Dec 1992.

[4] G.-O. Ahn, D. Tseng, C.-H. Liao, M. J. Dorie, A. Czechowicz, and J. M. Brown. Inhibition of Mac-1 (CD11b/CD18) enhances tumor response to radiation by reducing myeloid cell recruitment. *Proc Natl Acad Sci U S A*, 107(18):8363–8368, May 2010.

[5] B. Almand, J. I. Clark, E. Nikitina, J. van Beynen, N. R. English, S. C. Knight, D. P. Carbone, and D. I. Gabrilovich. Increased production of immature myeloid cells in cancer patients: a mechanism of immunosuppression in cancer. *J Immunol*, 166(1):678–689, Jan 2001.

[6] A. Á. d. Almeida, C. M. Bandeira, A. J. Gonçalves, and A. J. Araújo. Nicotine dependence and smoking habits in patients with head and neck cancer. *J Bras Pneumol*, 40(3):286–293, 2014.

[7] H. Arase, T. Saito, J. H. Phillips, and L. L. Lanier. Cutting edge: the mouse NK cell-associated antigen recognized by DX5 monoclonal antibody is CD49b (alpha 2 integrin, very late antigen-2). *J Immunol*, 167(3):1141–1144, Aug 2001.

[8] V. C. Ardi, P. E. Van den Steen, G. Opdenakker, B. Schweighofer, E. I. Deryugina, and J. P. Quigley. Neutrophil MMP-9 proenzyme, unencumbered by TIMP-1, undergoes efficient activation in vivo and catalytically induces angiogenesis via a basic fibroblast growth factor (FGF-2)/FGFR-2 pathway. *J Biol Chem*, 284(38):25854–25866, Sep 2009.

[9] C. E. Ayres-Sander, H. Lauridsen, C. L. Maier, P. Sava, J. S. Pober, and A. L. Gonzalez. Transendothelial migration enables subsequent transmigration of neutrophils through underlying pericytes. *PLoS One*, 8(3):e60025, 2013.

[10] D. Bausch, T. Pausch, T. Krauss, U. T. Hopt, C. Fernandez-del Castillo, A. L. Warshaw, S. P. Thayer, and T. Keck. Neutrophil granulocyte derived MMP-9 is a VEGF independent functional component of the angiogenic switch in pancreatic ductal adenocarcinoma. *Angiogenesis*, 14(3):235–243, Sep 2011.

[11] G. Bergers, R. Brekken, G. McMahon, T. H. Vu, T. Itoh, K. Tamaki, K. Tanzawa, P. Thorpe, S. Itohara, Z. Werb, and D. Hanahan. Matrix metalloproteinase-9 triggers the angiogenic switch during carcinogenesis. *Nat Cell Biol*, 2(10):737–744, Oct 2000.

[12] O. Boussif, F. Lezoualc'h, M. A. Zanta, M. D. Mergny, D. Scherman, B. Demeneix, and J. P. Behr. A versatile vector for gene and oligonucleotide transfer into cells in culture and in vivo: polyethylenimine. *Proc Natl Acad Sci U S A*, 92(16):7297–7301, Aug 1995.

[13] S. Brandau, C. A. Dumitru, and S. Lang. Protumor and antitumor functions of neutrophil granulocytes. *Semin Immunopathol*, 35(2):163–176, Mar 2013.

[14] S. Brandau, K. Moses, and S. Lang. The kinship of neutrophils and granulocytic myeloid-derived suppressor cells in cancer: cousins, siblings or twins? *Semin Cancer Biol*, 23(3):171–182, Jun 2013.

[15] S. Brandau, S. Trellakis, K. Bruderek, D. Schmaltz, G. Steller, M. Elian, H. Suttmann, M. Schenck, J. Welling, P. Zabel, and S. Lang. Myeloid-derived suppressor cells in the peripheral blood of cancer patients contain a subset of immature neutrophils with impaired migratory properties. *J Leukoc Biol*, 89(2):311–317, Feb 2011.

[16] J. A. Brennan, J. O. Boyle, W. M. Koch, S. N. Goodman, R. H. Hruban, Y. J. Eby, M. J. Couch, A. A. Forastiere, and D. Sidransky. Association between cigarette smoking and mutation of the p53 gene in squamous-cell carcinoma of the head and neck. *N Engl J Med*, 332(11):712–717, Mar 1995.

[17] V. Brinkmann, U. Reichard, C. Goosmann, B. Fauler, Y. Uhlemann, D. S. Weiss, Y. Weinrauch, and A. Zychlinsky. Neutrophil extracellular traps kill bacteria. *Science*, 303(5663):1532–1535, Mar 2004.

[18] V. Bronte, P. Serafini, E. Apolloni, and P. Zanovello. Tumor-induced immune dysfunctions caused by myeloid suppressor cells. *J Immunother*, 24(6):431–446, 2001.

[19] V. Bronte, P. Serafini, C. De Santo, I. Marigo, V. Tosello, A. Mazzoni, D. M. Segal, C. Staib, M. Lowel, G. Sutter, M. P. Colombo, and P. Zanovello. IL-4-induced arginase 1 suppresses alloreactive T cells in tumor-bearing mice. *J Immunol*, 170(1):270–278, Jan 2003.

[20] K. Bucher, F. Schmitt, S. E. Autenrieth, I. Dillmann, B. Nürnberg, K. Schenke-Layland, and S. Beer-Hammer. Fluorescent Ly6G antibodies determine macrophage phagocytosis of neutrophils and alter the retrieval of neutrophils in mice. *J Leukoc Biol*, May 2015.

[21] M. Burnet. Cancer; a biological approach. I. The processes of control. *Br Med J*, 1(5022):779–786, Apr 1957.

[22] S. Caielli, J. Banchereau, and V. Pascual. Neutrophils come of age in chronic inflammation. *Curr Opin Immunol*, 24(6):671–677, Dec 2012.

[23] D. W. Cain, P. B. Snowden, G. D. Sempowski, and G. Kelsoe. Inflammation triggers emergency granulopoiesis through a density-dependent feedback mechanism. *PLoS One*, 6(5):e19957, 2011.

[24] K. D. Carr, A. N. Sieve, M. Indramohan, T. J. Break, S. Lee, and R. E. Berg. Specific depletion reveals a novel role for neutrophil-mediated protection in the liver during Listeria monocytogenes infection. *Eur J Immunol*, 41(9):2666–2676, Sep 2011.

[25] A.-J. Casbon, D. Reynaud, C. Park, E. Khuc, D. D. Gan, K. Schepers, E. Passegué, and Z. Werb. Invasive breast cancer reprograms early myeloid differentiation in the bone marrow to generate immunosuppressive neutrophils. *Proc Natl Acad Sci U S A*, 112(6):E566–E575, Feb 2015.

[26] M. Champsaur and L. L. Lanier. Effect of NKG2D ligand expression on host immune responses. *Immunol Rev*, 235(1):267–285, May 2010.

[27] S. Chatterjee, S. Das, P. Chakraborty, A. Manna, M. Chatterjee, and S. K. Choudhuri. Myeloid derived suppressor cells (MDSCs) can induce the generation of Th17 response from naïve CD4+ T cells. *Immunobiology*, 218(5):718–724, May 2013.

[28] J. Choi, B. Suh, Y.-O. Ahn, T. M. Kim, J.-O. Lee, S.-H. Lee, and D. S. Heo. CD15+/CD16low human granulocytes from terminal cancer patients: granulocytic myeloid-derived suppressor cells that have suppressive function. *Tumor Biol.*, 33(1):121–129, Nov 2011.

[29] C. E. Clark, S. R. Hingorani, R. Mick, C. Combs, D. A. Tuveson, and R. H. Vonderheide. Dynamics of the immune reaction to pancreatic cancer from inception to invasion. *Cancer Res*, 67(19):9518–9527, Oct 2007.

[30] V. Cortez-Retamozo, M. Etzrodt, A. Newton, P. J. Rauch, A. Chudnovskiy, C. Berger, R. J. H. Ryan, Y. Iwamoto, B. Marinelli, R. Gorbatov, R. Forghani, T. I. Novobrantseva, V. Koteliansky, J.-L. Figueiredo, J. W. Chen, D. G. Anderson, M. Nahrendorf, F. K. Swirski, R. Weissleder, and M. J. Pittet. Origins of tumor-associated macrophages and neutrophils. *Proc Natl Acad Sci U S A*, 109(7):2491–2496, Feb 2012.

[31] J. Crawford, D. C. Dale, and G. H. Lyman. Chemotherapy-induced neutropenia: risks, consequences, and new directions for its management. *Cancer*, 100(2):228–237, Jan 2004.

[32] J. M. Daley, A. A. Thomay, M. D. Connolly, J. S. Reichner, and J. E. Albina. Use of Ly6G-specific monoclonal antibody to deplete neutrophils in mice. *J Leukoc Biol*, 83(1):64–70, Jan 2008.

[33] T. Dejima, K. Shibata, H. Yamada, H. Hara, Y. Iwakura, S. Naito, and Y. Yoshikai. Protective role of naturally occurring interleukin-17A-producing $\gamma\delta$ T cells in the lung at the early stage of systemic candidiasis in mice. *Infect Immun*, 79(11):4503–4510, Nov 2011.

[34] M. Di Maio, C. Gridelli, C. Gallo, F. Shepherd, F. V. Piantedosi, S. Cigolari, L. Manzione, A. Illiano, S. Barbera, S. F. Robbiati, L. Frontini, E. Piazza, G. P. Ianniello, E. Veltri, F. Castiglione, F. Rosetti, V. Gebbia, L. Seymour, P. Chiodini, and F. Perrone. Chemotherapy-induced neutropenia and treatment efficacy in advanced non-small-cell lung cancer: a pooled analysis of three randomised trials. *Lancet Oncol*, 6(9):669–677, Sep 2005.

[35] R. B. DuBridge, P. Tang, H. C. Hsia, P. M. Leong, J. H. Miller, and M. P. Calos. Analysis of mutation in human cells by using an Epstein-Barr virus shuttle system. *Mol Cell Biol*, 7(1):379–387, Jan 1987.

[36] I. Dufait, J. K. Schwarze, T. Liechtenstein, W. Leonard, H. Jiang, D. Escors, M. De Ridder, and K. Breckpot. Ex vivo generation of myeloid-derived suppressor cells that model the tumor immunosuppressive environment in colorectal cancer. *Oncotarget*, 6(14):12369–12382, May 2015.

[37] C. A. Dumitru, A. Bankfalvi, X. Gu, W. E. Eberhardt, R. Zeidler, S. Lang, and S. Brandau. Neutrophils Activate Tumoral CORTACTIN to Enhance Progression of Orohypopharynx Carcinoma. *Front Immunol*, 4:33, 2013.

[38] C. A. Dumitru, M. K. Fechner, T. K. Hoffmann, S. Lang, and S. Brandau. A novel p38-MAPK signaling axis modulates neutrophil biology in head and neck cancer. *J Leukoc Biol*, 91(4):591–598, Apr 2012.

[39] C. A. Dumitru, H. Gholaman, S. Trellakis, K. Bruderek, N. Dominas, X. Gu, A. Bankfalvi, T. L. Whiteside, S. Lang, and S. Brandau. Tumor-derived macrophage migration inhibitory factor modulates the biology of head and neck cancer cells via neutrophil activation. *Int J Cancer*, 129(4):859–869, Aug 2011.

[40] C. A. Dumitru, S. Lang, and S. Brandau. Modulation of neutrophil granulocytes in the tumor microenvironment: mechanisms and consequences for tumor progression. *Semin Cancer Biol*, 23(3):141–148, Jun 2013.

[41] C. A. Dumitru, K. Moses, S. Trellakis, S. Lang, and S. Brandau. Neutrophils and granulocytic myeloid-derived suppressor cells: immunophenotyping, cell biology and clinical relevance in human oncology. *Cancer Immunol Immunother*, 61(8):1155–1167, Aug 2012.

[42] K. J. Eash, A. M. Greenbaum, P. K. Gopalan, and D. C. Link. CXCR2 and CXCR4 antagonistically regulate neutrophil trafficking from murine bone marrow. *J Clin Invest*, 120(7):2423–2431, Jul 2010.

[43] B. Elenbaas, L. Spirio, F. Koerner, M. D. Fleming, D. B. Zimonjic, J. L. Donaher, N. C. Popescu, W. C. Hahn, and R. A. Weinberg. Human breast cancer cells generated by oncogenic transformation of primary mammary epithelial cells. *Genes Dev*, 15(1):50–65, Jan 2001.

[44] E. Elinav, R. Nowarski, C. A. Thaiss, B. Hu, C. Jin, and R. A. Flavell. Inflammation-induced cancer: crosstalk between tumours, immune cells and microorganisms. *Nat Rev Cancer*, 13(11):759–771, Nov 2013.

[45] M. Elkabets, V. S. G. Ribeiro, C. A. Dinarello, S. Ostrand-Rosenberg, J. P. Di Santo, R. N. Apte, and C. A. J. Vosshenrich. IL-1β regulates a novel myeloid-derived suppressor cell subset that impairs NK cell development and function. *Eur J Immunol*, 40(12):3347–3357, Dec 2010.

[46] R. J. Epstein. The CXCL12-CXCR4 chemotactic pathway as a target of adjuvant breast cancer therapies. *Nat Rev Cancer*, 4(11):901–909, Nov 2004.

[47] S. E. Erdman and T. Poutahidis. Roles for inflammation and regulatory T cells in colon cancer. *Toxicol Pathol*, 38(1):76–87, Jan 2010.

[48] G.-H. Fan, L. A. Lapierre, J. R. Goldenring, and A. Richmond. Differential regulation of CXCR2 trafficking by Rab GTPases. *Blood*, 101(6):2115–2124, Mar 2003.

[49] M. Faurschou and N. Borregaard. Neutrophil granules and secretory vesicles in inflammation. *Microbes Infect*, 5(14):1317–1327, Nov 2003.

[50] M. Faurschou, O. E. Sørensen, A. H. Johnsen, J. Askaa, and N. Borregaard. Defensin-rich granules of human neutrophils: characterization of secretory properties. *Biochim Biophys Acta*, 1591(1-3):29–35, Aug 2002.

[51] I. J. Fidler. Biological behavior of malignant melanoma cells correlated to their survival in vivo. *Cancer Res*, 35(1):218–224, Jan 1975.

[52] V. Finisguerra, G. Di Conza, M. Di Matteo, J. Serneels, S. Costa, A. A. R. Thompson, E. Wauters, S. Walmsley, H. Prenen, Z. Granot, A. Casazza, and M. Mazzone. MET is required for the recruitment of anti-tumoural neutrophils. *Nature*, 522(7556):349–353, Jun 2015.

[53] Z. G. Fridlender and S. M. Albelda. Tumor-associated neutrophils: friend or foe? *Carcinogenesis*, 33(5):949–955, May 2012.

[54] Z. G. Fridlender, J. Sun, S. Kim, V. Kapoor, G. Cheng, L. Ling, G. S. Worthen, and S. M. Albelda. Polarization of tumor-associated neutrophil phenotype by TGF-beta: "N1" versus "N2" TAN. *Cancer Cell*, 16(3):183–194, Sep 2009.

[55] Z. G. Fridlender, J. Sun, I. Mishalian, S. Singhal, G. Cheng, V. Kapoor, W. Horng, G. Fridlender, R. Bayuh, G. S. Worthen, and S. M. Albelda. Transcriptomic analysis comparing tumor-associated neutrophils with granulocytic myeloid-derived suppressor cells and normal neutrophils. *PLoS One*, 7(2):e31524, 2012.

[56] P. Friedland, A. Thomas, A. Naran, B. Amanuel, F. Grieu-Iacopetta, A. Carrello, G. Harnett, C. Meyer, and M. Phillips. Human papillomavirus and gene mutations in head and neck squamous carcinomas. *ANZ J Surg*, 82(5):362–366, May 2012.

[57] T. A. Fuchs, U. Abed, C. Goosmann, R. Hurwitz, I. Schulze, V. Wahn, Y. Weinrauch, V. Brinkmann, and A. Zychlinsky. Novel cell death program leads to neutrophil extracellular traps. *J Cell Biol*, 176(2):231–241, Jan 2007.

[58] S. Fujimoto, M. Greene, and A. H. Sehon. Immunosuppressor T cells in tumor bearing host. *Immunol Commun*, 4(3):201–217, 1975.

[59] M. Fujita, G. Kohanbash, W. Fellows-Mayle, R. L. Hamilton, Y. Komohara, S. A. Decker, J. R. Ohlfest, and H. Okada. COX-2 blockade suppresses gliomagenesis by inhibiting myeloid-derived suppressor cells. *Cancer Res*, 71(7):2664–2674, Apr 2011.

[60] D. I. Gabrilovich, M. P. Velders, E. M. Sotomayor, and W. M. Kast. Mechanism of immune dysfunction in cancer mediated by immature Gr-1+ myeloid cells. *J Immunol*, 166(9):5398–5406, May 2001.

[61] M. Garley, E. Jablonska, S. Z. Grabowska, and L. Piotrowski. IL-17 family cytokines in neutrophils of patients with oral epithelial squamous cell carcinoma. *Neoplasma*, 56(2):96–100, 2009.

[62] B. Geering, C. Stoeckle, S. Conus, and H.-U. Simon. Living and dying for inflammation: neutrophils, eosinophils, basophils. *Trends Immunol*, 34(8):398–409, Aug 2013.

[63] F. Ghiringhelli, P. E. Puig, S. Roux, A. Parcellier, E. Schmitt, E. Solary, G. Kroemer, F. Martin, B. Chauffert, and L. Zitvogel. Tumor cells convert immature myeloid dendritic cells into TGF-beta-secreting cells inducing CD4+CD25+ regulatory T cell proliferation. *J Exp Med*, 202(7):919–929, Oct 2005.

[64] M. L. Gillison, W. M. Koch, R. B. Capone, M. Spafford, W. H. Westra, L. Wu, M. L. Zahurak, R. W. Daniel, M. Viglione, D. E. Symer, K. V. Shah, and D. Sidransky. Evidence for a causal association between human papillomavirus and a subset of head and neck cancers. *J Natl Cancer Inst*, 92(9):709–720, May 2000.

[65] O. Goñi, P. Alcaide, and M. Fresno. Immunosuppression during acute Trypanosoma cruzi infection: involvement of Ly6G (Gr1(+))CD11b(+)immature myeloid suppressor cells. *Int Immunol*, 14(10):1125–1134, Oct 2002.

[66] Z. Granot, E. Henke, E. A. Comen, T. A. King, L. Norton, and R. Benezra. Tumor entrained neutrophils inhibit seeding in the premetastatic lung. *Cancer Cell*, 20(3):300–314, Sep 2011.

[67] W. E. Grizzle, X. Xu, S. Zhang, C. R. Stockard, C. Liu, S. Yu, J. Wang, J. D. Mountz, and H.-G. Zhang. Age-related increase of tumor susceptibility is associated with myeloid-derived suppressor cell mediated suppression of T cell cytotoxicity in recombinant inbred BXD12 mice. *Mech Ageing Dev*, 128(11-12):672–680, 2007.

[68] L. Guedez, S. Jensen-Taubman, D. Bourboulia, C. J. Kwityn, B. Wei, J. Caterina, and W. G. Stetler-Stevenson. TIMP-2 targets tumor-associated myeloid suppressor cells with effects in cancer immune dysfunction and angiogenesis. *J Immunother*, 35(6):502–512, Jul 2012.

[69] S. Hadrup, M. Donia, and P. Thor Straten. Effector CD4 and CD8 T cells and their role in the tumor microenvironment. *Cancer Microenviron*, 6(2):123–133, Aug 2013.

[70] D. Hanahan and R. A. Weinberg. The hallmarks of cancer. *Cell*, 100(1):57–70, Jan 2000.

[71] D. Hanahan and R. A. Weinberg. Hallmarks of cancer: the next generation. *Cell*, 144(5):646–674, Mar 2011.

[72] E. M. Hanson, V. K. Clements, P. Sinha, D. Ilkovitch, and S. Ostrand-Rosenberg. Myeloid-derived suppressor cells down-regulate L-selectin expression on CD4+ and CD8+ T cells. *J Immunol*, 183(2):937–944, Jul 2009.

[73] N.-B. Hao, M.-H. Lü, Y.-H. Fan, Y.-L. Cao, Z.-R. Zhang, and S.-M. Yang. Macrophages in tumor microenvironments and the progression of tumors. *Clin Dev Immunol*, 2012:948098, 2012.

[74] E. S. Harris, A. S. Weyrich, and G. A. Zimmerman. Lessons from rare maladies: leukocyte adhesion deficiency syndromes. *Curr Opin Hematol*, 20(1):16–25, Jan 2013.

[75] A. Hasenberg, M. Hasenberg, L. Männ, F. Neumann, L. Borkenstein, M. Stecher, A. Kraus, D. R. Engel, A. Klingberg, P. Seddigh, Z. Abdullah, S. Klebow, S. Engelmann, A. Reinhold, S. Brandau, M. Seeling, A. Waisman, B. Schraven, J. R. Göthert, F. Nimmerjahn, and M. Gunzer. Catchup: a mouse model for imaging-based tracking and modulation of neutrophil granulocytes. *Nat Methods*, 12(5):445–452, May 2015.

[76] J. M. Haverkamp, S. A. Crist, B. D. Elzey, C. Cimen, and T. L. Ratliff. In vivo suppressive function of myeloid-derived suppressor cells is limited to the inflammatory site. *Eur J Immunol*, 41(3):749–759, Mar 2011.

[77] R. B. Henderson, L. H. Lim, P. A. Tessier, F. N. Gavins, M. Mathies, M. Perretti, and N. Hogg. The use of lymphocyte function-associated antigen (LFA)-1-deficient mice to determine the role of LFA-1, Mac-1, and alpha4 integrin in the inflammatory response of neutrophils. *J Exp Med*, 194(2):219–226, Jul 2001.

[78] K. Hestdal, F. W. Ruscetti, J. N. Ihle, S. E. Jacobsen, C. M. Dubois, W. C. Kopp, D. L. Longo, and J. R. Keller. Characterization and regulation of RB6-8C5 antigen expression on murine bone marrow cells. *J Immunol*, 147(1):22–28, Jul 1991.

[79] S. L. Highfill, Y. Cui, A. J. Giles, J. P. Smith, H. Zhang, E. Morse, R. N. Kaplan, and C. L. Mackall. Disruption of CXCR2-mediated MDSC tumor trafficking enhances anti-PD1 efficacy. *Sci Transl Med*, 6(237):237ra67, May 2014.

[80] T. K. Hoffmann, E. Sonkoly, U. Hauser, A. van Lierop, T. L. Whiteside, J. P. Klussmann, D. Hafner, P. Schuler, U. Friebe-Hoffmann, K. Scheckenbach, K. Erjala, R. Grénman, J. Schipper, H. Bier, and V. Balz. Alterations in the p53 pathway and their association with radio- and chemosensitivity in head and neck squamous cell carcinoma. *Oral Oncol*, 44(12):1100–1109, Dec 2008.

[81] E.-H. Hong, S.-Y. Chang, B.-R. Lee, Y.-S. Kim, J.-M. Lee, C.-Y. Kang, M.-N. Kweon, and H.-J. Ko. Blockade of Myd88 signaling induces antitumor effects by skewing the immunosuppressive function of myeloid-derived suppressor cells. *Int J Cancer*, 132(12):2839–2848, Jun 2013.

[82] B. Huang, P.-Y. Pan, Q. Li, A. I. Sato, D. E. Levy, J. Bromberg, C. M. Divino, and S.-H. Chen. Gr-1+CD115+ immature myeloid suppressor cells mediate the development of tumor-induced T regulatory cells and T-cell anergy in tumor-bearing host. *Cancer Res*, 66(2):1123–1131, Jan 2006.

[83] S. J. Huh, S. Liang, A. Sharma, C. Dong, and G. P. Robertson. Transiently entrapped circulating tumor cells interact with neutrophils to facilitate lung metastasis development. *Cancer Res*, 70(14):6071–6082, Jul 2010.

[84] V. Hurez, B. J. Daniel, L. Sun, A.-J. Liu, S. M. Ludwig, M. J. Kious, S. R. Thibodeaux, S. Pandeswara, K. Murthy, C. B. Livi, S. Wall, M. J. Brumlik, T. Shin, B. Zhang, and T. J. Curiel. Mitigating age-related immune dysfunction heightens the efficacy of tumor immunotherapy in aged mice. *Cancer Res*, 72(8):2089–2099, Apr 2012.

[85] D. Ilkovitch and D. M. Lopez. Urokinase-mediated recruitment of myeloid-derived suppressor cells and their suppressive mechanisms are blocked by MUC1/sec. *Blood*, 113(19):4729–4739, May 2009.

[86] Y. Imai, Y. Kubota, S. Yamamoto, K. Tsuji, M. Shimatani, N. Shibatani, S. Takamido, M. Matsushita, and K. Okazaki. Neutrophils enhance invasion activity of human cholangiocellular carcinoma and hepatocellular carcinoma cells: an in vitro study. *J Gastroenterol Hepatol*, 20(2):287–293, Feb 2005.

[87] E. Jablonska, J. Jablonski, M. Marcinczyk, Z. Grabowska, and L. Piotrowski. The release of soluble forms of TRAIL and DR5 by neutrophils of oral cavity cancer patients. *Folia Histochem Cytobiol*, 46(2):177–183, 2008.

[88] E. Jablonska, L. Piotrowski, M. Kiluk, J. Jablonski, Z. Grabowska, and W. Markiewicz. Effect of IL-15 on the secretion of IL-1beta, IL-1Ra and sIL-1RII by PMN from cancer patients. *Cytokine*, 16(5):173–177, Dec 2001.

[89] E. Jablonska, W. Puzewska, Z. Grabowska, J. Jablonski, and L. Talarek. VEGF, IL-18 and NO production by neutrophils and their serum levels in patients with oral cavity cancer. *Cytokine*, 30(3):93–99, May 2005.

[90] J. Jablonska, S. Leschner, K. Westphal, S. Lienenklaus, and S. Weiss. Neutrophils responsive to endogenous IFN-beta regulate tumor angiogenesis and growth in a mouse tumor model. *J Clin Invest*, 120(4):1151–1164, Apr 2010.

[91] J. Jablonska, C.-F. Wu, L. Andzinski, S. Leschner, and S. Weiss. CXCR2-mediated tumor-associated neutrophil recruitment is regulated by IFN-β. *Int J Cancer*, 134(6):1346–1358, Mar 2014.

[92] T. Jamieson, M. Clarke, C. W. Steele, M. S. Samuel, J. Neumann, A. Jung, D. Huels, M. F. Olson, S. Das, R. J. B. Nibbs, and O. J. Sansom. Inhibition of CXCR2 profoundly suppresses inflammation-driven and spontaneous tumorigenesis. *J Clin Invest*, 122(9):3127–3144, Sep 2012.

[93] T. M. Jung and M. O. Dailey. Rapid modulation of homing receptors (gp90MEL-14) induced by activators of protein kinase C. Receptor shedding due to accelerated proteolytic cleavage at the cell surface. *J Immunol*, 144(8):3130–3136, Apr 1990.

[94] M. Kandasamy, B.-H. Bay, Y.-K. Lee, and R. Mahendran. Lactobacilli secreting a tumor antigen and IL15 activates neutrophils and dendritic cells and generates cytotoxic T lymphocytes against cancer cells. *Cell Immunol*, 271(1):89–96, 2011.

[95] H. T. Khong and N. P. Restifo. Natural selection of tumor variants in the generation of "tumor escape" phenotypes. *Nat Immunol*, 3(11):999–1005, Nov 2002.

[96] H.-J. Kim and H. Cantor. CD4 T-cell subsets and tumor immunity: the helpful and the not-so-helpful. *Cancer Immunol Res*, 2(2):91–98, Feb 2014.

[97] R. Kim, M. Emi, and K. Tanabe. Cancer immunoediting from immune surveillance to immune escape. *Immunology*, 121(1):1–14, May 2007.

[98] S. J. Klebanoff. Myeloperoxidase: friend and foe. *J Leukoc Biol*, 77(5):598–625, May 2005.

[99] M. Klemke, G. H. Wabnitz, F. Funke, B. Funk, H. Kirchgessner, and Y. Samstag. Oxidation of cofilin mediates T cell hyporesponsiveness under oxidative stress conditions. *Immunity*, 29(3):404–413, Sep 2008.

[100] B. Korkmaz, M. S. Horwitz, D. E. Jenne, and F. Gauthier. Neutrophil elastase, proteinase 3, and cathepsin G as therapeutic targets in human diseases. *Pharmacol Rev*, 62(4):726–759, Dec 2010.

[101] K. Kretschmer, I. Apostolou, E. Jaeckel, K. Khazaie, and H. von Boehmer. Making regulatory T cells with defined antigen specificity: role in autoimmunity and cancer. *Immunol Rev*, 212:163–169, Aug 2006.

[102] D.-M. Kuang, Q. Zhao, Y. Wu, C. Peng, J. Wang, Z. Xu, X.-Y. Yin, and L. Zheng. Peritumoral neutrophils link inflammatory response to disease progression by fostering angiogenesis in hepatocellular carcinoma. *J Hepatol*, 54(5):948–955, May 2011.

[103] M. Kujawski, M. Kortylewski, H. Lee, A. Herrmann, H. Kay, and H. Yu. Stat3 mediates myeloid cell-dependent tumor angiogenesis in mice. *J Clin Invest*, 118(10):3367–3377, Oct 2008.

[104] S. Kumar, J. Xu, C. Perkins, F. Guo, S. Snapper, F. D. Finkelman, Y. Zheng, and M.-D. Filippi. Cdc42 regulates neutrophil migration via crosstalk between WASp, CD11b, and microtubules. *Blood*, 120(17):3563–3574, Oct 2012.

[105] S. Kusmartsev, Y. Nefedova, D. Yoder, and D. I. Gabrilovich. Antigen-specific inhibition of CD8+ T cell response by immature myeloid cells in cancer is mediated by reactive oxygen species. *J Immunol*, 172(2):989–999, Jan 2004.

[106] I. Kuss, A. D. Donnenberg, W. Gooding, and T. L. Whiteside. Effector CD8+CD45RO-CD27-T cells have signalling defects in patients with squamous cell carcinoma of the head and neck. *Br J Cancer*, 88(2):223–230, Jan 2003.

[107] I. Kuss, B. Hathaway, R. L. Ferris, W. Gooding, and T. L. Whiteside. Decreased absolute counts of T lymphocyte subsets and their relation to disease in squamous cell carcinoma of the head and neck. *Clin Cancer Res*, 10(11):3755–3762, Jun 2004.

[108] Y. H. Kusumanto, W. A. Dam, G. A. P. Hospers, C. Meijer, and N. H. Mulder. Platelets and granulocytes, in particular the neutrophils, form important compartments for circulating vascular endothelial growth factor. *Angiogenesis*, 6(4):283–287, 2003.

[109] U. K. Laemmli. Cleavage of structural proteins during the assembly of the head of bacteriophage T4. *Nature*, 227(5259):680–685, Aug 1970.

[110] J. A. Lapinet, P. Scapini, F. Calzetti, O. Pérez, and M. A. Cassatella. Gene expression and production of tumor necrosis factor alpha, interleukin-1beta (IL-1beta), IL-8, macrophage inflammatory protein 1alpha (MIP-1alpha), MIP-1beta, and gamma interferon-inducible protein 10 by human neutrophils stimulated with group B meningococcal outer membrane vesicles. *Infect Immun*, 68(12):6917–6923, Dec 2000.

[111] M. Y. Lee, C. C. Liu, J. L. Lottsfeldt, S. A. Judkins, and G. A. Howard. Production of granulocyte-stimulating and bone cell-modulating activities from a neutrophilia hypercalcemia-inducing murine mammary cancer cell line. *Cancer Res*, 47(15):4059–4065, Aug 1987.

[112] C. Leurs, M. Jansen, K. E. Pollok, M. Heinkelein, M. Schmidt, M. Wissler, D. Lindemann, C. Von Kalle, A. Rethwilm, D. A. Williams, and H. Hanenberg. Comparison of three retroviral vector systems for transduction of nonobese diabetic/severe combined immunodeficiency mice repopulating human CD34+ cord blood cells. *Hum Gene Ther*, 14(6):509–519, Apr 2003.

[113] H. Li, Y. Han, Q. Guo, M. Zhang, and X. Cao. Cancer-expanded myeloid-derived suppressor cells induce anergy of NK cells through membrane-bound TGF-beta 1. *J Immunol*, 182(1):240–249, Jan 2009.

[114] G. J. Lieschke, D. Grail, G. Hodgson, D. Metcalf, E. Stanley, C. Cheers, K. J. Fowler, S. Basu, Y. F. Zhan, and A. R. Dunn. Mice lacking granulocyte colony-stimulating factor have chronic neutropenia, granulocyte and macrophage progenitor cell deficiency, and impaired neutrophil mobilization. *Blood*, 84(6):1737–1746, Sep 1994.

[115] F. Lin, C. M.-C. Nguyen, S.-J. Wang, W. Saadi, S. P. Gross, and N. L. Jeon. Neutrophil migration in opposing chemoattractant gradients using microfluidic chemotaxis devices. *Ann Biomed Eng*, 33(4):475–482, Apr 2005.

[116] B. Y. Liu, I. Soloviev, P. Chang, J. Lee, X. Huang, C. Zhong, N. Ferrara, P. Polakis, and C. Sakanaka. Stromal cell-derived factor-1/CXCL12 contributes to MMTV-Wnt1 tumor growth involving Gr1+CD11b+ cells. *PLoS One*, 5(1):e8611, 2010.

[117] C. Liu, S. Yu, J. Kappes, J. Wang, W. E. Grizzle, K. R. Zinn, and H.-G. Zhang. Expansion of spleen myeloid suppressor cells represses NK cell cytotoxicity in tumor-bearing host. *Blood*, 109(10):4336–4342, May 2007.

[118] F. Liu, H. Y. Wu, R. Wesselschmidt, T. Kornaga, and D. C. Link. Impaired production and increased apoptosis of neutrophils in granulocyte colony-stimulating factor receptor-deficient mice. *Immunity*, 5(5):491–501, Nov 1996.

[119] Y. Liu, A. T. Holdbrooks, G. P. Meares, J. A. Buckley, E. N. Benveniste, and H. Qin. Preferential Recruitment of Neutrophils into the Cerebellum and Brainstem Contributes to the Atypical Experimental Autoimmune Encephalomyelitis Phenotype. *J Immunol*, Jun 2015.

[120] K. J. Livak and T. D. Schmittgen. Analysis of relative gene expression data using real-time quantitative PCR and the 2(-Delta Delta C(T)) Method. *Methods*, 25(4):402–408, Dec 2001.

[121] R. D. Loberg, C. Ying, M. Craig, L. Yan, L. A. Snyder, and K. J. Pienta. CCL2 as an important mediator of prostate cancer growth in vivo through the regulation of macrophage infiltration. *Neoplasia*, 9(7):556–562, Jul 2007.

[122] J. B. Lubetsky, A. Dios, J. Han, B. Aljabari, B. Ruzsicska, R. Mitchell, E. Lolis, and Y. Al-Abed. The tautomerase active site of macrophage migration inhibitory factor is a potential target for discovery of novel anti-inflammatory agents. *J Biol Chem*, 277(28):24976–24982, Jul 2002.

[123] C. Ma, T. Kapanadze, J. Gamrekelashvili, M. P. Manns, F. Korangy, and T. F. Greten. Anti-Gr-1 antibody depletion fails to eliminate hepatic myeloid-derived suppressor cells in tumor-bearing mice. *J Leukoc Biol*, 92(6):1199–1206, Dec 2012.

[124] A. Mantovani, M. A. Cassatella, C. Costantini, and S. Jaillon. Neutrophils in the activation and regulation of innate and adaptive immunity. *Nat Rev Immunol*, 11(8):519–531, Aug 2011.

[125] B. Marcus, D. Arenberg, J. Lee, C. Kleer, D. B. Chepeha, C. E. Schmalbach, M. Islam, S. Paul, Q. Pan, S. Hanash, R. Kuick, S. D. Merajver, and T. N. Teknos. Prognostic factors in oral cavity and oropharyngeal squamous cell carcinoma. *Cancer*, 101(12):2779–2787, Dec 2004.

[126] I. Marigo, E. Bosio, S. Solito, C. Mesa, A. Fernandez, L. Dolcetti, S. Ugel, N. Sonda, S. Bicciato, E. Falisi, F. Calabrese, G. Basso, P. Zanovello, E. Cozzi, S. Mandruzzato, and V. Bronte. Tumor-induced tolerance and immune suppression depend on the C/EBPbeta transcription factor. *Immunity*, 32(6):790–802, Jun 2010.

[127] C. Martin, P. C. E. Burdon, G. Bridger, J. C. Gutierrez-Ramos, T. J. Williams, and S. M. Rankin. Chemokines acting via CXCR2 and CXCR4 control the release of neutrophils from the bone marrow and their return following senescence. *Immunity*, 19(4):583–593, Oct 2003.

[128] R. P. McEver. Selectins: lectins that initiate cell adhesion under flow. *Curr Opin Cell Biol*, 14(5):581–586, Oct 2002.

[129] D. Metcalf, C. G. Begley, G. R. Johnson, N. A. Nicola, A. F. Lopez, and D. J. Williamson. Effects of purified bacterially synthesized murine multi-CSF (IL-3) on hematopoiesis in normal adult mice. *Blood*, 68(1):46–57, Jul 1986.

[130] D. Metcalf, C. G. Begley, D. J. Williamson, E. C. Nice, J. De Lamarter, J. J. Mermod, D. Thatcher, and A. Schmidt. Hemopoietic responses in mice injected with purified recombinant murine GM-CSF. *Exp Hematol*, 15(1):1–9, Jan 1987.

[131] C. Meyer, A. Sevko, M. Ramacher, A. V. Bazhin, C. S. Falk, W. Osen, I. Borrello, M. Kato, D. Schadendorf, M. Baniyash, and V. Umansky. Chronic inflammation promotes myeloid-derived suppressor cell activation blocking antitumor immunity in transgenic mouse melanoma model. *Proc Natl Acad Sci U S A*, 108(41):17111–17116, Oct 2011.

[132] I. Mishalian, R. Bayuh, E. Eruslanov, J. Michaeli, L. Levy, L. Zolotarov, S. Singhal, S. M. Albelda, Z. Granot, and Z. G. Fridlender. Neutrophils recruit regulatory T-cells into tumors via secretion of CCL17–a new mechanism of impaired antitumor immunity. *Int J Cancer*, 135(5):1178–1186, Sep 2014.

[133] I. Mishalian, R. Bayuh, L. Levy, L. Zolotarov, J. Michaeli, and Z. G. Fridlender. Tumor-associated neutrophils (TAN) develop pro-tumorigenic properties during tumor progression. *Cancer Immunol Immunother*, 62(11):1745–1756, Nov 2013.

[134] K. Mizutani, S. Sud, N. A. McGregor, G. Martinovski, B. T. Rice, M. J. Craig, Z. S. Varsos, H. Roca, and K. J. Pienta. The chemokine CCL2 increases prostate tumor growth and bone metastasis through macrophage and osteoclast recruitment. *Neoplasia*, 11(11):1235–1242, Nov 2009.

[135] A. Mócsai. Diverse novel functions of neutrophils in immunity, inflammation, and beyond. *J Exp Med*, 210(7):1283–1299, Jul 2013.

[136] F. Mollinedo, M. Nakajima, A. Llorens, E. Barbosa, S. Callejo, C. Gajate, and A. Fabra. Major co-localization of the extracellular-matrix degradative enzymes heparanase and gelatinase in tertiary granules of human neutrophils. *Biochem J*, 327 (Pt 3):917–923, Nov 1997.

[137] B. Molon, S. Ugel, F. Del Pozzo, C. Soldani, S. Zilio, D. Avella, A. De Palma, P. Mauri, A. Monegal, M. Rescigno, B. Savino, P. Colombo, N. Jonjic, S. Pecanic, L. Lazzarato, R. Fruttero, A. Gasco, V. Bronte, and A. Viola. Chemokine nitration prevents intratumoral infiltration of antigen-specific T cells. *J Exp Med*, 208(10):1949–1962, Sep 2011.

[138] B. B. Moore, D. A. Arenberg, K. Stoy, T. Morgan, C. L. Addison, S. B. Morris, M. Glass, C. Wilke, Y. Y. Xue, S. Sitterding, S. L. Kunkel, M. D. Burdick, and R. M. Strieter. Distinct CXC chemokines mediate tumorigenicity of prostate cancer cells. *Am J Pathol*, 154(5):1503–1512, May 1999.

[139] J. K. Morales, M. Kmieciak, L. Graham, M. Feldmesser, H. D. Bear, and M. H. Manjili. Adoptive transfer of HER2/neu-specific T cells expanded with alternating gamma chain cytokines mediate tumor regression when combined with the depletion of myeloid-derived suppressor cells. *Cancer Immunol Immunother*, 58(6):941–953, Jun 2009.

[140] B. L. Mundy-Bosse, G. B. Lesinski, A. C. Jaime-Ramirez, K. Benninger, M. Khan, P. Kuppusamy, K. Guenterberg, S. V. Kondadasula, A. R. Chaudhury, K. M. La Perle, M. Kreiner, G. Young, D. C. Guttridge, and W. E. Carson, 3rd. Myeloid-derived suppressor cell inhibition of the IFN response in tumor-bearing mice. *Cancer Res*, 71(15):5101–5110, Aug 2011.

[141] V. R. Muthukkaruppan, L. Kubai, and R. Auerbach. Tumor-induced neovascularization in the mouse eye. *J Natl Cancer Inst*, 69(3):699–708, Sep 1982.

[142] P. Nair, M. Gaga, E. Zervas, K. Alagha, F. E. Hargreave, P. M. O'Byrne, P. Stryszak, L. Gann, J. Sadeh, P. Chanez, and S. I. . Safety and efficacy of a CXCR2 antagonist in patients with severe asthma and sputum neutrophils: a randomized, placebo-controlled clinical trial. *Clin Exp Allergy*, 42(7):1097–1103, Jul 2012.

[143] A. C. Ochoa, A. H. Zea, C. Hernandez, and P. C. Rodriguez. Arginase, prostaglandins, and myeloid-derived suppressor cells in renal cell carcinoma. *Clin Cancer Res*, 13(2 Pt 2):721s–726s, Jan 2007.

[144] A. F. Ochsenbein, P. Klenerman, U. Karrer, B. Ludewig, M. Pericin, H. Hengartner, and R. M. Zinkernagel. Immune surveillance against a solid tumor fails because of immunological ignorance. *Proc Natl Acad Sci U S A*, 96(5):2233–2238, Mar 1999.

[145] P. L. Olive, D. J. Chaplin, and R. E. Durand. Pharmacokinetics, binding and distribution of Hoechst 33342 in spheroids and murine tumours. *Br J Cancer*, 52(5):739–746, Nov 1985.

[146] S. Onizuka, I. Tawara, J. Shimizu, S. Sakaguchi, T. Fujita, and E. Nakayama. Tumor rejection by in vivo administration of anti-CD25 (interleukin-2 receptor alpha) monoclonal antibody. *Cancer Res*, 59(13):3128–3133, Jul 1999.

[147] V. Papayannopoulos, K. D. Metzler, A. Hakkim, and A. Zychlinsky. Neutrophil elastase and myeloperoxidase regulate the formation of neutrophil extracellular traps. *J Cell Biol*, 191(3):677–691, Nov 2010.

[148] W. C. Parks, C. L. Wilson, and Y. S. López-Boado. Matrix metalloproteinases as modulators of inflammation and innate immunity. *Nat Rev Immunol*, 4(8):617–629, Aug 2004.

[149] A. Passaniti, R. M. Taylor, R. Pili, Y. Guo, P. V. Long, J. A. Haney, R. R. Pauly, D. S. Grant, and G. R. Martin. A simple, quantitative method for assessing angiogenesis and antiangiogenic agents using reconstituted basement membrane, heparin, and fibroblast growth factor. *Lab Invest*, 67(4):519–528, Oct 1992.

[150] L. A. Pekarek, B. A. Starr, A. Y. Toledano, and H. Schreiber. Inhibition of tumor growth by elimination of granulocytes. *J Exp Med*, 181(1):435–440, Jan 1995.

[151] M. Phillipson, B. Heit, P. Colarusso, L. Liu, C. M. Ballantyne, and P. Kubes. Intraluminal crawling of neutrophils to emigration sites: a molecularly distinct process from adhesion in the recruitment cascade. *J Exp Med*, 203(12):2569–2575, Nov 2006.

[152] J. Pillay, I. den Braber, N. Vrisekoop, L. M. Kwast, R. J. de Boer, J. A. M. Borghans, K. Tesselaar, and L. Koenderman. In vivo labeling with 2H2O reveals a human neutrophil lifespan of 5.4 days. *Blood*, 116(4):625–627, Jul 2010.

[153] J. Pillay, T. Tak, V. M. Kamp, and L. Koenderman. Immune suppression by neutrophils and granulocytic myeloid-derived suppressor cells: similarities and differences. *Cell Mol Life Sci*, 70(20):3813–3827, Oct 2013.

[154] Z. Pojda and A. Tsuboi. In vivo effects of human recombinant interleukin 6 on hemopoietic stem and progenitor cells and circulating blood cells in normal mice. *Exp Hematol*, 18(9):1034–1037, Oct 1990.

[155] M. R. Porembka, J. B. Mitchem, B. A. Belt, C.-S. Hsieh, H.-M. Lee, J. Herndon, W. E. Gillanders, D. C. Linehan, and P. Goedegebuure. Pancreatic adenocarcinoma induces bone marrow mobilization of myeloid-derived suppressor cells which promote primary tumor growth. *Cancer Immunol Immunother*, 61(9):1373–1385, Sep 2012.

[156] B.-Z. Qian, J. Li, H. Zhang, T. Kitamura, J. Zhang, L. R. Campion, E. A. Kaiser, L. A. Snyder, and J. W. Pollard. CCL2 recruits inflammatory monocytes to facilitate breast-tumour metastasis. *Nature*, 475(7355):222–225, Jul 2011.

[157] M. M. Queen, R. E. Ryan, R. G. Holzer, C. R. Keller-Peck, and C. L. Jorcyk. Breast cancer cells stimulate neutrophils to produce oncostatin M: potential implications for tumor progression. *Cancer Res*, 65(19):8896–8904, Oct 2005.

[158] K. Radsak, R. Fuhrmann, R. P. Franke, D. Schneider, A. Kollert, K. H. Brücher, and D. Drenckhahn. Induction by sodium butyrate of cytomegalovirus replication in human endothelial cells. *Arch Virol*, 107(1-2):151–158, 1989.

[159] S. R. Rangan. A new human cell line (FaDu) from a hypopharyngeal carcinoma. *Cancer*, 29(1):117–121, Jan 1972.

[160] T. E. Reichert, L. Strauss, E. M. Wagner, W. Gooding, and T. L. Whiteside. Signaling abnormalities, apoptosis, and reduced proliferation of circulating and tumor-infiltrating lymphocytes in patients with oral carcinoma. *Clin Cancer Res*, 8(10):3137–3145, Oct 2002.

[161] G. Ren, X. Zhao, Y. Wang, X. Zhang, X. Chen, C. Xu, Z.-r. Yuan, A. I. Roberts, L. Zhang, B. Zheng, T. Wen, Y. Han, A. B. Rabson, J. A. Tischfield, C. Shao, and Y. Shi. CCR2-dependent recruitment of macrophages by tumor-educated mesenchymal stromal cells promotes tumor development and is mimicked by TNFα. *Cell Stem Cell*, 11(6):812–824, Dec 2012.

[162] S. I. Rennard, D. C. Dale, J. F. Donohue, F. Kanniess, H. Magnussen, E. R. Sutherland, H. Watz, S. Lu, P. Stryszak, E. Rosenberg, and H. Staudinger. CXCR2 Antagonist MK-7123. A Phase 2 Proof-of-Concept Trial for Chronic Obstructive Pulmonary Disease. *Am J Respir Crit Care Med*, 191(9):1001–1011, May 2015.

[163] E. Ribechini, P. J. M. Leenen, and M. B. Lutz. Gr-1 antibody induces STAT signaling, macrophage marker expression and abrogation of myeloid-derived suppressor cell activity in BM cells. *Eur J Immunol*, 39(12):3538–3551, Dec 2009.

[164] M. K. Richards, F. Liu, H. Iwasaki, K. Akashi, and D. C. Link. Pivotal role of granulocyte colony-stimulating factor in the development of progenitors in the common myeloid pathway. *Blood*, 102(10):3562–3568, Nov 2003.

[165] F. Rios-Santos, J. C. Alves-Filho, F. O. Souto, F. Spiller, A. Freitas, C. M. C. Lotufo, M. B. P. Soares, R. R. Dos Santos, M. M. Teixeira, and F. d. Q. Cunha. Down-regulation of CXCR2 on neutrophils in severe sepsis is mediated by inducible nitric oxide synthase-derived nitric oxide. *Am J Respir Crit Care Med*, 175(5):490–497, Mar 2007.

[166] A. G. Rosmarin, Z. Yang, and K. K. Resendes. Transcriptional regulation in myelopoiesis: Hematopoietic fate choice, myeloid differentiation, and leukemogenesis. *Exp Hematol*, 33(2):131–143, Feb 2005.

[167] A. Rot. Chemokine patterning by glycosaminoglycans and interceptors. *Front Biosci (Landmark Ed)*, 15:645–660, 2010.

[168] R. Rotondo, G. Barisione, L. Mastracci, F. Grossi, A. M. Orengo, R. Costa, M. Truini, M. Fabbi, S. Ferrini, and O. Barbieri. IL-8 induces exocytosis of arginase 1 by neutrophil polymorphonuclears in nonsmall cell lung cancer. *Int J Cancer*, 125(4):887–893, Aug 2009.

[169] U. J. H. Sachs, C. L. Andrei-Selmer, A. Maniar, T. Weiss, C. Paddock, V. V. Orlova, E. Y. Choi, P. J. Newman, K. T. Preissner, T. Chavakis, and S. Santoso. The neutrophil-specific antigen CD177 is a counter-receptor for platelet endothelial cell adhesion molecule-1 (CD31). *J Biol Chem*, 282(32):23603–23612, Aug 2007.

[170] J. Y. Sagiv, J. Michaeli, S. Assi, I. Mishalian, H. Kisos, L. Levy, P. Damti, D. Lumbroso, L. Polyansky, R. V. Sionov, A. Ariel, A.-H. Hovav, E. Henke, Z. G. Fridlender, and Z. Granot. Phenotypic diversity and plasticity in circulating neutrophil subpopulations in cancer. *Cell Rep*, 10(4):562–573, Feb 2015.

[171] Y. Sawanobori, S. Ueha, M. Kurachi, T. Shimaoka, J. E. Talmadge, J. Abe, Y. Shono, M. Kitabatake, K. Kakimi, N. Mukaida, and K. Matsushima. Chemokine-mediated rapid turnover of myeloid-derived suppressor cells in tumor-bearing mice. *Blood*, 111(12):5457–5466, Jun 2008.

[172] E. Schlecker, A. Stojanovic, C. Eisen, C. Quack, C. S. Falk, V. Umansky, and A. Cerwenka. Tumor-infiltrating monocytic myeloid-derived suppressor cells mediate CCR5-dependent recruitment of regulatory T cells favoring tumor growth. *J Immunol*, 189(12):5602–5611, Dec 2012.

[173] J. Schmielau and O. J. Finn. Activated granulocytes and granulocyte-derived hydrogen peroxide are the underlying mechanism of suppression of t-cell function in advanced cancer patients. *Cancer Res*, 61(12):4756–4760, Jun 2001.

[174] A. W. Segal. How neutrophils kill microbes. *Annu Rev Immunol*, 23:197–223, 2005.

[175] P. Serafini, I. Borrello, and V. Bronte. Myeloid suppressor cells in cancer: recruitment, phenotype, properties, and mechanisms of immune suppression. *Semin Cancer Biol*, 16(1):53–65, Feb 2006.

[176] P. Serafini, S. Mgebroff, K. Noonan, and I. Borrello. Myeloid-derived suppressor cells promote cross-tolerance in B-cell lymphoma by expanding regulatory T cells. *Cancer Res*, 68(13):5439–5449, Jul 2008.

[177] L. M. Shahbazian, L. J. Quinton, G. J. Bagby, S. Nelson, G. Wang, and P. Zhang. Escherichia coli pneumonia enhances granulopoiesis and the mobilization of myeloid progenitor cells into the systemic circulation. *Crit Care Med*, 32(8):1740–1746, Aug 2004.

[178] P. Shamamian, J. D. Schwartz, B. J. Pocock, S. Monea, D. Whiting, S. G. Marcus, and P. Mignatti. Activation of progelatinase A (MMP-2) by neutrophil elastase, cathepsin G, and proteinase-3: a role for inflammatory cells in tumor invasion and angiogenesis. *J Cell Physiol*, 189(2):197–206, Nov 2001.

[179] J. Shimizu, S. Yamazaki, and S. Sakaguchi. Induction of tumor immunity by removing CD25+CD4+ T cells: a common basis between tumor immunity and autoimmunity. *J Immunol*, 163(10):5211–5218, Nov 1999.

[180] S. Shresta, C. T. Pham, D. A. Thomas, T. A. Graubert, and T. J. Ley. How do cytotoxic lymphocytes kill their targets? *Curr Opin Immunol*, 10(5):581–587, Oct 1998.

[181] A. A. Shvedova, A. V. Tkach, E. R. Kisin, T. Khaliullin, S. Stanley, D. W. Gutkin, A. Star, Y. Chen, G. V. Shurin, V. E. Kagan, and M. R. Shurin. Carbon nanotubes enhance metastatic growth of lung carcinoma via up-regulation of myeloid-derived suppressor cells. *Small*, 9(9-10):1691–1695, May 2013.

[182] K. D. Simpson, D. J. Templeton, and J. V. Cross. Macrophage migration inhibitory factor promotes tumor growth and metastasis by inducing myeloid-derived suppressor cells in the tumor microenvironment. *J Immunol*, 189(12):5533–5540, Dec 2012.

[183] P. Sinha, V. K. Clements, and S. Ostrand-Rosenberg. Reduction of myeloid-derived suppressor cells and induction of M1 macrophages facilitate the rejection of established metastatic disease. *J Immunol*, 174(2):636–645, Jan 2005.

[184] T. R. Sippel, J. White, K. Nag, V. Tsvankin, M. Klaassen, B. K. Kleinschmidt-DeMasters, and A. Waziri. Neutrophil degranulation and immunosuppression in patients with GBM: restoration of cellular immune function by targeting arginase I. *Clin Cancer Res*, 17(22):6992–7002, Nov 2011.

[185] J. D. Spicer, B. McDonald, J. J. Cools-Lartigue, S. C. Chow, B. Giannias, P. Kubes, and L. E. Ferri. Neutrophils promote liver metastasis via Mac-1-mediated interactions with circulating tumor cells. *Cancer Res*, 72(16):3919–3927, Aug 2012.

[186] M. K. Srivastava, P. Sinha, V. K. Clements, P. Rodriguez, and S. Ostrand-Rosenberg. Myeloid-derived suppressor cells inhibit T-cell activation by depleting cystine and cysteine. *Cancer Res*, 70(1):68–77, Jan 2010.

[187] M. K. Srivastava, L. Zhu, M. Harris-White, U. K. Kar, U. Kar, M. Huang, M. F. Johnson, J. M. Lee, D. Elashoff, R. Strieter, S. Dubinett, and S. Sharma. Myeloid suppressor cell depletion augments antitumor activity in lung cancer. *PLoS One*, 7(7):e40677, 2012.

[188] M. A. Stark, Y. Huo, T. L. Burcin, M. A. Morris, T. S. Olson, and K. Ley. Phagocytosis of apoptotic neutrophils regulates granulopoiesis via IL-23 and IL-17. *Immunity*, 22(3):285–294, Mar 2005.

[189] A. Stoppacciaro, C. Melani, M. Parenza, A. Mastracchio, C. Bassi, C. Baroni, G. Parmiani, and M. P. Colombo. Regression of an established tumor genetically modified to release granulocyte colony-stimulating factor requires granulocyte-T cell cooperation and T cell-produced interferon gamma. *J Exp Med*, 178(1):151–161, Jul 1993.

[190] L. Strauss, C. Bergmann, and T. L. Whiteside. Functional and phenotypic characteristics of CD4+CD25highFoxp3+ Treg clones obtained from peripheral blood of patients with cancer. *Int J Cancer*, 121(11):2473–2483, Dec 2007.

[191] C. Strell, K. Lang, B. Niggemann, K. S. Zaenker, and F. Entschladen. Neutrophil granulocytes promote the migratory activity of MDA-MB-468 human breast carcinoma cells via ICAM-1. *Exp Cell Res*, 316(1):138–148, Jan 2010.

[192] Y. B. Su, A. J. Vickers, M. J. Zelefsky, D. H. Kraus, A. R. Shaha, J. P. Shah, A. M. Serio, L. B. Harrison, G. J. Bosl, and D. G. Pfister. Double-blind, placebo-controlled, randomized trial of granulocyte-colony stimulating factor during postoperative radiotherapy for squamous head and neck cancer. *Cancer J*, 12(3):182–188, 2006.

[193] H. Suttmann, J. Riemensberger, G. Bentien, D. Schmaltz, M. Stöckle, D. Jocham, A. Böhle, and S. Brandau. Neutrophil granulocytes are required for effective Bacillus Calmette-Guérin immunotherapy of bladder cancer and orchestrate local immune responses. *Cancer Res*, 66(16):8250–8257, Aug 2006.

[194] R. U. Svensson, J. M. Haverkamp, D. R. Thedens, M. B. Cohen, T. L. Ratliff, and M. D. Henry. Slow disease progression in a C57BL/6 pten-deficient mouse model of prostate cancer. *Am J Pathol*, 179(1):502–512, Jul 2011.

[195] S. Tabariès, V. Ouellet, B. E. Hsu, M. G. Annis, A. A. N. Rose, L. Meunier, E. Carmona, C. E. Tam, A.-M. Mes-Masson, and P. M. Siegel. Granulocytic immune infiltrates are essential for the efficient formation of breast cancer liver metastases. *Breast Cancer Res*, 17:45, 2015.

[196] O. Takeuchi and S. Akira. Pattern recognition receptors and inflammation. *Cell*, 140(6):805–820, Mar 2010.

[197] F. Talebian, J.-Q. Liu, Z. Liu, M. Khattabi, Y. He, R. Ganju, and X.-F. Bai. Melanoma cell expression of CD200 inhibits tumor formation and lung metastasis via inhibition of myeloid cell functions. *PLoS One*, 7(2):e31442, 2012.

[198] F. Tanaka, H. Goto, T. Yokosuka, M. Yanagimachi, R. Kajiwara, T. Naruto, S. Nishimaki, and S. Yokota. Suppressed neutrophil function in children with acute lymphoblastic leukemia. *Int J Hematol*, 90(3):311–317, Oct 2009.

[199] M. Tarnowski, K. Grymula, R. Liu, J. Tarnowska, J. Drukala, J. Ratajczak, R. A. Mitchell, M. Z. Ratajczak, and M. Kucia. Macrophage migration inhibitory factor is secreted by rhabdomyosarcoma cells, modulates tumor metastasis by binding to CXCR4 and CXCR7 receptors and inhibits recruitment of cancer-associated fibroblasts. *Mol Cancer Res*, 8(10):1328–1343, Oct 2010.

[200] H. Tazawa, F. Okada, T. Kobayashi, M. Tada, Y. Mori, Y. Une, F. Sendo, M. Kobayashi, and M. Hosokawa. Infiltration of neutrophils is required for acquisition of metastatic phenotype of benign murine fibrosarcoma cells: implication of inflammation-associated carcinogenesis and tumor progression. *Am J Pathol*, 163(6):2221–2232, Dec 2003.

[201] A. J. Templeton, M. G. McNamara, B. Šeruga, F. E. Vera-Badillo, P. Aneja, A. Ocaña, R. Leibowitz-Amit, G. Sonpavde, J. J. Knox, B. Tran, I. F. Tannock, and E. Amir. Prognostic role of neutrophil-to-lymphocyte ratio in solid tumors: a systematic review and meta-analysis. *J Natl Cancer Inst*, 106(6):dju124, Jun 2014.

[202] M. Terabe, S. Matsui, J.-M. Park, M. Mamura, N. Noben-Trauth, D. D. Donaldson, W. Chen, S. M. Wahl, S. Ledbetter, B. Pratt, J. J. Letterio, W. E. Paul, and J. A. Berzofsky. Transforming growth factor-beta production and myeloid cells are an effector mechanism through which CD1d-restricted T cells block cytotoxic T lymphocyte-mediated tumor immunosurveillance: abrogation prevents tumor recurrence. *J Exp Med*, 198(11):1741–1752, Dec 2003.

[203] S. Trellakis, K. Bruderek, C. A. Dumitru, H. Gholaman, X. Gu, A. Bankfalvi, A. Scherag, J. Hütte, N. Dominas, G. F. Lehnerdt, T. K. Hoffmann, S. Lang, and S. Brandau. Polymorphonuclear granulocytes in human head and neck cancer: enhanced inflammatory activity, modulation by cancer cells and expansion in advanced disease. *Int J Cancer*, 129(9):2183–2193, Nov 2011.

[204] S. Trellakis, H. Farjah, K. Bruderek, C. A. Dumitru, T. K. Hoffmann, S. Lang, and S. Brandau. Peripheral blood neutrophil granulocytes from patients with head and neck squamous cell carcinoma functionally differ from their counterparts in healthy donors. *Int J Immunopathol Pharmacol*, 24(3):683–693, 2011.

[205] M. Uehara and N. Sato. Impaired ability of neutrophils to produce oxygen-derived free radicals in patients with chronic liver disease and hepatocellular carcinoma. *Hepatology*, 20(2):326–330, Aug 1994.

[206] F. van Zijl, G. Krupitza, and W. Mikulits. Initial steps of metastasis: cell invasion and endothelial transmigration. *Mutat Res*, 728(1-2):23–34, 2011.

[207] J. Wang, Y. Jia, N. Wang, X. Zhang, B. Tan, G. Zhang, and Y. Cheng. The clinical significance of tumor-infiltrating neutrophils and neutrophil-to-CD8+ lymphocyte ratio in patients with resectable esophageal squamous cell carcinoma. *J Transl Med*, 12:7, 2014.

[208] J.-X. Wang, A. M. Bair, S. L. King, R. Shnayder, Y.-F. Huang, C.-C. Shieh, R. J. Soberman, R. C. Fuhlbrigge, and P. A. Nigrovic. Ly6G ligation blocks recruitment of neutrophils via a β2-integrin-dependent mechanism. *Blood*, 120(7):1489–1498, Aug 2012.

[209] K. Welte and L. A. Boxer. Severe chronic neutropenia: pathophysiology and therapy. *Semin Hematol*, 34(4):267–278, Oct 1997.

[210] A. M. Wengner, S. C. Pitchford, R. C. Furze, and S. M. Rankin. The coordinated action of G-CSF and ELR + CXC chemokines in neutrophil mobilization during acute inflammation. *Blood*, 111(1):42–49, Jan 2008.

[211] C. A. Wild, S. Brandau, M. Lindemann, R. Lotfi, T. K. Hoffmann, S. Lang, and C. Bergmann. Toll-like Receptors in Regulatory T Cells of Patients With Head and Neck Cancer. *Arch Otolaryngol Head Neck Surg*, 136(12):1253–1259, Dec 2010.

[212] C. A. Wild, S. Brandau, R. Lotfi, S. Mattheis, X. Gu, S. Lang, and C. Bergmann. HMGB1 is overexpressed in tumor cells and promotes activity of regulatory T cells in patients with head and neck cancer. *Oral Oncol*, 48(5):409–416, May 2012.

[213] R. Williams, D. W. Lee, B. D. Elzey, M. E. Anderson, B. S. Hostager, and J. H. Lee. Preclinical models of HPV+ and HPV- HNSCC in mice: an immune clearance of HPV+ HNSCC. *Head Neck*, 31(7):911–918, Jul 2009.

[214] A. Woodfin, M.-B. Voisin, and S. Nourshargh. Recent developments and complexities in neutrophil transmigration. *Curr Opin Hematol*, 17(1):9–17, Jan 2010.

[215] Q. D. Wu, J. H. Wang, C. Condron, D. Bouchier-Hayes, and H. P. Redmond. Human neutrophils facilitate tumor cell transendothelial migration. *Am J Physiol Cell Physiol*, 280(4):C814–C822, Apr 2001.

[216] Y. Wu, Y.-Y. Li, K. Matsushima, T. Baba, and N. Mukaida. CCL3-CCR5 axis regulates intratumoral accumulation of leukocytes and fibroblasts and promotes angiogenesis in murine lung metastasis process. *J Immunol*, 181(9):6384–6393, Nov 2008.

[217] Y. Wu, Q. Zhao, C. Peng, L. Sun, X.-F. Li, and D.-M. Kuang. Neutrophils promote motility of cancer cells via a hyaluronan-mediated TLR4/PI3K activation loop. *J Pathol*, 225(3):438–447, Nov 2011.

[218] L. Yang, L. M. DeBusk, K. Fukuda, B. Fingleton, B. Green-Jarvis, Y. Shyr, L. M. Matrisian, D. P. Carbone, and P. C. Lin. Expansion of myeloid immune suppressor Gr+CD11b+ cells in tumor-bearing host directly promotes tumor angiogenesis. *Cancer Cell*, 6(4):409–421, Oct 2004.

[219] L. Yang, J. Huang, X. Ren, A. E. Gorska, A. Chytil, M. Aakre, D. P. Carbone, L. M. Matrisian, A. Richmond, P. C. Lin, and H. L. Moses. Abrogation of TGF beta signaling in mammary carcinomas recruits Gr-1+CD11b+ myeloid cells that promote metastasis. *Cancer Cell*, 13(1):23–35, Jan 2008.

[220] W. Yang, D. Wang, and A. Richmond. Role of clathrin-mediated endocytosis in CXCR2 sequestration, resensitization, and signal transduction. *J Biol Chem*, 274(16):11328–11333, Apr 1999.

[221] J.-I. Youn, M. Collazo, I. N. Shalova, S. K. Biswas, and D. I. Gabrilovich. Characterization of the nature of granulocytic myeloid-derived suppressor cells in tumor-bearing mice. *J Leukoc Biol*, 91(1):167–181, Jan 2012.

[222] J.-I. Youn, S. Nagaraj, M. Collazo, and D. I. Gabrilovich. Subsets of myeloid-derived suppressor cells in tumor-bearing mice. *J Immunol*, 181(8):5791–5802, Oct 2008.

[223] I. H. Younos, A. J. Dafferner, D. Gulen, H. C. Britton, and J. E. Talmadge. Tumor regulation of myeloid-derived suppressor cell proliferation and trafficking. *Int Immunopharmacol*, 13(3):245–256, Jul 2012.

[224] A. Zarbock, C. A. Lowell, and K. Ley. Spleen tyrosine kinase Syk is necessary for E-selectin-induced alpha(L)beta(2) integrin-mediated rolling on intercellular adhesion molecule-1. *Immunity*, 26(6):773–783, Jun 2007.

[225] S.-L. Zhou, Z. Dai, Z.-J. Zhou, X.-Y. Wang, G.-H. Yang, Z. Wang, X.-W. Huang, J. Fan, and J. Zhou. Overexpression of CXCL5 mediates neutrophil infiltration and indicates poor prognosis for hepatocellular carcinoma. *Hepatology*, 56(6):2242–2254, Dec 2012.

[226] H. zur Hausen. Papillomaviruses and cancer: from basic studies to clinical application. *Nat Rev Cancer*, 2(5):342–350, May 2002.

Appendix

This sections lists supplementary figures and additional information in relation to the presented study.

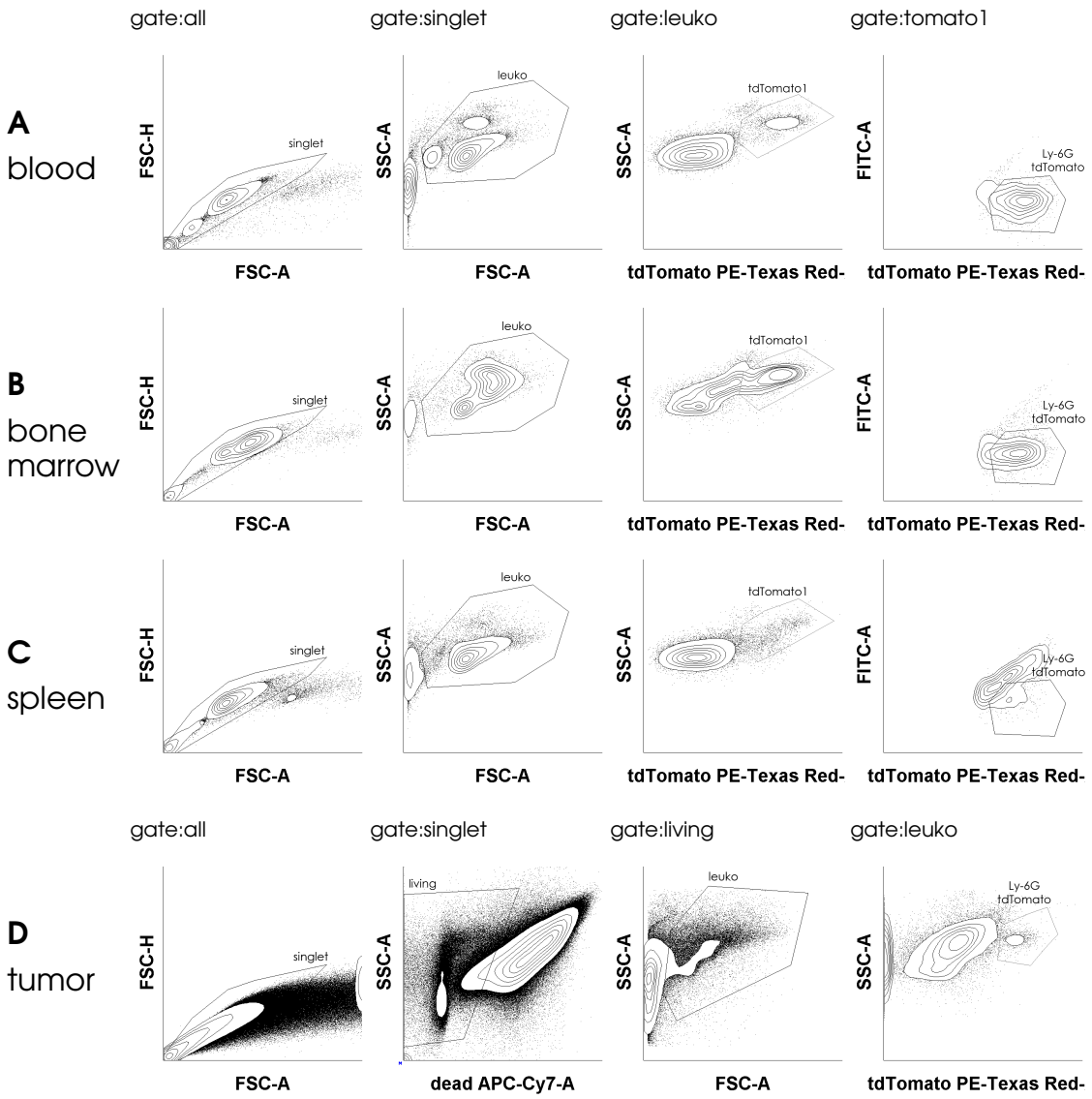

Figure A.1: Sorting strategy for Ly-6G$^+$ cell isolation from CatchUp animals. Cells were isolated from different organs of CatchUp animals and applied to FACS sorting. Representative density plots for blood (A), bone marrow (B), splenocytes (C) and tumor (D) are shown. tdTomato$^+$ cells were identified by gating on singlets (first panel), leukocytes (second panel), tdTomato$^+$ cells with high and intermediate SSC (panel 3) and by additionally excluding autofluorescent cells using the FITC channel (panel 4). For tumor infiltrating cells, gating on living cells (D panel 2) was added.

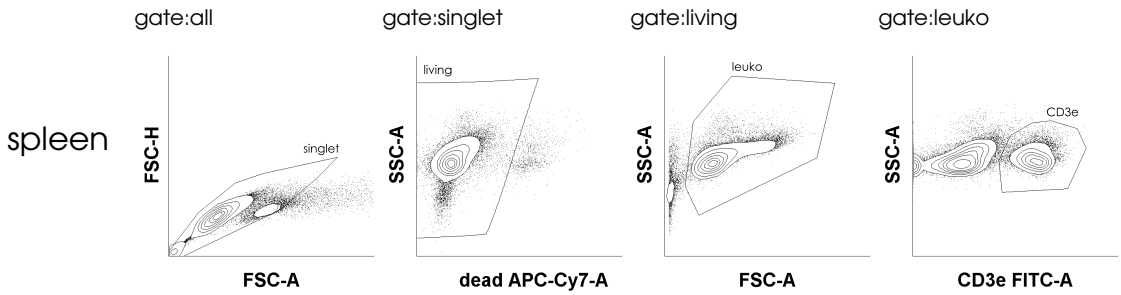

Figure A.2: Sorting strategy for CD3$^+$ T cell isolation. Cells were isolated from spleens of CatchUp animals, stained using anti-CD3ϵ-FITC and applied to FACS sorting. Representative density plots are shown. FITC$^+$ cells were identified by gating on singlets (first panel), living (second panel) leukocytes (panel 3) with high FITC fluorescence (panel 4).

Publications and presentations

Publications

[227] S. Brandau, K. Moses, and S. Lang. The kinship of neutrophils and granulocytic myeloid-derived suppressor cells in cancer: cousins, siblings or twins? *Semin Cancer Biol*, 23(3):171–182, Jun 2013.

[228] C. A. Dumitru, K. Moses, S. Trellakis, S. Lang, and S. Brandau. Neutrophils and granulocytic myeloid-derived suppressor cells: immunophenotyping, cell biology and clinical relevance in human oncology. *Cancer Immunol Immunother*, 61(8):1155–1167, Aug 2012.

Oral presentations

[229] K. Moses. Modulation of myeloid cells by tumor-derived macrophage migration inhibitory factor (MIF) in head and neck cancer. In *IRUN Symposium on Immune Recognition of Pathogens and Tumours in Mülheim an der Ruhr*, October 2011.

[230] K. Moses. Role of tumor-derived MIF in immunological tumor-host interactions. In *BIOME Graduate Seminar*, November 2011.

[231] K. Moses. Expansion and function of granulocytic cells during development and progression of head and neck cancer. In *BIOME Retreat on Cellular and Molecular Immunology/Tumour and Signalling in Hamminkeln*, November 2012.

[232] K. Moses. Expansion and function of granulocytic cells during development and progression of head and neck cancer. In *BIOME Graduate Seminar*, May 2013.

[233] K. Moses. Expansion and function of granulocytic cells during development and progression of head and neck cancer. In *BIOME Retreat on Cellular and Molecular Immunology/Tumour and Signalling in Essen*, November 2013.

[234] K. Moses. Expansion and function of granulocytic cells during development and progression of head and neck cancer. In *Workshop für experimentelle und klinische Forschung in der Kopf-Hals-Onkologie in Leipzig*, February 2013.

[235] K. Moses. Impact of polymorphonuclear cells (PMN) in head and neck cancer (HNC) progression - a mouse model to investigate time dependent functions of PMN. In *BIOME Retreat on Cellular and Molecular Immunology/Tumour and Signalling in Essen*, November 2014.

[236] K. Moses. Impact of polymorphonuclear cells (PMN) in head and neck cancer (HNC) progression. In *1st Internat. Symposium on Tumor Host Interaction in head and neck cancer in Essen*, January 2015.

Poster presentations

[237] K. Moses. Functional modulation of granulocytic cells by macrophage migration inhibitory factor (MIF) during development and progression of head and neck cancer. In *Forschungstag der medizinischen Fakultät des Univeristätsklinikums Essen*, November 2012.

[238] K. Moses. Expansion and function of granulocytic cells during development and progression of head and neck cancer. In *Annual Meeting of the German Societey of Immunology (Deutschen Gesellschaft für Immunologie, DGfI) in Mainz*, September 2013.

[239] K. Moses. Expansion and function of granulocytic cells during development and progression of head and neck cancer. In *Forschungstag der medizinischen Fakultät des Univeristätsklinikums Essen*, November 2013.

[240] K. Moses. Functional modulation of granulocytic cells by macrophage migration inhibitory factor (MIF) during development and progression of head and neck cancer. In *European Workshop on Immune Integrity (IRUN) at Radboud University, Nijmegen*, May 2013.

[241] K. Moses. Tumor-derived factors modulate neutrophil granulocytes to promote head and neck cancer development. In *International Symposium Neutrophil 2014 in Montreal*, June 2014.

Acknowledgments

At first, I like to thank Prof. Sven Brandau for his unbroken urge to collect money for our research, for hours of discussion about experimental layouts and for giving me the opportunity as well as the guidance for this thesis. Your side project, the fish tank, was always enjoyable to observe.

A very big thank you goes to the group of Prof. Matthias Gunzer who gave me a warm welcome for the work on the intravital imaging. I especially thank Anika Klingberg and Linda Männ in this context for your patience and the time you invested in helping me out at the microscope and with all my little special wishes. Thank you for not mentioning the mouse alarm any more as well.

Next, I like to thank the group of PD Bernd Giebel who provided the plasmid system and technical expertise for the establishment of the green fluorescent mouse HNC cell line. Special thanks go to Andre Görgens who supported me in the lab and was always available for any questions.

Furthermore, I would like to thank Claudia Dumitru for scientific guidance and enthusiastic experimental demonstrations. Disregarding your yelling attacks, one could learn a lot from working with you. I'll never forget our first cocktail night.

This is the section about the busy bees in our lab whom I like to thank so much. A big thank you is booked for the mistress of the ENT lab. Kirsten, thank you for organizing all the small things in the lab and keeping everything in place. I further thank Joanna for the IHC and TEM work. The next one in the line is Sebastian: Thanks for organizing the animal things and especially thank you for every single comic you sent to me. Last but not least, dear Petra, thank you for the IHC during my writing period and for all the cynical remarks that were always to the point.

Danksagung

Zuallererst möchte ich Prof. Sven Brandau meinen Dank aussprechen, der unermüdlich für die Finanzierung unserer Projekte gekämpft hat. Danken möchte ich Ihnen für die Zeit, die Sie sich nahmen, um das Projekt und verzwickte Experimente zu diskutieren ebenso wie für die Möglichkeit diese Arbeit überhaupt anzufertigen. Auch das Nebenprojekt Ihres Aquariums hat hierbei immer für interessante Beobachtungen und Aufmunterung gesorgt.

Ein großes Dankeschön soll an die Gruppe um Matthias Gunzer gehen, die mich für die intravitalen Experimente sehr nett und hilfsbereit in ihrem Labor aufgenommen haben. An dieser Stelle möchte ich besonders Linda Männ und Anika Klingberg hervorheben - ich danke euch für eure Geduld und all die Zeit, die für die vielen kleinen Sonderwünsche während meiner Experimente bei euch draufgegangen ist. Danke auch, dass der Mausalarm nicht mehr erwähnt wird.

Weiterhin gilt mein Dank der Gruppe von PD Bernd Giebel mit deren Hilfe ich die in dieser Arbeit genutzte grün fluoreszierende Mauszelllinie herstellen konnte. An dieser Stelle danke ich besonders Andre Görgens, der immer ein offenes Ohr für meine Fragen hatte und ohne den meine Arbeiten in der Transfusionsmedizin sicherlich weniger erfolgreich gewesen wären.

Hier möchte ich nun Claudia Dumitru danke sagen, die mir sowohl wissenschaftlich als auch experimentell oft weiterhelfen konnte. Wenn man gelernt hat, deine Wutanfälle zu ignorieren, konnte man eine Menge von dir lernen. Außerdem werde ich niemals den ersten Cocktail Abend vergessen.

Den fleißigen Bienchen unseres Labors gilt dieser Absatz. Allen voran gilt hier mein großer Dank der Meisterin unseres Labors, Kirsten. Danke, dass du alles organisierst, was so anfällt, und dass du alles an seinem Platz hältst (und diesen auch immer findest). Weiterhin danke ich Joanna für die gesamte IHC Arbeit und die vielen TEM Assays. Als nächster kommt nun Sebastian: Vielen Dank an dich für die Organisation der Mausgeschichten und vor allem für jeden einzelnen Comic (und Spruch), den du mir in den drei einhalb Jahren geschickt hast. Zu guter Letzt kommt hier die Petra an die Reihe. Dir danke ich für die letzten IHCs mit denen ich panisch in der Schreibphase angekommen bin und noch viel mehr für jede zynische Bemerkung, die des Pudels Kern entlarvt hat.

Thank you to all the proof readers of this thesis, you did a great job. And thank you, as well, to everyone in the lab who was helping me out with tips and fruitful discussions. But there was, of course, more than work to work during the time in the lab. Therefore, I like to say a big thank you to all the members and past members of the ENT lab. Thank you for being with me, making every day somehow enjoyable and being who you are. Thank you Johanna and Rob for the everyday motivation and for being great office mates, not to forget the bierskies. Thank you Cindy and Nina, both of you often gave me a new view on simple things. Thank you Clarissa and Tim for the good times we had also after you left. There would be so much more to say which does not fit in some pages of paper so don't feel sad about not being mentioned.

It is somehow probably a German thing to stick to the common order in this section. Therefore, it should be clear to everyone that the very last part contains the most important people. Here, I like to give thanks to the people who accompanied me for a long time. Most importantly, I want to say the biggest thank you to my parents who supported my way undoubtedly. Thank you for being so proud of me. Furthermore, thank you Max, for bearing with me, for spending hour in corrections for this thesis and for all the small things. More importantly, thank you for being with me all the time and for making our place homely nest to gain new energy from. At last, I don't want to forget about the good friends from Göttingen. Thank you for our meetings all over Germany and for making me trust in whatever may be is going to work out somehow.

Ich danke natürlich allen, die diese Arbeit korrekturgelesen haben, das war wirklich klasse. Außerdem möchte ich jedem aus dem Labor für die alltäglichen Tipps und anregenden Diskussion danken. Natürlich bestand Arbeit nicht immer nur aus Arbeit und dafür möchte ich mich auch bei allen Mitgliedern und Ehemaligen des HNO Labors herzlichst bedanken. Danke, dass ihr immer da ward, jeden Tag zu etwas Gutem gemacht habt und vor allem danke, dass ihr seid, wie ihr seid. Danke an Johanna und Rob für die tägliche Motivationseinheit und dafür, dass ihr klasse Büronachbarn gewesen seid. Danke an Nina und Cindy dafür, dass ihr irgendwie immer eine neue Blickweise auf einfache Dinge geliefert habt. Danke auch an Clarissa und Tim, dass wir auch weiterhin gute Zeiten miteinander haben. Es gäbe so viel mehr zu sagen, aber dafür gibt es hier keinen Platz. Daher sollte auch niemand traurig sein, wenn er nicht erwähnt wurde, denn ich danke euch allen sehr.

Die gegebene Reihenfolge einzuhalten ist irgendwie üblich und daher ist klar, dass im letzten Absatz die wichtigsten Leute ihren Platz finden. An dieser Stelle möchte ich mich ganz herzlich bei allen bedanken, die mich bis hier her begleitet haben. Allen voran geht mein größtes Danke schön an meine Eltern, die kompromisslos an mich geglaubt haben, mir meine Laufbahn ermöglicht haben und so unglaublich stolz auf mich sind. Außerdem möchte ich mich unbedingt bei dir bedanken, Max, dass du gewisse Launen ertragen hast, bis in die letzte Minute Korrekturen gemacht hast und die ganze Zeit über dafür gesorgt hast, dass ich bei uns zu Hause zur Ruhe kommen und neue Energie tanken konnte. Ich möchte auch die guten Freunde nicht vergessen, die zu großen Teilen den gleichen Weg beschritten haben oder auch andere Herausforderungen angegangen sind. Daher geht ein weiterer und sehr herzlicher Dank an den Kern der Göttinger MolMeds, denn unsere regelmäßigen Treffen haben mich immer ermutigt, dass was auch immer kommen mag auf jeden Fall geschafft werden kann.

Curriculum Vitae was removed due to protection of privacy in the online version.

Der Lebenslauf ist in der Online-Version aus Gründen des Datenschutzes nicht enthalten.

Affidavit

Erklärung:
Hiermit erkläre ich, gem. §6 Abs. 2, f der Promotionsordnung der Math.-Nat. Fakultäten zur Erlangung der Dr. rer. nat., dass ich das Arbeitsgebiet, dem das Thema "Analysis of Neutrophil Granulocytes in Experimental Head And Neck Cancer Development And Progression" zuzuordnen ist, in Forschung und Lehre vertrete und den Antrag von Frau Katrin Moses befürworte.

Essen, den	_____	Prof. Dr. Sven Brandau Name des wissenschaftl. Betreuers/Mitglieds der Universität Duisburg Essen	_____ Unterschrift des wissenschaftl. Betreuers/Mitglieds der Universität Duisburg Essen

Erklärung:
Hiermit erkläre ich, gem. §7 Abs. 2, c und e der Promotionsordnung der Math.-Nat. Fakultäten zur Erlangung des Dr. rer. nat., dass ich die vorliegende Dissertation selbständig verfasst und mich keiner anderen als der angegebenen Hilfsmittel bedient habe und alle wörtlich oder inhaltlich übernommenen Stellen als solche gekennzeichnet habe.

Essen, den	_____	_____ Katrin Moses

Erklärung:
Hiermit erkläre ich, gem. §7 Abs. 2, d und f der Promotionsordnung der Math.-Nat. Fakultäten zur Erlangung des Dr. rer. nat., dass ich keine anderen Promotionen bzw. Promotionsversuche in der Vergangenheit durchgeführt habe, dass diese Arbeit von keiner anderen Fakultät abgelehnt worden ist, und dass ich die Dissertation nur in diesem Verfahren einreiche.

Essen, den	_____	_____ Katrin Moses